

Regulons Revealed with Gene Expression Data and  
Studies on DNA Sequencing via Ion Conductance

A thesis presented  
by  
Frederick Phillip Roth  
to  
the Committee on Higher Degrees in Biophysics  
in partial fulfillment of the requirements  
for the degree of  
Doctor of Philosophy  
in the subject of  
Biophysics

Harvard University

Cambridge, Massachusetts

May 1998

© 1998 by Frederick Phillip Roth

I dedicate this thesis to my wife, Becca Marsh Roth,  
who means more to me than any of it.

## Table of Contents

Abstract	1
Acknowledgments	3
Chapter 1 — Introduction	1-1
Chapter 2 — Analyzing Affymetrix DNA microarrays	2-1
Overview of Affymetrix microarrays	2-2
Overview of data analysis	2-7
The GeneChip algorithm	2-8
Concerns with the GeneChip algorithm	2-14
An alternative method using median and median ratio	2-16
Chapter 3 — Revealing regulons with transcript data and sequence alignment	3-1
Credits	3-2
Introduction	3-3
Results and Discussion	3-4
Whole genome expression monitoring	3-4
Sequence motifs found	3-9
False positive and false negative motifs	3-19
Candidate sets of co-regulated genes	3-23
Experimental protocol	3-34
Chapter 4 — Prospects for DNA sequencing using ion conductance	4-1
Credits	4-2
Introduction	4-3
Results and Discussion	4-5
Modeling channel conductance	4-5
Conductance measurements of <i>Shigella</i> LamB and $\lambda$ bacteriophage	4-9
Experimental Protocol	4-18
Appendix A — Guide to Software	A-1
Applications for analyzing Affymetrix microarray data	A-2
Applications for noncoding DNA sequences	A-8
Appendix B — Assessing Similarity between Intergenic DNA Motifs	B-1
Appendix C — Absolute and Relative Abundance of Detectable Transcripts of Four <i>S. cerevisiae</i> Cultures, Ranked Alphabetically	C-1
Appendix D — ORFs Not Detected	D-1
ORFs not assayed by the Affymetrix microarrays used	D-2
Detection thresholds for each microarray experiment	D-3

ORFs assayed and not detected among any of four cultures	D-4
Appendix E — ORFs with the Highest Average Abundance	E-1
Appendix F — ORFs Most Changed in Abundance	F-1
In mating type $\alpha$ relative to mating type <b>a</b> strain	F-4
In mating type <b>a</b> relative to mating type $\alpha$ strain	F-6
In glucose-fed relative to galactose-fed culture	F-8
In galactose-fed relative to glucose-fed culture	F-10
In heat-shocked relative to 30 °C culture	F-12
In 30 °C relative to heat-shocked culture	F-14
Appendix G — Sizes of Intergenic Regions in <i>S. cerevisiae</i> , <i>E. coli</i> and <i>H. influenzae</i>	G-1
Intergenic regions in <i>S. cerevisiae</i>	G-5
Intergenic regions in <i>E. coli</i>	G-7
Intergenic regions in <i>H. influenzae</i>	G-9

## Abstract

The first part of this thesis contributes methods for the analysis of genome-scale transcript abundance data using oligonucleotide microarrays ('DNA chips'). This technique can reveal the genes most responsive to environmental or genotypic change. By searching for conserved elements among the upstream DNA sequences of these genes, one can identify candidate regulatory elements and corresponding candidate sets of co-regulated genes. This strategy was applied to three extensively studied regulatory systems in the yeast *Saccharomyces cerevisiae*. Galactose-response data yielded the known binding site of Gal4, and six of nine genes known to be induced by galactose, as well as two ORFs that are good candidates for galactose regulation. Heat shock data yielded a set of histone genes and CCA, a DNA element known to mediate cell-cycle dependent activation. Mating type a and  $\alpha$ -specificity data yielded most of the known a- and  $\alpha$ -specific genes and all of the four relevant DNA elements. This work validates a rapid approach for discovery of regulation mechanism and introduces 'AlignACE', a tool for extracting conserved motifs from unaligned DNA sequence.

In the second part of the thesis, a novel method for sequencing single molecules of DNA is proposed based on the hypothesis that DNA passing through a membrane-spanning channel can disrupt the flow of ions in a sequence-dependent fashion. The method's prospects are examined and an experimental system is suggested which uses bacteriophage  $\lambda$  and the outer-membrane protein LamB from *Shigella sonnei*. To characterize the components of this experimental system, the ion conductance through single channels of *Shigella* LamB was measured to be  $88 \pm 5$  picoSiemens (pS) and the

ion conductance through single channels associated with purified bacteriophage  $\lambda$  was measured to be  $2.1 \pm 0.7$  nS. The  $\lambda$  channels are present in the absence of LamB, suggesting that bacteriophage  $\lambda$ —rather than its receptor—provides the channel used for DNA transfer across the *E. coli* outer membrane.

## Acknowledgments

For the work of finding motifs from expression data described in Chapter 1, I have many people to thank. The direct and integral roles of Jason Hughes and Pete Estep are described in more detail in the preface to Chapter 1. Our collaborators at Affymetrix—particularly David Lockhart, Janet Warrington, Lisa Wodicka and Bob Blalock—made this work possible and shared a preprint of their yeast expression analysis article with us. George Church brought the Gibbs motif sampling algorithm to our attention initially, and Andrew Neuwald provided the Gibbs motif sampling computer code and advice in compiling it. Keith Robison brought DNA weight matrix methods and their power to my attention. Nearly every member of our lab contributed to conversations on how to analyze expression data from Affymetrix microarrays, but particularly Jason Hughes, Pete Estep, Saeed Tavazoie, George Church, John Aach, Jason Johnson, Martin Steffen and Tom Blackwell. Fred Winston and Aimee Dudley shared their expertise in yeast biology, with which we had little previous experience. Saeed Tavazoie suggested the use of clustering methods in the analysis of multiple gene expression data sets, an idea which is mentioned but not explored in Chapter 1. Temple Smith, Tom Schneider, and John Aach contributed to ideas on assessing similarity between sets of aligned sites. Dereth Phillips, Martha Bulyk, Saeed Tavazoie, Mark Johnston, Fred Winston, Temple Smith, Kevin Struhl, David Lockhart and Janet Warrington were kind enough to critically review our manuscript.

For the work on a single molecule method for DNA sequencing, I am indebted to many people. The central contributions of Richard Baldarelli and George Church are

described in detail in a preface to Chapter 2. Chuck Schultz aided Rich Baldarelli in making a working apparatus for measuring small electrical currents on a picoampere scale. Julie Gastier, Dereth Phillips, Martha Bulyk, Pete Estep were all laboratory rotation students involved at one time on this or related projects and provided enthusiastic help and advice. Pete Estep helped in developing a purification scheme for LamB porins. James Chou did some exploratory work on modeling of ion conductance in trans-membrane channels. Laura Richterich helped with figures used in earlier manuscript versions. I am indebted to Magdalena Tosteson for her help with planar bilayer methods. Jim Horn aided in design and constructed a Faraday cage and planar bilayer apparatus. Martin Steffen shared his knowledge of density gradient centrifugation. John Kasianowicz and Daniel Branton provided advice and collaboration. Howard Berg helped with DNA thermal motion calculations. Cliff Christian and Axon Instruments gave equipment and advice. John Greci and New England Biolabs generously supplied  $\lambda$  bacteriophage.

Through my graduate career, Matt Temple, Kristen Landry, and Paul Johnson have been invaluable in keeping things moving more smoothly than one could possibly expect and were tolerant of ambushes as they walked into their offices.

Support for the work described in this thesis came from a variety of sources. The National Science Foundation gave funding in the form of graduate fellowships for Jason Hughes and myself. George Church was an investigator with the Howard Hughes Medical Institute. Generous support came from the Department of Energy (grant # DE-FG02-87-ER60565), Office of Naval Research (grant # N00014-97-1-0865), National

Institutes of Health (grant # HG000811) and Lipper Foundation. Use of an SGI Power ChallengeArray was provided by the NCSA at the Univ. of Illinois at Urbana-Champaign.

Mary Beth Shertick, Abby Jacobs, Eva Marie Hylen and Bob Tanis have juggled our finances with humor and grace, and kept me replete with toys. Terri Broderick put up stoically with my tendency to ask for a FedEx package at exactly the last minute.

Members of the Church lab have been both good colleagues and good friends. In particular, Dereth Phillips has been my neighbor leading a parallel existence, and is always good for a spontaneous aria or a fierce hug. I owe Rich Baldarelli not only for allowing me to join his project, but for late night pizzas and conversation, and for dragging me out on a bike ride once in a while. Andy Link shared his knowledge of molecular biology, his skills in tequila concoctions and his many ideals, and gave me my first experience in thesis-writing. Pete Estep has been always willing to share his bagels and his hot stock tips while challenging my every scientific assumption. Jason Johnson and Martha Bulyk introduced me to the joys of ultimate frisbee, while Keith Robison, Cory Kostrub, and Eugene Chang helped divert me with competitive hand-eye coordination exercises. Saeed Tavazoie was always good for a pleasant conversation or a physics lesson. Martin Steffen was a source of motivation and enthusiasm. Mark Poritz gave lessons in bacteriology and in how to search for a job. Chris Harbison kept the shouting to a minimum. It has been a pleasure working in the past year in the close company of John Aach, Jason Hughes, Jason Johnson and Jong Park. They have been remarkably patient with me. Ting Wu, an honorary member of the Church Lab, gave praise and encouragement in some of my darkest moments in graduate school.

For what I have learned and accomplished in graduate school, thanks are due most to my advisor, George Church, who is remarkable man in that he ranks among both the kindest and most intelligent people I have ever known. George has created a chaotic place filled with creative people—a fantastic setting for thinking about science.

Meredith Wynne and Jim Hogle made me welcome in the Harvard Biophysics program. Jim and Gina DeVivo ('GB') have continued to make this program great and have always made time for helping and advising. Since arriving in graduate school, I've become indebted in the friendship of Stephen Chan, Shashi Mathew, Eliza and Paresh Shah, and Michelle Milne, Susan Alderman, Paul Diamond and Brian Gladstone. I thank Dan Jay and Jack Szostak for welcoming me into their laboratories.

Mentors, teachers and role models prior to graduate school include Irene MacKay, D. L. Smith, Barbara Woll, Craig Taylor, Richard Packard, Art Rosenfeld, Sumner Davis, Jasper Rine, Kevin Hurley, Alex Nichols, Adrianus Kalmijn, and Robert Saul.

I thank my mother, Uta, who gave me the confidence to think I could play the game of science, for knitting sweaters and sending cookies and calling often. I thank my father, John, for being a role model who makes a career in science look both fun and easy. He has given me good advice.

# Chapter 1

## An Introduction

The nature of an introduction encourages me to relate the two distinct parts of this thesis to one another. If there is one theme to this thesis, it is that both parts were motivated by a desire to develop more efficient methods in experimental molecular biology. One might also say that the two parts are complementary, in that one method uses DNA sequence information to develop hypotheses and guide experiments while the other method seeks more DNA sequence information. However, since unifying these two rather distinct topics seems contrived, I will treat them as the distinct subjects that they are.

Revealing Regulons. The first chapter of this thesis describes a method for developing hypotheses about the coordinate regulation of sets of genes, and the specific mechanisms that might regulate them. The first step in the approach is to measure the abundance of transcripts for every gene or putative gene in a genome (the yeast *Saccharomyces cerevisiae* was examined for the present study) under two or more conditions.

Recent technological developments have made the simultaneous quantitation of many mRNA transcripts more tractable. Although, it has long been possible to measure mRNA levels by a Northern blot assay<sup>1</sup>, scaling this approach up to thousands of genes is quite impractical. Currently, there are two general approaches to the problem of mRNA quantitation—hybridization-based methods and counting methods.

Hybridization-based methods involve a surface with arrayed nucleic acid, either oligonucleotides or larger gene fragments. These oligonucleotides or gene fragments are deposited in a known arrangement and are generally of known sequence. The mRNA to be quantitated is labeled fluorescently (or radioactively) and hybridized to the surface.

The level of fluorescence intensity (or radioactivity) is then used to infer the amount of each transcript in the mRNA population. Hybridization-based methods can be subclassified by the method used in producing the hybridization arrays. So-called ‘spotting methods’ produce DNA—generally by PCR—for deposition and subsequent cross-linking to the surface. This method was originally employed on the scale of hundreds of genes by Chuang et al.<sup>2</sup>, has been further miniaturized and refined in the laboratory of Patrick Brown<sup>3-6</sup>, and is currently commercially available from Incyte Pharmaceuticals and Molecular Dynamics, among others. *In situ*-synthesis methods involve synthesis of oligonucleotides in place, i.e., directly onto the surface on which hybridization will later occur. This method was developed by Affymetrix<sup>7-9</sup> and is also currently commercially available.

Counting methods are based on the determination of RNA sequences sampled randomly from the mRNA population to be quantitated. Sequence fragments of sufficient length can be uniquely assigned to a transcript, so that relative abundance can be calculated by simply counting the number of fragments obtained from each transcript. One example of this approach is the ‘shotgun’ sequencing of expressed sequence tags, assembly of these sequence fragments into contiguous sequences, and calculation of abundance for each contiguous sequence based on the number fragments assigned to each. Another example is the serial analysis of gene expression (SAGE) approach developed by Velculescu et al.<sup>10; 11</sup>, whereby very short sequence fragments are subcloned on the basis of neighboring restriction sites. These fragments are then concatenated and sequenced in a high-throughput manner. A third counting method has been developed by Lynx and has been mentioned in print<sup>12-14</sup>, although some details of

the method's capabilities remain obscure. The approach requires the creation of many beads, each bead containing many copies of a single DNA fragment isolated from an mRNA population. The sequence corresponding to each bead is sequenced by a clever process involving Type IIS restriction enzymes and sequence-dependent ligation of a Type IIS restriction site-containing linker.

Once one of these methods has been applied to cells grown in two or more conditions or to cells of two or more genotypes, relative transcript abundance in these mRNA populations can be examined. A set of genes which are similar in relative abundance are more likely to be coordinately regulated than a randomly chosen set of genes. Although not discussed here, there has been recent work on quantitating protein abundance on a whole-genome (or -proteome) scale. Finding a set of genes of similar relative protein abundance is another approach to finding a set of coordinately regulated genes. Whole-genome relative abundance approaches to finding a biologically interesting set of genes are comparable and complementary to genetic approaches which might be guided by isolation and identification of mutant genes. For example, a genetic approach to the study of gene regulation of galactose response (in the absence of prior knowledge) might be the isolation of mutants which will not grow in the presence of galactose, separation of mutant strains into complementation groups, and subsequent cloning and sequencing of the genes corresponding to complementation groups. The set of genes which, when mutated, impair growth on galactose is a biologically interesting set of genes.

Given a biologically interesting set of genes, we can ask if there is a subset of these genes that has a common DNA element in their upstream non-coding regions. Such

a subset is likely to be further enriched for coordinately regulated genes. There are several algorithms which have been previously developed for the purpose of finding conserved elements in unaligned sequence data. A recent review by Frech et al.<sup>15</sup> compared the methods CONSENSUS, WCONSENSUS<sup>16</sup>, Gibbs Site Sampling<sup>17</sup> and Gibbs Motif Sampling<sup>18</sup>, having found these to be the only algorithms that were readily available, currently recommended by their inventors, and which did not rely heavily on prior knowledge of the sought-after conserved element. A more recent method called Multiple Expectation Maximization for Motif Elicitation (MEME)<sup>19</sup> has been developed but has not been compared independently with other methods.

CONSENSUS and WCONSENSUS are based on a clustering algorithm for multiple sequence alignment, wherein the starting point is a pairwise comparison of all potentially conserved sites. The best-matching pairs are kept, and every possible comparison with a third sequence is made and the best sets of three are kept. This continues until one of several stopping criteria are met. A clustering algorithm is an example of a greedy algorithm, discussed further below.

MEME is based on expectation maximization, which is another example of a greedy algorithm. MEME chooses a number of starting estimates for the weight matrix describing a set of aligned site, each starting estimate being derived from one of the sites in the input set. Then, it calculates the probability that each site is a match to this matrix. Next, it updates the matrix based on these probabilities, with the greatest contribution to the weight matrix coming from the most probable sites. The preceding two steps are repeated until a locally optimal solution is reached.

A greedy algorithm assumes that a locally optimal solution is part of the globally optimal solution. In the case of CONSENSUS and WCONSENSUS this is the assumption that the best pair of sites (or one of the best pairs) will be a part of the best set of multiple aligned sites. In the case of MEME, it is the assumption that the globally optimal weight matrix will be reached by locally optimizing weight matrices derived from each site in the input set. That neither of these assumptions are necessarily true for subtle sequence motifs is a disadvantage. However, greedy algorithms are quite efficient and both CONSENSUS and MEME have had demonstrated success.

Gibbs Site Sampling and Gibbs Motif Sampling are both stochastic sampling approaches, i.e., unlike the greedy algorithms described above they do not proceed deterministically to a local optimum from a given starting point. The Gibbs sampling algorithm is similar to an expectation maximization approach except that it has an element of randomness, so that usually—but not always—it proceeds toward an optimal solution.

This allows the discovery of subtle sequence motifs, where the globally optimal alignment may be difficult to find using a deterministic greedy algorithm. One might think that this comes at some expense in efficiency for an exhaustive search, but Gibbs Site Sampling performs comparably to CONSENSUS using approximate 10 times fewer CPU cycles<sup>15</sup>.

Once a conserved DNA element has been found and a hypothesis has been generated that a set of genes is coordinately regulated, the hypothesis can guide experiments for verifying the functional importance of the conserved DNA element. Oligonucleotide-directed mutagenesis is a technique which allows one to make point

mutations at specific, desired locations. One can then assay for impaired gene regulation in the mutated strain.

We can contrast this approach to cases where there are no guiding hypotheses about the locations of regulatory DNA elements. There are two commonly used approaches in this case, both called ‘promoter-bashing’ in the common parlance. Promoter-bashing consists of creating many strains, each having a different mutation in the upstream region of the gene of interest. Linker-scanning mutagenesis is one such mutagenic approach where each strain has a different region deleted in its upstream sequence. Deletion strains in which differential transcription of a gene has been abolished can thus identify regions important to regulation. Smaller deletions are then constructed until the critical region(s) has been narrowed to a few base pairs. Once the size of the critical region(s) has been narrowed down sufficiently, oligonucleotide-directed mutagenesis can be used to make specific point mutations to determine the critical bases of the DNA element. Another promoter-bashing approach is cassette mutagenesis, wherein the upstream region is randomly point-mutagenized extensively and then used to replace the upstream sequence in an unmutagenized strain, so that any impairment of regulatory function can be attributed to mutations in this cassette region. Mutant strains impaired for gene regulation are then sequenced to identify critical regions. Both of the approaches described above are laborious, and would not be preferred in cases where there exist strong hypotheses for the location of regulatory sites.

Little or nothing is known about the transcriptional (or post-transcriptional) regulation of most *S. cerevisiae* genes, so that more efficient methods for developing and testing hypotheses about gene regulation are needed.

Single-molecule DNA sequencing. The second chapter of this thesis is an exploration of a method for sequencing single molecules of DNA that was first proposed by George Church in 1989.

At the time of this proposal, it was generally accepted that a dramatically improved method of DNA sequencing would be required to determine the sequence of the entire human genome at reasonable cost within a reasonable period of time<sup>20</sup>. Today's DNA sequencing technology of choice, Sanger dideoxy sequencing, was first described in 1977<sup>21</sup>. Radioactivity-based detection has evolved into fluorescence-based detection, different DNA polymerases have been employed and the method has become more automated, but the underlying method remains essentially the same<sup>22</sup>. Automation of the multiple steps required for Sanger dideoxy sequencing and the need for significant quantities of reagents contribute to the cost of this method. Methods which directly determine the sequence of a single molecule of DNA have the potential to reduce these costs significantly.

George Church's proposal was based on the principle that DNA passing through a transmembrane channel will impede ion flow through that channel. So, if each of the four (possibly modified) nucleotides block the channel to a unique extent, then the DNA can be sequenced by measuring ion conductance. George Church and Richard Baldarelli began exploring this idea and settled on a biological system for effecting DNA transport across a membrane—bacteriophage  $\lambda$ . Bacteriophage  $\lambda$  infects *E. coli* cells and is known to require a membrane receptor, the bacterial LamB porin, in order to inject its DNA

across the *E. coli* membrane. It has not been shown whether bacteriophage  $\lambda$  creates its own channel, or if it widens a pre-existing channel in the LamB pore.

That it is possible to measure ion current through a single molecular ‘hole’ in a lipid membrane has been long established<sup>23</sup>. Current blockages in single channels have previously been observed, e.g., in the case of a protein-conducting channel in the endoplasmic reticulum<sup>24</sup>. More critical questions to the proposed method are: Can nucleic acids be ‘threaded’ into a channel under suitable experimental conditions? Will different nucleotides block channel conductance to measurably different extents? If not, can modified nucleotides be used to achieve this aim? Will thermal diffusion of nucleic acids cause back-and-forth motion on the scale of single bases that will be more rapid than the time resolution in current measurement we are able to achieve?

Independently, another research group, consisting of David Deamer, Daniel Branton, John Kasianowicz and Eric Brandin, hit upon the same idea of using ion conductance to sequence nucleic acids. They decided to use *S. aureus*  $\alpha$ -hemolysin, a large channel which does not naturally transport nucleic acids, and use electrophoresis as a means to drive the nucleic acid (either RNA or DNA in this case) through the channel<sup>25</sup>.

I will briefly discuss the results of Kasianowicz et al. here, though since their results were published after completion of the work described in Chapter 2, this discussion might properly belong in an epilogue<sup>25</sup>. When ion current through a single channel of  $\alpha$ -hemolysin was measured in the presence of poly(U) single-stranded RNA, transient decreases of ion current were seen. These transient decreases were not seen in the absence of poly(U), so these decreases were attributed to channel blockage by the

nucleic acid. This was confirmed by repeating the experiment with poly(U) ranging in length from 150 to 450 nucleotides, and finding that the duration of channel blockage was proportional to poly(U) sequence length. Recently, it was reported that the same group was able to discern the difference between poly(A) and poly(C) by measuring ion current<sup>26</sup>. Using an RNA sequence of 70 As followed by 30 Cs, it was found that conductance changed during the transient decrease in ion current.

Apart from the proposed method of sequencing by ion conductance outlined in Chapter 2 and the method of Kasianowicz et al. discussed above, proposals for single-molecule sequencing fall into two categories. The first of these seeks to sequence DNA directly using scanning tunneling microscopy (STM). STM is a technique which uses a conductive probe to scan a surface. When the probe is in contact with the surface, there is a measurable electric current due to electrons ‘tunneling’ through the surface. If the probe is moved up and down so that the tunneling current remains constant, and the height of the probe is known, a topographical map of the surface can be constructed. Double-stranded DNA has been imaged by STM in aqueous solution with high enough resolution to resolve helical pitch<sup>27</sup>. Subsequently, individual adenine bases were resolved in single-stranded poly(dA), lending credence to the idea that DNA might be sequenced<sup>28</sup>. Since that time, there has been little reported progress towards sequencing DNA directly by STM. In 1994, a related proposal was made to cleave surface-deposited DNA at specific positions using incorporation of <sup>32</sup>P, and sequence by measuring the lengths of cleaved fragments using STM<sup>29</sup>. To date, no DNA sequencing by STM methods has been reported.

The second category of single-molecule DNA sequencing relies on the fluorescence-based detection of single-molecules in a flowing solution. It also requires that a DNA or RNA polymerase faithfully incorporate and extend from nucleotides that have been modified to be fluorescent. A single-stranded nucleic acid, having each of its four bases modified with one of four spectrally distinct fluorophores, is attached to a solid support. Fluid passes across this solid support, with the flow leading to a sensitive fluorescence detector. A 3'→5' exonuclease is used to remove bases sequentially from one end, and as the fluorescent bases are removed they are carried past the detector<sup>30</sup>. The sequence of the four different fluorescent bases moving past the detector will then correspond to the nucleic acid sequence.

Single-molecule fluorescence detection has been accomplished in a flow system using the fluorescent dye rhodamine-6G, with about 85% of molecules in the flow being detected<sup>30</sup>. Incorporation and extension of fluorescently labeled nucleotides has been accomplished, but low efficiency incorporation of modified nucleotides remains a technical problem<sup>31</sup>. No DNA sequence has yet been determined using this method.

In 1995, sequencing of the human genome began on a production scale using the conventional Sanger dideoxy method<sup>22</sup>. Incremental improvements in this method had made it possible to consider using this approach to complete the genome. At the same time, however, it was noted that uses for DNA sequencing would not end with completion of an individual human genome. Improved DNA sequencing would lead to improved methods for measuring mRNA expression levels, using the counting methods like the SAGE approach described above. Increased interest in genetic variation among

humans, and in genomes in all branches of life guarantees continued interest in revolutionary approaches to DNA sequencing.

## References

1. **Alwine, J.C., Kemp, D.J. and Stark, G.R.**, Method for detection of specific RNAs in agarose gels by transfer to diazobenzyloxymethyl-paper and hybridization with DNA probes, *Proceedings of the National Academy of Sciences of the United States of America*, 74(12), 5350-4, 1977.
2. **Chuang, S.E., Daniels, D.L. and Blattner, F.R.**, Global regulation of gene expression in Escherichia coli, *Journal of Bacteriology*, 175(7), 2026-2036, 1993.
3. **Shalon, D., Smith, S.J. and Brown, P.O.**, A DNA microarray system for analyzing complex DNA samples using two-color fluorescent probe hybridization, *Genome Research*, 6(7), 639-45, 1996.
4. **Schena, M., Shalon, D., Heller, R., Chai, A., Brown, P.O. and Davis, R.W.**, Parallel human genome analysis: microarray-based expression monitoring of 1000 genes, *Proceedings of the National Academy of Sciences of the United States of America*, 93(20), 10614-10619, 1996.
5. **Schena, M., Shalon, D., Davis, R.W. and Brown, P.O.**, Quantitative monitoring of gene expression patterns with a complementary DNA microarray [see comments], *Science*, 270(5235), 467-470, 1995.
6. **DeRisi, J., Penland, L., Brown, P.O., Bittner, M.L., Meltzer, P.S., Ray, M., Chen, Y., Su, Y.A. and Trent, J.M.**, Use of a cDNA microarray to analyse gene

expression patterns in human cancer [see comments], *Nature Genetics*, 14(4), 457-460, 1996.

7. **Chee, M., Yang, R., Hubbell, E., Berno, A., Huang, X.C., Stern, D., Winkler, J., Lockhart, D.J., Morris, M.S. and Fodor, S.P.**, Accessing genetic information with high-density DNA arrays, *Science*, 274(5287), 610-614, 1996.
8. **Lockhart, D.J., Dong, H.L., Byrne, M.C., Follettie, M.T., Gallo, M.V., Chee, M.S., Mittmann, M., Wang, C.W., Kobayashi, M., Horton, H. and Brown, E.L.**, Expression monitoring by hybridization to high-density oligonucleotide arrays, *Nature Biotechnology*, 14(13), 1675-1680, 1996.
9. **Wodicka, L., Dong, H., Mittmann, M., Ho, M.-H. and Lockhart, D.J.**, Genome-wide expression monitoring in *Saccharomyces cerevisiae*, *Nature Biotechnology*, 15(13), 1359-1366, 1997.
10. **Velculescu, V.E., Zhang, L., Zhou, W., Vogelstein, J., Basrai, M.A., Bassett, D., Jr., Hieter, P., Vogelstein, B. and Kinzler, K.W.**, Characterization of the yeast transcriptome, *Cell*, 88(2), 243-51, 1997.
11. **Zhang, L., Zhou, W., Velculescu, V.E., Kern, S.E., Hruban, R.H., Hamilton, S.R., Vogelstein, B. and Kinzler, K.W.**, Gene expression profiles in normal and cancer cells, *Science*, 276(5316), 1268-72, 1997.
12. **Marshall, A. and Hodgson, J.**, DNA chips: an array of possibilities. [Review] [4 refs], *Nature Biotechnology*, 16(1), 27-31, 1998.
13. **Brenner, S.**, Massively parallel sequencing of sorted polynucleotides, in *www.patents.ibm.com*, U.S., Lynx Therapeutics, Inc., 1997.

14. **Brenner, S.**, DNA sequencing by stepwise ligation and cleavage, in [www.patents.ibm.com](http://www.patents.ibm.com), U.S., Lynx Therapeutics, Inc., 1998.
15. **Frech, K., Quandt, K. and Werner, T.**, Software for the analysis of DNA sequence elements of transcription, *Computer Applications in the Biosciences*, 13(1), 89-97, 1997.
16. **Hertz, G.S. and Stormo, G.D.**, Identification of consensus patterns in unaligned DNA and protein sequences: a large deviation statistical basis for penalizing gaps., in *Proceedings of the 3rd International Conference on Bioinformatics and Genome Research*, Lim, H.A. and Cantor, C.R., Eds., Singapore, World Scientific Publishing Co., 1995, 201-216.
17. **Lawrence, C.E., Altschul, S.F., Boguski, M.S., Liu, J.S., Neuwald, A.F. and Wootton, J.C.**, Detecting subtle sequence signals: a Gibbs sampling strategy for multiple alignment, *Science*, 262(5131), 208-214, 1993.
18. **Neuwald, A.F., Liu, J.S. and Lawrence, C.E.**, Gibbs motif sampling: detection of bacterial outer membrane protein repeats, *Protein Science*, 4(8), 1618-1632, 1995.
19. **Bailey, T.L. and Elkan, C.**, Unsupervised learning of multiple motifs in biopolymers using expectation maximization, *Machine Learning Journal*, 21, 51-83, 1995.
20. **Olson, M.V.**, The human genome project. [Review] [80 refs], *Proceedings of the National Academy of Sciences of the United States of America*, 90(10), 4338-44, 1993.
21. **Sanger, F., Nicklen, S. and Coulson, A.R.**, DNA sequencing with chain-terminating inhibitors, *Proceedings of the National Academy of Sciences of the United States of America*, 74(12), 5463-7, 1977.

22. **Olson, M.V.**, A time to sequence, *Science*, 270(5235), 394-6, 1995.
23. **Bean, R.C., Shepherd, W.C., Chan, H. and Eichner, J.**, Discrete conductance fluctuations in lipid bilayer protein membranes, *J. Gen. Physiol.*, 53(6), 741-757, 1969.
24. **Simon, S.M. and Blobel, G.**, A protein-conducting channel in the endoplasmic reticulum, *Cell*, 65(3), 371-380, 1991.
25. **Kasianowicz, J.J., Brandin, E., Branton, D. and Deamer, D.W.**, Characterization of individual polynucleotide molecules using a membrane channel, *Proc. Natl. Acad. Sci. USA*, 93, 13770-13773, 1996.
26. **Zacks, R.**, Hole in the wall offers cheaper sequencing, *Technology Review*(May/June), 26, 1998.
27. **Lindsay, S.M. and Barris, B.**, Images of the DNA double helix in water, *Science*, 244, 1063-1064, 1989.
28. **Dunlap, D.D. and Bustamante, C.**, Images of single-stranded nucleic acids by scanning tunnelling microscopy, *Nature*, 342, 204-206, 1989.
29. **Kelson, I. and Nussinov, S.**, A scheme for sequencing large DNA molecules by identifying local nuclear-induced effects, *Proceedings of the National Academy of Sciences of the United States of America*, 91(15), 6963-6, 1994.
30. **Harding, J.D. and Keller, R.A.**, Single-molecule detection as an approach to rapid DNA sequencing. [Review] [17 refs], *Trends In Biotechnology*, 10(1-2), 55-7, 1992.
31. **Zhu, Z. and Waggoner, A.S.**, Molecular mechanism controlling the incorporation of fluorescent nucleotides into DNA by PCR, *Cytometry*, 28(3), 206-11, 1997.

## Chapter 2

### Analyzing Affymetrix DNA Microarrays

There were many, often intense, discussions among members of our laboratory on alternative ways to analyze fluorescence intensity data—the primary data from Affymetrix DNA microarrays ('chips'). It was during these discussions that my thoughts on chip data analysis became more clear. In this chapter, I will first describe the physical characteristics of Affymetrix chips, making liberal use of excerpts from several papers on the subject<sup>1-2</sup>. I will discuss the analysis algorithms used by Affymetrix and also our motivations for developing an alternative method. Finally, I will describe the method of analysis outlined in Chapter 1 in greater detail and describe limitations and future possibilities.

High-density synthetic oligonucleotide arrays. Synthetic oligonucleotide arrays have been used to quantitate transcript abundance in mammalian mRNA populations<sup>3</sup> and more recently in yeast mRNA populations<sup>1</sup>. Synthetic oligonucleotide arrays are essentially glass slides with oligonucleotides attached at the surface. Through the use of photolithographic masking it is possible to synthesize these oligonucleotides *in situ*, allowing for the creation of defined regions on the surface (also called 'features') which contain oligonucleotides of a single desired sequence (see Fig. 1).

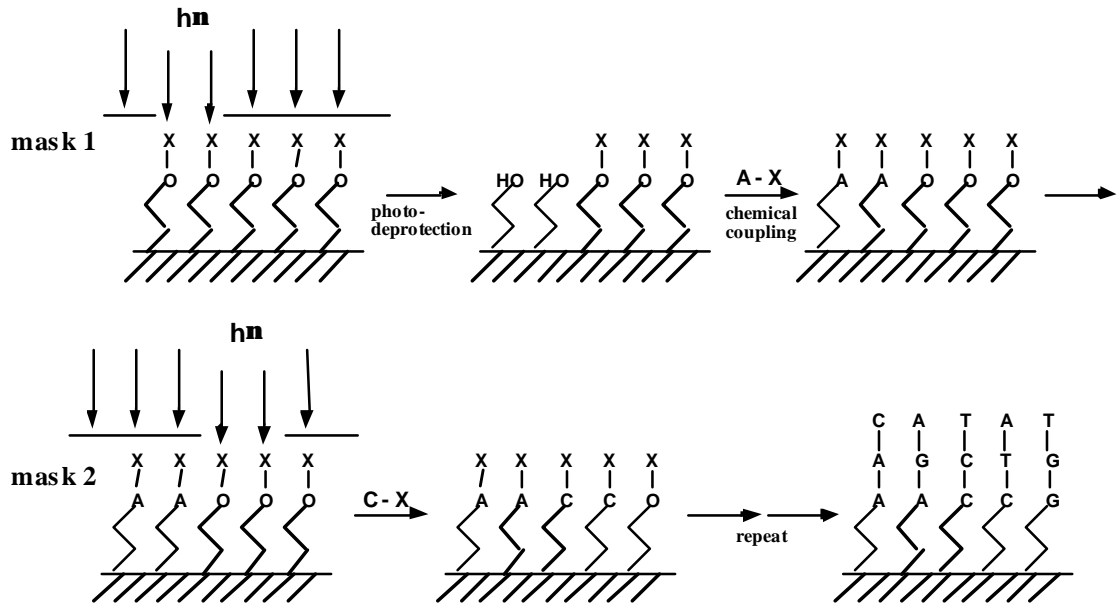


**Figure 1.** Light-directed synthesis of oligonucleotides. A surface bearing photoprotected hydroxyls (X-O) is illuminated through a photolithographic mask ('mask 1'), generating free hydroxyl groups in the photodeprotected region. The hydroxyl groups are then coupled to a deoxynucleoside phosphoramidite (5'-photoprotected). A new mask pattern ('mask 2') is applied, and a second photoprotected phosphoramidite is coupled. Rounds of illumination and coupling are repeated until the desired set of products is obtained. This figure legend was excerpted from ref. 2 and the figure was adapted from the same source by Martha L. Bulyk.

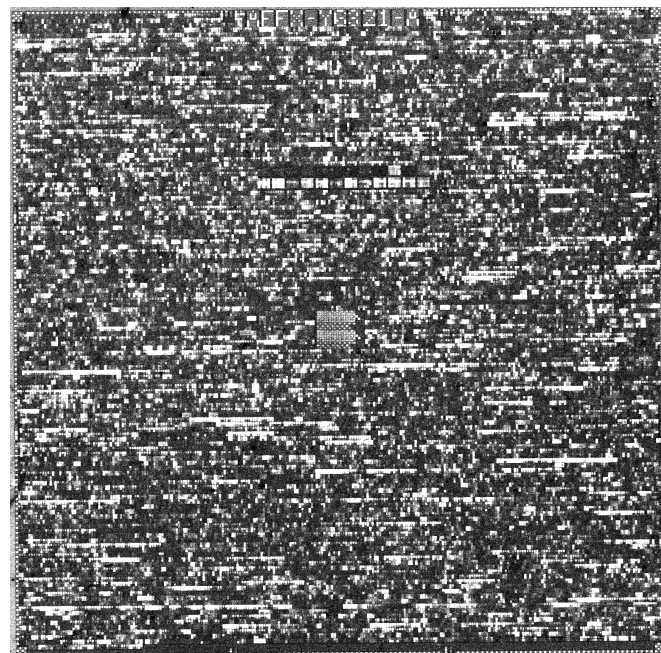
The oligonucleotide arrays used to monitor gene expression in *Saccharomyces cerevisiae* measure  $1.28 \times 1.28$  cm and contain more than 65,000  $50 \times 50$   $\mu\text{m}$  synthesis ‘features’. Each synthesis feature consists of more than  $10^7$  copies of a particular 25-mer oligonucleotide. The full set of oligonucleotide probes covering all open reading frames (ORFs) are divided among four different arrays, comprising a total area of approximately one square inch for the entire yeast genome. For each ORF, approximately 20 complementary 25-mers were chosen using selection criteria which have not been publicly revealed by Affymetrix, but which include tests for sequence uniqueness relative to the rest of the genome and the absence of sequence features (e.g., self-complementarity or clusters of single nucleotides) that have been determined to adversely affect hybridization on arrays.

Use of multiple oligonucleotides for each ORF provides redundancy in the detection and analysis of the data and mitigates the potentially confounding effects of occasional cross-hybridization. For each of the complementary 25-mers (called ‘PM’s, for ‘perfect matches’) there is a closely related 25-mer which differs by only one base (called an ‘MM’ for ‘mismatch’) at the central position. The MM probe of each pair serves as an internal control that allows consistent hybridization to be recognized (a PM signal larger than the corresponding MM signal). The difference between the PM and MM intensities of a probe pair will also be referred to as  $\Delta$ . Both of the algorithms discussed here are based on the difference of PM and MM partners, so that when the differences of several ‘probe pairs’ (a PM and its corresponding MM) are aggregated, cross-hybridization and background hybridization tends to cancel. Specific hybridization

signals, on the other hand, tend to add constructively across the set of probe pairs for each gene.

The chips are read out by hybridizing fluorescently labeled cDNA or ‘cRNA’ (produced from cDNA by reverse transcription) to the chip. Fluorescence intensity is quantitated by a scanning confocal microscope. This fluorescence intensity data is the primary data which must be interpreted to give the relative and/or absolute abundance of a transcript.

**A.**



**B.**

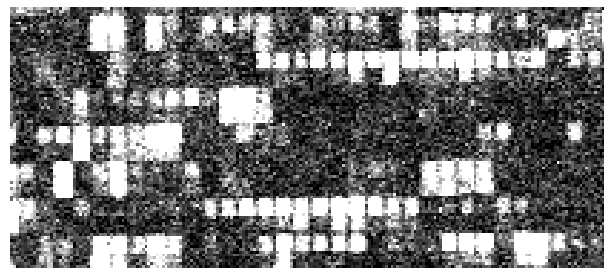


**Figure 2.** Fluorescence intensity images from an Affymetrix *S. cerevisiae* expression microarray. (A) contains the complete image of a yeast 'A' chip (the first of a set of 4 chips). The image was obtained from a chip which was hybridized with cRNA which was biotinylated and conjugated to phycoerythrin. The RNA was isolated from a culture grown in the presence of galactose, labeled and hybridized as described in Chapter 1. (B) is an enlargement of part of the chip shown in (A). In this image, a clustering of intense features can be seen within rows. These clusters are generally sets of PM probes derived from one ORF, while the corresponding MM probes are located in the next lowest row.

Overview of microarray fluorescence intensity data analysis. Analysis of fluorescence intensity data may be divided into four distinct steps:

- 1) **Obtain feature intensities.** Assign an intensity value to each feature on the chip. In Fig. 1A, a checkerboard pattern of intensity can be seen around the perimeter of the chip. Each of the intense features in this pattern is complementary to a fluorescently labeled control DNA sequence which has been added to the chip along with the labeled DNA or RNA to be examined. The checkerboard pattern aids the GeneChip software in its placement of a deformable grid over the intensity image, so that regions of intensity can be mapped to coordinates on the chip.
- 2) **Subtract Background.** Calculate and subtract background intensity from each feature. This step is employed in the methods used by both Affymetrix and myself, but is not essential to every method of analysis that might be envisioned, since MM features serve as an additional ‘background’ subtraction.
- 3) **Normalize.** Normalize feature intensity between chips within an experiment, and between experiments. Since the efficiency of mRNA isolation, labeling, and hybridization can vary from experiment to experiment, and the amount of *in situ*-synthesized oligonucleotide can vary considerably from chip to chip, normalization is an important step.
- 4) **Calculate ORF abundance.** First, group the feature intensities into sets of PM and MM intensities so that each correspond to a given gene or ORF, using the knowledge of the oligonucleotide sequence that corresponds to each feature coordinate on the chip. Then, use the set of background-subtracted, normalized, PM and MM features

for a given ORF to determine either a) the ORF's absolute transcript abundance or b) its abundance relative to another growth condition.

5) **Establish a measure of confidence.** Features with pixel intensities that are less variable should be more reliable. Feature sets that have more features, are less variable, or that are more easily distinguished from background are also likely to yield a more reliable measurement.

The GeneChip algorithm for interpreting fluorescence intensity. Here I describe the algorithm used by the Affymetrix GeneChip software. Past versions of the algorithm is known to me by personal communication, while the current version is as described in the help files of GeneChip 3.0, unless otherwise noted. I should mention that changes have been made in successive versions of the GeneChip software, so there is no guarantee the algorithm is the same as in previous versions of GeneChip, nor that it will be unchanged in future versions. My chief purpose in describing the GeneChip algorithm is to put the new method of data analysis in the context of an alternative method.

1) **Obtain feature intensities.** After the perimeter checkerboard is used to map a grid onto the features, a set of pixels is associated with each feature. The pixels near the edges of the feature are discarded, and a clustering algorithm is used to find a region of intense pixels among those remaining. The average pixel intensity of this region is then assigned to the feature. Details of this procedure have been unavailable to the general public, but I have been told more recently that the GeneChip 3.0 software has been altered so that, instead of choosing a cluster of intense pixels, the 75th percentile pixel intensity is assigned to the feature after discarding pixels near the feature edge.

2) **Subtract Background.** The total chip area is divided into sectors (with 16 as a default number of elements in a sector). The background is then calculated independently for the features in each sector by averaging the lowest N (80 is the default value for N) feature intensities in that sector.

3) **Normalize.** One of three different methods of normalization can be used, at the user's discretion: a) Normalize using selected genes. Typically the genes selected for normalization are transcripts not naturally present in yeast, e.g., transcripts from *E. coli*, that have been 'spiked' at known concentration into the hybridization mixture. This method is best for normalizing between different chips that have been exposed to the same hybridization mixture. This method can also be the best approach for normalizing between different preparations of hybridization mixture if the bacterial transcripts are 'spiked' into the nucleic acid preparation at an earlier step. If spiking occurs before total RNA is purified from cell lysate, variation in efficiencies of RNA isolation, mRNA, cDNA and cRNA production can be normalized. b) Normalize with user-defined constant. The user specifies the normalization factor to the GeneChip software. c) Normalize using the total intensity of all genes on the array. Although the exact procedure for doing this was not known to me at the time I developed our analysis method, I have since been told that this is done by dividing each feature intensity by the sum of PM – MM, i.e., the sum of  $\Delta$ , for all probe pairs.

4) **Calculate ORF abundance.** a) An ORF's absolute abundance is calculated by taking the average of  $\Delta$  for that ORF. For ORFs with few probe pairs ( $\leq 8$ ), no measures are taken to lessen the impact of outliers (surprisingly high or low values of  $\Delta$ ). For ORFs with ~20 probe pairs, a so-called 'Olympic scoring' method is employed

wherein the highest and lowest  $\Delta$  values are discarded before calculating the average of  $\Delta$ . For ORFs with ~50 probe pairs, so-called ‘super-Olympic’ scoring is used, wherein first the highest and lowest  $\Delta$  values are discarded, and then those  $\Delta$  values more than three standard deviations from the resulting mean are discarded, and abundance is taken to be the mean of the remaining  $\Delta$  values. b) To calculate abundance of an ORF relative to another growth condition, i.e., fold change, the absolute abundance is calculated in each case using the method described in (a), and fold change is simply calculated as the ratio of these two absolute abundances. In the case of abundance calculation, there is a heuristic method (described below) for determining whether a transcript is ‘present’ or ‘absent’. If the transcript is deemed absent, the abundance value calculated above is not reported. Similarly for fold change calculations, there is a heuristic method for determining if there is ‘no change’ in abundance, in which case the calculated value for fold change is not reported. If a transcript is deemed ‘present’ in one condition and ‘absent’ in the other, the lower transcript is set to 20 for the purposes of calculating an approximate fold change value.

5) **Establish a measure of confidence.** At this point, the GeneChip software does not provide a numeric measure of confidence, e.g., a 95% confidence interval for abundance measurements. However, GeneChip does use a heuristic method for declaring a transcript to be either ‘present’, ‘marginal’ or ‘absent’ among the pool of transcripts being assayed, although there is no measure of what the upper or lower limits of that transcript’s abundance might be, or with what confidence this decision was made. The presence, absence or marginality of a transcript is determined by some unknown combination of three measures: a) The average of  $\log(\text{PM}/\text{MM})$  for a given transcript.

This is a measure of how different the pattern of probe intensities is from random. An average  $\log(\text{PM/MM})$  of 0 would indicate perfectly random cross-hybridization. The GeneChip user is able to set ‘marginal’ or ‘present’ thresholds for this value. b) The ratio of the number of ‘positive’ probe pairs to the total number of probe pairs. A ‘positive’ probe pair is defined as one for which both  $\Delta$  and  $\text{PM/MM}$  are greater than user-defined thresholds (called ‘SDT’ and ‘SRT’, respectively). c) The ratio of number of ‘positive’ to number of ‘negative’ probe pairs. ‘Positive’ is defined as above, while a ‘negative’ probe pair is one for which  $-\Delta$  and  $\text{MM/PM}$  exceed those same user-defined thresholds employed in defining ‘positive’.

For measurements of expression change between two conditions, ‘fold change’ is calculated as the ratio of abundances (as calculated above) in each condition. As a non-quantitative measure of confidence a transcript is called ‘increased’ (I), ‘decreased’ (D), ‘increased moderately’ (MI), ‘decreased moderately’ (MD), or ‘not changed’ (NC). These determinations are made heuristically. There is also a measure called ‘Sig’ (short for significance) associated with each fold change value, using an empirical combination of ‘fold change’ and the absolute difference in abundance.

For ratios of transcript abundance, the determination of ‘NC’, ‘I’, ‘D’, ‘MI’, or ‘MD’ is made using an unknown combination of the following five measures: a) The ratio of the number of probe pairs ‘increased’ to the number of probe pairs ‘decreased’. A probe pair is considered ‘increased’ if  $(\Delta_{\text{experiment}} - \Delta_{\text{baseline}})$  is greater than a threshold ‘CT’, and  $(\Delta_{\text{experiment}} - \Delta_{\text{baseline}})/\Delta_{\text{baseline}}$  is greater than a threshold ‘PCT’. A probe pair is considered ‘decreased’ if  $(\Delta_{\text{baseline}} - \Delta_{\text{experiment}})$  is greater than a threshold ‘CT’, and  $(\Delta_{\text{baseline}} - \Delta_{\text{experiment}})/\Delta_{\text{baseline}}$  is greater than a threshold ‘PCT’. b) The fraction of probe

pairs that are ‘increased’, according to the above definition. c) The fraction of probe pairs that are ‘decreased’, according to the above definition. d) The difference in the ratio of the number of ‘positive’-scoring probe pairs to the number of ‘negative’-scoring probe pairs, i.e.,  $(\#Pos/\#Neg)_{\text{experiment}} - (\#Pos/\#Neg)_{\text{baseline}}$ . e) The difference in average log ratio for the set of probe pairs, i.e.,  $\text{avg}\{\log(\text{PM/MM})\}_{\text{experiment}} - \text{avg}\{\log(\text{PM/MM})\}_{\text{baseline}}$ . The exact method by which the ‘NC’, ‘I’, ‘D’, ‘MI’, and ‘MD’ calls are determined from the above measures has not been revealed to us.

With each fold change value, there is an associated measure of change in abundance called ‘Sig’. Although the name implies a measure of significance, it is not. It is an empirical formula combining difference in absolute fold change with the ratio of fold change, for ranking purposes. The formula is as follows:

$$\text{Sig} = 10^{(x-4/3)} \cdot \sqrt{\text{avg}\Delta_{\text{expt}} - \text{avg}\Delta_{\text{base}}} \cdot \log_{10} \left( \frac{\text{avg}\Delta_{\text{expt}}}{\text{avg}\Delta_{\text{base}}} \right)$$

where  $\text{avg}\Delta$  is the mean of the  $\Delta$  values for a given ORF for a given condition and

$$x = \frac{\left| \max(20, \text{avg}\Delta_{\text{expt}}) - \max(20, \text{avg}\Delta_{\text{base}}) \right|}{\max(20, \text{avg}\Delta_{\text{expt}}) + \max(20, \text{avg}\Delta_{\text{base}}) + 1}.$$

The preceding equation is heuristic and, although it may prove useful in ranking transcripts, has no direct connection that I can find with probability or significance of results.

Success of the GeneChip algorithm. Wodicka et al. have applied the GeneChip algorithm to chip data derived from *S. cerevisiae* cultures grown in both rich and minimal media <sup>1</sup>, with great success. These assays were shown to be largely reproducible: The

same RNA sample (from rich media) was hybridized to different chip sets from the same production lot, and of 6200 probe sets, only 14 showed a difference in abundance of more than two-fold between hybridizations while only two showed differences greater than three-fold. When independent preparations of labeled RNA from the same pellet of yeast cells were hybridized, 74 probe sets changed by more than two-fold, and six showed a greater than three-fold difference. Estimates of gene abundance from the GeneChip analysis reportedly agreed well for all but one of the genes for which absolute abundance had been measured in a previous study <sup>4</sup>, although details of this agreement were not presented <sup>1</sup>.

Concerns with the GeneChip algorithm. In Chapter 1, an alternative data analysis algorithm to the GeneChip algorithm above was presented. There were several motivations for developing an alternative approach. The first is simply that some aspects of the GeneChip algorithm are confidential, and it seems reasonable for one to know how one's data is being analyzed. A second, related, concern is that this algorithm has changed over time in subsequent versions of the GeneChip software in ways that may or may not have been shared with the public. Data analysis should be reproducible, and this is not necessarily the case if the GeneChip software is used and later upgraded.

Another concern is that the approaches used by the GeneChip algorithm use a number of parameters (thirty in GeneChip 3.0) set at the user's discretion. The default parameters used by GeneChip have reportedly been optimized by Affymetrix through a series of spiking experiments wherein several known amounts of transcripts are 'spiked' into a hybridization pool, and also through repeated hybridizations to determine the

algorithm's robustness to variation<sup>1</sup>. However, we have no information about how these parameters should vary depending upon the quality of the chip and nature of the hybridization. This was a key point for us, since the first DNA chips we had to work with had failed Affymetrix's quality control procedure, so that it was entirely possible that the algorithm parameters should be changed. For example, in the case where a transcript called absent, the detection threshold, i.e., the 'SDT' threshold above, was set to a value of 20. The default detection threshold then does not depend on the variance of the data. Since the chips we had failed the Affymetrix quality control criteria due to overall signal intensity, we expected that our detection threshold should be correspondingly higher.

We also had some concerns about how the GeneChip method deals with outliers. We and Affymetrix agree, I think, that the data acquired via Affymetrix chips contain a substantial amount of unavoidable 'contamination' due to cross-hybridization and variability in hybridization between probes of differing DNA sequence. Even in cases where there is no cross-hybridization, variable binding energy (due to differences in GC content) or secondary structure within a transcript can cause large differences in  $\Delta$ , even within a single transcript. The effect of data contamination should only increase with the use of lower quality chips. So, even if the GeneChip parameters have been optimized for most chips, they may not have been appropriate for ours. The GeneChip approach to outlier detection was to toss the high and low  $\Delta$  values, and then remove those  $\Delta$  values more than three standard deviations from the resulting mean. If we encounter more than one high or one low outlier, we should use a method which can handle this occurrence. Ideally, a method of outlier detection should be informed by a knowledge of the

distribution underlying  $\Delta$  values. Unfortunately, this distribution may be different for every transcript, since each transcript has probe pairs of different sequence. Many of the transcripts we analyzed have an asymmetric distribution of  $\Delta$  values, i.e., the median of  $\Delta$  values is consistently lower than the mean of  $\Delta$  values across the four conditions we measured. If this is the case, it is inappropriate to apply a symmetric outlier detection scheme since the distribution of  $\Delta$  is asymmetric. An alternative to outlier detection is to use statistics that are robust to outliers, e.g., the median as opposed to the mean.

A further concern stemmed from my objection that one of the measures used in deciding whether a transcript is ‘increased’ or ‘not changed’ between two conditions is inappropriate. The measure  $(\Delta_{\text{experiment}} - \Delta_{\text{baseline}})/\Delta_{\text{baseline}}$  depends on which of two conditions is considered the experimental condition and which is considered the baseline. It is then possible for a transcript to be considered ‘not changed’ with one choice of baseline, and ‘increased’ with the alternative choice. A representative of Affymetrix has recently informed me (20 April 1998) that the above formula is no longer used in GeneChip, but the literature distributed to users was not updated and unfortunately the formula in actual use is considered confidential until further notice. This highlights the potential danger of not being able to reproduce data analysis.

#### Median $\Delta$ and median $\Delta$ -ratio algorithms for interpreting fluorescence data.

Although there are minor differences in the way that I performed background subtraction and normalization in Chapter 1, I would not argue that the methods I used here were significantly different or superior. Our methods for dealing with background and normalization were developed without knowing the methods used by the GeneChip

software. With present knowledge, I would choose GeneChip's methods for background subtraction, and am ambivalent about the method of normalization. The GeneChip method for background subtraction is superior to the method that I used in that it accounts for variation in background levels across the chip, while the method I described in Chapter 1 does not.

An alternative to GeneChip's method of calculating transcript abundance is use of the median as a measure of central tendency of  $\Delta$  values. The median is a measure of central tendency that is robust to outliers. Use of a robust statistic seems preferable in a case where the underlying distribution of  $\Delta$  has not been characterized. A related measure of variance can then be used—median deviation. Median deviation is calculated in the following way: median deviation = median{ med $\Delta$  –  $\Delta_1$ , med $\Delta$  –  $\Delta_2$ , . . . , med $\Delta$  –  $\Delta_n$  }, where med $\Delta$  = median{ $\Delta_1, \Delta_2, \dots, \Delta_n$ }. This method was not described in Chapter 1, since only relative abundance was used for that work.

An alternative to the GeneChip method of calculating relative abundance (also described in Chapter 1) is the median  $\Delta$ -ratio method. Using this method, relative abundance is calculated in the following way: median { $(\Delta_{1,\text{expt}} / \Delta_{1,\text{base}})$ ,  $(\Delta_{2,\text{expt}} / \Delta_{2,\text{base}})$ ,  $(\Delta_{3,\text{expt}} / \Delta_{3,\text{base}})$ , . . . ,  $(\Delta_{n,\text{expt}} / \Delta_{n,\text{base}})$  }. This method has the advantage that variance associated with the sequence differences of different probes is eliminated. When absolute abundance is calculated for a given condition, individual probe intensities will vary because of the sequence-dependence of binding energy, secondary structure and hybridization kinetics. If the sequence in the transcript complementary to the probe has a propensity to form secondary structure, this will also create probe-specific variation in measured intensity. The sequence-dependence of intensity will create a large variance in

$\Delta$  intensities, which will be reflected in the ratio of two absolute abundances. The  $\Delta$ -ratio for a probe pair of given sequence is a less sequence-dependent measure than  $\Delta$ . The central tendency (I used the median) of these  $\Delta$ -ratios is then a good representation of ratio of abundance between conditions. An estimate of error in this number reflects primarily uncertainty in the abundance ratio, rather than sequence-dependent variation in hybridization kinetics.

An estimate of error in the ratio of abundance could be calculated by using the median deviation of  $\Delta$ -ratios, but since  $\Delta$ -ratios are ratios, it is perhaps better to estimate central tendency using the median of log-ratios and measure the error in this number by measuring the median deviation of log-ratios, so that:

$$M = \text{median} \left\{ \log \frac{\Delta_{1,\text{expt}}}{\Delta_{1,\text{base}}}, \log \frac{\Delta_{2,\text{expt}}}{\Delta_{2,\text{base}}}, \log \frac{\Delta_{3,\text{expt}}}{\Delta_{3,\text{base}}}, \dots, \log \frac{\Delta_{n,\text{expt}}}{\Delta_{n,\text{base}}} \right\}$$

$$E = \text{median} \left\{ \left| \log \frac{\Delta_{1,\text{expt}}}{\Delta_{1,\text{base}}} - M \right|, \left| \log \frac{\Delta_{2,\text{expt}}}{\Delta_{2,\text{base}}} - M \right|, \left| \log \frac{\Delta_{3,\text{expt}}}{\Delta_{3,\text{base}}} - M \right|, \dots, \left| \log \frac{\Delta_{n,\text{expt}}}{\Delta_{n,\text{base}}} - M \right| \right\}$$

where  $M$  is the median of log( $\Delta$ -ratios) and  $E$  is an estimate of error in this number.

The methods described here of calculating absolute and relative abundance have the advantages that they are simpler, and allow for an estimate of error. What the user of chip data would really like is a confidence interval for abundance and relative abundance, i.e., a range of values and a statement that the true value lies within that range with a confidence. Unfortunately, a supportable method for assigning confidence intervals to this data does not exist. To assign a confidence interval, one should first obtain an understanding of the underlying distribution of  $\Delta$  values for each ORF (or the underlying distribution of  $\Delta$  ratios). This will almost be certainly done empirically, with data sets that are not available to us at present. Several types of experiments will be required for

this purpose. To characterize the cross-hybridization of a transcript to all probes on a chip, one might label and hybridize each probe alone to the chip. This would require about 24,000 experiments (6,000 genes  $\times$  four chips), so one might envision hybridizing with pools containing a small number of labeled transcripts to reduce the number of required hybridizations. One caveat to this already arduous experiment is that differential mRNA degradation, differential transcription initiation or termination sites, and differential splicing may make the total number of possible transcripts much greater than 6,000.

Neglecting cross-hybridization, the distribution of  $\Delta$  could be found by simply hybridizing labeled genomic DNA to a chip, since the relative amount of ‘transcript’ is the same for each ORF being assayed. To determine the relationship of  $\Delta$  ratios to the true ratio of transcript abundance, one could hybridize with different mixtures each ‘spiked’ with known amounts of one or more transcripts.

## References

1. **Wodicka, L., Dong, H., Mittmann, M., Ho, M.-H. and Lockhart, D.J.**, Genome-wide expression monitoring in *Saccharomyces cerevisiae*, *Nature Biotechnology*, 15(13), 1359-1366, 1997.
2. **Pease, A.C., Solas, D., Sullivan, E.J., Cronin, M.T., Holmes, C.P. and Fodor, S.P.**, Light-generated oligonucleotide arrays for rapid DNA sequence analysis, *Proceedings of the National Academy of Sciences of the United States of America*, 91(11), 5022-6, 1994.
3. **Lockhart, D.J., Dong, H.L., Byrne, M.C., Follettie, M.T., Gallo, M.V., Chee, M.S., Mittmann, M., Wang, C.W., Kobayashi, M., Horton, H. and Brown, E.L.**, Expression monitoring by hybridization to high-density oligonucleotide arrays, *Nature Biotechnology*, 14(13), 1675-1680, 1996.
4. **Iyer, V. and Struhl, K.**, Absolute mRNA levels and transcription initiation rates in *Saccharomyces cerevisiae*., *Proceedings of the National Academy of Sciences of the United States of America*, 93, 5208-5212, 1996.

## Chapter 3

# Revealing Regulons Using Transcript Abundance Data and Upstream Sequence Alignment

## Allocating Credit among Co-authors

Since the following chapter represents more than one person's efforts, it seems appropriate to a doctoral thesis that I describe which parts were my own work.

Contributions made by those who were not coauthors are credited—I sincerely hope adequately—elsewhere in the acknowledgments. The central concept of searching for conserved upstream elements among genes chosen by expression analysis originated jointly with Jason Hughes and myself. The work of growing cultures, isolating and labeling RNA, and performing microarray hybridization experiments was performed entirely by Preston Estep. The tools for data analysis were developed collaboratively by Jason Hughes and myself, but our contributions are separable. Jason's focus was on rewriting the computer code for AlignACE, and implementing the changes that we made from the original Gibbs motif sampling algorithm. Design and implementation of the algorithms for analyzing data from Affymetrix microarrays and for assessing similarity between two sets of aligned sites were primarily my own. I wrote the computer code used for retrieving upstream DNA sequence for given ORFs, scoring motifs discovered by AlignACE against the yeast genome by the Berg and von Hippel method, integrating site locations with expression data, and for calculating consensus sequences by the method of Day and McMorris. I applied the above-described tools to the galactose, heat shock and mating type data sets, and assessed false negatives and the expected number of false positives.

Complete DNA sequence is now known for more than ten different organisms<sup>1</sup>. For even the most intensely studied of these organisms, a large fraction of genes is completely uncharacterized — about 40% and 50% for *Escherichia coli* and *Saccharomyces cerevisiae*, respectively<sup>2; 3</sup>. Furthermore, annotation of non-coding regions has typically lagged behind discovery and prediction of gene function. Given that sequence elements in non-coding regions often control gene expression, and that knowing a gene's place in the larger regulatory network of a cell is essential to understanding its function, it is critical that we develop methods for rapidly characterizing non-coding regions.

A common approach to the discovery of regulatory elements entails the construction of a series of deletions or replacements in the 5' untranslated region (UTR) sequence of a gene, followed by a screen for altered regulation. An efficient method for predicting the most likely locations of regulatory sequences can guide experiments more quickly to the sought-after elements. Where there is a set of genes ‘enriched’ for co-regulated members (obtained for example by genetic evidence), this prediction can be based on sequence conservation among the upstream regions of several genes<sup>4</sup>.

Recently, it has become possible to measure the abundance of mRNA transcripts on a whole-genome scale<sup>5-9</sup>. By comparing transcript levels in different conditions (or different strains), we can find the set of genes whose transcript levels respond to a difference in environment (or genotype). With this set of genes in hand, a number of questions naturally arise: Which of these changes in expression constitute a primary response to an environmental change, and which are indirect effects? Which are most

critical for adaptation to a new condition? By what mechanisms are changes in transcript abundance achieved? What DNA (or RNA) sequence elements mediate the regulation of transcript abundance?

Given a set of induced (or repressed) genes, one can use a computational algorithm to search the regions upstream of translation start for short conserved DNA sequence motifs. Such a conserved motif is a good candidate for a transcriptional control element. Although they have been less extensively studied, sequence elements in the 5' UTR may also be determinants of mRNA stability<sup>10; 11</sup>. It has also been suggested that long conserved sequences in the 5' UTR are candidate sites for regulation by antisense transcripts<sup>12</sup>. Regardless of mechanism, a set of genes with similar expression responses that also share a conserved upstream motif is a candidate for a set of co-regulated genes, i.e., a regulon.

## Results and Discussion

Whole genome expression monitoring. To test our strategy of combined expression analysis and upstream sequence alignment, we examined three transcriptionally-regulated systems in the yeast *S. cerevisiae*: galactose utilization, heat shock response, and mating type regulation. We measured mRNA transcript abundances in *S. cerevisiae* in each of four different cultures, which allowed three whole-genome comparisons to be made: 1) growth on galactose vs. glucose; 2) strains of mating type **a** vs. mating type **α** and 3) growth at 30 °C continuously vs. after a 39 °C heat shock.

Expression was measured for each of these three systems using photolithographically synthesized oligonucleotide microarrays ('chips')<sup>7; 9</sup>. Change in

transcript abundance for each open reading frame (ORF) was calculated for each comparison described above by a variation on a previously described method (see Protocols). Fig. 1 shows the distribution of change in expression for each of the three systems. Complete data sets are available, including ranked lists of those ORFs that were most changed between each pair of conditions <sup>13</sup>.

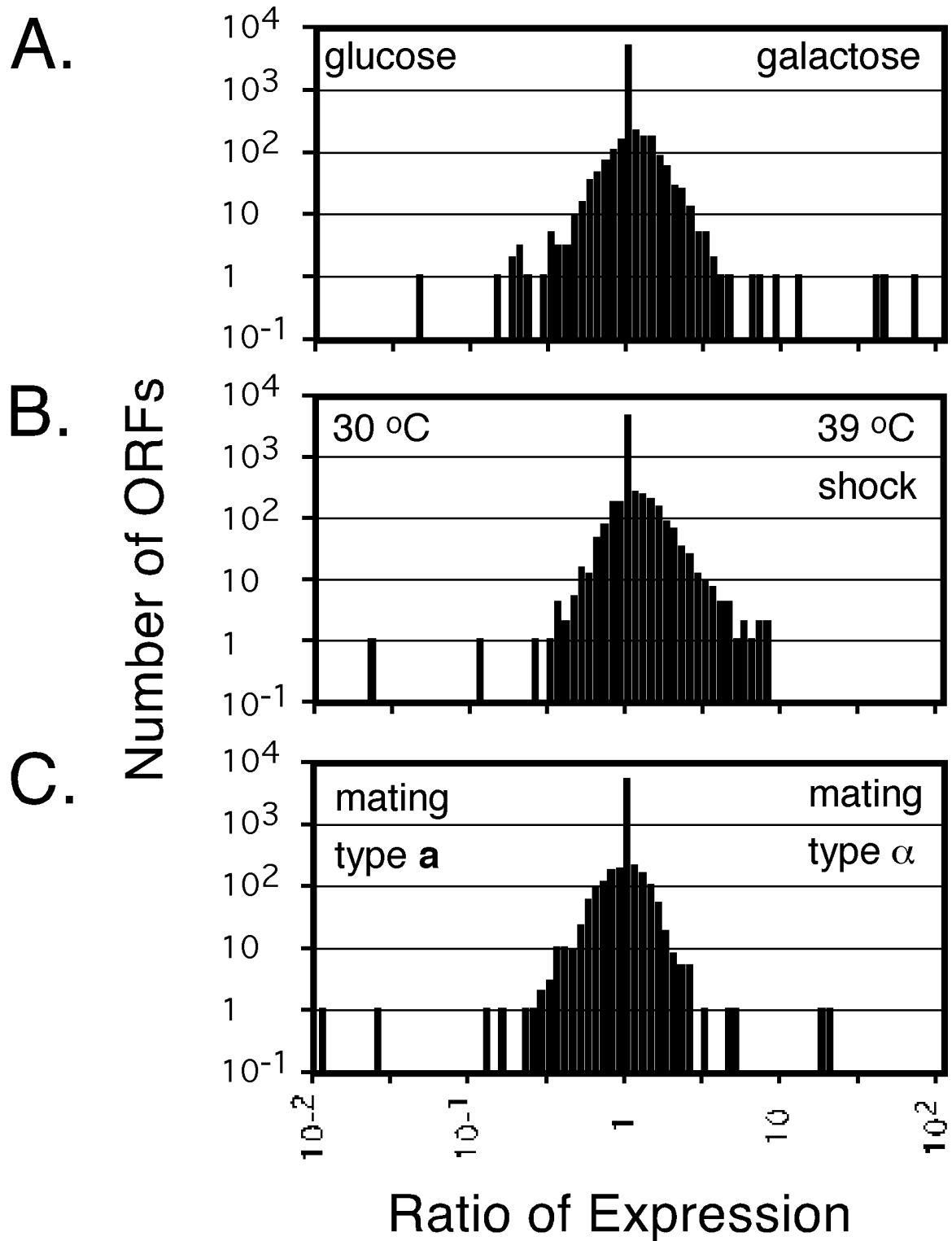


**Figure 1.** Histograms of log ratio of expression level in each of three whole-genome expression comparisons. (A) reflects the comparison between growth in galactose vs. glucose, with transcripts more abundant in galactose having a higher log ratio. (B) reflects the comparison of heat shock vs. 30 °C, with transcripts increased under heat shock conditions having a higher log ratio. (C) reflects the comparison of mating type  $\alpha$  with **a**, where transcripts more abundant in mating type  $\alpha$  have a higher log ratio. Transcripts with low measured abundance in both conditions were assigned a log ratio value of 1 for the purposes of this figure. The fraction of all ORFs in the yeast genome which were below detection threshold in both conditions was 70%, 62% and 68% for figures (A), (B) and (C) respectively.

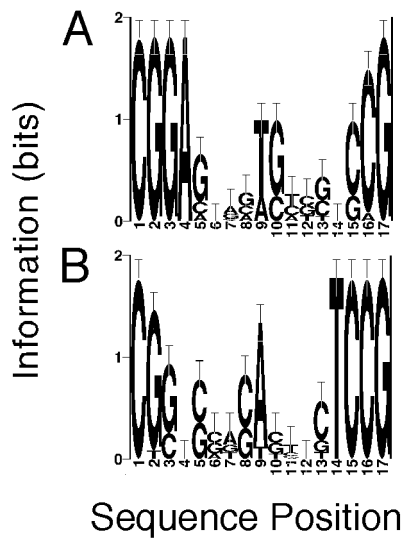
Examining upstream non-coding DNA sequence. For each of the whole-genome expression comparisons described above, we examined sets of upstream DNA sequences from 1) the top ten ORFs, as ranked by ratio of first-condition to second-condition abundance, e.g., ratio of galactose to glucose expression, 2) the top ten ORFs, as ranked by ratio of second-condition to first-condition abundance, e.g., ratio of glucose to galactose expression, and 3) the combination of the two preceding ORF sets. Upstream DNA sequence for each ORF was bounded at the 3' (or downstream) end by the ORF's translation start. The 5' end was bounded by the translation start or stop of the nearest upstream ORF, with the exception that this boundary was never more than 600 DNA base pairs (bp) or less than 300 bp from translation start.

Several algorithms which discover recurring motifs in unaligned sequences have been developed, and have been compared in Frech et al.<sup>14</sup>. ‘Gibbs motif sampling’ is one such algorithm that is both computationally efficient and tends not to become ‘trapped’ in sub-optimal alignments<sup>15; 16</sup>. Although the Gibbs sampling strategy has been applied primarily to protein sequence alignments, it has been applied previously to DNA<sup>14; 17</sup>. The Gibbs motif sampling algorithm<sup>15</sup> was modified in several ways, primarily to make it more amenable to alignment of DNA (as opposed to protein) sequence and to allow iterative searches for multiple motifs.

The modified Gibbs motif sampling algorithm (‘AlignACE’) was applied to each set of upstream DNA sequence. Of the many resulting DNA site alignments, we considered further only those motifs which: 1) exceeded a threshold AlignACE score—a measure of ‘goodness’ of sequence alignment; and 2) had a specificity score—a measure of the fraction of genes in the yeast genome with matching upstream sites—below 1% of

the ORFs in yeast. The latter criterion requires that motifs be selective, i.e., not similar to elements (such as the TATA Box) commonly found among upstream regions.

DNA sequence motifs found from expression data. We first consider alignment results from the galactose vs. glucose comparison. With the set of ten ORFs more abundant in galactose than glucose, we identified a motif, ‘gal-1’ (Fig. 2A), which matches the galactose upstream activation sequence (UAS<sub>G</sub>) motif. It should be noted that we developed an objective measure to assess the similarity of the motifs identified here with previously described motifs, and that this measure is—to our knowledge—the only published method for quantitatively assessing similarity between DNA-binding site motifs (see Protocols). UAS<sub>G</sub> is known to regulate galactose-utilization genes via the Gal4/Gal80 activation complex <sup>18</sup>. No motif which met our criteria was obtained when the top ten ORFs ranked more abundant in glucose were used. Another UAS<sub>G</sub>-like motif, ‘gal-glu-1’ (Fig. 2B), was obtained when the preceding two ORF sets (a total of twenty ORFs) were combined. Fig. 2C summarizes the motifs found by AlignACE and those that might have been expected *a priori* given their previously defined roles in transcriptional regulation.



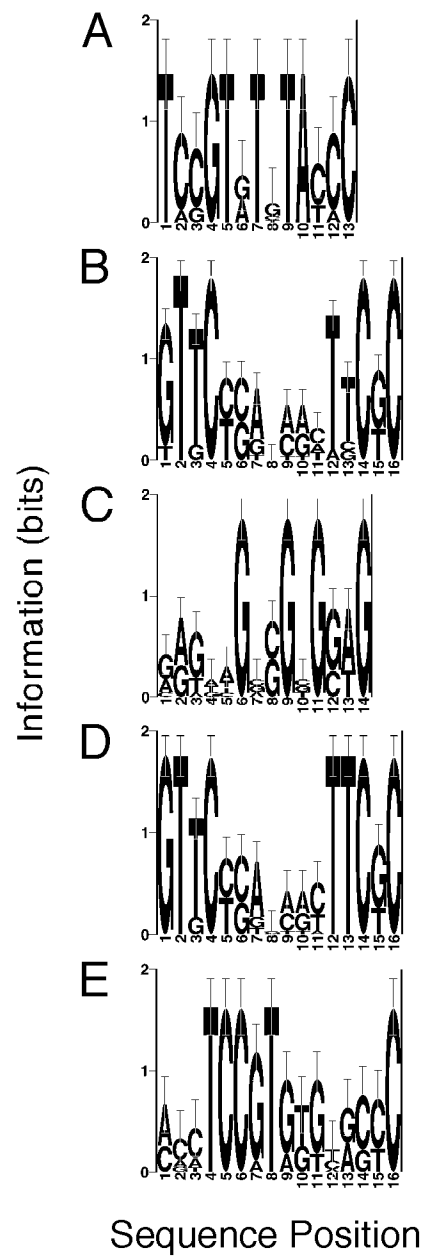
### C.

Motif	Score	Specif	Consensus	Similarity
gal-1 (A)	33.1	0.16	CGGAGNRVTSYBBNCCG	gal-glu-1*, UAS <sub>G</sub>
gal-glu-1	24.9	0.20	CGSBSVWSABYNBTCCG	UAS <sub>G</sub> , gal-1*

Expected	DNABP	Consensus	Ref.
UAS <sub>G</sub>	Gal4/Gal8	TTCGGMGVDMTSTBVHCC	19
URS <sub>G</sub>	Mig1	CCCCRSNTWWWW	19
Rap1-binding	Rap1	WRCACCAKACAYY	19
Gcr1-binding	Gcr1	CKRGCTTCCWNTWK	19

**Figure 2.** DNA sequence motifs obtained from a comparison between growth on galactose- and glucose-containing media. (**A**) Motif ('gal-1') obtained from the ten ORFs most abundant in galactose relative to glucose while (**B**) Motif ('gal-glu-1') obtained by combining the preceding set with the ten ORFs most abundant in glucose relative to galactose, and matches UAS<sub>G</sub>. See Protocols for a description of sequence logos. (**C**) lists those motifs returned by AlignACE as well as motifs which might have been expected a priori. 'Score' refers to AlignACE score, 'Specif' is the specificity score, and 'DNABP' refers to the protein which binds an element, where known. Consensus sequences and motif similarity were obtained by objective criteria (see Protocols). A '\*' indicates a motif's reverse complement.

The ten ORFs most abundant in the heat shocked culture relative to 30 °C yielded a single motif, ‘39C-1’ (Fig. 3A), which is similar to ‘39C-30C-2’ (Fig. 3E), but not similar to any of the known binding sites considered in this study. The ten ORFs more abundant in 30 °C relative to heat-shocked culture yielded two motifs. The first of these, ‘30C-1’ (Fig. 3B), matches the cell cycle activation (CCA) motif, a previously known activator of histone genes<sup>20; 21</sup>. The second motif, ‘30C-2’ (Fig. 3C), has not been previously noted. When the combined set of twenty ORFs was used (genes abundant either in heat shock or 30 °C), another CCA-like motif—‘39C-30C-1’ (Fig. 3D)—was identified along with ‘39C-30C-2’ (Fig. 3E), a motif similar to ‘39C-1’. Fig. 3F summarizes the motifs found by AlignACE and those that might have been expected *a priori* given their previously defined roles in transcriptional regulation.



**F.**

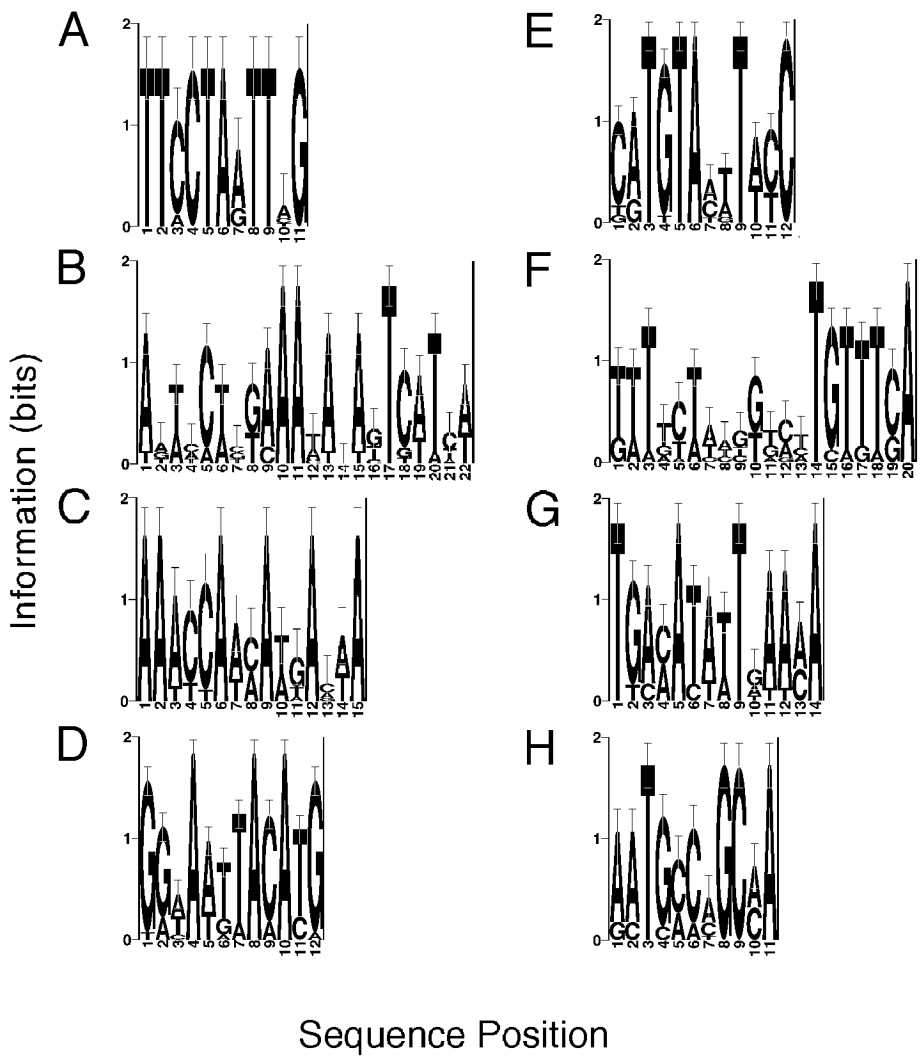
<b>Found</b>	<b>Score</b>	<b>Specif</b>	<b>Consensus</b>	<b>Similarity</b>
39C-1 (A)	5.1	0.04	TCCGTRTBTAYCC	39C-30C-2
30C-1 (B)	40.1	0.26	GTTCYSANMRHTTCK	39C-30C-1, CCA*
30C-2 (C)	5.5	0.44	RRKDWGVSGBGSWG	-
39C-30C-1 (D)	30.1	0.20	GTTCYSAVMRYTTCK	30C-1, CCA*
39C-30C-2 (E)	8.5	0.10	MMMTCCGTRKKYRSY	39C-1

<b>Expected</b>	<b>DNABP</b>	<b>Consensus</b>	<b>Ref.</b>
HSE	HSF	CNVGAANNTTCBMG	22
STRE	Msn2/Msn4	HHAGGGGV	23; 24
CCA	?/Hir1/Hir2	GCGAARWWNTSRGAAC	20
NEG	?	TDDACGCTMAAWSWC	21
MCB	Mbp1	ACGCGTWAM	25
SCB	Swi4/Swi6	RDDYCACGAAAA	25
ECB	Mcm1	TTWCCCDWTTAGGAAA	26

**Figure 3.** DNA sequence motifs obtained from a comparison of growth between heat shock and 30 °C conditions. **(A)**, Motif ('39C-1') obtained from the ten ORFs most abundant in heat shock relative to 30 °C, **(B)** and **(C)** Motifs ('30C-1' and '30C-2', respectively) obtained from the ten ORFs most abundant in 30 °C relative to heat shock, while **(D)** and **(E)** Motifs ('39C-30C-1' and '39C-30C-2' respectively) obtained from the combined set of twenty ORFs. See Protocols for a description of sequence logos. **(F)** lists those motifs returned by AlignACE as well as motifs which might have been expected a priori. 'Score' refers to AlignACE score, 'Specif' is the specificity score, and 'DNABP' refers to the protein which binds an element, where known. Consensus sequences and motif similarity were obtained by objective criteria (see Protocols). A '\*' indicates a motif's reverse complement.

When the ten ORFs most abundant in mating type  $\alpha$  relative to type **a** were examined, the motif ‘mt $\alpha$ -1’ (Fig. 4A) was found. ‘mt $\alpha$ -1’ matches the P-Box and the early cell cycle box (ECB; mediates activation of M/G<sub>1</sub>-specific transcription <sup>25; 26</sup>), as well as the Gcr1-binding site and the heat shock element (HSE). The P-box and ECB elements are both known to be bound by Mcm1 <sup>27</sup>. Using the ten ORFs more abundant in mating type **a** than type  $\alpha$ , three motifs emerged. The first two of these, ‘mt**a**-1’ and ‘mt**a**-2’ (Fig. 4B,C) have not been previously noted. The third motif, ‘mt**a**-3’ (Fig. 4D), matches the binding site of Mat $\alpha$ 2 <sup>27</sup>.

When the combined set of twenty ORFs was used, four motifs emerged. The first of these, ‘mt $\alpha$ -mt**a**-1’ (Fig. 4E), matches the known Mat $\alpha$ 2-binding site. The second, ‘mt $\alpha$ -mt**a**-2’ (Fig. 4F), matches the pheromone-response element (PRE)—the known binding site of Ste12 <sup>27</sup>. ‘mt $\alpha$ -mt**a**-2’ is interesting, since a weak second match to the PRE consensus suggests a conserved spacing of 7 bp between PRE elements. The third motif, ‘mt $\alpha$ -mt**a**-3’ (Fig. 4G), bears some resemblance to the PRE consensus, but had a similarity score below the threshold applied here (see Protocols). The fourth motif, ‘mt $\alpha$ -mt**a**-4’ (Fig. 4H), corresponds to the Q-Box element, which is known to bind Mat $\alpha$ 1 <sup>27</sup>. Fig. 4I summarizes the motifs found by AlignACE and those that might have been expected *a priori* given their previously defined roles in transcriptional regulation.



## I.

Motif	Score	Specif	Consensus	Similarity
mt $\alpha$ -1 (A)	8.9	0.22	TTCCTTAATTHG	P-Box*, ECB*, Gcr1-binding, HSE
mt $\alpha$ -1 (B)	8.5	0.10	ADWHCWBKAAAWANAKTCWTH	-
mt $\alpha$ -2 (C)	5.0	0.20	AAAYCAWMMAWKAMWA	-
mt $\alpha$ -3 (D)	28.1	0.62	GRWAWTTACATG	$\alpha$ 2-binding*, mt $\alpha$ -mt $\alpha$ -1*
mt $\alpha$ -mt $\alpha$ -1 (E)	20.7	0.68	CATGTAMWTWYC	$\alpha$ 2-binding, mt $\alpha$ -3*
mt $\alpha$ -mt $\alpha$ -2 (F)	5.3	0.26	TWTDYWWHBKKMWTGTTSA	PRE*
mt $\alpha$ -mt $\alpha$ -3 (G)	8.6	0.54	TGAMATAWTDAAMA	-
mt $\alpha$ -mt $\alpha$ -4 (H)	5.3	0.62	AATGMCMGCMA	Q-Box

Expected	DNABP	Consensus	Ref.
P-Box	Mcm1	TTTCCTTAATTAGGNAN	27
Q-Box	Mat $\alpha$ 1	TCAATGVCAG	27
$\alpha$ 2-binding	Mat $\alpha$ 2	CRTGTAAWT	27
PRE	Ste12	TGAAACA	27

**Figure 4.** DNA sequence motifs obtained from a comparison of growth between mating type **a** and  $\alpha$  strains. **(A)** Motif ('mt $\alpha$ -1') obtained from the ten ORFs most abundant in mating type  $\alpha$  relative to mating type **a**. **(B), (C), (D)** Motifs ('mt $\alpha$ -1', 'mt $\alpha$ -2' and 'mt $\alpha$ -3' respectively) obtained from the ten ORFs most abundant in mating type **a** relative to mating type  $\alpha$ . **(E), (F), (G), (H)** Motifs ('mt $\alpha$ -mt $\alpha$ -1', 'mt $\alpha$ -mt $\alpha$ -2', 'mt $\alpha$ -mt $\alpha$ -3' and 'mt $\alpha$ -mt $\alpha$ -4' respectively) obtained from the combined set of twenty ORFs. See Protocols for a description of sequence logos. **(I)** lists motifs returned by AlignACE as well as motifs which might have been expected a priori. 'Score' refers to AlignACE score, 'Specif' is the specificity score, and 'DNABP' refers to the protein which binds an element, where known. Consensus sequences and motif similarity were obtained by objective criteria (see Protocols). A '\*' indicates a motif's reverse complement.

How do these results compare with what one might have expected from previous work on these regulatory systems? Motifs common to many genes, e.g., the TATA box, were neither found nor expected since these are excluded by the selectivity constraint discussed above. In the case of ORFs more abundant in glucose than galactose, we might have expected motifs corresponding to Rap1 or Gcr1-binding sites, but found neither of these. Rap1 and Gcr1 are general transcription factors with diverse roles, including regulation of glycolytic enzymes and ribosomal proteins<sup>28</sup>. In the case of ORFs more abundant in galactose than glucose we might have expected to find URS<sub>G</sub> (bound by Mig1<sup>28</sup>), but did not. As expected, our procedure did find UAS<sub>G</sub>, an essential regulatory element for galactose-utilizing genes.

The heat shock (HSE) and stress response promoter elements (STRE), known to mediate heat shock response<sup>29; 30</sup>, were notably absent from the motifs found by AlignACE. Heat shock is known to have broad effects, including transient cell cycle arrest in G1<sup>31</sup>. As a result, we might also have expected to find genes with cell cycle-specific expression among genes affected by heat shock. Histone genes are strongly transcribed during S phase, and are regulated both by a negative regulatory sequence (NEG) and activated by the CCA motif (Fig. 3B, D)<sup>20; 21</sup>. Not found among heat shock data were the NEG motif, the Swi4/6-dependent cell cycle box (SCB) or MluI cell cycle box (MCB) motifs which regulate G<sub>1</sub>/S-specific transcription, or the ECB element<sup>25; 26</sup>. AlignACE did find the CCA motif among a set of histone genes.

The  $\alpha$ 2 operator, P-Box, PRE and Q-Box elements represent the complete set of DNA elements responsible for regulation of mating type-specific genes<sup>27</sup>. All four of these elements were found by AlignACE (Fig. 4C-H). The similarity of ‘mt $\alpha$ -1’ to both

HSE and the Gcr1-binding site was unexpected, and may represent false positive determinations of motif similarity.

False positive and false negative motifs. We estimated the number of expected false positives by generating and examining negative control sets of randomly chosen genes and asking how many motifs passed both AlignACE and specificity criteria. The AlignACE score criterion used here was chosen permissively, so that few biologically relevant motifs would be excluded. The permissive AlignACE score threshold (5) was examined as well as more stringent thresholds (8 and 20). For the permissive threshold, an average of 1.7 motifs (Poisson distributed with a coefficient of dispersion (CD) of 0.9) was obtained from negative control gene sets, which is consistent with the observation that four motifs identified in this study from sets of 10 ORFs (Fig. 3A, 3C, 4B, 4C) did not match known regulatory elements. The chance that a motif is a false positive decreases with increasing AlignACE score, so that if a threshold score of 8 is applied the mean number of false positives is reduced to 0.8 (CD = 1.0). If a threshold score of 20 is applied, the mean number of false positives is further reduced to 0.2 (CD = 1.6). The number of expected false positives for a variety of alternative AlignACE and specificity score thresholds can be found in Fig. 5. All six of the six motifs identified in this study which meet the most stringent threshold of 20 are similar to known regulatory elements. This shows that these methods can be applied—at the discretion of the user—to either generate an inclusive set of testable hypotheses with a significant false positive rate, or to more confidently predict a subset of biologically relevant motifs.

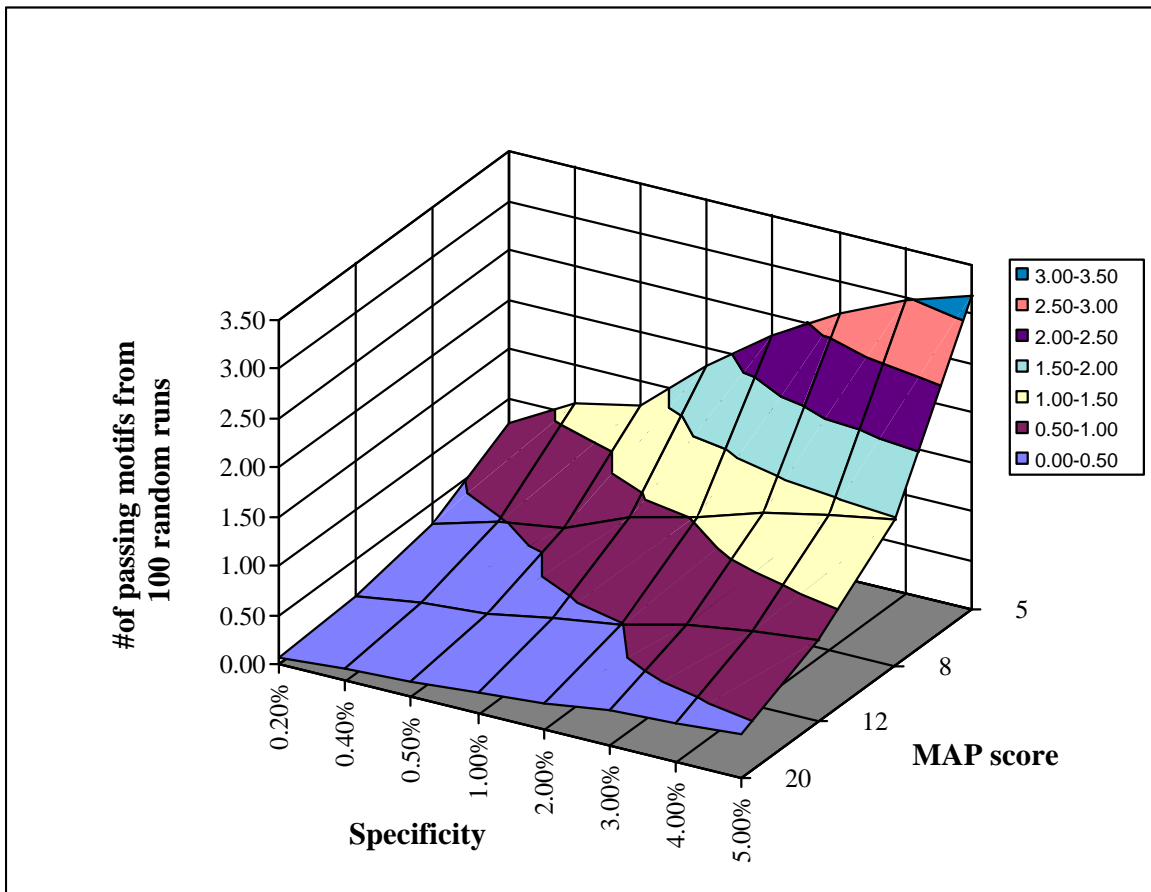


**Figure 5.** Sets of 10 ORFs were drawn randomly 100 times from the complete set of yeast ORFs. AlignACE was used to find conserved motifs for each random set. AlignACE score and specificity score were obtained for each motif. The number of motifs found that passed both AlignACE and specificity score thresholds is plotted as a function of the thresholds chosen.

We were interested in understanding why our approach had ‘false negatives’, i.e., did not find all of the motifs we might have expected *a priori*. For each expected motif, we applied our method to an ‘ideal’ set of genes derived from the literature. Motifs corresponding to the URS<sub>G</sub> and NEG elements were not found among ‘ideal’ gene sets using the permissive AlignACE score threshold, so that we attribute not finding these motifs to AlignACE. Motifs corresponding to the Gcr1-binding, STRE and MCB elements were obtained which passed both AlignACE score (13.9, 12.1, 10.6 respectively) and specificity score criteria (0.4%, 0.9% and 1.0%, respectively), so that we attribute not finding these motifs to the input sets of ORFs derived from expression data. Motifs corresponding to the Rap1-binding, HSE, SCB and ECB elements were found using ‘ideal’ gene sets with passing AlignACE scores (8.1, 14.8, 20.2 and 12.1, respectively) but unacceptable specificity scores (4.1%, 7.3%, 5.3% and 1.6%, respectively). We re-examined the appropriate 10 most-increased genes using relaxed specificity score criterion and still did not find these motifs, so that we also attribute not finding these motifs to the input set of ORFs. However, even if Rap1-binding, HSE, SCB and ECB motifs had been found, they would likely not have passed our chosen specificity criterion of 1%.

That input sets of upstream regions contained too few sites for AlignACE to align can be verified by scanning the upstream regions of the appropriate 10 most-increased genes for matches to motifs found from among ideal gene sets. Among the 10 genes most increased in heat shock, HSE matched only 2 sites upstream of HSP26 while STRE matched a total of only 3 sites upstream of HSP12 and HSP26. Among the 10 genes most decreased in heat shock, MCB matched no sites, SCB matched 1 site upstream of LYS1,

and ECB matched only 1 site in the upstream region shared by HHT1 and HHF1. Among the 10 genes most decreased in galactose neither the Rap1-binding site nor the Gcr1-binding motif matched any upstream sites.

Candidate sets of co-regulated genes. Once a candidate regulatory motif has been found, we are particularly interested in those ORFs that are both altered in expression and contain an upstream match to this motif. First, we search the complete *S. cerevisiae* genome to find the set of ORFs that contain matches to each motif in the 600 bp region upstream of translation start. Second, we consider the intersection of this set of ORFs with those ORFs that changed more than two-fold in abundance between conditions. We consider the resulting ORFs to be good candidates for membership in a transcriptionally co-regulated set of genes.

ORFs that have a measured change of more than two-fold in expression between galactose and glucose, and have an upstream match to at least one of the UAS<sub>G</sub>-like motifs ‘gal-1’ and ‘gal-glu-1’ are shown in Table 1, along with the remaining genes known previously to be regulated by UAS<sub>G</sub>. There are nine genes known previously to be regulated by the Gal4/Gal80 complex: GAL1, GAL2, GAL3, GAL7, GAL10, GAL80, GCY1, MEL1 and PGM2. The candidate set derived from Table 1 contains six of these nine. One of the missing three is MEL1, which codes for alpha-galactosidase. The strain used for this experiment (FY4) is a *mel-* strain. Furthermore, we could not find a good match to UAS<sub>G</sub> in the MEL1 upstream sequence from this strain, so that we should not have necessarily expected to find MEL1 in our candidate set. Also missing from our candidate set were PGM2 and GAL80, which are known to be Gal4/Gal80 regulated. For

both of these genes, absolute expression levels were too low in both galactose and glucose for an accurate estimate of change in expression.

The candidate set for galactose vs. glucose contains three ORFs not previously thought to be regulated by Gal4/Gal80. Two of these, YPL066W and YPL067C, are particularly interesting since they have approximately the same measured change in expression, and are divergently transcribed from the same intergenic region which contains a single match to each of the UAS<sub>G</sub>-like motifs. Another site in this intergenic region matches the consensus CGG(N)<sub>10</sub>CCG, to which weak Gal4-binding has also been shown in vitro <sup>32</sup>. Both YPL066W and YPL067C are of unknown function according to the *Saccharomyces* Genome Database (SGD) <sup>33</sup>, with no significant homology to any gene of known function. Also in the candidate set was YMR318C, which has a strong homology to zinc-containing alcohol dehydrogenases <sup>33</sup>. We are currently exploring the possibility that these ORFs are regulated by Gal4/Gal80.

ORFs that have a measured change of more than two-fold in expression between heat shock and 30 °C, and have an upstream match to at least one of the motifs in Fig. 3 are shown in Table 2, along with the remaining histone genes. There are eight genes—four functionally redundant gene pairs—in *S. cerevisiae* that code for the four nucleosomal proteins: HTA1, HTA2, HTB1, HTB2, HHT1, HHT2, HHF1, and HHF2. The candidate set of co-regulated genes with matches to both of the CCA-like motifs ('30C-1' and '39C-30C-1') contains five of these genes—collectively coding for the complete set of *S. cerevisiae* nucleosomal proteins. It is important to note that our results by themselves do not necessarily indicate a role for the CCA motif in heat shock regulation or in cell cycle regulation, since we seek any motif common to a set of ORFs

without information about which motif (if any) might be responsible for the observed changes in expression. RPS8A (coding for ribosomal protein rp19), HOR2 (DL-glycerol-3-phosphatase), YDR070C (an ORF of unknown function), and GSY1 (glycogen synthase) have upstream matches to one of the CCA-like motifs ('30C-1')<sup>33</sup>. None of these genes have previously been noted to be heat shock repressed or to be regulated by CCA. However, GSY2—a homolog of GSY1—is reportedly induced by heat shock<sup>34</sup>. This suggests, together with our data showing reduced abundance of GSY1 in heat shock, that GSY2 is a thermotolerant variant of glycogen synthase. It is also worth mentioning that along with the other histone genes discussed above we found the gene HHO1 (histone H1) to be reduced by more than two-fold in heat shock. HHO1 does not, however, contain an upstream match to the CCA motif.

Another candidate set of co-regulated genes can be derived from heat shock data, using those ORFs in Table 2 with upstream matches to the motifs '39C-1' and '39C-30C-2'. This set contains the genes HSP26, GND2, GCV1, UBI4, ERG11, SOL4, and YHB1. Of these, only HSP26 and UBI4 have been reported to be differentially expressed as a result of heat shock<sup>29</sup>. We can see no apparent rationale for co-regulation of this set of genes or of the set derived from '30C-2'. None of the motifs '39C-1', '30C-2', or '39C-30C-2' have previously been implicated as regulatory elements.

ORFs that have a measured change of more than two-fold in expression between mating types **a** and  $\alpha$ , and have an upstream match to at least one of the mating type-derived motifs (Fig. 4) are shown in Table 3, along with the remaining genes known to have mating type-specific expression. Genes MF $\alpha$ 1, MF $\alpha$ 2, STE3, SAG1, MAT $\alpha$ 1 and MAT $\alpha$ 2 are known previously to have mating type  $\alpha$ -specific expression. The genes

MFA1, MFA2, STE2, STE6, BAR1, AGA2, MAT $\alpha$ 1 and MAT $\alpha$ 2 are known previously to have mating type **a**-specific expression <sup>35</sup>. The candidate set of co-regulated genes corresponding to the P-Box-like motif ‘mt $\alpha$ -1’ contains twelve genes, including four of fourteen known mating type-specific genes. Candidate sets derived from those motifs not known to be involved in transcriptional regulation, ‘mt $\alpha$ -1’ and ‘mt $\alpha$ -2’, each contained seven ORFs, two of which are mating type-specific. The candidate set of genes with matches to either of the Mat $\alpha$ 2 binding site-like motifs (‘mt $\alpha$ -3’ and ‘mt $\alpha$ -mt $\alpha$ -1’) contains seventeen genes—including five of the eight known **a**-specific genes. That MAT $\alpha$ 1 and MAT $\alpha$ 2 genes had an upstream match to ‘mt $\alpha$ -mt $\alpha$ -1’ in their shared intergenic region is consistent with the fact that this locus is repressed by the Mat $\alpha$ 2/Mata1 complex in **a/α** cells <sup>35</sup>.

The candidate set of genes having upstream sites matching ‘mt $\alpha$ -mt $\alpha$ -2’—a PRE-like element—contains nine genes, five of which are mating type regulated. The candidate set for ‘mt $\alpha$ -mt $\alpha$ -3’ (weakly similar to PRE as noted above) contains thirteen genes, two of which are mating-type specific. The gene STE18 has an upstream match to ‘mt $\alpha$ -mt $\alpha$ -3’. STE18 codes for the G $\gamma$  subunit of the G protein coupled to both **a** and  $\alpha$  mating factor receptors, and is known to be regulated via the PRE element. Although STE18 is not thought to have mating type-specific expression, we found the STE18 transcript to be three-fold more abundant in **a** than  $\alpha$  <sup>35</sup>. The candidate set of genes with upstream matches to the Q-Box-like motif, ‘mt $\alpha$ -mt $\alpha$ -4’, contained seven genes, including one **a**-specific and two  $\alpha$ -specific genes. In all, forty genes were contained in at

least one of the candidate sets of co-regulated genes described above, and among those forty were nine of fourteen known mating type-specific genes.

ORF ID	Gene	Change	gal-1	gal-glu-1
YBR020W	GAL1	>1.8	5	4
YBR018C	GAL7	>1.6	2	2
YBR019C	GAL10	>1.6	5	4
YOR120W	GCY1	>1.1	1	1
YLR081W	GAL2	>0.9	4	4
YPL066W	-	>0.8	1	1
YPL067C	-	>0.8	1	1
YMR318C	-	0.6	1	1
YDR009W	GAL3	>0.5	2	2
<i>YML051W</i>	<i>GAL80</i>	<i>ND</i>	2	2
<i>YMR105C</i>	<i>PGM2</i>	<i>ND</i>	<i>I</i>	<i>I</i>
<i>YBR184W</i>	<i>MEL1</i>	<i>ND</i>	-	-

**Table 1.** The number of matching sites that lie within 600 bp upstream of translation start of genes/ORFs that were either measurably changed in expression or are known to be galactose-responsive. Genes/ORFs in plain text had a greater than 0.3 (two-fold) between galactose and glucose growth conditions. Genes/ORFs in italics have been shown previously to be regulated by the Gal4/Gal80 complex, but had a measured change of less than 0.3. Change calculation is as described (see Protocols) with positive change indicating higher transcript abundance in galactose than glucose.

<u>ORF ID</u>	<u>Gene</u>	<u>Change</u>	<u><math>^{39}\text{C}^1</math></u>	<u><math>^{30}\text{C}_1</math></u>	<u><math>^{30}\text{C}_2</math></u>	<u><math>^{39}\text{C}-^{30}\text{C}_1</math></u>	<u><math>^{39}\text{C}-^{30}\text{C}_2</math></u>
YPL223C	-	>0.8	1	-	-	-	-
YBR072W	HSP26	0.7	2	-	-	-	2
YGR256W	GND2	0.7	1	-	-	-	1
YDR219C	GCV1	0.6	1	-	-	-	1
YLL039C	UBI4	0.6	2	-	-	-	1
YDR070C	-	0.5	-	2	-	-	-
YER062C	HOR2	0.5	-	1	-	-	-
YER103W	SSA4	0.5	1	-	-	-	-
YHR007C	ERG11	0.5	1	-	-	-	1
YER042W	-	0.4	1	-	-	-	-
YDL223C	-	0.4	-	-	1	-	-
YGR038W	ORM1	0.4	-	-	1	-	-
YDL048C	STP3	>0.3	1	-	-	-	-
YMR090W	-	>0.3	1	-	-	-	-
YGR248W	SOL4	0.3	1	-	-	-	1
YOR185C	GSP2	0.3	1	-	-	-	-
YOR259C	CRL13	0.3	-	-	1	-	-
YNL241C	ZWF1	0.3	-	-	1	-	-
YNL156C	-	0.3	1	-	-	-	-
YPL135W	-	0.3	1	-	-	-	-
YHR057C	CYP2	0.3	1	-	-	-	-
YNL031C	HHT2	ND	-	2	1	2	1
YDR224C	HTB1	-0.1	-	4	1	2	-
YDR225W	HTA1	-0.2	-	4	1	2	-
YBL015W	ACH1	-0.3	-	-	-	-	1
YNL030W	HHF2	-0.4	-	2	1	2	1
YBR009C	HHF1	<-0.4	-	4	3	4	-
YFR015C	GSY1	<-0.5	2	1	1	-	-
YBL003C	HTA2	-0.5	-	5	-	4	-
YBL002W	HTB2	-0.5	-	5	-	4	-
YBL072C	RPS8A	-0.5	-	1	-	-	1
YBR010W	HHT1	-0.5	-	4	3	4	-
YGR234W	YHB1	<-0.6	2	-	2	-	1
YJL052W	TDH1	<-1.7	-	-	1	-	-

**Table 2.** The number of matching sites that lie within 600 bp upstream of translation start of genes/ORFs that were either measurably changed in expression or are known to code for nucleosomal proteins. Genes/ORFs in plain text had a measured change of greater than 0.3 (two-fold) between the heat shock and 30 °C growth conditions. Genes/ORFs in italics are known to code for nucleosomal proteins, but had a measured change of less than 0.3. Change calculation is as described (see Protocols) with positive change indicating higher transcript abundance in heat shock than 30 °C.

<u>ORF ID</u>	<u>Gene</u>	<u>Change</u>	mt $\alpha$ -1	mt a-1	mt a-2	mt a-3	mt $\alpha$ -mt a-1	mt $\alpha$ -mt a-2	mt $\alpha$ -mt a-3	mt $\alpha$ -mt a-4
YPL187W	MF $\alpha$ 1	>1.3	4	-	-	-	1	1	-	1
YGL089C	MF $\alpha$ 2	>1.2	1	-	-	-	-	1	-	1
YCL066W	MAT $\alpha$ 1	>0.7	-	-	-	-	1	-	-	-
YCR040W	MAT $\alpha$ 1	>0.6	-	-	-	-	1	-	-	-
YJR004C	SAG1	0.5	1	-	-	-	-	2	1	-
YLR040C	-	>0.4	-	-	-	-	-	-	1	1
YHR053C	CUP1	0.4	1	-	-	-	-	-	-	2
YHR128W	FUR1	0.4	-	-	-	-	-	1	-	-
YHR141C	MAK18	0.4	-	-	-	-	-	-	1	-
YGR038W	ORM1	0.3	-	-	-	-	-	1	-	-
YLR355C	ILV5	0.3	-	-	-	-	-	-	-	1
<i>YCR097W</i>	<i>MATA1</i>	<i>ND</i>	-	-	-	-	-	-	-	-
<i>YCR096C</i>	<i>MATA2</i>	<i>ND</i>	-	-	-	-	-	-	-	-
<i>YCR039C</i>	<i>MATA2</i>	<i>ND</i>	-	-	-	-	1	-	-	-
<i>YCL067C</i>	<i>MATA2</i>	<i>ND</i>	-	-	-	-	1	-	-	-
<i>YKL178C</i>	<i>STE3</i>	<i>ND</i>	1	-	-	-	-	-	-	-
<i>YKL209C</i>	<i>STE6</i>	<i>ND</i>	-	-	-	3	3	-	-	-
YDR301W	YHH1	-0.3	-	-	-	-	-	-	1	-
YLR438W	CAR2	-0.3	1	-	-	-	-	-	-	-
YBR107C	-	-0.3	-	-	-	-	-	-	1	-
YKL080W	VMA5	-0.3	-	-	-	-	-	1	-	-
YML133C	-	-0.3	1	-	-	-	-	-	-	-
YDR342C	HXT7	-0.3	-	-	-	-	-	-	1	-
YLR028C	ADE16	-0.3	1	-	-	-	-	-	-	-
YJR103W	URA8	-0.4	1	-	-	-	-	-	-	-
YML075C	HMG1	-0.4	-	-	-	-	1	-	-	-
YKL128C	PMU1	-0.4	1	-	-	-	-	-	-	-
YCR012W	PGK1	-0.4	1	-	-	-	-	-	-	-
YMR003W	-	-0.4	-	-	1	-	-	-	-	-
YAL061W	-	-0.4	-	-	-	2	2	-	-	-
YPL271W	ATP15	<-0.4	1	-	-	-	-	-	-	-
YBR011C	IPP1	-0.5	-	1	-	-	-	-	-	-
YMR119W	-	-0.5	-	-	-	-	-	-	1	-
YKL214C	-	-0.5	-	-	-	-	-	-	1	-
YKR018C	-	-0.5	-	-	-	1	1	-	-	-
YJR086W	STE18	-0.5	-	-	1	-	-	-	1	-
YBR147W	-	-0.5	-	2	1	-	-	-	-	-
YKR071C	-	-0.5	-	2	-	1	-	-	2	-
YLL040C	VPS13	-0.6	-	1	2	-	-	-	1	-
YJL164C	SRA3	-0.6	-	1	-	-	-	1	1	1
YCR024C-A	PMP1	-0.6	-	-	1	-	-	-	-	-
YIL015W	BAR1	<-0.7	-	-	2	3	2	-	-	-
YFL026W	STE2	<-0.8	1	-	-	2	2	-	-	1
YGL032C	AGA2	<-0.9	-	1	-	2	2	2	1	-
YNL145W	MFA2	<-1.6	-	-	-	3	2	-	-	-
YDR461W	MFA1	2.0	-	1	1	2	2	1	-	-

**Table 3.** The number of matching sites that lie within 600 bp upstream of translation start of genes/ORFs that were either measurably changed in expression or are known to be mating type-specific. Genes/ORFs in plain text had a measured change of greater than 0.3 (two-fold) between mating types **a** and  $\alpha$ . Genes/ORFs in italics have been shown previously to have mating-type specific expression, but had a measured change of less than 0.3. Change calculation is as described (see Protocols) with positive change indicating higher transcript abundance in mating type  $\alpha$  than **a**.

The success of this approach in finding regulatory DNA sequence motifs was dramatic. The same criteria, when applied to three whole-genome expression comparisons, uncovered at least one biologically important regulatory motif in each case. In the case of galactose vs. glucose, UAS<sub>G</sub> — one of the two motifs involved in regulating galactose-utilization genes — was found along with most of the known UAS<sub>G</sub>-regulated genes. In the case of heat shock vs 30 °C, a motif known to function in nucleosomal gene regulation was found, along with a set of genes collectively coding for every nucleosomal protein. In the case of mating type **a** vs.  $\alpha$ , every one of the four motifs involved in mating type-specific gene regulation was found, along with most of the known mating type-specific genes.

Our experiments showed lower sensitivity to transcripts of low abundance compared with previously published *S. cerevisiae* expression studies <sup>9</sup>. As a result, some ORFs which are known from previous studies to be differentially expressed between the examined conditions fell below our detection threshold for transcript abundance and thus were not measurably changed in our results. Our approach for finding co-regulated genes should then become even more successful as we optimize experimental methods in whole-genome expression measurement.

In this work, we have restricted ourselves to a search for upstream sequence elements. However, this approach could also be applied to 3' UTR sequences to discover conserved determinants of transcript termination, stability, or post-transcriptional processing (as in the case of higher eukaryotic histone genes <sup>21</sup>). The search for DNA (or RNA) sequence elements in coding regions of co-expressed genes is complicated by codon usage bias, which will tend to increase the likelihood of obtaining strong

alignments by chance. However, a search for protein (as opposed to nucleic acid) sequence motifs among co-expressed genes may prove useful, e.g., in the discovery of shared N-terminal signal sequences.

The AlignACE algorithm promises to be more generally useful in finding motifs in unaligned DNA sequences. Although we used whole-genome expression analysis to obtain sets of genes enriched for conserved sites, AlignACE may also prove useful in finding regulatory motifs among a variety of enriched sequence sets. A common example of this might be the upstream sequence from a collection of genes whose mutants share a phenotype. For gene expression data sets taken from many cell types or growth environments, it will be useful to find clusters of genes that are correlated in their expression<sup>36</sup> and apply the sequence analysis described here. AlignACE and all other software written for this work is publicly available<sup>13</sup>.

## Experimental Protocol

Strains and growth conditions. *S. cerevisiae* strain FY4 MAT $\alpha$  was used for all growth conditions except as noted. FY4 is a prototroph whose genome is completely sequenced<sup>3; 37</sup>. Cultures were grown with aeration in yeast nitrogen base plus ammonium sulfate without amino acids (YNB) at 30 °C in a rotary incubator, and supplemented with 2% glucose except as noted. All cultures were harvested in mid log phase ( $2 - 4 \times 10^7$  cells/ml) as determined by cell count and dilution plating. Cells were pelleted, quickly washed once with 50 ml dH<sub>2</sub>O, frozen in a dry ice-isopropanol bath, and stored at -80 °C. For galactose growth, 2% galactose was used in place of glucose. For the heat shocked culture, cells were transferred at mid-log phase to a 39 °C shaking water bath. After 13

minutes the culture had reached 39 °C, and the incubation was continued for an additional 20 minutes. This temperature profile was chosen since heat shock-related transcripts are at maximal levels between 10 and 20 minutes after reaching the higher temperature<sup>38</sup>. For mating type  $\alpha$  cultures, strain FY5—isogenic to FY5 except that it is MAT $\alpha$ —was used in place of FY4. All strains were kindly provided by A. Dudley and F. Winston, Harvard Medical School.

RNA preparation and hybridization. Total cellular RNA was prepared from the frozen cell pellets by hot phenol extraction method (Current protocols in Molecular Bio, Ausubel et.al.). An additional phenol extraction and a phenol/chloroform/isoamyl alcohol extraction were done before ethanol precipitation. The poly-A fraction of total cellular RNA was purified by a PolyATract kit (Promega , Madison, WI). The resulting eluant was lyophilized and resuspended in 1-2  $\mu$ l H<sub>2</sub>O. Synthesis, purification, and fragmentation of biotinylated RNA antisense to mRNA transcripts (cRNA) was performed as previously described<sup>9</sup>. For each culture, expression data was acquired using a set of four chips (Affymetrix yeast ‘antisense’ A - D) designed for expression monitoring of *S. cerevisiae*<sup>9</sup>.

Hybridization, washing, and scanning were carried out as previously described<sup>9</sup> except where noted below. For all hybridizations, 15  $\mu$ g fragmented cRNA in 250  $\mu$ l buffer. Hybridizations were carried out either in Affy buffer (Affymetrix, Inc.) at 40 °C or in 6X SSPE-T (0.9 M NaCl, 60 mM NaH<sub>2</sub>PO<sub>4</sub>, 6mM EDTA, 0.005% Triton X-100, pH 7.6) at 45 °C for 14 to 18 hours. For a given chip type, hybridizations were carried out identically for each culture. After hybridization and washing, the chips were stained for 10 minutes at room temperature with 2 $\mu$ g/ml streptavidin-phycoerythrin conjugate

(SAPE; Molecular Probes , Eugene, OR) in 6X SSPE-T with 1 mg/ml acetylated BSA (New England Biolabs , Beverly, MA). Unbound SAPE was removed by rinsing with 6X SSPE-T at 45 °C.

Expression data analysis. Perfect match (PM) and single-base mismatch (MM) probe intensities are calculated from raw intensities by the GeneChip™ software (Affymetrix, Inc.) as described <sup>9</sup>. For this analysis, genes with MM probes that are perfect matches to a sequence within the genome, e.g., YBL087C and YKL006W, were not considered further. Intensities for PM and MM probes are background-subtracted using the average intensity of a set of 36 chip features with consistently low intensity in all of our experiments. For a given chip, PM and MM data are then normalized using the average background-subtracted PM intensity on that chip. This is likely more reliable than normalizing to transcripts of ‘constant’ expression level, e.g., ACT1 or PDA1, since these can vary between conditions by more than three-fold <sup>39</sup>. PM – MM ( $\Delta$ ) is then calculated for each probe pair, and if  $\Delta$  is less than detection threshold, then  $\Delta$  is set to this threshold. A detection threshold for PM or MM values on a given chip was chosen to be  $s$ , the standard deviation of background probe intensities on that chip; the threshold for  $\Delta$  values is then  $\sqrt{2} * s$  by propagation of error. The ratio  $\Delta_A / \Delta_B$  of transcript abundance in one condition (A) vs. another (B) is calculated for each corresponding pair of  $\Delta$  values. Application of the detection threshold prevents unreasonably high (or negative) values for ( $\Delta_A / \Delta_B$ ) where a transcript is absent or undetectable in one or both conditions. The change in expression for a given ORF is then calculated as  $\log(\text{median}\{(\Delta_{A1} / \Delta_{B1}), (\Delta_{A2} / \Delta_{B2}), \dots, (\Delta_{An} / \Delta_{Bn})\})$ , where n is the number of probe pairs for that ORF. If the median is

calculated using a  $\Delta_A/\Delta_B$  value where both or the greater of  $\Delta_A$  and  $\Delta_B$  were threshold-adjusted, then change in expression for this ORF is not calculated ('ND'). Otherwise, if the median is calculated using a  $\Delta_A/\Delta_B$  value where either  $\Delta_A$  or  $\Delta_B$  were threshold-adjusted, change in expression is stated as being greater than (or less than) the calculated value. The median, as opposed to the mean, was chosen as a measure of central tendency that is robust to outliers. Our rationale for using the median of  $\Delta$  ratios rather than the ratio of  $\Delta$  medians was that while the magnitude of  $\Delta$  for features of different sequence can vary considerably,  $\Delta_A/\Delta_B$  should be less variant. An alternative measure of expression change (not used here) is 'fractional change': median  $\{(\Delta_{A1}-\Delta_{B1})/(\Delta_{A1}+\Delta_{B1}), (\Delta_{A2}-\Delta_{B2})/(\Delta_{A2}+\Delta_{B2}), \dots, (\Delta_{An}-\Delta_{Bn})/(\Delta_{An}+\Delta_{Bn})\}$ . This measure should be robust to cases where a transcript is below detection threshold in one condition but not the other.

Optimality of these or previous methods<sup>9</sup> for intensity data analysis have yet to be demonstrated experimentally. However, the lists of most-changed genes for each of our condition comparisons were not greatly affected by the analysis method used.

Modifications to Gibbs motif sampling alteration. Alterations of the Gibbs motif sampling algorithm described in ref.<sup>15</sup> are the following: 1) Consideration of both strands of DNA, so that when a potential site is examined, either the site or its reverse complement—but not both—may be added to the alignment; 2) Near-optimum sampling method was improved so that it tends to result in higher scoring alignments and so that all columns spanned by the initially-chosen columns were considered; 3) Simultaneous multiple motif searching was replaced with an iterative masking approach, allowing a more efficient search for subtle motifs; 4) The model for base frequencies of non-site sequence was fixed using the background nucleotide frequencies of *S. cerevisiae*. 5) The

code is now portable to DEC Unix and Windows platforms, in addition to Silicon Graphics and Sun Unix systems.

AlignACE settings. The program ‘AlignACE’ was used with the following settings: initial alignment used a ‘column-sampling’ approach with 10 columns; the expected number of sites was 10; maximum number of initial sampling runs was 500; iterative masking to find multiple motifs was performed a maximum of 100 times; near-optimum sampling commenced after 50 consecutive sampling runs without an increase in alignment score; iterative masking was terminated after three consecutive cases of non-convergence or non-positive alignment score.

AlignACE implemented a scoring method for ‘goodness’ of a site alignment that has previously been described by eq. 10 in ref. <sup>40</sup>, and motifs below a threshold AlignACE score of five were not considered further. To ensure that this criterion was sufficiently permissive, we searched for conserved motifs among randomly chosen sets of 10 upstream intergenic DNA sequences with AlignACE settings as described above except that a maximum of three motifs were sought from each intergenic sequence set. Each of 1000 randomly chosen sequence sets returned at least one motif with a score greater than our threshold of five. In 674 cases, all three motifs returned had scores greater than five.

Finding sites which match motifs and calculating motif specificity. Sites were scored against motifs using the method of Berg and von Hippel <sup>41</sup>. To define a threshold score for a ‘good’ matching site, we first calculated the mean score  $\mu$  and standard deviation  $\sigma$  for the set of sites that were aligned by AlignACE. We determined our specificity score—the estimated fraction of genes bound by the putative protein corresponding to a given motif—in the following way: We found the fraction of genes with upstream

matches, defining a matching site as one with a Berg-Von Hippel score greater than or equal to  $\mu$ . The specificity score is then twice this fraction, since half of ‘real’ sites will have scores better than  $\mu$  if ‘real’ sites have a symmetric score distribution. For discovery of specific upstream sites, the threshold score for a ‘good’ match was lowered to  $\mu - 3\sigma$  to avoid missing potential binding sites.

Measuring similarity between DNA motifs. To identify previously described motifs that might be similar to the newly identified motif, the relevant literature was searched. Additionally, the TRANSFAC Release 3.2 was searched<sup>19</sup> using PatternSearch or MatInspector 2.1<sup>42</sup> with a threshold of 85% identity for ‘core’ nucleotides and 60% for overall identity. To assess similarity more quantitatively once a putatively similar motif has been identified, DNA site weight matrices<sup>41</sup> were examined pairwise in all possible alignments. The alignment which minimizes the sum of squared differences between matrix elements is chosen. When necessary, as in the case of imperfectly overlapping matrices, matrix elements are taken as their expectation value, based on the base composition of *S. cerevisiae*. If aligned matrices do not overlap by more than 5 bases, they are considered not similar. To further compare a given matrix A with a matrix B, a submatrix of A defined by the region of overlap between aligned A and B matrices is constructed. Each site used in generating the A and B matrices is scored against submatrix A. Student’s *t*-statistic is calculated from the set of A site scores and the set of B site scores. Matrix A is said to ‘detect’ matrix B if *t* is above a threshold (described below). The procedure is repeated using a submatrix of B, and matrix A is then said to be ‘similar’ to matrix B if either matrix detects the other. The threshold for *t* was obtained using a negative control set of fourteen literature-derived matrices that are each bound by

different proteins (all of the ‘expected’ motifs in Fig. 2C, 3F, and 4I except the P-Box, which is bound by the same protein as ECB). False positive rate for matrix similarity was calculated to be the number of similar pairs in the negative control set divided by 91(the number of pairwise comparisons). The value of  $t$  corresponding to a 5% false positive rate was found to be 3.26 by linear interpolation.

Assessing false positives. To estimate the number of ‘passing’ motifs that we might expect by chance, we ran AlignACE on 100 randomly chosen sets of 10 upstream sequences with settings identical to those above, where a ‘passing’ motif has a AlignACE score greater than a set threshold (alternative thresholds of 5, 8, and 20 were examined) and a less than 1% specificity score.

Ideal Gene Lists. In trying to determine why our approach failed to find certain regulatory motifs, the following ‘ideal’ ORF sets were used to search for these motifs: ECB: CDC 6, CDC46, CDC47, CLN3 and SWI4; Gcr1-binding site: ADH1, CDC19, ENO1, PGK1 and TPI1; HSE: CUP1, HSC82, HSP26, HSP82, PGK1, SIS1, SSA1 and SSA3; MCB: CDC8, CDC9, CDC21 and CLB5; URS<sub>G</sub>: FBP1, FPS1, GAL1, GAL3, GAL4, HAP4, MEL1, PDC1 and SUC2; NEG: HHT1, HHT2 and HTA1; Rap1-binding site: CDC19, ENO1, PGK1, PDC1, PHO5, RNR2, Rpl16A, SRA1, TEF1, TEF2 and TPI1; SCB: CLN1, CLN2, HO and PCL1; STRE: CTT1, CYC7, DDR2, GAC1, HSP12, HSP26, HSP104, NTH2, PTP2 and TPS2.

Methods for visually representing sequence alignments. In sequence ‘logos’, the height of each letter is made proportional to its frequency, and the letters are sorted so the most common one is on top. The height of the entire stack is then adjusted to signify the information content of the sequences at that position <sup>43</sup>. Consensus sequences were

determined using the plurality method of Day and McMorris<sup>44</sup>. From a set of equally valid consensus bases, we choose the most precise base (e.g., A is more precise than N) that has a precision unique to this set. For example, V is chosen from the set {M, R, V, N}.

## References

1. **Pennisi, E.**, Laboratory workhorse decoded [news], *Science*, 277(5331), 1432-1434, 1997.
2. **Blattner, F.R., Plunkett, G.r., Bloch, C.A., Perna, N.T., Burland, V., Riley, M., Collado-Vides, J., Glasner, J.D., Rode, C.K., Mayhew, G.F., Gregor, J., Davis, N.W., Kirkpatrick, H.A., Goeden, M.A., Rose, D.J., Mau, B. and Shao, Y.**, The complete genome sequence of Escherichia coli K-12, *Science*, 277(5331), 1453-1474, 1997.
3. **Goffeau, A., Barrell, B.G., Bussey, H., Davis, R.W., Dujon, B., Feldmann, H., Galibert, F., Hoheisel, J.D., Jacq, C., Johnston, M., Louis, E.J., Mewes, H.W., Murakami, Y., Philippsen, P., Tettelin, H. and Oliver, S.G.**, Life with 6000 genes [see comments]. [Review] [86 refs], *Science*, 274(5287), 563-567, 1996.
4. **Chen, P., Ailion, M., Bobik, T., Stormo, G. and Roth, J.**, Five promoters integrate control of the cob/pdu regulon in *Salmonella typhimurium*, *Journal of Bacteriology*, 177(19), 5401-5410, 1995.
5. **Chuang, S.E., Daniels, D.L. and Blattner, F.R.**, Global regulation of gene expression in *Escherichia coli*, *Journal of Bacteriology*, 175(7), 2026-2036, 1993.

6. **Schena, M., Shalon, D., Davis, R.W. and Brown, P.O.**, Quantitative monitoring of gene expression patterns with a complementary DNA microarray [see comments], *Science*, 270(5235), 467-470, 1995.
7. **Lockhart, D.J., Dong, H.L., Byrne, M.C., Follettie, M.T., Gallo, M.V., Chee, M.S., Mittmann, M., Wang, C.W., Kobayashi, M., Horton, H. and Brown, E.L.**, Expression monitoring by hybridization to high-density oligonucleotide arrays, *Nature Biotechnology*, 14(13), 1675-1680, 1996.
8. **DeRisi, J., Penland, L., Brown, P.O., Bittner, M.L., Meltzer, P.S., Ray, M., Chen, Y., Su, Y.A. and Trent, J.M.**, Use of a cDNA microarray to analyse gene expression patterns in human cancer [see comments], *Nature Genetics*, 14(4), 457-460, 1996.
9. **Wodicka, L., Dong, H., Mittmann, M., Ho, M.-H. and Lockhart, D.J.**, Genome-wide expression monitoring in *Saccharomyces cerevisiae*, *Nature Biotechnology*, 15(13), 1359-1366, 1997.
10. **Muhlrad, D., Decker, C.J. and Parker, R.**, Turnover mechanisms of the stable yeast PGK1 mRNA, *Molecular & Cellular Biology*, 15(4), 2145-2156, 1995.
11. **Jacobson, A. and Peltz, S.W.**, Interrelationships of the pathways of mRNA decay and translation in eukaryotic cells. [Review] [400 refs], *Annual Review of Biochemistry*, 65, 693-739, 1996.
12. **Lipman, D.J.**, Making (anti)sense of non-coding sequence conservation. [Review] [54 refs], *Nucleic Acids Research*, 25(18), 3580-3583, 1997.
13. <http://arep.med.harvard.edu/AlignACE/>.

14. **Frech, K., Quandt, K. and Werner, T.**, Software for the analysis of DNA sequence elements of transcription, *Computer Applications in the Biosciences*, 13(1), 89-97, 1997.
15. **Neuwald, A.F., Liu, J.S. and Lawrence, C.E.**, Gibbs motif sampling: detection of bacterial outer membrane protein repeats, *Protein Science*, 4(8), 1618-1632, 1995.
16. **Lawrence, C.E., Altschul, S.F., Boguski, M.S., Liu, J.S., Neuwald, A.F. and Wootton, J.C.**, Detecting subtle sequence signals: a Gibbs sampling strategy for multiple alignment, *Science*, 262(5131), 208-214, 1993.
17. **Liu, J.S.**, The collapsed Gibbs sampler in Bayesian computations with applications to a gene regulation problem, *Journal of the American Statistical Association*, 89(427), 958-966, 1994.
18. **Lohr, D., Venkov, P. and Zlatanova, J.**, Transcriptional regulation in the yeast GAL gene family: a complex genetic network. [Review] [59 refs], *Faseb Journal*, 9(9), 777-787, 1995.
19. **Wingender, E., Kel, A.E., Kel, O.V., Karas, H., Heinemeyer, T., Dietze, P., Knuppel, R., Romaschenko, A.G. and Kolchanov, N.A.**, TRANSFAC, TRRD and COMPEL: towards a federated database system on transcriptional regulation, *Nucleic Acids Research*, 25(1), 265-268, 1997.
20. **Freeman, K.B., Karns, L.R., Lutz, K.A. and Smith, M.M.**, Histone H3 transcription in *Saccharomyces cerevisiae* is controlled by multiple cell cycle activation sites and a constitutive negative regulatory element, *Molecular & Cellular Biology*, 12(12), 5455-5463, 1992.

21. **Osley, M.A.**, The regulation of histone synthesis in the cell cycle. [Review] [230 refs], *Annual Review of Biochemistry*, 60, 827-861, 1991.
22. **Simon, J.A. and Lis, J.T.**, A germline transformation analysis reveals flexibility in the organization of heat shock consensus elements, *Nucleic Acids Research*, 15(7), 2971-2988, 1987.
23. **Schuller, C., Brewster, J.L., Alexander, M.R., Gustin, M.C. and Ruis, H.**, The HOG pathway controls osmotic regulation of transcription via the stress response element (STRE) of the *Saccharomyces cerevisiae* CTT1 gene, *Embo Journal*, 13(18), 4382-4389, 1994.
24. **Martinez-Pastor, M.T., Marchler, G., Schuller, C., Marchler-Bauer, A., Ruis, H. and Estruch, F.**, The *Saccharomyces cerevisiae* zinc finger proteins Msn2p and Msn4p are required for transcriptional induction through the stress response element (STRE), *Embo Journal*, 15(9), 2227-2235, 1996.
25. **Breeden, L.**, Start-specific transcription in yeast. [Review] [112 refs], *Current Topics in Microbiology & Immunology*, 208, 95-127, 1996.
26. **McInerny, C.J., Partridge, J.F., Mikesell, G.E., Creemer, D.P. and Breeden, L.L.**, A novel Mcm1-dependent element in the SWI4, CLN3, CDC6, and CDC47 promoters activates M/G1-specific transcription, *Genes & Development*, 11(10), 1277-1288, 1997.
27. **Herskowitz, I., Rine, J. and Strathern, J.**, Mating-type determination and mating-type interconversion in *Saccharomyces cerevisiae*, in *Gene Expression*, Vol. 2, Jones, E.W., Pringle, J.R. and Broach, J.R., Eds., Cold Spring Harbor, NY, Cold Spring Harbor Laboratory Press, 1992, 583-656.

28. **Johnston, M. and Carlson, M.**, Regulation of Carbon and Phosphate Utilization, in *Gene Expression*, Vol. 2, Jones, E.W., Pringle, J.R. and Broach, J.R., Eds., Cold Spring Harbor, NY, Cold Spring Harbor Laboratory Press, 1992, 193-281.
29. **Craig, E.A.**, The Heat-Shock Response of *Saccharomyces cerevisiae*, in *Gene Expression*, Vol. 2, Jones, E.W., Pringle, J.R. and Broach, J.R., Eds., Cold Spring Harbor, NY, Cold Spring Harbor Laboratory Press, 1992, 501-537.
30. **Schmitt, A.P. and McEntee, K.**, Msn2p, a zinc finger DNA-binding protein, is the transcriptional activator of the multistress response in *Saccharomyces cerevisiae*, *Proc Natl Acad Sci U S A*, 93(12), 5777-5782, 1996.
31. **Rowley, A., Johnston, G.C., Butler, B., Werner-Washburne, M. and Singer, R.A.**, Heat shock-mediated cell cycle blockage and G1 cyclin expression in the yeast *Saccharomyces cerevisiae*, *Molecular & Cellular Biology*, 13(2), 1034-1041, 1993.
32. **Vashee, S., Xu, H., Johnston, S.A. and Kodadek, T.**, How do "Zn2 cys6" proteins distinguish between similar upstream activation sites? Comparison of the DNA-binding specificity of the GAL4 protein in vitro and in vivo, *Journal of Biological Chemistry*, 268(33), 24699-24706, 1993.
33. <http://genome-www.stanford.edu/Saccharomyces>.
34. **Ni, H.T. and LaPorte, D.C.**, Response of a yeast glycogen synthase gene to stress, *Molecular Microbiology*, 16(6), 1197-1205, 1995.
35. **Sprague, G.F. and Thorner, J.W.**, Pheromone Response and Signal Transduction during the Mating Process of *Saccharomyces cerevisiae*, in *Gene Expression*, Vol. 2, Jones, E.W., Pringle, J.R. and Broach, J.R., Eds., Cold Spring Harbor, NY, Cold Spring Harbor Laboratory Press, 1992, 657-744.

36. **Wen, X., Fuhrman, S., Michaels, G.S., Carr, D.B., Smith, S., Barker, J.L. and Somogyi, R.**, Large-scale temporal gene expression mapping of central nervous system development, *Proceedings of the National Academy of Sciences of the United States of America*, 95(1), 334-339, 1998.
37. **Winston, F., Dollard, C. and Ricupero-Hovasse, S.L.**, Construction of a set of convenient *Saccharomyces cerevisiae* strains that are isogenic to S288C, *Yeast*, 11(1), 53-55, 1995.
38. **Miller, M.J., Xuong, N.H. and Geiduschek, E.P.**, Quantitative analysis of the heat shock response of *Saccharomyces cerevisiae*, *Journal of Bacteriology*, 151(1), 311-327, 1982.
39. **Wenzel, T.J., Teunissen, A.W. and de Steensma, H.Y.**, PDA1 mRNA: a standard for quantitation of mRNA in *Saccharomyces cerevisiae* superior to ACT1 mRNA, *Nucleic Acids Research*, 23(5), 883-884, 1995.
40. **Liu, J.S., Neuwald, A.F. and Lawrence, C.E.**, Bayesian models for multiple local sequence alignment and Gibbs sampling strategies, *Journal of the American Statistical Association*, 90(432), 1156-1170, 1995.
41. **Berg, O.G. and von Hippel, P.H.**, Selection of DNA binding sites by regulatory proteins. Statistical-mechanical theory and application to operators and promoters, *Journal of Molecular Biology*, 193(4), 723-750, 1987.
42. **Quandt, K., Frech, K., Karas, H., Wingender, E. and Werner, T.**, MatInd and MatInspector: new fast and versatile tools for detection of consensus matches in nucleotide sequence data, *Nucleic Acids Research*, 23(23), 4878-4884, 1995.

43. **Schneider, T.D. and Stephens, R.M.**, Sequence logos: a new way to display consensus sequences, *Nucleic Acids Research*, 18(20), 6097-6100, 1990.
44. **Day, W.H. and McMorris, F.R.**, A consensus program for molecular sequences, *Computer Applications in the Biosciences*, 9(6), 653-656, 1993.

## Chapter 4

Prospects for Single Molecule DNA Sequencing

Using Ion Conductance

## Allocating Credit among Co-authors

Since the following chapter represents more than one person's efforts, it seems appropriate to a doctoral thesis that I describe which parts were my own work.

Contributions made by those who were not coauthors are credited—I sincerely hope adequately—elsewhere in the acknowledgments. Computer modeling of channel conductance was done primarily by George Church, with minor help from me in choosing pore dimensions and producing the van der Waals representation in Fig. 1. Estimation of thermal motion of phage DNA during injection was my own work. Dr. Richard Baldarelli expressed and purified *Shigella* LamB pores, and tested activity with an in vitro time course of bacteriophage  $\lambda$  injection. Dr. Baldarelli initiated work with this system by purchasing and assembling the apparatus for measuring ion currents on a picoampere scale, and performing preliminary experiments with LamB and bacteriophage  $\lambda$  using patch-clamp methods. The observation of a channel activity associated with purified bacteriophage  $\lambda$  in the absence of LamB was my own. Experiments which established the single-channel conductance of LamB, and that of the bacteriophage  $\lambda$ -associated channel (data shown in Fig. 2 & 3) were also entirely my own work. I used the planar bilayer method of conductance measurement which I reduced to practice in our laboratory with advice from Dr. Baldarelli. Modifications of this method—including a novel apparatus for static discharge production of narrow apertures in thin polymer film, and the use of FEP fluoropolymer film—were my own innovations.

Advances in electrophoretic gel-based DNA sequencing, automated fluorescent and multiplex methods, have made feasible the complete sequencing of genomes<sup>1-3</sup>. Given the growing desire to sequence other large genomes and to genotype many individual human genomes, there remains a need to explore alternative approaches that can increase data yields and decrease costs without increasing errors. Single-molecule DNA sequencing approaches have the potential to overcome some limitations of gel-based sequencing<sup>4-6</sup>, e.g., to reduce time, reagent costs, and amplification artifacts associated with conventional sequencing approaches. However, no single-molecule method has yet produced reliable sequence.

Observation of voltage-induced flow of ions through a single transmembrane channel was first reported in 1969<sup>7</sup> and observations of transient blocking and rapid gating of single ion channels are now made routinely. Within the last few years, measurements of channel conductance blockage by individual polymers have been reported. These include peptide transport through channels of the endoplasmic reticulum, protein transport across nuclear pore complexes, poly(ethylene glycol) diffusion through alamethicin channels, and supercoiled DNA interactions with bilayers<sup>8-11</sup>. More recently, conductance blockage of *S. aureus*  $\alpha$ -hemolysin channels due to the passage of ssDNA has been reported<sup>12</sup>.

We propose a single-molecule DNA sequencing method that takes advantage of the remarkable sensitivity of single-channel recording techniques. A DNA molecule passing through a transmembrane channel will interfere with ion flow through that channel. If it each of four nucleotide bases (or base pairs) of a DNA molecule forms a blockage of a unique size, it may then be possible to correlate variations in ion

conductance with DNA sequence as DNA is passed through a transmembrane channel. If the canonical four nucleotides are too similar in size, we might then consider the use of modifying DNA with larger bases.

The low cost of solid state amplifiers and the routine data acquisition rate of 300,000 samples per second make an ion conductance-based system for sequencing DNA attractive. Any such system will have three basic requirements: an ion channel with suitable geometry (discussed below), some form of nucleic acid, and a means of delivering the nucleic acid to the channel. A system consisting of ssDNA or ssRNA driven electrophoretically through  $\alpha$ -hemolysin channels has recently been proposed <sup>12</sup>. We have focused our attention on dsDNA and on a bacteriophage/receptor system to deliver dsDNA to a channel, since dsDNA has more predictable and less variable secondary structure than ssDNA or RNA and since the observation of DNA injection by a single bacteriophage would be of great biological interest. The rate of phage DNA injection (about 1000 bp/sec <sup>13</sup>), the potentially large read length (50 kb for  $\lambda$  bacteriophage), and the ease of packaging exogenous DNA into phage particles <sup>14</sup> also make a bacteriophage/receptor system a good choice.

## Results and discussion

Model for a hypothetical DNA-containing channel. To illustrate the proposed method and to examine its feasibility, we explored a simple geometrical model for the conductance of a hypothetical channel containing dsDNA (Fig. 1A). The ion conductance of a channel is determined by the channel's surface charge distribution,

bulk conductivity of its solution, the structure of water within the channel and, of course, the geometric size and shape of the channel<sup>15</sup>. Theory of ion channel conductance has not advanced to the point where conductance can be accurately predicted given a channel's three-dimensional structure. The conductance of large cylindrical water-filled channels has, however, been modeled with some success as  $g = \frac{\sigma \cdot A}{L}$ , where  $\sigma$  is the bulk conductivity of the solution,  $A$  is the ion-accessible cross-sectional area, and  $L$  is the length of the channel<sup>16</sup>. Although this approximation is an overestimate for smaller channels,  $g$  is in any case a monotonically increasing function of  $A$  if all non-geometric factors are held constant; i.e., if a channel conducts ions, a decrease in cross-sectional area results in a decrease in channel conductance. We draw only qualitative conclusions from our model since it incorporates only steric effects on channel conductance.

So that the conductance might be principally determined by passage of only one base pair at a time, we designed a hypothetical channel with a single narrow constriction or 'bottleneck'. The constriction was designed to be slightly wider than the diameter of dsDNA and have a thickness that is small compared to nucleotide spacing along dsDNA. Conductance (in units relative to the channel's conductance without DNA present) was calculated as the position of either canonical (Fig. 1B, black line) or modified (Fig. 1B, red line) dsDNA was shifted along the axis of the channel (see materials and methods). The modified dsDNA has an identical base sequence, but for one of its strands, every dT was replaced by dU and every dC replaced by d-5-methyl-C (dmC).

We draw three conclusions from the output of the model for unmodified dsDNA.

- (i) There is a periodic pattern of conductance peaks and valleys as a function of dsDNA

position along the channel axis, reflecting the periodic structure of dsDNA. (ii) Conductance ‘valleys’ follow a pattern, so that dG-dC base pairs are distinguishable from dA-dT base pairs; i.e., dA-dT base pairs block a greater fraction of channel conductance than do dG-dC base pairs. (iii) By observing the conductance ‘valleys’ of canonical DNA, one cannot distinguish dA-dT from dT-dA or dC-dG from dG-dC. For the modified dsDNA conductance trace, ‘valleys’ corresponding to dmC -dG base pairs can now be distinguished from those of dC-dG, and dA-dT can be distinguished from dA-dU. One can envision the use of bulkier modifications if more base-dependent contrast in conductance is required.

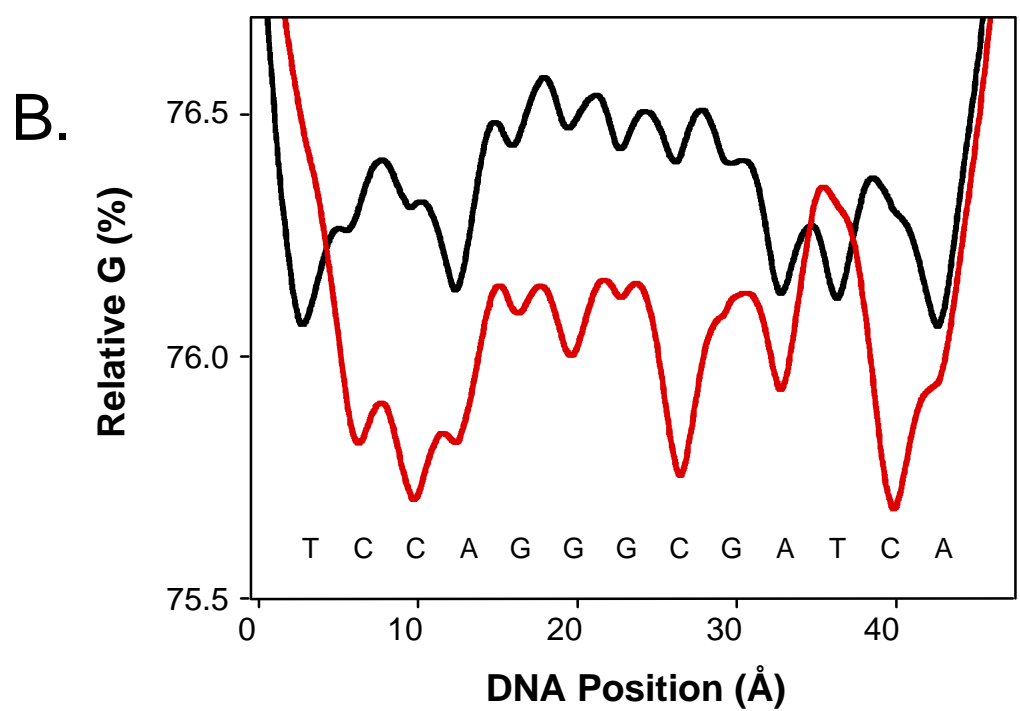
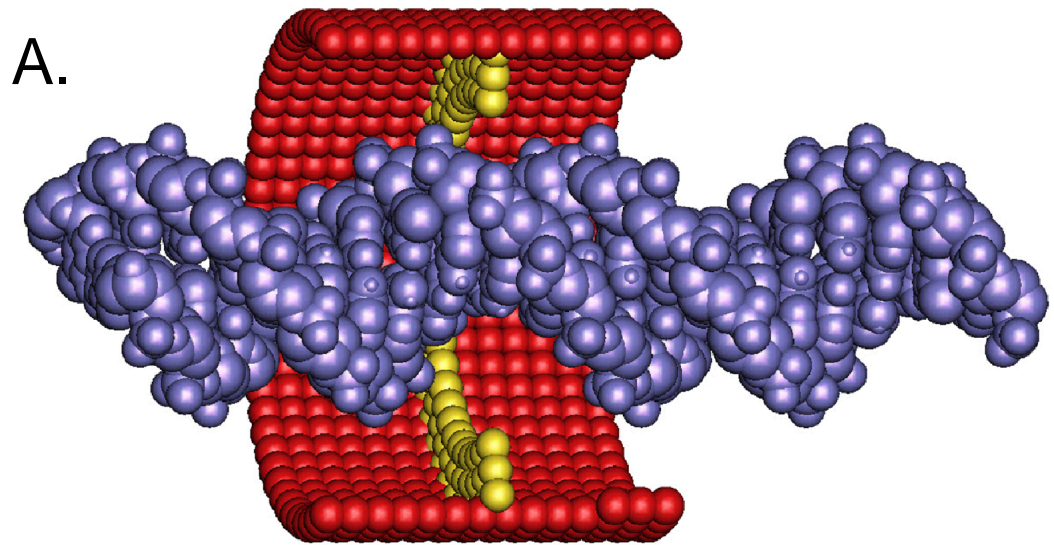


**Figure 1.** Modeling conductance through an idealized DNA-containing channel to examine feasibility of DNA sequencing. (A) The idealized pore (shown in red) is 38 Å in diameter and 26 Å in length (the approximate length of the hydrophobic region of a lipid bilayer). The channel has a constriction 28 Å in diameter (in yellow) which has the thickness of one keto-oxygen (3.1 Å), so that it admits dsDNA (in blue) with surrounding space to allow the passage of small ions. Fig. 1A was generated using RASMOL, which can be obtained from <http://klaatu.oit.umass.edu/microbio/rasmol/>. (B) Conductance of a dsDNA-containing channel as a function of DNA position along the idealized channel axis in 0.1 Å increments (see materials and methods). Conductance is plotted for the indicated sequence of canonical B-form dsDNA (black line) and dsDNA modified as described in the text (red line). Comparing unmodified DNA with DNA modified in one strand identifies which parts of the conductance curve are sensitive to which atoms of the DNA helix. In terms of the base sequence of the modified strand, the conductance of the valleys follow a pattern of  $dC = dG > dA = dT$  for canonical DNA and  $dU > dG > dA > d5mC$  for the modified DNA.

Conductance measurements of *Shigella* LamB and bacteriophage  $\lambda$ . We chose to investigate this approach experimentally using bacteriophage  $\lambda$  and its receptor, the outer membrane porin LamB of *Shigella sonnei*. The advantages of this system are that  $\lambda$  is genetically and structurally the best understood bacteriophage, and for the following additional reasons: in vitro conditions for *Shigella* LamB-dependent DNA ejection have been determined<sup>17</sup>; bacteriophage  $\lambda$ , in combination with LamB, has previously been shown to form stable transmembrane channels<sup>18</sup>; and the structure of *E. coli* LamB has been determined<sup>19</sup>. *Shigella* rather than *E. coli* LamB was chosen for these studies, since *E. coli* LamB requires ethanol or chloroform to trigger  $\lambda$ 's DNA ejection in vitro<sup>20; 21</sup>. Other bacteriophages for which in vitro DNA ejection has been studied include T4 and T5<sup>22; 23</sup>.

LamB is a trimeric outer membrane protein whose physiological function is to passively transport maltose<sup>19; 24</sup>. The  $\lambda$  tail fiber initiates the phage/receptor interaction by docking reversibly to surface-exposed residues of LamB<sup>21; 25</sup>. This is followed by irreversible association of  $\lambda$  with LamB and subsequent DNA ejection at a rate of 1000 base pairs per second<sup>13</sup>. After DNA ejection, the complex of  $\lambda$  and LamB remains associated, and a channel is present that is stable and permeable to larger molecules than LamB alone can admit<sup>18</sup>.

Although the conductance of *E. coli* LamB has been characterized<sup>26; 27</sup>, the conductance of *Shigella* LamB has not been reported. The LamB protein of *Shigella* differs from that of *E. coli* by only a few residues on the outer surface of the molecule<sup>28</sup>, so that the overall structure and conductance of the two porins should be very similar.

We developed a method for affinity-purifying *Shigella* LamB (see materials and methods) and have shown the single (trimeric) channel conductance of *Shigella* LamB to be  $88 \pm 5$  pS (based on 75 transitions measured) in 0.5 M KCl in a lipid bilayer (Fig. 2), with occasional subconductance transitions of  $29 \pm 3$  pS (based on 37 transitions). Subconductance states have been described for mutants of *E. coli* LamB, but have not been observed in wild-type LamB<sup>26; 27</sup>. We ascribe the 29 pS transitions to transient closure of monomers. For a direct comparison of *Shigella* LamB with its *E. coli* counterpart, we measured *Shigella* LamB conductance to be  $174 \pm 7$  pS (based on 63 transitions) in conditions (bilayer potential 20 mV, bath solution 1 M KCl, 10 mM Tris (pH 7.5), 10 mM MgCl<sup>2</sup>) similar to those in which *E. coli* LamB conductance is known to be 155 pS<sup>26; 27</sup>.

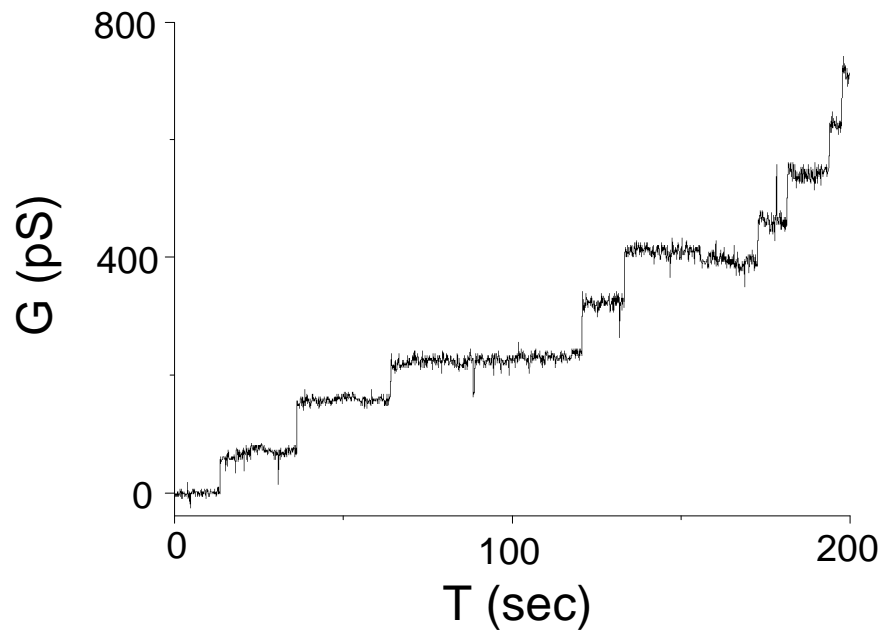


**Figure 2.** Discrete conductance transitions due to single *Shigella* LamB trimers. Channel conductance measurements were obtained by adding *Shigella* LamB detergent micelles to a bath of 0.5 M KCl adjacent to a voltage-clamped asolectin bilayer. Conductance of the trimers was found to be  $88 \pm 5$  pS.

The conductance of single channels associated with bacteriophage T5 and with filamentous phage fd has been studied<sup>23; 24</sup>, and some inferences about behavior of individual bacteriophage T4-induced channels have been made<sup>29</sup>. Although previous in vitro experiments suggested that the bacteriophage  $\lambda$ /LamB complex forms a channel<sup>18</sup>, single channel conductance has not been measured. We attempted to characterize the conductance of the  $\lambda$ /LamB complex. When a preincubated mixture of  $\lambda$  and *Shigella* LamB was added to a voltage-clamped lipid bilayer, large channels were observed (data not shown). The initial conductance transition of these channels is to a level of  $2.4 \pm 0.5$  nS (based on 88 transitions measured), followed by a drop to  $2.1 \pm 0.2$  nS (based on 25 transitions) after a characteristic time of about 20 seconds. Subsequent to this drop, a variety of gating behaviors between lower conductance levels was observed in some channels. Estimating a characteristic time for complete channel closure was problematic, since these events were quite rare. Observations of a single channel have persisted as long as 2.8 hours, and were generally terminated by a second channel insertion or by breakage of the lipid bilayer.

To our surprise, when  $\lambda$  was added to a lipid bilayer in the absence of LamB, channels with similar characteristics were observed (Fig. 3). Examples of the gating behaviors mentioned above are shown in Fig. 3A and 3B. The mean initial conductance transition for these channels is  $2.1 \pm 0.7$  nS (based on 54 transitions), which is statistically indistinguishable from the mean transition of the  $\lambda$ /LamB mixture. The number of channels present with bacteriophage  $\lambda$  alone was not significantly different from the number of channels present when  $\lambda$  was premixed with LamB. These channels

were not observed in experiments with bilayer alone, or with bilayer and *Shigella* LamB. Therefore we conclude that purified  $\lambda$  bacteriophage can form a channel in vitro without the aid of its in vivo receptor, LamB. We do not know if the channel is formed by intact phage or by a subpopulation of phage, e.g., ‘ghosts’ that have spontaneously ejected their DNA. The  $\lambda$ -associated channel is unlikely to be an *E. coli* porin contaminant, since further equilibrium CsCl density-gradient purification of phage and extensive dialysis with a 500,000 MWCO membrane did not significantly alter the amount of channel activity. Also, the channel is unlike any described naturally occurring *E. coli* channel in its behavior and conductance.

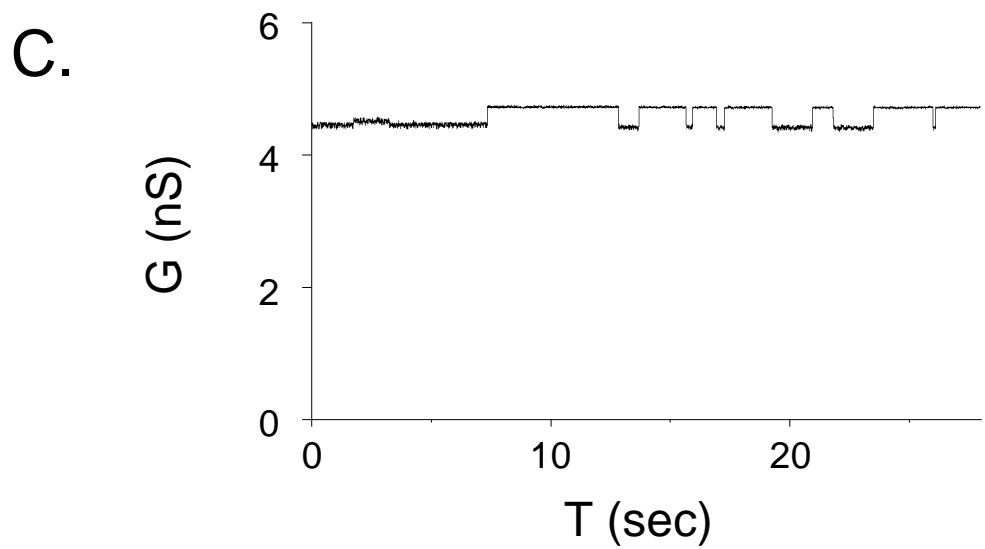
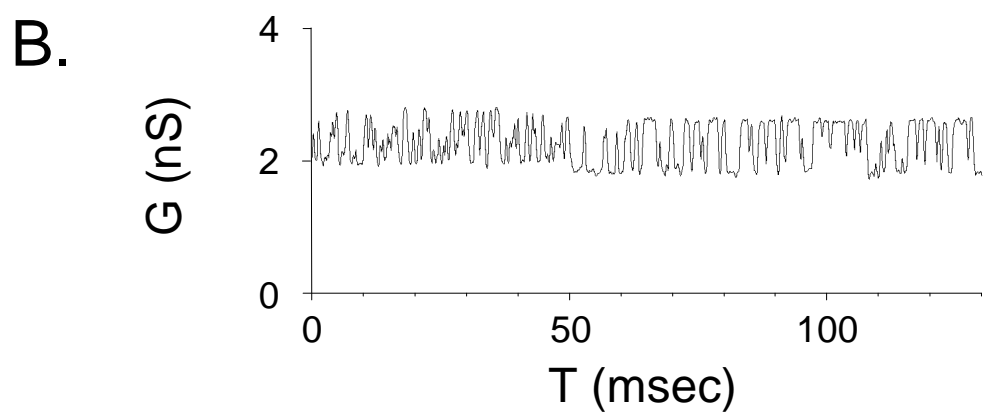
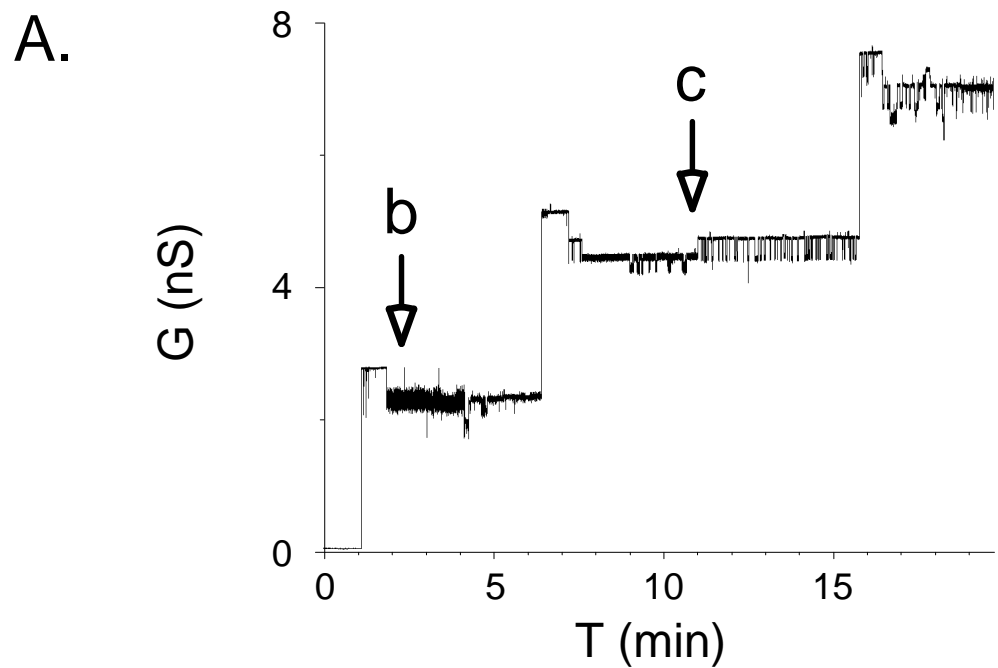


**Figure 3.** A conductance trace of single channels associated with  $\lambda$  bacteriophage. **(A)**

Discrete conductance transitions of three individual channels. Channel conductance measurements were obtained by adding purified  $\lambda$  phage to a bath of 0.5 M KCl adjacent to a voltage-clamped asolectin bilayer. **(B)** An expansion of the conductance profile indicated by the **b** arrow in Fig. 3 A **(C)** An expansion of the conductance profile indicated by the **c** arrow in Fig. 3 A.

Receptor-independent channel formation was unexpected, since previous work showed that  $\lambda$  does not trigger release of ATP from *E. coli* LamB-containing liposomes, but does trigger ATP release from *Shigella* LamB-containing liposomes<sup>18</sup>. However, several possibilities reconcile this observation with our own: receptor-independent channel formation by  $\lambda$  may be particular to lipid composition (we used soy rather than egg phosphatidylcholine) or lower salt conditions; *E. coli* LamB may inhibit channel formation by  $\lambda$  in vitro; the  $\lambda$  channel may form, but only be permeable to ATP when complexed with *Shigella* LamB; or the channel-forming activity of  $\lambda$  alone may be below the sensitivity of the ATP detection assay used. Experiments demonstrating a *Shigella* LamB requirement for  $\lambda$  DNA injection<sup>13; 17; 30</sup> do not conflict with our observations, since channel-formation and DNA ejection may be independent processes. We do not believe that DNA transfer is occurring during our observations of  $\lambda$  phage alone, since previous work has clearly shown that LamB is required for in vitro DNA ejection<sup>13</sup>. Nor do we expect DNA transfer in our mixtures of LamB and  $\lambda$ , since any DNA ejection would have taken place before conductance is measured.

Conductance measurements of the  $\lambda$  channel allow us to make general inferences about the nature of the channel used by  $\lambda$  for DNA transfer across the outer membrane. It has not been known whether  $\lambda$  widens a channel in LamB for DNA transport or if it forms a distinct transmembrane channel. Using a cylindrical water-filled channel model (described above) with the 58.5 mS/cm conductivity of 0.5M KCl<sup>31</sup>, a channel with 2.1 nS conductance has the 2 nm diameter of dsDNA if it has an ‘effective’ length of 9 nm. Although the phage tail is about 150 nm long, its ‘effective’ length will be determined by

the permeability of the tail wall to ions, so that 9 nm does not seem unreasonable. The conductance of the  $\lambda$  channel is comparable to the 2.1 nS conductance of FhuA/T5 bacteriophage channel under similar salt conditions<sup>23</sup> and to the 3.0 nS conductance of the adsorption protein of filamentous phage fd (observed in 1M rather than 0.5M KCl)<sup>24</sup>. The observation that  $\lambda$  can by itself form a channel large enough to pass DNA removes any need to invoke LamB as the pore used for DNA transfer, but does not rule out this possibility.

Experiments critical to the success of the proposed sequencing method will involve the addition of  $\lambda$  bacteriophage to a LamB-containing bilayer, so that conductance during DNA transport may then be observed. We do not know if  $\lambda$ 's DNA transport channel contains a single 'bottleneck' as we have modeled above, and so we cannot predict whether the channel will have sequence-dependent variations in ion conductance which exceed the noise inherent in our experimental system. We also cannot be certain that random thermal motion of DNA as it passes through  $\lambda$ 's tail tube will permit unidirectional motion of DNA as we have modeled it above. However, a calculation of the rate of this random motion based on frictional considerations indicates that it will be slow when compared with achievable data acquisition rates. In any case, distinguishing the conductance signature of DNA transport from that of  $\lambda$  alone is possible now that the conductance of  $\lambda$  and *Shigella* LamB have been observed individually.

We suggest bacteriophage  $\lambda$ /*Shigella* LamB as a system for investigating single-molecule DNA sequencing. In addition, this system may allow us to elucidate details of

$\lambda$  phage's mechanism of DNA transfer. Although other virus-associated channels have been previously described, e.g., bacteriophage T5/FhuA, filamentous phage fd adsorption protein, mammalian reovirus, and influenza A virus, no detailed mechanism for transmembrane nucleic acid transfer has been established for these systems<sup>23; 24; 32-34</sup>. Details of other DNA transport systems, e.g., bacterial conjugation or specific uptake of DNA by *Haemophilus influenzae* are also unknown<sup>35</sup>.

### Experimental protocol

Bacteriophage  $\lambda$  and LamB preparations. Purified bacteriophage  $\lambda$  of strain cI857ind1Sam7 was obtained from New England Biolabs and was purified further by CsCl equilibrium density centrifugation<sup>36</sup>. Yield was determined to be  $\sim 10^{12}$  pfu/ml. *Shigella* LamB protein was affinity-purified from *E. coli* strain Pop154, which carries a *Shigella* LamB gene in place of the endogenous gene<sup>25</sup>. Solubilized outer membranes prepared from 2 L culture as described<sup>37</sup> were mixed with 15 ml amylose/agarose affinity resin (New England Biolabs) and equilibrated with 10 mM CAPS/10 mM Tris (pH 8.0), 1% triton X-100 and 100 mM NaCl. The column was washed with 20 mls equilibration buffer. LamB protein was eluted with a continuous pH gradient established between equilibration buffer and otherwise-identical pH 11 buffer. Fractions were neutralized and those containing LamB were pooled and dialyzed against an excess volume of 10 mM Tris (pH 7.5), 1% triton X- 100, 100 mM NaCl. The yield of LamB protein was  $49 \mu\text{g}/\text{ml}$  ( $2.1 \times 10^{14}$  trimers/ml). Consistent with its maltose-binding function, LamB can also be eluted using 2% maltooligosaccharide mix (Pfanstiehl

Laboratories, Inc.). We tested *Shigella* LamB and  $\lambda$  by mixing the two preparations 1:250 by volume and assaying for  $\lambda$  DNA release using ethidium bromide-stained agarose gel electrophoresis. Fluorescence increased upon  $\lambda$  addition -- plateauing after ~1 minute at 37° -- but did not increase when LamB dialysis buffer was used in place of LamB. In preparation for conductance measurements, a mixture of 1:250 by volume of LamB:  $\lambda$  preparations was incubated at 37° for 3 hours, and then mixed 1:1 with 1M KCl to approximately equalize salt concentrations to bath solution. 150  $\mu$ l of this mixture was added to bilayer chamber. For lambda-only channel measurements, phage was prepared in the same manner, replacing the LamB preparation with 10 mM Tris (pH 7.5), 1% triton X-100, 100 mM NaCl.

Estimation of thermal motion of DNA. To obtain an order of magnitude estimate for the diffusion constant (D) of DNA during injection, we first assumed that -- in the manner of a spring -- the driving force of DNA transport is that stored in the densely packed DNA of the head. If the packaging energy for  $\lambda$  is similar to that measured for other bacteriophages -- ~1 ATP for every 2 bp packaged<sup>38; 39</sup> -- and if about 10% of this energy is available to drive DNA transport, then a force (F) of  $1.6 * 10^{-11}$  J m<sup>-1</sup> would drive DNA the length of 48,500 bp ( $F \cdot$  distance = energy). We can relate F to a frictional coefficient (f) for our situation if we assume the ‘terminal velocity’ v of DNA transport --where frictional force balances motive force -- to be the rate previously measured (~10<sup>3</sup> bp/sec)<sup>13</sup>, since  $f \cdot v = F$ . Finally, using the Einstein-Smoluchowski

relation  $D = \frac{k \cdot T}{f}$ , we can estimate D to be  $\sim 10^{-16}$  meter<sup>2</sup>/sec. Knowing D, and using the one-dimensional diffusion equation  $X_{RMS} = \sqrt{2 \cdot D \cdot t}$ , where  $X_{RMS}$  is the root-mean-

square distance traveled by DNA in a time  $t$ , we can conclude that the characteristic time for the segment of DNA which experiences the friction calculated above to move a distance of 1 bp by random thermal motion is  $\sim 1$  millisecond. This is slow compared with our data acquisition time of 3 microseconds per sample. See ref. <sup>40</sup> for a discussion of diffusion.

Model for conductance of a DNA-containing channel. Conductance was calculated using

$$g(x) = \frac{1}{R(x)} = \frac{1}{\sum_{i=1}^N \left( \frac{t}{A(i, x)} \right)}, \text{ where } g(x) \text{ and } R(x) \text{ are the conductance and resistance,}$$

respectively, of the DNA-containing channel as a function of DNA position  $x$ ,  $A(i, x)$  is the ion-accessible area of a particular ‘slice’  $i$  for the DNA-containing channel, respectively, and  $N$  is the number of axial ‘slices’ of thickness  $\tau$  into which the channel can be divided. We set  $\tau$  at 0.1 Å, and chose the ion  $\text{Be}^{++}$  for its small radius (0.35 Å).

The total resistance of the channel is the sum of the resistances of all the ‘slices’. For each slice, the resistance is proportional to slice thickness  $\tau$  and inversely proportional to the ion-accessible area. The ion-accessible area of each slice was calculated by adding the ion radius to the van der Waals radius of each channel and DNA atom, and then counting the number of points on a 0.1 Å grid that are not contained within any atom’s resultant radius.

Conductance measurements. All conductance measurements employed a Teflon<sup>TM</sup> block with two chambers, each of  $\sim 1$  ml capacity. The chambers are separated by a .0005 inch-thick Teflon<sup>TM</sup> or Korton<sup>TM</sup> FEP film (Norton Performance Plastics) with a small ( $\sim 25\text{-}30$  μm) aperture. The aperture is produced by static discharge from a Zerostat<sup>TM</sup>

piezoelectric gun (Discwasher). Unless otherwise indicated, bath solution was 0.5 M KCl, 5 mM Tris (pH 7.5), 5 mM MgCl<sup>2</sup>. Bilayers were produced by the folded bilayer method<sup>41</sup> using 3 µl of a 20 mg/ml solution of asolectin (Sigma #P-5638) in pentane for each chamber, and with light application of 1% squalene in pentane to the aperture. Unless otherwise indicated, all bilayers were voltage-clamped at 25 mV. Electrodes were Ag/AgCl (Axon Instruments). An Axopatch 200A amplifier (Axon Instruments) was used to monitor pipette current in the capacitive-feedback configuration with a CV201A headstage. Internal low-pass Bessel filter was set at 1 KHz, and a sampling interval of 100 µsec was used. A TL-1 DMA A/D converter interface transferred data to acquisition software PCLAMP 6.0.2 (Axon Instruments). Data were analyzed with PCLAMP 6.0.2 and Axograph 2.0 (Axon Instruments). *Shigella* LamB measurements were digitally filtered at 10 Hz.

## References

1. **Hunkapiller, T., Kaiser, R.J., Koop, B.F. and Hood, L.**, Large-scale and automated DNA sequence determination, *Science*, 254(5028), 59-67, 1991.
2. **Fleischmann, R.D., Adams, M.D., White, O., Clayton, R.A., Kirkness, E.F., Kerlavage, A.R., Bult, C.J., Tomb, J.F., Dougherty, B.A., Merrick, J.M. and et, a.,** Whole-genome random sequencing and assembly of Haemophilus influenzae Rd [see comments], *Science*, 269(5223), 496-512, 1995.
3. **Church, G.M. and Kieffer-Higgins, S.**, Multiplex DNA sequencing, *Science*, 240(4849), 185-188, 1988.

4. **Davis, L.M., Fairfield, F.R., Harger, C.A., Jett, J.H., Keller, R.A., Hahn, J.H., Krakowski, L.A., Marrone, B.L., Martin, J.C., Nutter, H.L. and et al.**, Rapid DNA sequencing based upon single molecule detection, *Gen. Anal. Tech. Appl.*, 8(1), 1-7, 1991.
5. **Lindsay, S.M. and Philipp, M.**, Can the scanning tunneling microscope sequence DNA?, *Gen. Anal. Tech. Appl.*, 8(1), 8-13, 1991.
6. **Hansma, H.G., Weisenhorn, A.L., Gould, S.A.C., Sinsheimer, R.L., Guab, H.E., Stucky, G.D., Zaremba, C.M. and Hansma, P.K.**, Progress in sequencing deoxyribonucleic acid with an atomic force microscope, *J. Vacuum Science and Technol.*, 9(2), 1282-1284, 1991.
7. **Bean, R.C., Shepherd, W.C., Chan, H. and Eichner, J.**, Discrete conductance fluctuations in lipid bilayer protein membranes, *J. Gen. Physiol.*, 53(6), 741-757, 1969.
8. **Simon, S.M. and Blobel, G.**, A protein-conducting channel in the endoplasmic reticulum, *Cell*, 65(3), 371-380, 1991.
9. **Bustamante, J.O., Oberleithner, H., Hanover, J.A. and Liepins, A.**, Patch clamp detection of transcription factor translocation along the nuclear pore complex channel, *J. Membrane Biol.*, 146(3), 253-261, 1995.
10. **Bezrukova, S.M., Vodyanoy, I. and Parsegian, V.A.**, Counting polymers moving through a single ion channel, *Nature*, 370(6487), 279-281, 1994.
11. **Spassova, M., Tsoneva, I., Petrov, A.G., Petkova, J.I. and Neumann, E.**, Dip patch clamp currents suggest electrodifusive transport of the polyelectrolyte DNA through lipid bilayers, *Biophys. Chem.*, 52(3), 267-274, 1994.

12. **Kasianowicz, J.J., Brandin, E., Branton, D. and Deamer, D.W.**, Characterization of individual polynucleotide molecules using a membrane channel, *Proc. Natl. Acad. Sci. USA*, 93, 13770-13773, 1996.
13. **Novick, S.L. and Baldeschwieler, J.D.**, Fluorescence measurement of the kinetics of DNA injection by bacteriophage lambda into liposomes, *Biochemistry*, 27(20), 7919-7924, 1988.
14. **Enquist, L. and Sternberg, N.**, Packaging of bacteriophage lambda in vitro, *Meth. Enz.*, 68, 281-298, 1979.
15. **Eisenberg, R.S.**, Computing the field in proteins and channels, *J. Membrane Biol.*, 150, 1-25, 1996.
16. **Benz, R., Schmid, A. and Hancock, R.E.W.**, Ion selectivity of gram-negative bacterial porins, *J. Bact.*, 162(2), 722-727, 1985.
17. **Schwartz, M. and Le Minor, L.**, Occurrence of the bacteriophage lambda receptor in some enterobacteriaceae, *J. Virol.*, 15(4), 679-685, 1975.
18. **Roessner, C.A. and Ihler, G.M.**, Formation of transmembrane channels in liposomes during injection of lambda DNA Bacteriophage lambda PaPa: not the mother of all lambda phages, *J. Biol. Chem.*, 261(1), 386-390, 1986.
19. **Schirmer, T., Keller, T.A., Wang, Y.F. and Rosenbusch, J.P.**, Structural basis for sugar translocation through maltoporin channels at 3.1 Å resolution [see comments], *Science*, 267(5197), 512-514, 1995.
20. **Randall-Hazelbauer, L. and Schwartz, M.**, Isolation of the bacteriophage lambda receptor from Escherichia coli, *J. Bact.*, 116(3), 1436-1446, 1973.

21. **Mackay, D.J. and Bode, V.C.**, Binding to isolated phage receptors and lambda DNA release in vitro, *Virology*, 72(1), 167-181, 1976.
22. **Furukawa, H., Kuroiwa, T. and Mizushima, S.**, DNA injection during bacteriophage T4 infection of Escherichia coli, *J. Bact.*, 154, 938-945, 1983.
23. **Bonhivers, M., Ghazi, A., Boulanger, P. and Letellier, L.**, FhuA, a transporter of the *E. coli* outer membrane, is converted into a channel upon binding of bacteriophage T5, *EMBO J.*, 15(8), 1850-1856, 1996.
24. **Szmelcman, S. and Hofnung, M.**, Maltose transport in Escherichia coli K-12: involvement of the bacteriophage lambda receptor, *J Bact.*, 124(1), 112-118, 1975.
25. **Roa, M. and Scandella, D.**, Multiple steps during the interaction between coliphage lambda and its receptor protein in vitro, *Virology*, 72(1), 182-194, 1976.
26. **Benz, R., Schmid, A. and Vos-Scheperkeuter, G.H.**, Mechanism of sugar transport through the sugar-specific LamB channel of Escherichia coli outer membrane, *J. Membrane Biol.*, 100(1), 21-29, 1987.
27. **Dargent, B., Charbit, A., Hofnung, M. and Pattus, F.**, Effect of point mutations on the in-vitro pore properties of maltoporin, a protein of Escherichia coli outer membrane, *J. Mol. Biol.*, 201(3), 497-506, 1988.
28. **Roessner, C.A. and Ihler, G.M.**, Sequence of amino acids in lamB responsible for spontaneous ejection of bacteriophage lambda DNA, *J. Mol. Biol.*, 195(4), 963-966, 1987.
29. **Boulanger, P. and Letellier, L.**, Characterization of ion channels involved in the penetration of phage T4 DNA into Escherichia coli cells, *J. Biol. Chem.*, 263(20), 9767-9775, 1988.

30. **Roessner, C.A., Struck, D.K. and Ihler, G.M.**, Injection of DNA into liposomes by bacteriophage lambda, *J. Biol. Chem.*, 258(1), 643-648, 1983.
31. **Weast, R., Ed.**, CRC Handbook of Chemistry and Physics, CRC Press, Inc., Boca Raton, FL, 1987.
32. **Tosteson, M.T., Nibert, M.L. and Fields, B.N.**, Ion channels induced in lipid bilayers by subvirion particles of the nonenveloped mammalian reovirus, *Proc. Natl. Acad. Sci. USA*, 90, 10549-10552, 1993.
33. **Tosteson, M.T., Pinto, L.H., Holsinger, L.J. and Lamb, R.A.**, Reconstitution of the influenza virus M<sub>2</sub> ion channel in lipid bilayers, *J. Membrane Biol.*, 142, 117-126, 1994.
34. **Glaser-Wuttke, G., Keppner, J. and Rasched, I.**, Pore-forming properties of the adsorption protein of filamentous phage fd, *Bioch. Biophys. Acta*, 985, 239-247, 1989.
35. **Dreiseikelmann, B.**, Translocation of DNA across bacterial membranes, *Microbiol. Rev.*, 58(3), 293-316, 1994.
36. **Sambrook, J., Fritsch, E.F. and Maniatis, T.**, *Molecular Cloning: A Laboratory Manual*, Vol. 1, Cold Spring Harbor Laboratory Press, Cold Spring Harbor, NY, 1989.
37. **Gabay, J. and Schwartz, M.**, Monoclonal antibody as a probe for structure and function of an Escherichia coli outer membrane protein, *J. Biol. Chem.*, 257(12), 6627-6630, 1982.
38. **Morita, M., Tasaka, M. and Fujisawa, H.**, DNA Packaging ATPase of Bacteriophage T3, *Virology*, 193, 748-752, 1993.

39. **Guo, P., Peterson, C. and Anderson, D.**, Prohead and DNA-gp3-dependent ATPase activity of the DNA packaging protein gp16 of bacteriophage phi 29, *J. Mol. Biol.*, 197(2), 229-236, 1987.
40. **Berg, H.C.**, *Random Walks in Biology*, Princeton University Press, Princeton, NJ, 1993.
41. **Montal, M. and Mueller, P.**, Formation of bimolecular membranes from lipid monolayers and a study of their electrical properties, *Proc. Natl. Acad. Sci. USA*, 69, 3561-3566, 1972.

## Appendix A

### A Software Guide

Quite a number of applications, small and large, were written in the course of this work. So that others may make some use of these, I've made an attempt here to list the applications, their purpose, their proper usage, and the naming of input and output files. For the sake of simplicity, I've divided the applications into two categories: 1) applications for processing and analyzing Affymetrix microarray ('chip') data; 2) applications for analyzing upstream noncoding DNA sequences. All of the applications listed were written in Perl5, with the exception of 'AlignACE', which was written in C. Usage for each of these applications can also be determined from the command line by typing the name of the application with no arguments.

Applications for processing and analyzing Affymetrix microarray data. The following is a summary table of chip analysis applications:

Application	Input Files	Output File	Purpose
make_SUM_file	.txt	.SUM	Converts Affymetrix chip summary file to less ambiguous .SUM format
make_FEA_file	.SUM, .CEL	.FEA	Groups Affymetrix .CEL file feature data by ORF
make_BKG_file	.FEA	.BKG	Background-subtracts feature intensity data
make_NRM_file	.BKG	.NRM	Normalizes between chips within an experiment using in vitro transcription controls
make_ALL_file	.BKG or .NRM	.ALL	Collection of data from complete chip set for a given experiment
chipbatch	.CEL	.ALL	Batch file for running make_FEA_file, make_BKG_file, make_NRM_file, make_ALL_file
make_XP_file	.ALL	.XP	Computes absolute expression levels for each ORF in an experiment
make_DIF_file	.ALL	.DIF	Computes relative expression levels for each ORF between two experiments

### **'make\_SUM\_file'**

Usage: "make\_SUM\_file ?.txt -o ?.SUM".

Example: “`make_SUM_file 1228a.txt -o Sc_A.SUM`”.

The starting point for our analysis was a ‘.CEL’ file created by the Affymetrix GeneChip software. The ‘.CEL’ file contains the mean and variance of fluorescence intensity for every coordinate on the chip. An essential step in calculating abundance of an ORF is knowing which positions on the chip correspond to which ORFs. To this end, we received files from Affymetrix which give the number of probes for each ORF, and the X and Y coordinates of the ‘upper leftmost’ and ‘lower rightmost’ positions for each feature set. Unfortunately, this description is ambiguous in cases where this feature set has been interrupted, since the two defining coordinates given do not tell us where the interruption occurs. Examples of interruptions include some features near the chip edge which do not contain DNA, and checkerboards of features complementary to a control DNA sequence located at the center and periphery of the chip. The ‘.SUM’ file was designed as an unambiguous format which contains the start and stop coordinates of uninterrupted blocks of features. ‘`make_SUM_file`’ takes the Affymetrix ‘.txt’ files and converts them to .SUM files, notifying the user of ambiguities. To resolve ambiguities, a ‘dummy’ .CEL file was created containing intensities each of which encodes its corresponding coordinate, e.g., the feature at coordinate (133,54) is given the intensity 133054. When this .CEL file is examined using the GeneChip software, the intensities corresponding to a given ORF determine the corresponding coordinates. The .SUM files which have been hand-edited to remove ambiguities are called ‘Sc\_A.SUM’, ‘Sc\_B.SUM’, ‘Sc\_C.SUM’, and ‘Sc\_D.SUM’, corresponding to chips A through D in a complete chip set for yeast.

#### **‘`make_FEA_file`’**

Usage: “make\_FEA\_file ?.CEL ?.SUM”.

Example: “make\_FEA\_file 062697GALA.CEL Sc\_A.SUM”.

Given the unambiguous locations of features corresponding to a given chip set, we can now group intensity data by ORF. ‘make\_FEA\_file’ does this, putting the result into a ‘.FEA’ file. In addition, ‘make\_FEA\_file’ groups a set of intensities drawn from 36 non-DNA-containing features into a feature set called ‘BACKGROUND’, for the purpose of determining background and detection threshold levels.

#### **‘make\_BKG\_file’**

Usage: “make\_BKG\_file ?.FEA”.

Example: “make\_BKG\_file 062697GALA.FEA”.

This program finds the mean of 36 non-DNA-containing features and subtracts it from every intensity value in a .FEA file. The results are written to a .BKG file.

#### **‘make\_NRM\_file’**

Usage: “make\_NRM\_file ?.BKG”.

Example: “make\_NRM\_file 062697GALA.BKG”.

If one would like to compare absolute abundance of ORFs which were measured on different chip types within the same experiment, it is important to normalize the results between the four different .BKG files of a chip set, since the average amount of oligonucleotide on a chip can vary. This is true even if each chip has been hybridized with the same pool of labeled nucleic acid under identical conditions. A reasonable approach to normalization is to spike the pool of nucleic acid with a fixed amount of a known sequence which can be assayed on each chip in the set. The chips have been designed with this in mind, so that each chip in a set contains probes for several bacterial

transcripts. ‘make\_NRM\_file’ gets the median value of  $\Delta$  for each of these transcripts and averages it to obtain a normalization factor. This program was not used for the work in this thesis, since we sought only to calculate transcript abundance in each ‘experimental’ condition relative to a ‘baseline’ condition, and were not interested in comparing abundances of different ORFs within the same condition. Consequently, absolute abundance values of ORFs found in the appendices should be compared with absolute abundances of other ORFs measured on different chip types only with some hesitation.

#### **‘make\_ALL\_file’**

Usage: “make\_ALL\_file ?A.NRM ?B.NRM ?C.NRM ?D.NRM or

make\_ALL\_file ?A.BKG ?B.BKG ?C.BKG ?D.BKG”.

Example: “make\_ALL\_file 062697GALA.NRM 062797GALB.NRM

062797GALC.NRM 062997GALD.NRM”.

Since measuring abundance of all transcripts in a single condition requires four chip experiments, the data from these experiments should be gathered together and treated as a single data set (a .ALL file). ‘make\_ALL\_file’ also normalizes the complete data set so that it will be comparable to data sets from other .ALL files. Normalization is as discussed in Chapters 2 and 3. Each intensity value is divided by a normalization factor. The normalization factor is the average PM intensity over all four chip data sets within a .ALL file.

#### **‘chipbatch’**

Usage: “chipbatch ?A.CEL ?B.CEL ?C.CEL ?D.CEL [-d]”.

Example: “chipbatch 062697GALA.CEL 062797GALB.CEL  
062797GALC.CEL 062997GALD.CEL”.

This is simply a script which shepherds a set of .CEL files from the four chips through ‘make\_FEA\_file’, ‘make\_BKG\_file’, ‘make\_NRM\_file’ (optional) and ‘make\_ALL\_file’. The -d option indicates a decision to skip the normalization between chips using the in vitro transcription controls provided by ‘make\_NRM\_file’.

#### **‘make\_XP\_file’**

Usage: “make\_XP\_file ?.ALL ?.XP”.

Example: “make\_XP\_file 062697GALA.ALL”.

This program calculates absolute abundance for every ORF by the median of  $\Delta$  values method described in Chapters 2 and 3. The .XP output file contains a threshold column. A value of 1 in this column indicates that the value (or one of the two values if the feature set contains an even number of probes) used to calculate the  $\Delta$  median is below the detection threshold determined for that chip’s hybridization. If there are MM probes among the features for an ORF which are not unique in the genome, this fact is indicated and the calculation is based on the median of PM values rather than the median of  $\Delta$  values.

#### **‘make\_DIF\_file’**

Usage: “make\_DIF\_file ?.ALL ?.ALL ?.DIF”.

Example: “make\_DIF\_file 062697GALA.ALL 062697FY4A.ALL  
GAL,GLU.DIF”.

Calculates relative abundance by the median of  $\Delta$ -ratios method described in Chapters 2 and 3. Median deviation of log  $\Delta$ -ratios is calculated as described in Chapter

2. ORFs are categorized based on whether or not they exceeded detection thresholds for the two conditions being compared. This categorization is based on the  $\Delta$  values used to calculate the median log  $\Delta$ -ratio value (there are two such values for features with an odd number of probes, four for an even number). The following table is a guide to interpreting the threshold codes returned by ‘make\_DIF\_file’.

$D_{\text{expt}}$ value(s) <sup>3</sup>	$D_{\text{base}}$ value(s) <sup>3</sup>	$D_{\text{expt}}$ value(s) <sup>3</sup>	$D_{\text{base}}$ value(s) <sup>3</sup>	Threshold Code	Comment
$T_{\text{expt}}$	$T_{\text{base}}$	$T_{\text{base}}$	$T_{\text{expt}}$		
yes	yes	-	-	none	Detected in both conditions
no	yes	-	yes	1	Detected in condition 2 only
yes	no	yes	-	2	Detected in condition 1 only
no	yes	-	no	3	Detected in both conditions, but in condition 2 is below threshold for condition 1
yes	no	no	-	4	Detected in both conditions, but in condition 1 is below threshold for condition 2
no	no	-	-	5	Detected in neither condition

For the preceding table, the .ALL file that is first in the argument list is considered to be the experimental condition, and the second .ALL in the argument list is the baseline condition.  $T_{\text{expt}}$  and  $T_{\text{base}}$  refer to the detection threshold in the experimental condition and the baseline condition, respectively. If there are MM probes among the features for an ORF which are not unique in the genome, this fact is indicated, and the calculation is based on the median of PM-ratios rather than the median of  $\Delta$ -ratios.

Applications for analyzing upstream noncoding DNA sequences. The following is a summary table of upstream sequence analysis applications:

Application	Input Files	Output File	Purpose
-------------	-------------	-------------	---------

pickup	.up, Sc_table, yeastseq	.dat	selects upstream regions from yeast sequence
makeseqfile	.ascii	yeastseq	concatenates a set of SGD raw sequence files w/o line feeds
AlignACE	.dat	.out	finds and aligns conserved sequences
make_LGO_files	.out	.LGO	creates logos from gibbs output file
make_aln_files	.out	.aln	extracts set of aligned sites from gibbs into FASTA format
matrix_comp	.aln	.cmp	assesses similarity between sets of aligned sites
find_consensus	.aln	.cns	gets consensus sequence for aligned sites
scoresites	.out	.sco	finds sites matching an aligned sequence set
assignsites	.sco	.ass,.as2	assigns each site upstream of coding regions to its ORF(s)
mergeORFs	.DIF,.as2	.MRG	takes a list of ORFs ranked by expression and merges with site info

## ‘pickup’

Usage: “pickup yeastseq?? Sc\_table?? [-l ?.up] [-r #ofrandom]  
[-m widthmin] [-w widthmax] [-c]”.

Example: “pickup yeastseq8\_97 Sc\_table9\_97 -l coolORFs.up -o  
coolORFs.dat -m 300 -w 600”.

This application returns a FASTA-format file containing upstream non-coding regions, given an input (.up) file with a list of ORF names, e.g., YJL052W. All of the work described in this thesis used yeastseq8\_97 and Sc\_table9\_97, which are the raw DNA sequence and ORF tables from *S. cerevisiae* as obtained from SGD. The program can be used without an input file to generate an upstream sequence file from randomly chosen ORFs. The upstream region is delimited at one end by the translation start of the ORF specified and at the other end by the start or stop of the nearest upstream ORF, except where a minimum or maximum upstream sequence length is specified. The -c option can be used to generate both forward and reverse strands of the upstream

sequence. If two ORFs which share an upstream region are listed in the input file, that upstream sequence is returned without duplication of sequence.

### **‘makeseqfile’**

Usage: “makeseqfile ?? [-s seqdir]”.

Example: “makeseqfile yeastseq8\_97 -s ~/yeast/all\_raw/”.

This program takes a set of raw sequence files (one per chromosome) that have been obtained from SGD and are in the specified directory, concatenates them and writes them into one file. Line feeds are removed for faster loading of raw sequence data by the program ‘pickup’.

### **‘AlignACE’**

Usage: “AlignACE [-? -? -? ...]”.

Example: “gibbs -w10 -x10 -t500 -r100 -u50 -q3 -igoodORFs.dat -ogoodORFs.out”.

This is an application which finds conserved motifs among DNA (or RNA) sequence. The ‘.dat’ input file contains the sequence data to be examined in FASTA format. Differences between this application and Gibbs Motif Sampling are described in Chapter 3.

AlignACE performs a series of motif searches. After each successful motif search, bases at the most information-rich position in the discovered motif are ‘masked out’ so that they cannot be found in subsequent motif searches. We call this an iterative masking approach.

Each motif search consists of a series of ‘sampling runs’, after which the highest scoring motif found thus far is further optimized in a ‘near-optimum sampling run’.

Each run consists of a ‘column sampling step’, a ‘pass’ through the input sequence, and a recalculation of the motif (or ‘MAP’) score. If the MAP score is higher than any previously encountered in the current run, the current alignment is saved.

When column sampling is employed, only the number of columns (sequence positions) specified is used to optimize the alignment, even though the element may span a larger number of bases (e.g., the Gal4 binding site spans 17 bases even though only about 8 bases show conservation).

The command line options for AlignACE are summarized in the table below.

Switch	Default Value	Description
-c	1	Number of cycles per column shift
-d	-	Turn off column sampling
-e	<i>stderr_outfile</i>	Save debugging information to a file
-f	0.1	Ratio of pseudocounts to real counts
-i	none	Input file name
-m	3× (#columns)	Maximum width of site
-n	500	Number of iterations of near-optimum sampling
-o	<i>infileoptions.out</i>	Output file name
-p	0.8	Fractional weight on prior expectation of # of sites
-q	10	Exit after this number of failed motif searches
-r	10	Maximum total number of iteratively masked motif searches
-s	100	Cease sampling run after this many passes without improvement
-t	100	Maximum number of sampling runs in motif search
-u	100	Cease motif search after this many sampling runs without improvement
-w	10	Number of columns (maximum number of conserved positions expected)
-x	10	Expected # of elements in input sequence data
-z	-	Show stderr output

### **‘make\_LGO\_files’**

Usage: “`make_LGO_files ? .out [-r ?] [-n]`”.

Example: “`make_LGO_files goodORFs.out -r 10`”.

This application is a front end for a set of programs developed by Tom Schneider for generating sequence logos (described in Chapter 3). The input is a .out file generated by AlignACE, and the output is a set of .LGO files containing logos in postscript format. Run numbers 1 through the maximum specified by the -r switch are used to make logos (the default is all motifs in the AlignACE file). The -n switch is used to specify that the name of the file not be included next to the logo image.

#### **‘make\_aln\_files’**

Usage: “make\_aln\_files ? .out [-r ?]”.

Example: “make\_aln\_files goodORFs.out -r 10”.

This application parses a AlignACE output file (.out) and writes each motif to a separate output (.aln) file. The .aln file is a FASTA format file containing the sites aligned by AlignACE. The -r switch is used to limit the number of motifs parsed.

#### **‘matrix\_comp’**

Usage: “matrix\_comp A.aln B.aln [C.aln D.aln etc.]”.

Example: “matrix\_comp \*.aln”.

This application takes as input a set of .aln files (FASTA format files containing aligned sites). By a process outlined in Appendix B, each set of aligned sites is compared against every other set, and the resulting similarity score (best t statistic) is printed out for matrices which are found to be similar. Currently, the default output is printed to the screen, but this can be redirected to an output file, e.g. “matrix\_comp \*.aln > all\_against\_all.cmp”.

#### **‘find\_consensus’**

Usage: “find\_consensus A.aln [C.aln D.aln etc.] [-a]”.

Example: “`find_consensus *.aln`”.

This application takes as input one or more .aln files (FASTA format files containing aligned sites). By the method of Day and McMorris, a consensus sequence is determined for each set of aligned sites. Currently, the default output is printed to the screen, but this can be redirected to an output file, e.g. “`find_consensus *.aln > all.cns`”.

### **‘scoresites’**

Usage: “`scoresites ? .out ? [-t Sc_table??] [-s yeastseq??]`  
[`-o ?`] [`-z ?`] [`-d`]”.

Example: “`scoresites goodORFs.out 2 -t Sc_table9_97 -s yeastseq8_97 -d -z 0`”.

This application takes as input a AlignACE (.out) output file, a table of ORFs, and a raw sequence file. It creates a weight matrix by the Berg and von Hippel method described in Appendix B, and scores every site in the raw sequence file. This weight matrix is also used to score each of the aligned sites from which the weight matrix was derived. Based on the mean and standard deviation of the aligned site scores, a threshold score can be set such that only scores better than this threshold will be recorded. The -z switch is used to set this threshold: A -z switch setting of ‘0’ corresponds to a threshold equal to the mean score of the aligned sites, while a -z setting of 3 corresponds to 3 standard deviations below (worse) than the mean of the aligned sites. The -o switch can be used to specify the name of the output file (default is a .sco file of the same prefix as the input file). ‘scoresites’ saves the distribution of scores across the whole genome, unless the -d switch is applied.

### **‘assignsites’**

Usage: “`assignsites ?.sco [-t Sc_table??] [-w ?]  
[-n ?] [-z ?] [-d]`”.

Example: “`assignsites goodORFs.sco -t Sc_table9_97 -w 600 -n  
50 -z 0`”.

This application takes as input a ‘.sco’ file produced by ‘scoresites’ which contains high-scoring sites matching a motif found by ‘AlignACE’. Each site is examined and if it lies within 600 bases (or some other distance specified with the -w switch) upstream of an ORF’s translation start, the site is assigned to that ORF. A site may be assigned to more than one ORF, as will be the case if the site lies within a divergent intergenic region. The output is saved in both of two alternative formats in .ass and .as2 files.

The -n switch is used to limit the output to the specified number of top-ranked ORFs. The -z switch is used to only consider sites better than a certain threshold, and is used in the same way as ‘scoresites’, described above. The -d switch is used to automatically fetch brief descriptions of the top-ranked ORFs from the web sites of YPD, SwissProt, and MIPS. This should be avoided unless the list of ORFs is short, as this can be time-consuming and may be considered an unfriendly act by the managers of the databases being accessed.

### **‘mergeORFs’**

Usage: “`mergeORFs ?.DIF ?.as2 [?.as2 ?.as2...] [-o OUTFILE]`”.

Example: “`mergeORFs GAL,GLU.DIF goodORFs.as2`”.

This application merges a .as2 file with a .DIF file, so that each ORF in a .DIF file is associated with the number of upstream matching sites and the highest score of its upstream sites.

## Appendix B

### Method for Quantitatively Assessing Similarity Between Intergenic DNA Element Motifs

Since much of this appendix is concerned with weight matrices as a representation of an aligned set of DNA sequences, I will first devote some attention to weight matrices. A weight matrix of size  $4 \times L$  can be used to described a set of sites of maximum length L. There are four rows since there are four nucleotides. Elements of the matrix are measures of the propensity of a ‘real’ site (one which is presumably bound by a DNA-binding protein) to have a given base at a given position. This matrix can then be used to assign an objective score to any DNA sequence, where the score reflects the similarity of that sequence to the set of aligned sequences. A number of methods have been used for deciding what values to put in each of the matrix elements. The method we used for building weight matrices throughout this work was that of Berg and von Hippel

<sup>1</sup>, wherein each element is given by  $\ln\left(\frac{n(b, p) + 0.5}{n_{\max}(p) + 0.5}\right)$ . Here,  $n(b,p)$  is the number of occurrences of base b at position p in the set of aligned sites, and  $n_{\max}$  is the number of occurrences of the most commonly occurring base at position p. The result of this equation is that the most common base at a position is given weight 0, while less common bases are given increasingly negative weights. The addition of 0.5 in the numerator and denominator is a pseudocount, which has the effect of lessening the penalty for bases that do not occur in the aligned sites. The reduction in penalty is most dramatic in cases where the matrix has been generated from very few aligned sites. If a base occurs commonly in upstream regions, we may want to adjust the score to reflect this. Imagine a case where ten examples of the sequence AAAAAAA have been aligned to generate a weight matrix. It would hardly be surprising to find a sequence matching this matrix in a 95% AT genome, but it would be very surprising to find matches to this matrix in a 5%

AT genome. The matrix weights can be adjusted based on the background nucleotide frequency in upstream regions, i.e., the prior probability of a base's occurrence, by adding  $\ln\left(\frac{f_{bkg}(b)}{f_{max}}\right)$  to each matrix element, where  $f_{bkg}(b)$  is the background frequency of the base b corresponding to the matrix element and  $f_{max}$  is the background frequency of the most common base.

Along with developing methods for discovery of regulatory sequence elements, a major goal of the work described in Chapter 3 was to validate these methods. For this purpose, yeast growth conditions and/or genotypes were chosen where we might predict the outcome. In other words, conditions were chosen where we already knew which upstream sequence motifs we might expect *a priori*. Having obtained a set of sequence motifs by the ‘AlignACE’ method of sequence alignment and the specificity scoring approach, we must then ask, “Did we find the motifs we expected”. It would be all too easy to simply look at a motif and conclude that it ‘looks like’ the motif we expected, and in some cases this would be perfectly reasonable and reliable. It is in the borderline cases of similarity where a visual examination is subject to the risk of a bias based on expectations. When confronted with the need for an objective method for quantifying similarity between two sets of DNA elements, I was surprised to discover that no such method existed in the literature.

The problem of comparing two sets of aligned sites can be separated into two parts. The first part is alignment of the two motifs or site sets with each other. I viewed this problem as equivalent to aligning two weight matrices. To achieve this, I simply tried all possible alignments of the two matrices with each other. For each alignment, I

calculated the sum of the squared differences between corresponding matrix elements.

The alignment which minimized the sum of the squared differences is then the best alignment. You may have noticed a difficulty with this approach. How do we handle the fact that matrices may be of a different width, since they may represent aligned sequences of differing widths? How do we handle the fact that even matrices of the same width will overhang one another in all but one possible alignment? At overhanging positions there will be 'missing' elements in one of the matrices. For these 'missing' elements, I use the expectation value of elements, given the known background nucleotide frequencies. The matrix elements are then just the background frequency adjustment used above:

$\ln\left(\frac{f_{\text{bkg}}(b)}{f_{\text{max}}}\right)$ . A weight matrix is also calculated for the reverse complement of one set of aligned sites, and all possible alignments are scored as above so that the best alignments of two sets of sites are chosen from either forward or reverse complement orientations.

The second step of motif comparison is quantitating similarity between the now-aligned sets of sites. The general approach is to reduce this problem to that of comparison of two distributions of numbers. There are accepted measures of similarity between two distributions in classical statistics. One such measure which is commonly

used is Student's t-statistic,  $t = \frac{\mu_1 - \mu_2}{s\sqrt{1/N_1 + 1/N_2}}$ , where  $\mu_1$  and  $\mu_2$  are the means of the

two distributions,  $N_1$  and  $N_2$  are the number of samples in each distribution, and

$s = \sqrt{\frac{N_1 \cdot s_1^2 + N_2 \cdot s_2^2}{N_1 + N_2 - 2}}$ , where  $s_1$  and  $s_2$  are the standard deviations of the two

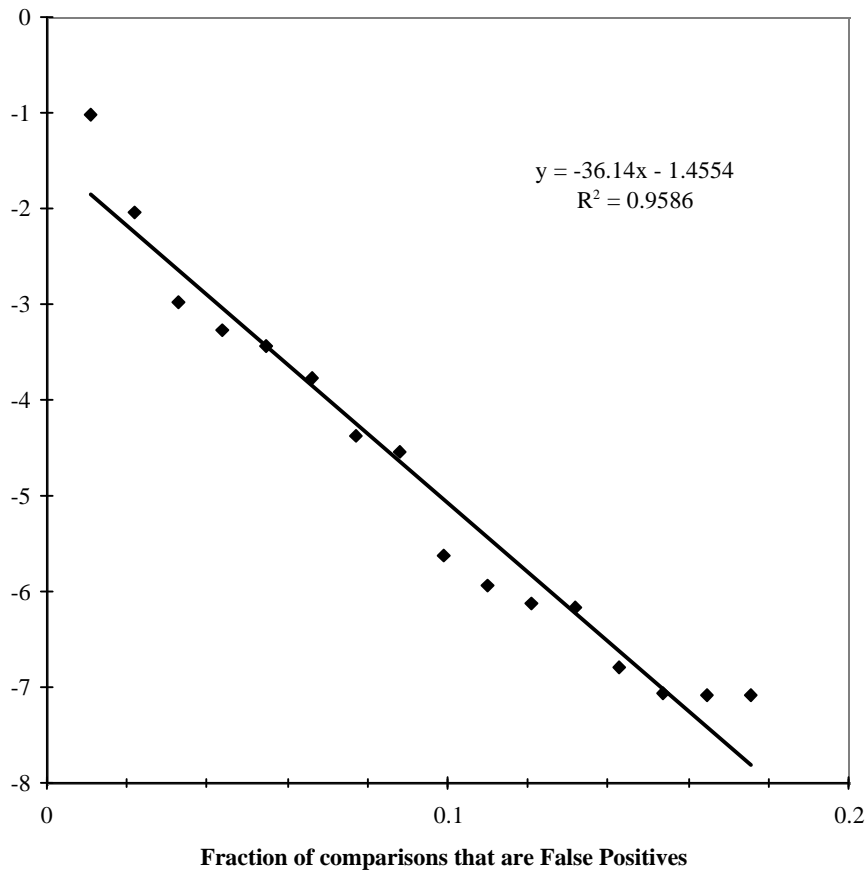
distributions. The smaller the absolute value of the t-statistic, the more similar the two distributions.

The question remaining is how to assign a number (score) to each site, and then how to decide on a value of t that indicates a significant similarity. Consider sets of sites A and B and their corresponding weight matrices A and B. After aligning matrix A and matrix B, we can define two submatrices A and B of equal width by taking the overlapping portions of each matrix. Using submatrix A, we can assign a score to each A sequence and each B sequence, and calculate the t-statistic for the two scores. Likewise, we can calculate a t-statistic for the scores of A sites and B sites generated using submatrix B. The measure of similarity between matrix A and matrix B is then  $t_{min}$ , the t-statistic with the smallest absolute value.

How then do we assign a threshold for  $t_{min}$ , below which the two matrices are considered similar? In Chapter 3, we described fifteen regulatory motifs that we might have expected from the literature. Sites corresponding to these motifs were derived from the literature, and weight matrices were generated for each. These fifteen sets of DNA elements provided 105 ( $\frac{15 \cdot 14}{2}$ ) that can serve as negative controls, since I did not expect any of these motifs to be similar to one another. I calculated a t-statistic such that a false positive rate of 5% is expected, and was surprised to see that the ECB and P-Box motifs had a  $t_{min}$  which was well below the calculated threshold of similarity. The reason for this similarity became apparent on further examination: ECB and P-Box elements are both bound by the same transcription factor Mcm1, so that I should in fact have expected the motifs to be similar. After removing one of these motifs, the P-Box, from the

negative control set, I was left with 91 pairwise comparisons as negative controls with which to calculate a threshold for  $t_{\min}$ . The graph below shows the fraction of these pairwise comparisons deemed similar, based on different possible thresholds of  $t_{\min}$ . By linear interpolation, a 5% false positive rate was achieved using a  $t_{\min}$  of -3.26.

**Fraction of Negative Control Comparisons Deemed Similar for Various Cutoffs Threshold of Best t-Value**



In addition to the criteria above, we also require that the best alignment of sites has an overlap of at least five bases, since DNA regulatory sites generally have more than five conserved positions.

## References.

1. **Berg, O.G. and von Hippel, P.H.**, Selection of DNA binding sites by regulatory proteins. Statistical-mechanical theory and application to operators and promoters, *Journal of Molecular Biology*, 193(4), 723-750, 1987.

## Appendix C

Absolute and Relative Abundance of Detectable Transcripts  
in Four *Saccharomyces cerevisiae* Cultures Organized  
Alphabetically by ORF Identifier.

This appendix contains a table of those absolute and relative transcript abundances that were detectable in at least one of four *Saccharomyces cerevisiae* cultures. The genotype and growth conditions of these cultures are described in Chapter 3, as are the method of data collection, background subtraction and normalization. Since I took only one approach of many towards analyzing this rich data set in Chapter 3, it is my hope that this appendix will serve as a resource to others in the future.

In addition to conclusions drawn from this data in Chapter 3, there are minor observations drawn from this data with regard to ‘housekeeping’ genes commonly used as standards in Northern mRNA quantitation experiments. Transcripts for TBP (YER148W; TATA-binding protein, also known as SPT15 or TFIID), ACT1 (YFL039C; actin), SRB4 (YER022W; subunit of RNA polymerase II holoenzyme), and PDA1 (YER178W; subunit of pyruvate dehydrogenase) are commonly used standards for quantitating mRNA. Neither TBP nor SRB4 were above detection threshold in all of our experiments, so that these are not useful standards for our data. The absolute abundance of ACT1 is more promising as a standard, in that it is well above detection threshold in all conditions and its measured absolute abundance varies by only about 20% at most (between mating type  $\alpha$  and heat-shock). Measured absolute abundance of PDA1 was above detection threshold in all conditions but was low in galactose (more than seven-fold lower than in heat-shock). This is surprising, given that PDA1 transcript level has been cited as being more invariant to varying growth conditions than that of ACT1<sup>1</sup>. The RPS2 gene (YGL123W; also known as RPS4 or SUP44) is one of few genes whose absolute transcript abundance has been reliably quantitated. It was found to be at  $28 \pm 5$  copies per cell under growth conditions similar to those for our ‘baseline’ culture (glucose minimal

medium without casamino acids grown at 30 °C to mid-log phase)<sup>2</sup>. Measured in the absolute abundance units of the table below, RPS2 has an absolute abundance of 7.1 in our ‘baseline’ (mating type **a**, glucose, 30 °C) condition. Based on this, 0.25 absolute abundance units corresponds roughly with a single transcript per cell. This is necessarily approximate since growth conditions and strains varied..

Guide to abundance table. The first column in the abundance table (“ID”) contains—excepting the ribosomal RNA genes at top—the ORF identifier as issued by the Saccharomyces Genome Database. An ORF identifier printed in italics indicates that the sequence of some of the mismatch probes for this ORF were not unique in the *cerevisiae* genome. In this case PM values were substituted for Δ values in calculating absolute and relative abundance, so that the quantitation for these ORFs should be viewed more critically.

The second column (“Gene”) contains the common gene names corresponding to each ORF identifier. The gene names were taken from the current (10 April 98) SGD table of gene names.

The third column (“Chip”) indicates which of the four Affymetrix microarrays contain the probe pairs corresponding to this transcript. Some transcripts are measured on all four of the microarrays, so that they are labeled “A-D”.

The fourth column (“#PP”) is the number of probe pairs corresponding to this transcript contained on the microarrays. Most transcripts employed 20 or 21 probe pairs but a few ‘housekeeping’ genes, namely YFL039C (ACT1), YER 148W (SPT15), and

YER022W (SRB4) employed many more probe pairs and were measured on all four microarrays in each condition.

The fifth through the eighth columns (“**a**”, “ $\alpha$ ”, “gal”, and “heat”) contain absolute transcript abundances. These values are calculated by taking the median of normalized  $\Delta$  values. If the central-most  $\Delta$  value—or either of the central-most  $\Delta$  values in cases where there is an even number of  $\Delta$  values—in a ranked list is below detection threshold (described in Chapters 2 and 3) then a transcript is considered to be below detection threshold. Transcripts which fell below the detection threshold of the corresponding hybridization experiment are indicated by abundance values in italics. In this case,  $\Delta$  values used to calculate the abundance value were adjusted to the detection threshold if they fell below it.

The last three columns (“log ( $\alpha/a$ )”, “log (gal/a)” and “log (heat/a)”) contain transcript abundances relative to the ‘**a**’ culture—strain FY4 (MAT **a**), grown on glucose at 30 °C. These values are calculated by taking the median of the log-ratios of normalized  $\Delta$  values. If any of the  $\Delta$  values used to calculate the ratios of the central-most  $\Delta$  ratio value(s) in a ranked list are below detection threshold (described in Chapters 2 and 3) then a transcript is considered to be below detection threshold in one or both of the conditions being compared. Transcripts considered below detection threshold in one or both conditions being compared are indicated by median log  $\Delta$ -ratio values in italics. If a transcript is below detection threshold in both conditions being compared, the median log  $\Delta$ -ratio is set to zero.

For each of the relative abundance values, a measure of significance is calculated by dividing the median log  $\Delta$ -ratio by the median deviation of log  $\Delta$ -ratios. If this measure of significance is one or greater, and the median log  $\Delta$ -ratio is 0.2 or greater, the median log  $\Delta$ -ratio value is in bold type.

The following table contains abundance values for 3399 *Saccharomyces cerevisiae* ORFs. Appendix D contains a list of those ORFs which both fell below detection threshold in all four cultures measured and were not measurably changed between pairs of conditions, along with a list of ORFs not represented on the microarray set. Appendix D also contains a table of detection thresholds for each microarray assayed.

### Absolute and Relative Abundance of Transcripts in Four Assayed Cultures

ID	Gene	Chip	#PP	a	$\alpha$	gal	heat	log ( $\alpha/a$ )	log (gal/a)	log (heat/a)
18srRnaa		A-D	84	0.17	0.12	0.16	0.15	0	-0.12	0
18srRnab		A-D	80	0.11	0.09	0.09	0.1	0	0	0
25srRnaa		A-D	84	1.54	1.02	0.32	0.84	-0.17	<b>-0.51</b>	<b>-0.22</b>
25srRnab		A-D	80	0.11	0.08	0.07	0.09	-0.1	0	0
25srRnac		A-D	84	0.11	0.08	0.07	0.09	<b>-0.2</b>	0	0
25srRnae		A-D	84	0.35	0.26	0.25	0.24	0.08	0	0
YAL003W	EFB1	A	41	1.58	1.47	1.28	1.01	-0.1	-0.12	-0.18
YAL005C	SSA1	A	20	1.37	0.99	1.38	2.42	<b>-0.29</b>	-0.04	<b>0.21</b>
YAL007C		A	20	0.26	0.16	0.22	0.13	-0.13	-0.04	-0.11
YAL008W	FUN14	A	20	0.18	0.15	0.14	0.16	-0.14	-0.2	-0
YAL009W	SPO7	A	21	0.09	0.04	0.07	0.09	0	0	0
YAL012W	CYS3	A	20	1.53	1.72	1.19	1.42	0.03	-0.12	0
YAL014C		A	21	0.15	0.12	0.1	0.09	<b>-0.22</b>	0	0.01
YAL016W	TPD3	A	20	0.32	0.23	0.26	0.31	-0.1	-0.04	0.01
YAL017W	FUN31	A	20	0.09	0.05	0.07	0.09	0	0	0
YAL019W	FUN30	A	20	0.09	0.04	0.07	0.09	0	0	0
YAL021C	CCR4	A	20	0.09	0.08	0.1	0.09	0	0	0
YAL022C	FUN26	A	20	0.1	0.08	0.08	0.09	-0.15	0	0
YAL023C	PMT2	A	21	0.38	0.29	0.29	0.24	<b>-0.23</b>	0	-0.08
YAL027W		A	21	0.09	0.05	0.07	0.09	0	0	0
YAL030W	SNC1	A	42	0.42	0.29	0.31	0.27	-0.13	-0.07	-0.1
YAL033W	FUN53	A	20	0.13	0.12	0.1	0.09	-0.17	0	0
YAL035W	FUN12	A	21	0.26	0.18	0.21	0.14	-0.15	0	0
YAL036C	FUN11	A	21	0.09	0.1	0.11	0.09	-0.1	0.02	0
YAL038W	CDC19	A	20	7.32	4.36	4.35	5.25	-0.11	<b>-0.26</b>	-0.1
YAL039C	CYC3	A	20	0.22	0.11	0.16	0.15	<b>-0.26</b>	0	-0.09
YAL040C	CLN3	A	21	0.12	0.09	0.14	0.09	-0.16	0	0
YAL042W	FUN9	A	20	0.2	0.19	0.19	0.17	-0.01	0	-0
YAL043C	PTA1	A	21	0.09	0.05	0.07	0.09	0	0	0
YAL044C	GCV3	A	20	0.83	0.52	0.71	1.13	-0.11	-0.12	0.09
YAL045C		A	21	0.09	0.04	0.07	0.09	0	0	0
YAL046C		A	20	0.16	0.07	0.15	0.14	0	0	0
YAL049C		A	20	0.36	0.32	0.49	0.87	-0.05	0.05	<b>0.24</b>
YAL051W	YAF1	A	21	0.09	0.04	0.07	0.09	0	0	0
YAL053W		A	20	0.14	0.07	0.17	0.12	0	0.06	0
YAL054C	ACS1	A	21	0.09	0.04	0.08	0.09	0	0	0
YAL055W		A	21	0.09	0.04	0.07	0.09	0	0	0
YAL056W		A	20	0.09	0.05	0.07	0.09	0	0	0
YAL060W		A	21	0.56	0.17	0.66	0.48	0	-0.03	0
YAL061W		A	21	0.46	0.16	0.28	1.07	<b>-0.45</b>	-0.1	<b>0.32</b>
YAL062W	GDH3	A	20	0.09	0.08	0.09	0.09	0	0	0
YAL063C		A	20	0.09	0.1	0.07	0.09	0.06	0	0
YAL068C		A	20	0.24	0.21	0.26	0.17	<b>-0.21</b>	0	-0.1
YAR002AC		A	20	0.56	0.57	0.72	0.43	-0.09	-0.02	-0.1
YAR003W		A	20	0.09	0.09	0.07	0.11	0	0	0.09
YAR007C	RFA1	A	20	0.09	0.05	0.07	0.09	0	0	0
YAR009C		A	46	0.56	0.31	0.5	0.97	-0.13	-0.03	<b>0.32</b>
YAR010C		A	20	0.12	0.08	0.16	0.23	0	-0.01	<b>0.21</b>
YAR015W	ADE1	A	20	0.12	0.05	0.19	0.15	0	0.01	0
YAR020C		A	20	0.26	0.11	0.2	0.16	0	0	-0.05

YAR023C		A	21	0.09	0.04	0.08	0.09	0	0	0
YAR027W		A	21	0.29	0.22	0.17	0.16	<b>-0.21</b>	0	0.01
YAR028W		A	20	0.09	0.08	0.08	0.11	0	0	0
YAR033W		A	24	0.09	0.06	0.07	0.09	0	0	0
YAR035W	YAT1	A	21	0.13	0.11	0.1	0.09	-0.17	0	-0.1
YAR042W	SWH1	A	21	0.1	0.15	0.07	0.09	0	-0.1	-0
YAR066W		A	20	0.09	0.06	0.12	0.09	0	0	0
YAR071W	PHO11	A	20	0.09	0.05	0.07	0.09	0	0	0
YAR073W		A	22	0.11	0.04	0.08	0.09	0	0	-0
YAR075W		A	20	0.22	0.22	0.2	0.16	0	0	-0.13
YBL001C	ECM15	A	20	0.51	0.24	0.54	0.7	-0.13	0	<b>0.26</b>
YBL002W	HTB2	A	20	2.74	2.63	1.92	0.73	0.08	-0.08	<b>-0.48</b>
YBL003C	HTA2	A	16	1.31	1.11	1.39	0.47	-0.05	-0.01	<b>-0.48</b>
YBL005W	PDR3	A	21	0.09	0.05	0.07	0.09	<b>-0.25</b>	0	0
YBL006C		A	21	0.19	0.12	0.16	0.15	<b>-0.23</b>	0	-0.02
YBL007C	SLA1	A	21	0.16	0.13	0.17	0.14	<b>-0.24</b>	0	0
YBL011W	SCT1	A	20	0.13	0.06	0.1	0.1	0	0	0
YBL015W	ACH1	A	21	0.46	0.11	0.66	0.14	<b>-0.44</b>	0.17	<b>-0.33</b>
YBL016W	FUS3	A	20	0.11	0.06	0.07	0.09	-0.18	0	0
YBL017C	PEP1	A	21	0.09	0.06	0.15	0.12	-0.19	0	0
YBL021C	HAP3	A	20	0.09	0.04	0.08	0.09	0	0	0
YBL022C	PIM1	A	20	0.11	0.08	0.1	0.11	0	0	0
YBL024W		A	21	0.09	0.1	0.07	0.09	-0.14	0	0
YBL025W	RRN10	A	21	0.09	0.1	0.07	0.1	0.04	0	0
YBL026W	SNP3	A	36	0.09	0.04	0.08	0.09	0	0	0
YBL027W	RPL19B	A	54	0.64	0.57	0.37	0.23	-0.06	0	<b>-0.3</b>
YBL030C	PET9	A	20	2.41	1.44	2.61	1.98	-0.19	0	<b>-0.2</b>
YBL032W		A	20	0.17	0.11	0.13	0.09	0	0	-0.12
YBL033C	RIB1	A	21	0.13	0.05	0.28	0.15	0	<b>0.26</b>	0
YBL034C	STU1	A	21	0.09	0.04	0.07	0.09	0	0	0
YBL038W	MRPL16	A	21	0.09	0.1	0.13	0.09	<b>-0.23</b>	-0.08	0
YBL039C	URA7	A	20	0.11	0.14	0.11	0.1	-0.1	0	0
YBL040C	ERD2	A	20	0.24	0.12	0.18	0.11	<b>-0.27</b>	0	-0.2
YBL041W	PRE7	A	20	0.26	0.11	0.16	0.24	<b>-0.28</b>	0	0
YBL042C	FUI1	A	20	0.1	0.04	0.12	0.11	0	0.01	0
YBL043W	ECM13	A	21	0.09	0.05	0.07	0.09	0	0	0
YBL045C	COR1	A	21	0.4	0.17	0.78	0.33	<b>-0.37</b>	0.18	-0.11
YBL047C		A	20	0.09	0.05	0.09	0.09	0	0	0
YBL048W		A	21	0.09	0.04	0.07	0.18	0	0	<b>0.29</b>
YBL049W		A	20	0.09	0.06	0.07	0.1	0	0	0
YBL050W	SEC17	A	20	0.1	0.18	0.17	0.16	-0.05	-0.08	0
YBL051C		A	20	0.09	0.07	0.07	0.09	0	0	0
YBL053W		A	21	0.09	0.15	0.07	0.09	0.01	0	0
YBL055C		A	20	0.09	0.04	0.1	0.09	0	0	0
YBL056W	PTC3	A	20	0.09	0.05	0.09	0.09	0	0	0
YBL057C		A	20	0.09	0.06	0.07	0.09	0	0	0
YBL058W	SHP1	A	21	0.21	0.05	0.15	0.21	0	0	0
YBL063W	KIP1	A	20	0.09	0.04	0.07	0.09	0	0	0
YBL064C		A	20	0.34	0.18	0.73	0.54	<b>-0.2</b>	0.14	0.09
YBL068W	PRS4	A	21	0.25	0.24	0.22	0.22	0	0	-0.01
YBL069W	AST1	A	21	0.09	0.04	0.07	0.1	0	0	0
YBL071C		A	21	0.09	0.05	0.07	0.09	0	0	0
YBL072C	RPS8A	A	16	23.04	18.06	17.16	7.03	-0.13	-0.13	<b>-0.49</b>
YBL076C	ILS1	A	20	0.41	0.48	0.37	0.4	0.06	-0.06	0
YBL077W		A	20	0.09	0.06	0.07	0.09	0	0	0

YBL078C		A	20	0.09	0.05	0.11	0.13	0	0	0.05
YBL081W		A	21	0.09	0.08	0.08	0.09	<b>-0.2</b>	0	0
YBL082C	RHK1	A	20	0.09	0.05	0.08	0.09	0	0	0
YBL083C		A	26	0.2	0.13	0.23	0.1	-0.19	-0.04	-0.1
YBL084C	CDC27	A	20	0.09	0.05	0.08	0.09	0	0	0
YBL085W	BOI1	A	21	0.09	0.06	0.07	0.09	-0.16	0	0
YBL087C	RPL23A	A	53	2.07	1.37	1.01	2.2	-0.2	<b>-0.4</b>	-0.11
YBL089W		A	21	0.09	0.06	0.07	0.12	<b>-0.26</b>	0	0
YBL091C	MAP2	A	20	0.41	0.37	0.42	0.36	0	-0.04	0
YBL092W	RPL32	A	20	3.47	2.96	2.1	1.7	-0.06	<b>-0.22</b>	<b>-0.32</b>
YBL099W	ATP1	A	21	1.71	0.68	1.2	1.02	0	0.01	-0.12
YBL101C	ECM21	A	21	0.12	0.09	0.07	0.14	<b>-0.3</b>	0	0
YBL101W-A		A	20	0.09	0.05	0.08	0.1	0	0	0
YBL102W	SFT2	A	21	0.51	0.35	0.42	0.3	-0.16	0	0.02
YBL103C	RTG3	A	21	0.09	0.04	0.07	0.09	0	0	0
YBL106C	SNI2	A	21	0.09	0.04	0.07	0.09	0	0	0
YBL112C		A	20	0.09	0.08	0.07	0.1	0	0	0
YBL113C		A	24	0.75	0.49	0.53	0.69	-0.14	0	0.03
YBR001C	NTH2	A	20	0.09	0.04	0.08	0.11	0	0	0
YBR004C		A	21	0.15	0.14	0.16	0.19	-0.11	-0.08	0
YBR005W		A	20	0.36	0.2	0.23	0.13	0	0	0
YBR006W		A	20	0.12	0.04	0.1	0.28	0	0	0.16
YBR008C	FLR1	A	21	0.33	0.24	0.16	0.28	-0.18	<b>-0.23</b>	-0.1
YBR009C	HHF1	A	20	1.7	1.06	1.47	0.55	-0.11	-0.09	<b>-0.4</b>
YBR010W	HHT1	A	20	5.04	3.84	5.29	1.29	-0.11	-0.02	<b>-0.53</b>
YBR011C	IPP1	A	20	1.17	0.63	0.41	1.46	<b>-0.46</b>	<b>-0.58</b>	0.01
YBR012W-A		A	20	0.21	0.17	0.25	0.57	-0.14	0.01	<b>0.36</b>
YBR012W-B		A	40	0.09	0.09	0.19	0.22	0	0.01	0
YBR013C		A	21	0.09	0.04	0.09	0.09	0	-0.09	0
YBR014C		A	21	0.09	0.13	0.14	0.15	0.01	0.02	0
YBR015C	TTP1	A	21	0.11	0.07	0.07	0.13	<b>-0.26</b>	0	0
YBR016W		A	21	0.96	0.6	0.77	0.68	<b>-0.22</b>	-0.16	-0.15
YBR018C	GAL7	A	21	0.09	0.04	3.59	0.09	0	<b>1.62</b>	0
YBR019C	GAL10	A	20	0.09	0.04	3.24	0.09	0	<b>1.57</b>	0
YBR020W	GAL1	A	21	0.09	0.04	7.12	0.09	0	<b>1.81</b>	0
YBR022W		A	20	0.1	0.04	0.07	0.09	0	0	0
YBR023C	CHS3	A	21	0.11	0.13	0.07	0.13	-0.01	0	0.04
YBR024W	SCO2	A	21	0.09	0.05	0.07	0.09	0	0	0
YBR025C		A	21	0.75	0.76	0.72	1.06	0.01	-0.08	0.07
YBR026C	MRF1'	A	20	0.09	0.1	0.09	0.21	0	0	<b>0.22</b>
YBR028C		A	20	0.09	0.04	0.08	0.09	0	0	0
YBR029C	CDS1	A	21	1.12	1.09	0.89	0.84	-0.07	-0.07	-0.13
YBR031W	RPL4A	A	20	17.42	15.97	11.76	11.71	-0.04	-0.14	-0.14
YBR034C	HMT1	A	20	0.1	0.1	0.11	0.1	0	0.05	0
YBR035C	PDX3	A	20	0.48	0.35	0.54	0.44	-0.14	0.06	0.06
YBR036C	CSG2	A	20	0.62	0.44	0.38	0.57	-0.16	-0.1	-0
YBR037C	SCO1	A	20	0.1	0.05	0.08	0.11	0	0	0
YBR038W	CHS2	A	20	0.09	0.05	0.1	0.09	0	0	0
YBR039W	ATP3	A	21	0.65	0.41	0.98	0.63	-0.09	0.19	-0.07
YBR041W	FAT1	A	20	0.31	0.23	0.18	0.23	-0.16	-0.11	0
YBR042C		A	20	0.1	0.11	0.15	0.13	0	0	0
YBR043C		A	20	0.1	0.04	0.07	0.09	0	0	0
YBR046C	ZTA1	A	20	0.31	0.2	0.14	0.46	-0.13	<b>-0.1</b>	<b>0.16</b>
YBR048W	RPS11B	A	84	0.32	0.37	0.37	0.31	0.02	0	-0.02
YBR049C	REB1	A	20	0.09	0.07	0.07	0.09	0	0	0

YBR050C	REG2	A	21	0.09	0.04	0.08	0.09	0	0	0
YBR052C		A	20	0.69	0.34	0.68	0.93	<b>-0.2</b>	-0.07	0.11
YBR053C		A	21	0.32	0.29	0.31	0.55	-0.15	-0.06	0.15
YBR054W	YRO2	A	21	1.05	0.91	0.85	2.94	-0.16	-0.17	<b>0.39</b>
YBR056W		A	20	0.12	0.05	0.1	0.16	0	0	0
YBR058C	UBP14	A	20	0.09	0.08	0.07	0.09	<b>-0.23</b>	0	0
YBR061C		A	21	0.09	0.06	0.15	0.09	0	0.11	0
YBR062C		A	20	0.23	0.2	0.22	0.36	-0.04	0	0.18
YBR063C		A	21	0.09	0.06	0.07	0.1	0	0	0
YBR066C		A	20	0.09	0.05	0.12	0.1	0	0	0
YBR067C	TIP1	A	21	2.24	2.16	2.05	4.78	-0.03	-0.03	<b>0.29</b>
YBR068C	BAP2	A	20	0.52	0.38	0.32	0.57	-0.12	-0.14	0.03
YBR069C	VAP1	A	20	0.24	0.23	0.27	0.22	<i>0.03</i>	0	0
YBR070C		A	20	0.19	0.13	0.17	0.13	0	-0.09	0
YBR071W		A	20	0.13	0.05	0.09	0.09	0	0	0
YBR072W	HSP26	A	20	0.68	0.24	0.18	4.62	<b>-0.4</b>	<b>-0.39</b>	<b>0.75</b>
YBR073W	RDH54	A	20	0.09	0.07	0.07	0.09	0	0	0
YBR077C		A	21	0.1	0.06	0.11	0.09	<b>-0.25</b>	0	0
YBR078W	ECM33	A	41	0.8	0.64	0.55	0.69	-0.03	-0.13	0.01
YBR079C	RPG1	A	20	0.17	0.25	0.15	0.27	0.04	0	0
YBR080C	SEC18	A	21	0.14	0.13	0.14	0.16	0	0	0
YBR082C	UBC4	A	26	1.58	1.2	1.69	2.78	-0.06	0.07	<b>0.24</b>
YBR083W	TEC1	A	20	0.12	0.07	0.09	0.34	0	0	0.13
YBR084C-A	RPL19A	A	46	0.43	0.33	0.24	0.5	0.02	0	0
YBR084W	MIS1	A	20	0.1	0.1	0.07	0.12	0	0	0
YBR085W	AAC3	A	20	0.09	0.12	0.07	0.09	-0.08	0	0
YBR086C		A	20	0.98	1.04	0.68	1.01	-0.04	-0.2	0
YBR087W	RFC5	A	20	0.11	0.11	0.08	0.09	0	0	0
YBR088C	POL30	A	20	0.38	0.43	0.44	0.13	0.04	0.03	-0.1
YBR090C		A	54	0.12	0.08	0.13	0.22	<b>-0.26</b>	-0.06	0.03
YBR090C-A	NHP6B	A	21	0.39	0.3	0.25	0.59	-0.07	-0.07	0.19
YBR091C	MRS5	A	20	0.09	0.11	0.14	0.1	0	0.08	0
YBR092C	PHO3	A	20	0.35	0.41	0.15	0.4	0.07	<b>-0.28</b>	0
YBR093C	PHO5	A	21	0.15	0.14	0.07	0.19	-0.11	0	0
YBR096W		A	20	0.39	0.33	0.23	0.55	-0.02	0	0.15
YBR101C		A	20	0.29	0.23	0.11	0.17	-0.1	<b>-0.32</b>	-0.18
YBR105C		A	20	0.15	0.06	0.12	0.22	0	0	0.17
YBR106W	PHO88	A	21	2.11	0.76	0.34	1.85	<b>-0.46</b>	<b>-0.7</b>	-0.03
YBR107C		A	21	0.09	0.06	0.07	0.09	<b>-0.32</b>	0	0
YBR108W		A	21	0.09	0.04	0.07	0.09	0	0	0
YBR109C	CMD1	A	21	1.34	0.96	1.1	1.52	-0.05	-0.01	0.06
YBR111C	YSA1	A	21	0.73	0.63	0.71	0.93	-0.11	-0.01	0.14
YBR115C	LYS2	A	21	1.82	0.72	0.9	0.66	<b>-0.29</b>	<b>-0.26</b>	<b>-0.28</b>
YBR116C		A	21	0.09	0.05	0.09	0.17	0	0	0.17
YBR117C	TKL2	A	20	0.09	0.04	0.07	0.3	0	0	<b>0.44</b>
YBR118W	TEF2	A	20	16.27	7.88	7.86	9.63	-0.14	<b>-0.24</b>	-0.1
YBR121C	GRS1	A	20	0.46	0.41	0.31	0.41	0.03	-0.05	0
YBR122C	MRPL36	A	20	0.11	0.1	0.11	<i>0.11</i>	-0.09	0	0
YBR123C	TFC1	A	20	0.09	0.04	0.1	0.09	0	0	0
YBR125C		A	20	0.09	0.07	0.09	0.09	0	0	0
YBR126C	TPS1	A	20	0.91	0.58	0.68	1.53	<b>-0.23</b>	-0.14	0.12
YBR127C	VMA2	A	21	0.79	0.87	0.64	0.86	-0.01	-0.09	0.06
YBR129C	OPY1	A	20	0.09	0.04	0.08	0.09	0	0	0
YBR132C	AGP2	A	20	0.12	0.07	0.07	0.09	0	0	0
YBR133C	HSL7	A	21	0.09	0.1	0.07	0.09	0	0	0

YBR135W	CKS1	A	20	0.18	0.16	0.14	0.12	0	0.01	0
YBR137W		A	20	0.13	0.1	0.2	0.14	0	0.13	0
YBR139W		A	21	0.36	0.19	0.13	0.46	<b>-0.25</b>	-0.15	0
YBR140C	IRA1	A	20	0.11	0.07	0.07	0.11	0	0	0
YBR143C	SUP45	A	21	0.22	0.2	0.16	0.18	0.01	-0.04	0
YBR145W	ADH5	A	20	0.58	0.22	0.59	0.26	<b>-0.29</b>	0.04	<b>-0.22</b>
YBR146W	MRPS9	A	21	0.15	0.16	0.14	0.18	<b>-0.21</b>	0	0
YBR147W		A	20	0.39	0.11	0.37	0.18	<b>-0.52</b>	-0.03	-0.17
YBR149W		A	20	0.69	0.45	0.87	1.05	-0.17	0.06	<b>0.25</b>
YBR151W		A	20	0.19	0.09	0.07	0.19	0	-0.15	0.01
YBR154C	RPB5	A	21	0.11	0.1	0.11	0.19	0	-0.03	0.14
YBR157C		A	20	0.1	0.06	0.08	0.09	0	0	0
YBR158W		A	20	0.58	0.57	0.69	0.81	-0.01	0.04	0.14
YBR159W		A	20	0.88	0.72	1.01	0.77	-0.14	0	-0.02
YBR160W	CDC28	A	20	0.21	0.23	0.21	0.26	0	0	0
YBR162C		A	21	0.6	0.61	0.54	0.48	0.05	-0.07	-0.05
YBR162W-A	YSY6	A	21	0.09	0.13	0.15	0.14	-0.18	0	0
YBR163W		A	20	0.09	0.06	0.07	0.09	0	0	0
YBR164C	ARL1	A	20	0.09	0.09	0.07	0.11	0	0	0
YBR165W	UBS1	A	20	0.11	0.12	0.11	0.09	-0.02	0.01	0
YBR166C	TYR1	A	20	0.09	0.04	0.07	0.09	0	0	0
YBR169C	SSE2	A	20	0.2	0.06	0.07	0.26	0	<b>-0.2</b>	0.17
YBR171W	SEC66	A	20	0.21	0.18	0.15	0.14	-0.04	0.02	0
YBR173C	UMP1	A	20	0.11	0.11	0.14	0.14	-0.02	0.01	0.16
YBR175W		A	21	0.11	0.09	0.12	0.09	-0.12	0	0
YBR177C		A	20	0.6	0.4	0.45	0.46	-0.14	0	-0.11
YBR181C	RPS6B	A	40	0.85	0.86	0.9	1.07	-0.01	-0.09	0
YBR183W		A	20	0.24	0.22	0.2	0.38	<b>-0.2</b>	-0.13	0
YBR185C	MBA1	A	21	0.28	0.29	0.36	0.4	-0.09	-0.02	0.09
YBR187W		A	21	0.93	0.7	0.54	0.61	0	<b>-0.23</b>	-0.15
YBR188C	NTC20	A	20	0.09	0.05	0.08	0.09	0	0	0
YBR189W	RPS9B	A	20	2.94	2.79	1.98	1.94	-0.08	-0.15	<b>-0.21</b>
YBR191W	RPL21A	A	17	28.82	26.13	15.15	13.93	0	-0.1	-0.18
YBR196C	PGI1	A	20	1.85	1.73	1.52	1.88	-0.02	-0.14	0
YBR198C	TAF90	A	21	0.09	0.07	0.07	0.09	-0.18	0	0
YBR199W	KTR4	A	20	0.14	0.09	0.15	0.19	-0.19	0	0
YBR201W	DER1	A	20	0.09	0.05	0.15	0.09	0	0.12	0
YBR205W	KTR3	A	20	0.11	0.08	0.07	0.11	0	0	0
YBR206W		A	21	0.09	0.05	0.07	0.11	0	0	0
YBR207W		A	21	0.42	0.32	0.31	0.37	-0.07	-0.04	0
YBR210W		A	20	0.1	0.06	0.12	0.09	0	0	0
YBR211C	MAE1	A	21	0.09	0.04	0.07	0.09	0	0	0
YBR212W	NGR1	A	21	0.09	0.04	0.07	0.09	0	0	0
YBR213W	MET8	A	21	0.09	0.04	0.1	0.09	0	-0.05	0
YBR214W		A	20	0.34	0.2	0.23	0.53	<b>-0.27</b>	0	0.09
YBR218C	PYC2	A	20	0.24	0.09	0.11	0.09	0	0	-0.1
YBR220C		A	21	0.22	0.14	0.17	0.13	-0.1	-0.08	-0.1
YBR221C	PDB1	A	21	0.75	0.63	0.61	0.62	-0.08	-0.09	-0.11
YBR222C	FAT2	A	20	0.15	0.16	0.21	0.27	0.01	0.07	0.18
YBR227C		A	20	0.09	0.04	0.07	0.09	0	0	0
YBR230C		A	21	0.87	0.35	0.78	0.76	<b>-0.32</b>	-0.06	-0.1
YBR231C		A	20	0.09	0.04	0.07	0.11	0	0	0
YBR234C		A	20	0.62	0.56	0.51	0.63	-0.14	-0.1	0.01
YBR235W		A	21	0.09	0.09	0.07	0.09	0	0	0
YBR239C		A	21	0.09	0.06	0.07	0.09	-0.17	0	0

YBR241C		A	21	0.49	0.18	0.31	0.58	<b>-0.23</b>	0	0.14
YBR242W		A	21	0.09	0.07	0.07	0.09	0	0	0
YBR243C	ALG7	A	21	0.17	0.11	0.1	0.09	0	0	-0.08
YBR244W		A	20	0.09	0.06	0.07	0.09	0	0	0
YBR246W		A	21	0.11	0.08	0.11	0.15	-0.13	0	0.04
YBR248C	HIS7	A	20	0.09	0.08	0.15	0.12	0	0.01	0
YBR249C	ARO4	A	20	2.24	1.79	2.23	0.92	0.06	0.11	-0.17
YBR252W	DUT1	A	21	0.55	0.58	0.62	0.35	-0.01	-0.03	-0.18
YBR253W	SRB6	A	20	0.09	0.04	0.12	0.09	0	0.01	0
YBR254C		A	21	0.09	0.1	0.1	0.09	0.01	0	0
YBR256C	RIB5	A	20	0.09	0.09	0.14	0.09	<b>-0.21</b>	0	0
YBR258C		A	20	0.09	0.06	0.07	0.09	-0.19	0	0
YBR260C		A	21	0.09	0.06	0.07	0.09	0	0	0
YBR261C		A	21	0.15	0.18	0.22	0.12	-0.08	-0.07	0
YBR262C		A	21	0.27	0.21	0.37	0.26	-0.13	0.12	0
YBR263W	SHM1	A	21	0.75	0.55	0.5	0.52	-0.05	-0.06	-0.11
YBR264C		A	21	0.09	0.06	0.08	0.09	0	-0.05	0
YBR265W		A	20	0.38	0.26	0.38	0.21	-0.1	-0.05	-0.1
YBR268W	MRPL37	A	20	0.26	0.05	0.14	0.11	<b>-0.42</b>	-0.12	<b>-0.24</b>
YBR269C		A	21	0.39	0.18	0.32	0.33	-0.11	0.1	0.08
YBR274W		A	21	0.09	0.07	0.08	0.09	0	0	0
YBR276C	PPS1	A	20	0.1	0.11	0.13	0.18	-0.02	0	0
YBR279W	PAF1	A	20	0.09	0.06	0.14	0.12	<b>-0.25</b>	0.05	0
YBR280C		A	21	0.12	0.08	0.07	0.09	0	0	0
YBR282W	MRPL27	A	21	0.13	0.08	0.14	0.13	0	0	0
YBR283C	SSH1	A	21	0.52	0.43	0.31	0.42	-0.01	-0.12	-0.02
YBR286W	APE3	A	20	3.04	2.18	2.54	4.85	-0.13	-0.15	0.15
YBR287W		A	20	0.48	0.31	0.38	0.54	0	-0.06	0.14
YBR288C	APM3	A	20	0.09	0.05	0.07	0.09	0	0	0
YBR290W	BSD2	A	20	0.09	0.07	0.07	0.09	<b>-0.25</b>	0	0
YBR291C	CTP1	A	21	0.9	0.47	0.46	0.56	<b>-0.21</b>	<b>-0.21</b>	<b>-0.22</b>
YBR293W		A	20	0.09	0.04	0.08	0.11	0	0	0
YBR297W	MAL33	A	20	0.09	0.04	0.08	0.09	0	0	0
YBR301W		A	20	0.14	0.08	0.08	0.15	0	0	0
YBR302C		A	20	0.93	0.54	0.58	0.65	-0.17	0	-0.06
YCL001W	RER1	A	20	0.1	0.08	0.07	0.09	0	0	0
YCL002C		A	20	0.19	0.2	0.14	0.16	-0.06	-0.1	0
YCL008C		A	20	0.15	0.12	0.07	0.1	-0.15	0	0
YCL009C	ILV6	A	20	1.26	0.91	1.04	0.75	-0.1	-0.01	-0.12
YCL011C	GBP2	A	21	0.25	0.25	0.26	0.27	0.01	0	0
YCL016C		A	20	0.09	0.05	0.07	0.09	0	0	0
YCL017C	NFS1	A	21	0.52	0.64	0.52	0.45	0.01	0.03	0
YCL018W	LEU2	A	20	1.04	0.85	1.17	1.21	<b>-0.22</b>	-0.08	0
YCL019W		A	20	0.1	0.09	0.15	0.09	0	0	0
YCL025C	AGP1	A	20	0.51	0.27	0.47	0.65	<b>-0.2</b>	-0.02	0
YCL027W	FUS1	A	21	0.09	0.08	0.07	0.09	0	0	0
YCL028W		A	21	0.24	0.16	0.18	0.21	-0.19	0	0
YCL029C	BIK1	A	21	0.09	0.06	0.07	0.11	0	0	0
YCL030C	HIS4	A	21	0.38	0.32	0.33	0.36	-0.1	-0.08	0
YCL033C		A	20	0.16	0.2	0.27	0.33	-0.08	0.12	<b>0.23</b>
YCL034W		A	20	0.27	0.14	0.27	0.26	-0.13	-0.06	-0.05
YCL035C		A	20	1.16	0.43	1.09	1.7	-0.16	0.03	<b>0.39</b>
YCL036W		A	21	0.09	0.04	0.07	0.09	0	0	0
YCL037C	SRO9	A	20	0.11	0.11	0.08	0.11	-0.06	0	0
YCL038C		A	20	0.12	0.07	0.11	0.2	0	0	0.15

YCL039W		A	20	0.09	0.05	0.08	0.09	0	0	0
YCL040W	GLK1	A	21	4.56	2.52	5.11	4.42	<b>-0.32</b>	-0.09	0.01
YCL042W		A	20	0.31	0.15	0.19	0.37	0	0	0
YCL043C	PDI1	A	21	2.02	1.06	2.34	2.3	-0.1	0.12	0.12
YCL044C		A	20	0.09	0.05	0.08	0.09	0	0	0
YCL045C		A	20	0.11	0.05	0.1	0.09	0	0	0
YCL047C		A	20	0.11	0.07	0.12	0.09	0	-0.01	0
YCL049C		A	20	0.18	0.09	0.15	0.2	0	0	0
YCL050C	APA1	A	20	0.42	0.37	0.35	0.52	-0.04	0	0.09
YCL056C		A	20	0.09	0.11	0.14	0.13	-0.09	-0.09	0
YCL057W	PRD1	A	21	0.09	0.04	0.08	0.11	0	0	0
YCL064C	CHA1	A	20	0.7	0.62	0.7	1	-0.07	0	0.12
YCL066W	ALPHA1	A	20	0.09	0.51	0.07	0.09	<b>0.67</b>	0	0
YCL067C	ALPHA2	A	20	0.09	0.12	0.13	0.12	0	0	0
YCL073C		A	20	0.12	0.12	0.11	0.11	0	0	0
YCLX06C		A	20	0.09	0.07	0.1	0.12	0	0	0
YCLX12W		A	21	0.09	0.06	0.07	0.09	<b>-0.28</b>	0	0
YCR002C	CDC10	A	21	0.51	0.48	0.35	0.3	-0.09	-0.03	-0.06
YCR004C	YCP4	A	21	0.5	0.5	0.57	0.84	-0.14	0	0.04
YCR005C	CIT2	A	20	1.05	0.53	0.19	0.48	<b>-0.21</b>	<b>-0.52</b>	<b>-0.24</b>
YCR008W	SAT4	A	21	0.09	0.05	0.07	0.09	0	0	0
YCR009C	RVS161	A	20	0.3	0.31	0.48	0.44	-0.01	0.1	0.07
YCR011C	ADP1	A	20	0.09	0.07	0.08	0.15	0	0	0.09
YCR012W	PGK1	A	20	23.1	5.85	9.14	8.72	<b>-0.44</b>	<b>-0.35</b>	<b>-0.23</b>
YCR013C		A	21	0.14	0.14	0.09	0.15	<b>-0.21</b>	0	0
YCR017C		A	21	0.33	0.25	0.17	0.26	-0.11	-0.19	-0.09
YCR018C	SRD1	A	21	0.09	0.04	0.13	0.09	0	0.06	0
YCR020C	PET18	A	20	0.09	0.08	0.13	0.1	0	0	0
YCR020C-A	MAK31	A	20	0.09	0.11	0.13	0.1	-0.05	0	0
YCR021C	HSP30	A	21	2.85	2.05	3.07	7.83	-0.18	0.02	<b>0.35</b>
YCR023C		A	21	0.28	0.16	0.17	0.13	-0.12	0	-0.03
YCR024C-A	PMP1	A	20	1.83	0.54	0.8	1.02	<b>-0.6</b>	<b>-0.38</b>	<b>-0.32</b>
YCR029C		A	21	0.09	0.09	0.07	0.11	<b>-0.27</b>	0	0
YCR029C-A	RIM1	A	40	0.88	0.53	0.95	0.71	-0.06	0.03	-0.1
YCR030C		A	20	0.09	0.05	0.07	0.09	0	0	0
YCR031C	RPS14A	A	20	8.73	4.9	6.89	6.4	0	-0.09	<b>-0.2</b>
YCR034W	FEN1	A	20	0.75	0.4	0.55	0.22	0	<b>-0.2</b>	<b>-0.37</b>
YCR035C	RRP43	A	21	0.09	0.08	0.07	0.11	0	0	0
YCR036W	RBK1	A	20	0.09	0.08	0.07	0.09	0	0	0
YCR037C	PHO87	A	20	0.09	0.06	0.08	0.14	0	0	0
YCR039C	ALPHA2	A	20	0.09	0.14	0.14	0.1	<i>0.01</i>	0	0
YCR040W	ALPHA1	A	20	0.09	0.37	0.07	0.09	<b>0.63</b>	0	0
YCR043C		A	21	0.21	0.22	0.2	0.15	-0.06	0	-0.14
YCR044C		A	20	0.25	0.26	0.23	0.29	-0.11	0	0
YCR046C	IMG1	A	20	0.36	0.19	0.34	0.32	0	-0.05	0
YCR047C		A	20	0.09	0.06	0.07	0.09	0	0	0
YCR048W	ARE1	A	21	0.16	0.06	0.1	0.17	<b>-0.26</b>	0	0
YCR051W		A	20	0.17	0.2	0.16	<i>0.14</i>	0.02	0	0
YCR052W	RSC6	A	20	0.11	0.07	0.09	0.09	<b>-0.27</b>	0	0
YCR053W	THR4	A	20	0.87	1.16	0.76	0.83	0.08	-0.02	0.06
YCR057C	PWP2	A	20	0.09	0.06	0.07	0.09	0	0	0
YCR059C		A	21	0.17	0.2	0.23	0.22	0	0.01	0
YCR060W		A	20	0.11	0.12	0.13	<i>0.13</i>	-0.09	-0.08	0
YCR061W		A	20	0.28	0.11	0.1	0.14	<b>-0.3</b>	0	0
YCR062W		A	20	0.17	0.11	0.12	0.19	<b>-0.22</b>	0	0

YCR065W	HCM1	A	21	0.13	0.07	0.07	0.09	0	0	-0.07
YCR067C	SED4	A	21	0.09	0.08	0.1	0.14	-0.14	0	0
YCR069W	SCC3	A	20	0.37	0.14	0.21	0.2	0	-0.12	-0.02
YCR070W	SCC3	A	20	0.38	0.27	0.27	0.38	-0.17	-0.1	0
YCR071C	IMG2	A	21	0.09	0.04	0.08	0.09	0	0	0
YCR072C		A	20	0.09	0.04	0.09	0.09	0	0	0
YCR075C	ERS1	A	21	0.13	0.1	0.1	0.09	-0.12	-0.1	-0.03
YCR076C		A	20	0.12	0.09	0.18	0.19	-0.15	0	0
YCR077C	PAT1	A	20	0.16	0.21	0.15	0.19	-0.05	0	0
YCR079W		A	20	0.27	0.24	0.24	0.25	-0.02	0.02	0
YCR080W		A	21	0.09	0.08	0.07	0.09	-0.05	0	0
YCR082W		A	20	0.15	0.1	0.16	0.21	-0.16	-0.01	0.1
YCR083W		A	20	0.24	0.18	0.27	0.42	-0.1	0.08	<b>0.35</b>
YCR084C	TUP1	A	20	0.25	0.32	0.19	0.21	-0.05	0	0
YCR087W		A	21	0.09	0.04	0.07	0.09	0	0	0
YCR088W	ABP1	A	21	0.11	0.11	0.07	0.1	-0.19	0	0
YCR090C		A	20	0.09	0.09	0.11	0.09	0.01	0.02	0
YCR096C	A2	A	20	0.12	0.17	0.18	0.17	0.01	0.02	0
YCR104W	PAU3	A	20	0.15	0.22	0.12	0.16	-0.08	0	0
YCRX07W		A	21	0.09	0.06	0.1	0.09	0	0	0
YCRX08W		A	20	0.11	0.14	0.08	0.17	-0.12	0	0.03
YCRX13W	SOL2	A	20	0.3	0.2	0.22	0.3	-0.11	-0.04	0.07
YCRX17W		A	20	0.3	0.22	0.25	0.48	-0.05	0.03	0.16
YCRX19W		A	21	0.09	0.06	0.07	0.09	0	0	0
YCRX21C		A	21	0.09	0.05	0.07	0.09	0	0	0
YDL001W		A	21	0.09	0.05	0.07	0.09	0	0	0
YDL004W	ATP16	A	20	1.08	0.83	3.21	0.77	-0.16	<b>0.21</b>	-0.08
YDL005C	MED2	A	21	0.09	0.06	0.09	0.09	<b>-0.28</b>	0	0
YDL007W	RPT2	A	20	0.18	0.19	0.2	0.39	-0.12	-0.05	<b>0.26</b>
YDL008W	APC11	A	20	0.14	0.13	0.13	0.15	0	0	0
YDL009C		A	21	0.11	0.1	0.14	0.09	-0.13	0	0
YDL010W		A	20	0.12	0.07	0.07	0.09	0	0	0
YDL012C		A	41	0.24	0.17	0.19	0.19	0	0	-0
YDL014W	NOP1	A	20	0.63	0.94	0.77	0.71	0.13	-0.06	-0.04
YDL015C		A	20	0.46	0.29	0.39	0.49	-0.17	0	0.01
YDL018C		A	20	0.09	0.06	0.07	0.12	0	0	0
YDL022W	GPD1	A	20	4.4	2.94	2.84	3.92	<b>-0.21</b>	-0.13	-0.06
YDL024C		A	21	0.09	0.04	0.07	0.14	0	0	0
YDL029W	ARP2	A	20	0.52	0.4	0.63	0.54	-0.05	0.12	0.05
YDL033C		A	20	0.09	0.07	0.07	0.09	-0.13	0	0
YDL038C		A	21	0.09	0.14	0.09	0.2	-0.08	0	0.13
YDL039C		A	21	0.14	0.1	0.12	0.23	-0.16	-0.05	0.05
YDL040C	NAT1	A	21	0.09	0.06	0.15	0.09	0	-0.03	0.02
YDL042C	SIR2	A	20	0.09	0.06	0.07	0.1	0	0	0
YDL046W		A	21	0.78	0.43	0.47	0.62	-0.15	-0.18	0.06
YDL047W	SIT4	A	21	0.09	0.05	0.08	0.09	<b>-0.33</b>	0	0
YDL048C	STP4	A	20	0.83	0.35	1.1	1.77	-0.18	<b>0.21</b>	<b>0.29</b>
YDL049C	KNH1	A	21	0.09	0.04	0.1	0.09	0	0.07	0
YDL051W	YLA1	A	21	0.11	0.1	0.12	0.16	0	0.01	0
YDL052C	SLC1	A	20	0.44	0.35	0.42	0.42	-0.11	-0.02	0
YDL053C		A	20	0.33	0.23	0.4	0.4	-0.15	0.04	0
YDL054C		A	20	0.09	0.06	0.13	0.12	0	0.07	0
YDL055C	PSA1	A	20	1.88	1.18	1.55	2.28	-0.11	0.02	0.05
YDL057W		A	21	0.09	0.05	0.07	0.09	<b>-0.27</b>	0	0
YDL059C	RAD59	A	21	0.09	0.05	0.07	0.09	0	0	0

YDL061C	RPS29B	A	22	3.87	3.76	2.79	2.04	-0.07	-0.14	<b>-0.22</b>
YDL064W		A	21	0.25	0.25	0.17	0.28	0	-0.02	0
YDL066W	IDP1	A	20	0.64	0.5	0.92	0.54	-0.08	0.18	-0.03
YDL067C	COX9	A	20	1.43	1.01	2.49	1.15	-0.07	<b>0.28</b>	-0.09
YDL072C		A	20	1.46	0.79	1.3	1.58	-0.12	-0.08	0
YDL075W	RPL31A	A	66	1.57	1.75	1.45	1.03	-0.07	0	-0.1
YDL076C		A	20	0.09	0.08	0.07	0.1	0	0	0
YDL078C	MDH3	A	21	0.3	0.25	0.25	0.37	-0.17	-0.01	0.09
YDL080C	THI3	A	20	0.1	0.05	0.1	0.09	0	0	0
YDL081C	RPP1A	A	20	7.2	5.21	6.1	2.72	-0.08	<b>-0.26</b>	<b>-0.31</b>
YDL082W	RPL13A	A	20	2.42	4.59	2.31	2.23	0.11	-0.05	-0.03
YDL083C	RPS16B	A	20	5.9	4.64	3.26	3.72	-0.04	-0.16	<b>-0.21</b>
YDL084W		A	20	0.53	0.37	0.43	0.42	-0.07	0	-0.1
YDL085W		A	21	0.09	0.04	0.12	0.09	0	0	0
YDL086W		A	20	0.51	0.15	0.25	0.31	0	0	0
YDL092W	SRP14	A	20	0.09	0.07	0.07	0.11	0	0	0
YDL093W	PMT5	A	20	0.11	0.05	0.11	0.09	0	0	-0
YDL095W	PMT1	A	20	0.29	0.16	0.2	0.28	-0.14	0	0
YDL097C	RPN6	A	20	0.13	0.08	0.11	0.21	0	0	0.16
YDL100C		A	20	0.46	0.3	0.59	0.6	-0.12	0.06	0.08
YDL102W	CDC2	A	20	0.09	0.05	0.07	0.09	0	0	0
YDL103C	QRI1	A	20	0.09	0.07	0.12	0.09	<b>-0.2</b>	0	0
YDL109C		A	21	0.1	0.06	0.09	0.14	-0.17	-0.08	0
YDL110C		A	21	0.19	0.13	0.22	0.21	<b>-0.25</b>	0.03	0
YDL111C	RRP42	A	20	0.14	0.12	0.11	0.24	-0.09	-0.03	0.11
YDL112W		A	21	0.1	0.08	0.1	0.1	-0.04	0	0
YDL120W	YFH1	A	20	0.1	0.09	0.19	0.13	0	0.13	0
YDL122W	UBP1	A	20	0.09	0.07	0.11	0.09	0	-0.07	0
YDL123W		A	20	0.17	0.11	0.09	0.12	0	0	0
YDL124W		A	21	1.19	0.81	2.02	1.83	-0.18	0.13	<b>0.21</b>
YDL125C	HNT1	A	41	4.95	3.51	8.1	4.01	-0.14	<b>0.2</b>	-0.08
YDL126C	CDC48	A	20	0.57	0.3	0.57	0.78	-0.18	0.02	0.15
YDL128W	VCX1	A	21	1.07	0.8	1.22	1.58	-0.07	-0.03	0.16
YDL130W	RPP1B	A	41	20.92	22.16	14.29	13.86	0.02	-0.16	<b>-0.25</b>
YDL131W	LYS21	A	20	1.46	0.62	1.4	0.8	<b>-0.26</b>	-0.02	<b>-0.22</b>
YDL132W	CDC53	A	21	0.09	0.07	0.07	0.09	<b>-0.26</b>	0	0
YDL133W		A	21	0.09	0.04	0.07	0.09	0	0	0
YDL134C	PPH21	A	20	0.13	0.08	0.13	0.13	<b>-0.2</b>	0.03	0
YDL135C	RDI1	A	20	0.13	0.09	0.1	0.11	0	0	0
YDL136W	RPL35B	A	20	1.57	1.19	1.52	0.87	-0.01	-0.05	-0.18
YDL137W	ARF2	A	20	2.71	1.8	3.3	1.96	-0.16	0.05	-0.07
YDL140C	RPO21	A	20	0.13	0.09	0.2	0.19	0	0	0
YDL141W	BPL1	A	20	0.09	0.04	0.08	0.09	0	0	0
YDL142C	CRD1	A	20	0.13	0.07	0.07	0.1	0	0	0
YDL143W	CCT4	A	20	0.1	0.09	0.1	0.11	-0.09	0	0
YDL144C		A	21	0.26	0.29	0.24	0.33	-0.01	-0.05	0
YDL145C	COP1	A	20	0.09	0.11	0.07	0.09	0	0	0
YDL147W	RPN5	A	21	0.09	0.05	0.07	0.13	0	0	0.06
YDL153C	SAS10	A	20	0.09	0.05	0.07	0.09	0	0	0
YDL155W	CLB3	A	20	0.09	0.05	0.07	0.09	0	0	0
YDL157C		A	20	0.22	0.21	0.28	0.21	0	0.04	0.01
YDL158C		A	20	0.11	0.1	0.07	0.09	<b>-0.21</b>	-0.2	0
YDL160C	DHH1	A	21	0.23	0.15	0.15	0.18	<b>-0.21</b>	0	0
YDL165W	CDC36	A	20	0.26	0.15	0.31	0.27	-0.11	0.07	0.08
YDL168W	SFA1	A	20	0.25	0.15	0.27	0.41	-0.17	-0.08	0.13

YDL171C	GLT1	A	20	0.29	0.27	0.27	0.32	-0.05	-0.06	0
YDL173W		A	20	0.09	0.06	0.07	0.12	0	0	0
YDL174C	DLD1	A	21	0.25	0.18	0.19	0.31	<b>-0.24</b>	-0.13	-0.03
YDL178W	AIP2	A	20	0.09	0.06	0.11	0.1	0	0	0
YDL179W	PCL9	A	21	0.09	0.04	0.07	0.09	0	-0.08	0
YDL180W		A	20	0.09	0.05	0.07	0.09	0	0	0
YDL181W	INH1	A	20	1.31	1.63	1.78	1.27	-0.03	0.12	-0.05
YDL182W	LYS20	A	21	6.35	3.03	4.98	3.4	<b>-0.29</b>	-0.15	<b>-0.27</b>
YDL185W	TFP1	A	21	0.77	0.52	0.64	0.94	-0.13	-0.09	0.08
YDL188C	PPH22	A	20	0.9	0.78	0.9	0.72	-0.13	-0.08	0
YDL190C	UFD2	A	20	0.1	0.07	0.1	0.1	0	0	0
YDL191W	RPL35A	A	20	2.15	2.03	2.42	1.82	0	-0.03	-0.13
YDL192W	ARF1	A	20	3.84	4.11	7.41	4.11	0.06	0.13	0.04
YDL193W		A	20	0.09	0.05	0.1	0.15	0	-0	0
YDL195W	SEC31	A	21	0.41	0.31	0.17	0.32	-0.12	0	0.02
YDL198C	YHM1	A	21	0.56	0.38	0.54	0.36	-0.16	-0.05	-0.06
YDL200C	MGT1	A	21	0.09	0.06	0.08	0.1	<b>-0.25</b>	0	0
YDL201W		A	21	0.09	0.08	0.07	0.09	0	0	0
YDL202W	MRPL11	A	20	0.09	0.07	0.11	0.09	-0.15	0	0
YDL204W		A	20	0.17	0.1	0.08	0.46	0	-0.1	<b>0.37</b>
YDL205C	HEM3	A	20	0.09	0.07	0.07	0.09	0	0	0
YDL208W	NHP2	A	20	0.46	0.72	0.57	0.44	0.17	0.07	0
YDL212W	SHR3	A	20	0.7	0.51	0.54	0.36	-0.15	0	-0.13
YDL213C		A	21	0.09	0.04	0.07	0.09	0	0	0
YDL215C	GDH2	A	20	0.11	0.07	0.12	0.14	0	0	0.05
YDL217C	TIM22	A	20	0.09	0.08	0.11	0.09	0	0	0
YDL220C	CDC13	A	20	0.13	0.07	0.07	0.09	0	0	0
YDL222C		A	21	0.23	0.05	0.07	0.97	0	<b>-0.2</b>	<b>0.45</b>
YDL223C		A	20	0.11	0.06	0.07	0.42	0	0	<b>0.39</b>
YDL224C	WHI4	A	20	0.09	0.11	0.07	0.1	0	0	0
YDL226C	GCS1	A	20	0.17	0.1	0.17	0.18	-0.13	-0.06	0
YDL228C		A	21	0.09	0.05	0.08	0.1	0	0	0
YDL229W	SSB1	A	20	5.02	5.31	3.74	3.35	0.04	-0.14	-0.15
YDL230W	PTP1	A	21	0.09	0.04	0.07	0.11	0	0	0.07
YDL232W	OST4	A	21	1.16	1.19	1.12	1.17	-0.06	-0.08	-0.02
YDL234C	GYP7	A	20	0.09	0.04	0.08	0.09	0	0	0
YDL235C	YPD1	A	20	0.09	0.05	0.12	0.1	0	0	0
YDL236W	PHO13	A	21	0.25	0.18	0.27	0.32	-0.11	-0.01	0.07
YDL237W		A	21	0.34	0.25	0.3	0.29	-0.13	-0.05	0.08
YDL241W		A	20	0.09	0.05	0.07	0.09	0	0	0
YDL246C		A	20	0.14	0.15	0.16	0.09	<b>-0.23</b>	-0.01	0
YDR001C		A	20	0.17	0.09	0.11	0.28	0	0	<b>0.31</b>
YDR002W		A	20	0.52	0.3	0.46	0.32	-0.15	-0.03	-0.1
YDR003W		A	20	0.13	0.08	0.13	0.09	-0.18	0	0
YDR005C		A	21	0.12	0.06	0.1	0.11	<b>-0.25</b>	-0.05	0
YDR006C		A	20	0.09	0.04	0.1	0.1	0	-0.03	0.07
YDR007W	TRP1	A	21	0.21	0.12	0.27	0.27	<b>-0.28</b>	0.03	0.12
YDR009W	GAL3	A	20	0.09	0.04	0.29	0.09	0	<b>0.49</b>	0
YDR011W	SNQ2	A	20	0.24	0.1	0.17	0.3	-0.17	0	0
YDR012W	RPL4B	A	35	8.95	6.22	4.99	5.42	-0.11	-0.18	-0.17
YDR016C		A	20	0.11	0.07	0.07	0.09	-0.14	0	0
YDR017C	KCS1	A	21	0.09	0.04	0.07	0.09	0	0	0
YDR019C	GCV1	A	21	0.16	0.17	0.13	1	-0.13	-0.07	<b>0.64</b>
YDR020C		A	20	0.09	0.05	0.07	0.09	0	0	0
YDR023W	SES1	A	20	0.47	0.38	0.33	0.42	-0.05	-0.1	-0.07

YDR024W		A	20	0.09	0.08	0.08	0.09	0	0	0
YDR025W	RPS11A	A	94	1.05	1.34	1.27	1.25	0.03	-0.05	-0.03
YDR027C		A	20	0.09	0.05	0.07	0.09	0	0	0
YDR031W		A	20	0.09	0.04	0.09	0.1	0	0	0
YDR032C		A	20	1.87	1.2	1.29	3.17	<b>-0.25</b>	<b>-0.2</b>	0.16
YDR033W		A	20	9.07	6.59	5.58	6.13	-0.06	-0.16	<b>-0.22</b>
YDR035W	ARO3	A	20	0.73	0.63	1.11	0.66	-0.08	0.17	0
YDR036C		A	21	0.09	0.1	0.1	0.15	0	-0.09	0.1
YDR037W	KRS1	A	20	0.34	0.42	0.43	0.43	0.03	0.02	0.1
YDR038C	ENA5	A	20	0.11	0.08	0.09	0.09	0	0	0
YDR039C	ENA2	A	20	0.24	0.27	0.24	0.38	-0.01	-0.02	0.1
YDR041W		A	20	0.1	0.06	0.12	0.09	0	0.07	0
YDR043C		A	20	0.09	0.07	0.07	0.1	0	0	0
YDR044W	HEM13	A	20	0.4	0.22	0.39	0.31	0	0	0.01
YDR045C		A	20	0.11	0.07	0.08	0.11	0	0	0
YDR046C	BAP3	A	20	0.31	0.21	0.19	0.37	-0.15	0	0.18
YDR047W	HEM12	A	21	0.25	0.23	0.28	0.3	-0.09	-0.09	0.03
YDR050C	TPI1	A	21	20.73	18.17	15.12	12.24	-0.1	<b>-0.2</b>	-0.12
YDR051C		A	20	0.09	0.05	0.1	0.09	0	0	0
YDR055W		A	21	1.54	1.32	1.82	5.63	-0.14	0.08	<b>0.57</b>
YDR056C		A	20	0.17	0.18	0.34	0.23	-0.13	0.04	0
YDR059C	UBC5	A	38	0.17	0.12	0.22	0.23	-0.16	0.04	0.1
YDR062W	LCB2	A	20	0.52	0.22	0.13	0.19	0	-0.19	-0.1
YDR063W		A	20	0.25	0.23	0.32	0.28	-0.06	-0.04	-0.08
YDR064W	RPS13	A	21	7.08	6.41	4.79	4.32	-0.08	<b>-0.22</b>	<b>-0.26</b>
YDR067C		A	20	0.09	0.09	0.08	0.09	0	-0.05	0
YDR070C		A	21	0.51	0.08	0.52	2.18	0	-0.05	<b>0.52</b>
YDR071C		A	20	0.17	0.12	0.16	0.16	0	-0.02	0
YDR072C	IPT1	A	21	0.37	0.27	0.32	0.43	-0.13	-0.06	0
YDR073W	SNF11	A	20	0.09	0.06	0.07	0.09	0	0	0
YDR074W	TPS2	A	20	0.29	0.09	0.15	0.21	0	-0.11	0
YDR077W	SED1	A	20	6.78	5.06	6.65	7.48	-0.14	-0.1	0.03
YDR079W	PET100	A	21	0.12	0.09	0.13	0.13	-0.17	0.06	0
YDR082W	STN1	A	21	0.09	0.04	0.07	0.09	0	0	0
YDR084C		A	20	0.45	0.3	0.34	0.36	-0.12	0	-0.05
YDR086C	SSS1	A	21	0.88	0.62	0.66	0.48	-0.09	-0.08	-0.15
YDR090C		A	21	0.16	0.11	0.15	0.18	-0.1	-0.08	0
YDR091C		A	20	0.13	0.16	0.16	0.19	0	0	0
YDR092W	UBC13	A	20	0.44	0.42	0.73	0.66	-0.04	0.1	0.09
YDR093W		A	20	0.09	0.05	0.1	0.09	0	0	0
YDR094W		A	21	0.1	0.04	0.11	0.1	0	-0.06	0
YDR097C	MSH6	A	20	0.09	0.06	0.07	0.09	0	0	0
YDR098C		A	21	0.12	0.1	0.1	0.13	-0.17	0	0
YDR099W	BMH2	A	20	0.72	0.56	0.48	0.7	-0.12	0	0.05
YDR100W		A	20	0.87	0.46	0.5	0.82	<b>-0.26</b>	-0.2	-0.03
YDR101C		A	20	0.09	0.06	0.08	0.09	0	0	0
YDR103W	STE5	A	20	0.09	0.05	0.07	0.09	0	0	0
YDR105C		A	20	0.19	0.11	0.24	0.18	<b>-0.2</b>	0	0
YDR107C		A	21	0.29	0.18	0.23	0.15	-0.14	-0.07	-0.06
YDR111C		A	21	0.09	0.08	0.07	0.09	-0.16	0	0
YDR115W		A	20	0.2	0.15	0.23	0.24	-0.07	0	0.09
YDR116C		A	20	0.11	0.05	0.07	0.09	0	0	0
YDR117C		A	20	0.09	0.07	0.07	0.09	0	0	0
YDR119W		A	20	0.11	0.1	0.08	0.14	0	0	0
YDR120C	TRM1	A	20	0.09	0.05	0.07	0.09	0	0	0

YDR121W		A	20	0.09	0.05	0.07	0.09	0	0	0
YDR123C	INO2	A	21	0.09	0.06	0.09	0.09	<b>-0.31</b>	0	0
YDR126W		A	20	0.09	0.12	0.07	0.14	-0.16	0	0
YDR127W	ARO1	A	21	0.2	0.16	0.21	0.19	-0.1	0	0
YDR128W		A	21	0.09	0.04	0.07	0.09	0	0	0
YDR129C	SAC6	A	21	0.41	0.2	0.31	0.3	-0.18	-0.07	-0.04
YDR130C		A	20	0.09	0.05	0.07	0.09	0	0	0
YDR133C		A	16	10.29	8.07	6.47	5.16	-0.13	-0.19	<b>-0.24</b>
YDR134C		A	34	14.56	12.15	12.18	9.7	-0.12	-0.13	-0.18
YDR138W	HPR1	A	21	0.09	0.04	0.07	0.09	0	0	0
YDR139C	RUB1	A	40	0.24	0.17	0.19	0.22	-0.11	-0.02	0.01
YDR140W		A	21	0.12	0.22	0.12	0.33	-0.1	-0.01	0.09
YDR141C		A	20	0.09	0.04	0.08	0.09	0	0	0
YDR142C	PEX7	A	20	0.09	0.06	0.09	0.1	<b>-0.23</b>	0	0
YDR143C	SAN1	A	21	0.09	0.04	0.07	0.09	0	0	0
YDR144C	MKC7	A	21	0.09	0.09	0.07	0.09	-0.18	0	0
YDR146C	SWI5	A	20	0.09	0.06	0.07	0.09	<b>-0.22</b>	0	0
YDR147W		A	20	0.09	0.04	0.07	0.12	0	0	0.09
YDR148C	KGD2	A	20	0.31	0.17	0.4	0.19	0	0.11	-0.05
YDR151C	CTH1	A	20	0.09	0.08	0.07	0.1	-0.11	0	0
YDR152W		A	20	0.09	0.08	0.07	0.09	0	0	0
YDR153C		A	20	0.1	0.05	0.12	0.09	0	0	0
YDR154C		A	21	39.53	32.8	36.58	35.26	-0.06	-0.1	-0.02
YDR155C	CPH1	A	20	9.71	8.33	8.09	10.17	-0.11	-0.14	0
YDR156W	RPA14	A	20	0.5	0.42	0.54	0.44	0	-0.01	0
YDR158W	HOM2	A	20	2.28	1.68	2.78	1.61	-0.07	0.14	-0
YDR160W	SSY1	A	21	0.09	0.04	0.07	0.09	0	0	0
YDR161W	TCI1	A	20	0.09	0.07	0.07	0.09	0	0	0
YDR163W		A	21	0.09	0.06	0.07	0.09	0	0	0
YDR165W		A	20	0.09	0.06	0.07	0.09	0	0	0
YDR166C	SEC5	A	21	0.09	0.05	0.07	0.09	0	0	0
YDR167W	TAF25	A	20	0.1	0.04	0.09	0.09	0	0	0
YDR170C	SECT	A	21	0.09	0.06	0.07	0.09	<b>-0.22</b>	0	0
YDR171W	HSP42	A	20	0.5	0.34	0.27	0.36	<b>-0.3</b>	<b>-0.3</b>	-0.15
YDR172W	SUP35	A	20	0.23	0.27	0.23	0.26	-0.19	0	0
YDR174W		A	21	0.57	0.42	0.49	0.9	-0.13	0	0.09
YDR177W	UBC1	A	21	0.21	0.21	0.26	0.24	-0.04	0.11	0.06
YDR178W	SDH4	A	20	2.47	1.95	4.61	2.07	-0.14	<b>0.2</b>	-0.06
YDR182W	CDC1	A	20	0.13	0.1	0.21	0.11	-0.1	-0.02	0
YDR185C		A	20	0.09	0.05	0.08	0.09	0	0	0
YDR187C		A	20	0.09	0.06	0.07	0.09	0	0	0
YDR188W	CCT6	A	20	0.32	0.26	0.26	0.32	-0.06	-0.06	0.07
YDR190C		A	20	0.15	0.18	0.16	0.23	<i>0.01</i>	0	0
YDR194C	MSS116	A	20	0.11	0.09	0.07	0.09	0	0	0
YDR196C		A	20	0.1	0.07	0.1	<i>0.1</i>	0	0	0
YDR204W	COQ4	A	21	0.12	0.11	0.11	0.23	<b>-0.3</b>	0	0.19
YDR205W		A	21	0.09	0.06	0.07	0.1	0	0	0
YDR208W	MSS4	A	20	0.09	0.05	0.07	0.09	0	0	0
YDR209C		A	21	0.09	0.07	0.07	0.09	<b>-0.21</b>	0	0
YDR210W		A	20	0.25	0.23	0.3	0.22	-0.15	0.08	-0.01
YDR212W	TCP1	A	21	0.18	0.11	0.11	0.17	<b>-0.24</b>	-0.18	0.05
YDR214W		A	20	0.27	0.16	0.23	1.09	<b>-0.24</b>	-0.02	<b>0.53</b>
YDR216W	ADR1	A	20	0.09	0.07	0.08	0.09	0	0	0
YDR220C		A	20	0.09	0.1	0.07	0.09	-0.17	0	0
YDR222W		A	21	0.09	0.12	0.08	0.26	-0.15	0	<b>0.3</b>

YDR224C	HTB1	A	19	1.72	2	1.75	1.31	-0.01	0.02	-0.13
YDR225W	HTA1	A	32	4.13	2.61	3.02	2.54	-0.07	-0.07	-0.19
YDR226W	ADK1	A	20	3.57	2.45	4.6	3.44	-0.11	0.02	-0.05
YDR231C		A	20	0.29	0.1	0.29	0.17	-0.18	0.13	0
YDR232W	HEM1	A	21	0.7	0.57	0.6	0.71	-0.08	-0.04	0
YDR233C		A	20	2.35	2.2	2.24	2.57	-0.06	-0.05	-0.01
YDR234W	LYS4	A	20	1.09	0.81	0.87	0.46	-0.15	0	-0.19
YDR235W	PRP42	A	20	0.09	0.04	0.07	0.09	0	0	0
YDR236C		A	21	0.13	0.13	0.11	0.17	0	0	0
YDR238C	SEC26	A	21	0.19	0.19	0.25	0.31	-0.12	0.01	0.02
YDR239C		A	21	0.1	0.05	0.07	0.09	0	0	0
YDR242W	AMD2	A	21	0.09	0.05	0.09	0.09	0	0.02	0
YDR245W	MNN10	A	20	0.13	0.11	0.11	0.12	0	0	0
YDR247W		A	20	0.23	0.16	0.29	0.28	<b>-0.21</b>	0.03	0.11
YDR248C		A	20	0.11	0.07	0.11	0.12	-0.17	0	0
YDR252W	BTT1	A	20	0.09	0.04	0.08	0.09	0	-0.07	0
YDR258C	HSP78	A	20	0.13	0.04	0.08	0.19	0	0	0.17
YDR260C		A	20	0.09	0.09	0.14	0.09	0	0	0
YDR261C	EXG2	A	21	0.18	0.14	0.13	0.29	-0.11	0	0.1
YDR262W		A	21	0.18	0.11	0.11	0.2	-0.17	-0.01	0.09
YDR264C	AKR1	A	20	0.11	0.06	0.12	0.2	0	0	0.16
YDR266C		A	21	0.11	0.08	0.07	0.09	<b>-0.23</b>	0	0
YDR267C		A	21	0.09	0.06	0.1	0.1	0	0	0
YDR271C		A	20	0.09	0.06	0.07	0.09	0	0	0
YDR272W	GLO2	A	20	0.21	0.16	0.26	0.33	0	0.06	0.16
YDR275W		A	20	0.11	0.1	0.13	0.24	-0.05	0.02	0.18
YDR276C		A	21	8.06	5.35	6.18	6.68	<b>-0.21</b>	-0.11	-0.03
YDR280W		A	21	0.09	0.09	0.09	0.09	-0.08	0	0
YDR284C	DPP1	A	21	0.54	0.3	0.26	0.33	<b>-0.21</b>	-0.19	-0.15
YDR286C		A	20	0.1	0.07	0.08	0.13	0	0	0
YDR287W		A	20	0.09	0.05	0.07	0.09	0	0	0
YDR291W		A	20	0.09	0.06	0.07	0.09	0	0	0
YDR292C	SRP101	A	20	0.09	0.06	0.09	0.13	0	0	0
YDR293C	SSD1	A	21	0.09	0.06	0.07	0.1	0	0	0
YDR294C	DPL1	A	20	0.16	0.15	0.17	0.3	0	0	0.15
YDR296W		A	20	0.17	0.11	0.18	0.16	<b>-0.24</b>	0	0
YDR297W	SUR2	A	20	1.38	0.95	1.3	1.66	0	-0.03	0.11
YDR298C	ATP5	A	20	2.2	1.67	3.27	1.49	-0.09	0.12	-0.15
YDR300C	PRO1	A	20	0.09	0.07	0.13	0.09	-0.12	0	0
YDR301W	CFT1	A	21	0.09	0.04	0.07	0.09	<b>-0.31</b>	0	0
YDR302W		A	20	0.09	0.1	0.09	0.09	<b>-0.23</b>	0	0
YDR303C		A	20	0.09	0.05	0.07	0.09	0	0	0
YDR304C	CYP5	A	21	1.16	0.83	1.11	1.48	-0.09	-0.06	0.09
YDR306C		A	20	0.09	0.05	0.12	0.11	0	0	0
YDR307W		A	21	0.11	0.08	0.07	0.09	<b>-0.25</b>	0	0
YDR308C	SRB7	A	20	0.09	0.05	0.07	0.09	0	0	0
YDR309C		A	21	0.13	0.14	0.22	0.12	0	-0.03	0
YDR315C		A	20	0.09	0.04	0.07	0.09	0	0	0
YDR318W	MCM21	A	21	0.09	0.04	0.09	0.09	0	0	0
YDR319C		A	21	0.11	0.1	0.16	0.11	0	-0.09	0
YDR320C		A	21	0.09	0.05	0.07	0.1	0	0	0.07
YDR321W	ASP1	A	20	0.26	0.2	0.18	0.17	-0.09	0	-0.1
YDR322W	MRPL35	A	20	0.12	0.1	0.16	0.17	0	0	0
YDR323C	PEP7	A	20	0.09	0.06	0.07	0.09	0	0	0
YDR328C	SKP1	A	20	0.93	0.84	1.16	1.18	-0.05	0.04	0

YDR329C	PEX3	A	20	0.09	0.06	0.07	0.1	0	0	0
YDR335W	MSN5	A	21	0.09	0.06	0.1	0.09	0	-0.02	0
YDR337W	MRPS28	A	20	0.12	0.05	0.12	0.12	0	-0.04	0
YDR338C		A	20	0.09	0.06	0.08	0.09	0	0	0
YDR339C		A	20	0.09	0.14	0.15	0.18	-0.02	0.06	0.04
YDR341C		A	20	0.32	0.26	0.36	0.29	-0.05	-0.01	-0.03
YDR342C	HXT7	A	20	6.13	3.01	4.56	4.07	<b>-0.33</b>	<b>-0.24</b>	-0.19
YDR343C	HXT6	A	20	6	2.42	4.84	3.68	<b>-0.42</b>	-0.16	-0.18
YDR345C	HXT3	A	20	3.77	2.58	0.09	2.42	-0.16	<b>-1.4</b>	-0.18
YDR346C		A	20	0.11	0.13	0.13	0.09	-0.17	0	0
YDR347W	MRP1	A	21	0.22	0.18	0.32	0.3	-0.19	1E-16	0
YDR348C		A	20	0.09	0.05	0.07	0.09	0	0	0
YDR349C	YPS4	A	20	0.24	0.24	0.24	0.24	-0.09	0	0.1
YDR350C	TCM10	A	21	0.09	0.04	0.07	0.09	0	0	0
YDR352W		A	21	0.14	0.1	0.14	0.09	-0.18	0	0
YDR353W	TRR1	A	20	2.74	2.43	2.49	2.49	-0.01	-0.02	-0.06
YDR354W	TRP4	A	20	0.19	0.16	0.22	0.09	-0.05	-0.06	-0.1
YDR357C		A	20	0.09	0.08	0.09	0.09	<b>-0.22</b>	0	0
YDR358W		A	21	0.09	0.05	0.08	0.09	<b>-0.25</b>	-0.06	0
YDR362C	TFC6	A	21	0.09	0.05	0.07	0.09	0	0	0
YDR364C	CDC40	A	20	0.09	0.04	0.08	0.09	0	0	0
YDR365C		A	20	0.09	0.08	0.07	0.09	0	0	0
YDR367W		A	20	0.34	0.31	0.41	0.37	-0.1	-0.07	0.01
YDR368W	YPR1	A	20	0.91	0.78	1.03	1.03	-0.13	0.03	0.08
YDR373W		A	20	0.09	0.05	0.07	0.1	0	0	0
YDR375C	BCS1	A	21	0.09	0.04	0.07	0.09	0	0	0
YDR376W	ARH1	A	20	0.09	0.07	0.07	0.09	-0.17	0	0
YDR377W	ATP17	A	20	0.48	0.33	0.62	0.39	<b>-0.2</b>	0.19	-0.05
YDR378C		A	20	0.13	0.15	0.16	0.18	<b>-0.2</b>	0	0
YDR381W	YRA1	A	20	0.41	0.47	0.5	0.26	0	-0.01	-0.16
YDR382W	RPP2B	A	20	30.31	23.08	17.09	13.72	-0.08	<b>-0.25</b>	<b>-0.33</b>
YDR384C		A	21	0.5	0.37	0.12	0.34	-0.07	<b>-0.25</b>	-0.07
YDR385W	EFT2	A	20	3.6	3.35	2.35	3	-0.07	-0.19	-0.09
YDR387C		A	21	0.09	0.04	0.09	0.11	0	0	0
YDR388W	RVS167	A	21	2.09	1.5	1.57	2.45	-0.11	-0.11	0.04
YDR389W	SAC7	A	21	0.09	0.05	0.07	0.09	0	0	0
YDR390C	UBA2	A	20	0.09	0.05	0.07	0.09	0	0	0
YDR391C		A	20	0.31	0.22	0.27	0.34	<b>-0.24</b>	-0.07	0.07
YDR392W	SPT3	A	21	0.09	0.04	0.09	0.09	0	-0.02	0
YDR394W	RPT3	A	21	0.15	0.1	0.09	0.16	<b>-0.23</b>	0	0
YDR395W	SXM1	A	20	0.1	0.11	0.13	0.13	-0.06	-0.06	0
YDR397C	NCB2	A	20	0.09	0.04	0.13	0.1	0	0	0
YDR398W		A	21	0.09	0.11	0.15	0.09	0.1	0.07	0.04
YDR399W	HPT1	A	21	0.22	0.38	0.22	0.29	0.12	-0.04	0.11
YDR400W		A	21	0.11	0.11	0.18	0.09	-0.11	0.18	0
YDR404C	RPB7	A	20	1.63	1.23	0.9	1.17	-0.04	-0.14	-0.07
YDR407C		A	20	0.09	0.06	0.07	0.09	0	0	0
YDR408C	ADE8	A	21	0.26	0.27	0.24	0.27	-0.06	0	0.01
YDR409W		A	20	0.09	0.05	0.07	0.09	0	0	0
YDR410C	STE14	A	20	0.4	0.27	0.25	0.42	-0.16	0	0.06
YDR411C		A	20	0.33	0.33	0.59	0.28	-0.05	0.18	-0.04
YDR415C		A	20	0.09	0.06	0.07	0.11	0	0	0
YDR418W	RPL12B	A	20	4.88	4.53	3.91	2.88	-0.09	-0.17	-0.18
YDR422C	SIP1	A	20	0.09	0.05	0.07	0.09	0	0	0
YDR423C	CAD1	A	21	0.11	0.07	0.09	0.09	0	0	0

YDR424C	DYN2	A	20	0.12	0.08	0.15	0.14	<b>-0.2</b>	0.07	0.04
YDR427W	RPN9	A	21	0.19	0.16	0.22	0.28	-0.16	-0.05	0.14
YDR429C	TIF35	A	20	0.35	0.32	0.3	0.35	-0.04	0	0
YDR432W	NPL3	A	20	0.19	0.13	0.1	0.14	-0.19	0	0
YDR433W		A	31	1.23	1.3	0.93	1.98	0.02	-0.08	0.17
YDR434W		A	20	0.17	0.28	0.26	0.29	-0.01	0.14	0.11
YDR435C		A	21	0.13	0.07	0.16	0.09	0	0	-0
YDR436W	PPZ2	A	20	0.09	0.04	0.07	0.09	0	0	0
YDR441C	APT2	A	20	0.33	0.46	0.36	0.34	0.02	-0.01	0
YDR447C	RPS17B	A	20	3.3	3.09	3.09	1.85	-0.03	-0.11	-0.14
YDR450W	RPS18A	A	26	1.45	3.12	2.91	2.15	<b>0.2</b>	<b>0.23</b>	0.01
YDR451C		A	20	0.09	0.06	0.07	0.09	0	0	0
YDR452W		A	20	0.15	0.11	0.17	0.22	0	0	0
YDR453C		A	20	0.2	0.07	0.14	1.66	0	0	<b>0.88</b>
YDR454C	GUK1	A	21	3.37	2.96	3.18	2.07	-0.06	-0.02	<b>-0.21</b>
YDR456W	NHX1	A	20	0.09	0.14	0.07	0.11	-0.19	0	0
YDR457W	TOM1	A	21	0.09	0.12	0.11	0.09	0.06	-0.05	0
YDR459C		A	21	0.19	0.12	0.17	0.2	<b>-0.23</b>	0	-0.03
YDR461W	MFA1	A	21	4.42	0.04	4.53	5.25	<b>-1.98</b>	0.02	0.08
YDR462W	MRPL28	A	21	0.1	0.08	0.18	0.17	0	0.07	0.13
YDR463W	STP1	A	21	0.09	0.09	0.1	0.11	0	0	0.06
YDR464W	SPP41	A	20	0.1	0.12	0.11	0.09	0.01	0	0
YDR465C		A	21	0.09	0.09	0.07	0.09	-0.05	0	0
YDR466W		A	20	0.09	0.08	0.07	0.09	<b>-0.2</b>	0	0
YDR468C	TLG1	A	21	0.09	0.05	0.09	0.11	<b>-0.3</b>	0	0
YDR470C		A	20	0.09	0.08	0.07	0.09	0	0	0
YDR471W	RPL27B	A	20	0.82	1.28	1.39	1.35	<b>0.21</b>	<b>0.25</b>	0.19
YDR472W		A	20	0.14	0.11	0.17	0.17	0	0.07	0.13
YDR474C		A	20	0.09	0.06	0.1	0.1	0	0	0.06
YDR476C		A	21	0.72	0.52	0.93	0.62	-0.05	0.08	-0.03
YDR477W	SNF1	A	21	0.29	0.16	0.13	0.29	-0.1	0	0
YDR479C		A	21	0.15	0.09	0.1	0.13	-0.19	-0.07	0
YDR481C	PHO8	A	21	0.25	0.26	0.26	0.37	-0.04	0	0.16
YDR482C		A	21	0.09	0.04	0.1	0.09	0	0	0
YDR483W	KRE2	A	20	0.67	0.58	0.85	1.13	0	0.02	0.16
YDR486C		A	20	0.09	0.06	0.09	0.09	0	-0.06	0
YDR487C	RIB3	A	20	0.13	0.21	0.35	0.22	0.09	<b>0.31</b>	0.19
YDR489W		A	21	0.09	0.06	0.07	0.09	<b>-0.25</b>	0	0
YDR490C		A	21	0.12	0.05	0.08	0.09	<b>-0.33</b>	0	0
YDR492W		A	21	0.24	0.28	0.4	0.42	0.09	0.12	0.18
YDR493W		A	20	0.09	0.06	0.08	0.09	<b>-0.24</b>	0	0
YDR494W		A	21	0.09	0.04	0.07	0.09	0	0	0
YDR497C	ITR1	A	20	4.04	3.86	6.05	3.14	0.01	<b>0.25</b>	-0.13
YDR498C	SEC20	A	21	0.11	0.11	0.2	0.14	-0.02	0.11	0
YDR500C	RPL37B	A	21	5.12	7.72	8.36	5.04	0.15	<b>0.21</b>	-0.01
YDR502C	SAM2	A	20	2.5	2.08	2.09	2.01	-0.04	-0.04	-0.07
YDR503C	LPP1	A	20	0.14	0.12	0.18	0.14	<b>-0.21</b>	0	0.05
YDR504C		A	20	0.18	0.16	0.18	0.22	-0.12	0	0
YDR505C	PSP1	A	20	0.09	0.06	0.07	0.1	0	0	0
YDR506C		A	21	0.09	0.07	0.07	0.09	<b>-0.33</b>	0	0
YDR508C	GNP1	A	20	0.53	0.66	0.5	0.69	0.1	0	0
YDR510W	SMT3	A	21	0.28	0.5	0.55	0.36	0.12	0.18	0
YDR511W		A	20	0.09	0.07	0.18	0.16	0	0.07	0.09
YDR512C		A	20	0.09	0.04	0.11	0.09	0	0	0
YDR513W	TTR1	A	21	0.68	0.55	1.36	1.2	-0.01	<b>0.28</b>	<b>0.25</b>

YDR514C		A	21	0.09	0.05	0.07	0.09	0	0	0
YDR516C		A	21	0.54	0.32	0.51	0.26	<b>-0.31</b>	-0.02	<b>-0.3</b>
YDR517W		A	20	0.4	0.27	0.37	0.21	-0.15	-0.09	-0.02
YDR518W	EUG1	A	21	0.14	0.17	0.2	0.2	-0.14	0.01	0
YDR519W	FKB2	A	20	0.97	0.92	0.84	1.13	0.02	0.14	0.05
YDR520C		A	20	0.09	0.07	0.07	0.09	0	0	0
YDR529C	QCR7	A	21	0.75	0.24	1.27	0.46	<b>-0.3</b>	<b>0.23</b>	-0.17
YDR531W		A	20	0.09	0.08	0.1	0.09	0	0	0
YDR533C		A	20	1.53	1.01	2.53	9.8	-0.16	0.16	<b>0.65</b>
YDR534C		A	21	0.09	0.09	0.07	0.09	0	0	0
YDR538W	PAD1	A	20	0.09	0.14	0.08	0.14	-0.11	0	0
YDR539W		A	20	0.09	0.05	0.1	0.12	0	0	0
YDR541C		A	20	0.09	0.06	0.07	0.16	0	0	0.1
YDR542W		A	20	0.26	0.21	0.29	0.21	-0.12	0	0
YDR543C		A	20	0.14	0.11	0.09	0.13	0	0	0
YDR545W		A	20	0.65	0.39	0.62	0.75	<b>-0.24</b>	0.04	0.05
YEL001C		B	20	0.44	0.61	0.57	0.38	0	0.1	0.11
YEL002C	WBP1	B	20	0.31	0.23	0.27	0.31	0	0	0.01
YEL006W		B	20	0.16	0.08	0.18	0.16	0	0	0.05
YEL007W		B	20	0.1	0.14	0.22	0.3	0.08	0.15	<b>0.32</b>
YEL009C	GCN4	B	20	4.55	3.37	3.05	4.88	-0.09	0.01	0.02
YEL011W	GLC3	B	21	0.12	0.11	0.23	0.05	0	0.06	0
YEL012W	UBC8	B	21	0.07	0.07	0.07	0.05	0	0	0
YEL013W	VAC8	B	20	0.11	0.07	0.1	0.14	-0.1	0	0
YEL015W		B	20	0.07	0.07	0.07	0.08	0	0	0
YEL017C-A	PMP2	B	31	4.02	3.44	3.85	6.39	-0.11	-0.05	<b>0.15</b>
YEL017W		B	21	0.13	0.12	0.07	0.21	0	0	0.01
YEL020C		B	21	0.07	0.07	0.07	0.08	0	0	-0.1
YEL021W	URA3	B	21	0.14	0.13	0.14	0.13	0	-0.01	-0.08
YEL024W	RIP1	B	20	0.7	0.33	1.21	0.58	-0.18	0.18	-0.09
YEL026W		B	20	1.59	2.96	2.14	3.21	<b>0.24</b>	0.14	<b>0.27</b>
YEL027W	CUP5	B	21	6.11	8.08	4.37	7.51	0.02	-0.06	0.07
YEL031W	SPF1	B	21	0.21	0.07	0.21	0.51	<b>-0.32</b>	0	<b>0.29</b>
YEL034W	HYP2	B	20	3.65	2.59	4.14	5.92	-0.05	0	-0.01
YEL036C	ANP1	B	21	0.13	0.14	0.22	0.18	0	0.01	0.1
YEL037C	RAD23	B	21	0.07	0.07	0.12	0.13	0	0	0.16
YEL038W	UTR4	B	20	0.19	0.17	0.21	0.25	-0.04	0	-0.01
YEL040W	UTR2	B	21	0.36	0.75	0.28	0.36	<b>0.2</b>	-0.03	0
YEL042W	GDA1	B	20	0.16	0.07	0.29	0.25	0	0.18	0.07
YEL043W		B	21	0.07	0.07	0.07	0.09	0	0	0.09
YEL046C	GLY1	B	20	0.51	0.35	0.86	0.96	-0.2	<b>0.2</b>	0.12
YEL047C		B	21	0.18	0.12	0.18	0.27	0	0	<b>0.21</b>
YEL049W	PAU2	B	20	0.15	0.08	0.13	0.13	0	0	-0.08
YEL050C	RML2	B	20	0.15	0.11	0.13	0.18	0	0	-0.07
YEL051W	VMA8	B	20	0.15	0.09	0.17	0.26	-0.1	0.03	0.13
YEL052W	AFG1	B	20	0.09	0.08	0.11	0.15	0	0	0.1
YEL054C	RPL12A	B	21	1.73	1.94	2.37	1.57	0	0.08	-0.01
YEL056W	HAT2	B	20	0.12	0.07	0.08	0.12	-0.12	0	0
YEL057C		B	20	0.07	0.07	0.13	0.05	0	<b>0.24</b>	0
YEL058W	PCM1	B	21	0.31	0.17	0.2	0.27	-0.14	0.15	0.01
YEL059C-A	SOM1	B	21	0.16	0.17	0.34	0.29	0	<b>0.21</b>	0.12
YEL059W		B	21	0.07	0.07	0.07	0.05	0	0	0
YEL060C	PRB1	B	20	0.26	0.17	0.4	0.49	-0.15	0.16	0.16
YEL063C	CAN1	B	20	0.09	0.07	0.07	0.1	0	0	-0.09
YEL066W	HPA3	B	20	0.07	0.07	0.19	0.28	0	<b>0.27</b>	<b>0.38</b>

YEL071W		B	20	0.2	0.16	0.21	0.31	-0.1	0	0.15
YEL073C		B	20	0.26	0.15	0.25	0.26	<b>-0.21</b>	0.05	0
YEL074W		B	10	0.07	0.07	0.07	0.06	0	0	0
YEL075C		B	20	0.07	0.07	0.07	0.05	0	0	0
YEL077C		B	22	0.29	0.22	0.35	0.44	-0.11	0	<b>0.2</b>
YER001W	MNN1	B	21	0.07	0.07	0.08	0.1	0	0	0.03
YER003C	PMI40	B	21	0.23	0.07	0.27	0.18	<b>-0.2</b>	0.19	0
YER004W		B	21	0.36	0.27	0.62	0.38	-0.1	0.13	0.15
YER005W		B	20	0.07	0.07	0.07	0.13	0	0	0.08
YER007C-A		B	21	0.13	0.07	0.07	0.09	0	0	0
YER009W	NTF2	B	20	1.33	1.02	1.42	0.9	0.06	0.07	-0.08
YER010C		B	20	0.14	0.1	0.17	0.23	-0.01	0	0.16
YER011W	TIR1	B	20	2.52	3.07	1.9	2.23	0.06	-0.03	0.03
YER012W	PRE1	B	21	0.27	0.22	0.18	0.41	0	0.11	<b>0.27</b>
YER014W	HEM14	B	21	0.07	0.07	0.07	0.05	0	0	0
YER016W	BIM1	B	20	0.1	0.07	0.07	0.05	-0.03	0	0
YER017C	AFG3	B	21	0.07	0.07	0.07	0.06	0	0	-0.11
YER019C-A	SBH2	B	20	0.93	0.56	0.61	0.63	-0.1	-0.03	-0.06
YER019W		B	21	0.16	0.11	0.11	0.15	-0.02	-0.02	0
YER020W	GPA2	B	21	0.28	0.19	0.37	0.4	-0.08	0.01	0.04
YER021W	RPN3	B	21	0.09	0.09	0.18	0.23	0	0.1	0.17
YER022W	SRB4	A-D	625	0.11	0.08	0.07	0.09	-0.11	0	0
YER023W	PRO3	B	20	0.94	1.03	1.4	0.5	-0.05	0.07	-0.07
YER024W		B	20	0.08	0.07	0.07	0.06	0	0	0
YER025W	GCD11	B	21	0.21	0.2	0.12	0.15	0	0	0
YER026C	CHO1	B	20	0.97	0.41	0.64	0.67	<b>-0.32</b>	-0.19	<b>-0.2</b>
YER027C	GAL83	B	21	0.09	0.07	0.07	0.1	-0	0	-0.07
YER028C		B	21	0.09	0.07	0.07	0.05	0	0	0
YER029C	SMB1	B	20	0.07	0.07	0.08	0.05	0	0	0
YER030W		B	20	0.07	0.07	0.09	0.09	0	0	0.05
YER031C	YPT31	B	20	0.29	0.12	0.34	0.23	-0.1	0	-0.08
YER034W		B	21	0.07	0.07	0.07	0.05	0	0	0
YER035W		B	20	0.31	0.18	0.21	0.98	0	0	<b>0.3</b>
YER036C		B	20	0.16	0.17	0.21	0.3	0	0	<b>0.22</b>
YER037W		B	21	0.07	0.07	0.07	0.15	0	0	<b>0.28</b>
YER039C	HVG1	B	21	0.07	0.07	0.07	0.05	0	0	0
YER042W		B	20	0.07	0.07	0.07	0.29	0	0	<b>0.41</b>
YER043C	SAH1	B	21	4.32	2.8	3.21	2.86	-0.16	-0.14	<b>-0.2</b>
YER044C		B	21	0.65	0.33	0.44	0.72	-0.19	-0.19	0
YER045C		B	21	0.07	0.07	0.07	0.12	0	0	0.19
YER046W		B	21	0.07	0.07	0.07	0.08	0	0	-0.14
YER048C	CAJ1	B	20	0.07	0.07	0.08	0.1	0	0	0
YER049W		B	20	0.07	0.07	0.07	0.05	0	0	0
YER050C		B	20	0.07	0.07	0.07	0.1	0	0	0
YER052C	HOM3	B	20	0.16	0.17	0.27	0.24	0	<b>0.31</b>	0.14
YER053C		B	20	0.75	0.33	0.71	1.03	<b>-0.26</b>	0	0.15
YER055C	HIS1	B	20	0.97	0.6	0.86	0.79	-0.19	-0.01	-0.12
YER056C	FCY2	B	20	0.68	0.79	0.79	1.41	-0.05	-0.05	0.17
YER056C-A	RPL34A	B	20	2.49	1.66	1.83	1.35	0	-0.14	-0.17
YER057C	HIG1	B	21	0.89	0.77	1.13	1.21	0.02	0.06	0.08
YER058W	PET117	B	20	0.07	0.07	0.07	0.07	0	0	0
YER060W	FCY21	B	20	0.07	0.07	0.07	0.16	0	0	0.18
YER060W-A	FCY22	B	20	0.09	0.07	0.07	0.16	0	0	0.01
YER061C	CEM1	B	20	0.07	0.07	0.07	0.07	0	0	0
YER062C	HOR2	B	20	0.59	0.65	0.4	2.05	-0.07	-0.04	<b>0.5</b>

YER063W		B	21	0.15	0.07	0.08	0.05	-0.06	0	0
YER064C		B	20	0.08	0.07	0.09	0.14	0	0	0.11
YER066W		B	20	0.11	0.08	0.12	0.06	-0.08	0	0
YER067W		B	21	0.35	0.22	1.03	0.23	-0.19	<b>0.36</b>	-0.17
YER068W	MOT2	B	20	0.07	0.08	0.07	0.1	0	0	-0.03
YER069W	ARG5,6	B	20	0.27	0.13	0.5	0.27	-0.07	<b>0.37</b>	0.03
YER072W		B	21	1.02	1.05	0.91	1.14	0.07	0.11	0.16
YER073W		B	21	0.1	0.13	0.18	0.13	0.09	0.11	0.15
YER074W	RPS24A	B	42	0.49	0.72	0.57	0.63	0.17	0.07	0.02
YER076C		B	21	0.11	0.08	0.08	0.06	0	0	-0.14
YER078C		B	20	0.07	0.07	0.07	0.07	0	0	0
YER079W		B	21	0.08	0.09	0.12	0.11	0	0	-0.05
YER080W		B	21	0.08	0.07	0.09	0.1	0.02	0	0
YER081W		B	21	0.07	0.07	0.07	0.09	0	0	0.03
YER082C		B	20	0.07	0.07	0.07	0.07	0	0	0
YER083C		B	20	0.24	0.24	0.64	0.55	0	0.12	0.12
YER084W		B	21	0.07	0.07	0.08	0.05	0	0	0
YER086W	ILV1	B	20	0.13	0.36	0.3	0.27	<b>0.21</b>	0.13	0.03
YER087C-A	SBH1	B	20	0.47	0.56	0.83	0.48	0	0.07	-0.04
YER087W		B	20	0.07	0.07	0.07	0.1	0	0	0.03
YER088C	DOT6	B	21	0.25	0.26	0.51	0.57	-0	0	<b>0.29</b>
YER089C	PTC2	B	20	0.41	0.17	0.33	0.34	-0.1	0	-0.03
YER090W	TRP2	B	21	0.08	0.07	0.13	0.13	0	0.05	0
YER091C	MET6	B	20	2.23	3.16	1.47	3.65	0	<b>-0.21</b>	0.15
YER092W		B	21	0.07	0.07	0.07	0.06	0	0	0
YER093C-A		B	41	0.07	0.07	0.07	0.06	0	0	-0.12
YER094C	PUP3	B	20	0.68	0.7	1.18	1.14	0	0.1	<b>0.3</b>
YER095W	RAD51	B	21	0.15	0.17	0.13	0.16	0	0	-0.07
YER099C	PRS2	B	21	0.1	0.07	0.08	0.18	0	0	0.08
YER100W	UBC6	B	20	0.14	0.07	0.09	0.09	0	0	-0.03
YER102W	RPS8B	B	33	6.12	5.21	5.47	4	0.01	-0.08	<b>-0.23</b>
YER103W	SSA4	B	20	0.26	0.09	0.12	0.84	-0.16	-0.1	<b>0.5</b>
YER106W		B	20	0.07	0.07	0.07	0.05	0	0	0
YER107C	GLE2	B	20	0.11	0.13	0.1	0.11	0	0.06	-0.05
YER112W	USS1	B	20	0.08	0.07	0.07	0.1	0	0	0
YER113C		B	20	0.07	0.07	0.07	0.06	0	0	0
YER114C	BOI2	B	20	0.1	0.07	0.07	0.06	0	0	0
YER115C	SPR6	B	20	0.16	0.19	0.21	0.13	0	0	-0.04
YER117W	RPL23B	B	50	1.82	3.53	1.68	1.83	<b>0.21</b>	0.03	0.07
YER118C	SSU81	B	20	0.27	0.25	0.27	0.38	-0.03	-0.05	0.03
YER119C		B	21	0.07	0.09	0.11	0.19	0	0	0.11
YER120W	SCS2	B	20	1.47	1.53	0.98	2.03	0.07	-0.05	0.1
YER121W		B	20	0.07	0.07	0.07	0.09	0	0	0
YER122C	GLO3	B	20	0.09	0.09	0.15	0.12	-0.01	0	0
YER124C		B	21	0.07	0.07	0.07	0.15	0	0	<b>0.33</b>
YER125W	RSP5	B	20	0.14	0.11	0.13	0.17	0	0	-0.12
YER126C		B	21	0.07	0.07	0.07	0.07	0	0	-0.09
YER127W	LCP5	B	20	0.07	0.07	0.07	0.07	0	0	0
YER130C		B	20	0.07	0.09	0.07	0.17	0	0	0.12
YER131W	RPS26B	B	21	0.6	0.76	0.46	0.41	0	0	0
YER133W	GLC7	B	40	0.07	0.07	0.07	0.08	0	0	-0.05
YER134C		B	20	0.18	0.1	0.16	0.17	-0.04	0	0
YER136W	GDI1	B	20	0.17	0.16	0.19	0.39	-0.01	0	0.18
YER138C		B	40	0.27	0.17	0.24	0.55	0	0.05	<b>0.29</b>
YER141W	COX15	B	20	0.58	0.54	0.54	1.24	-0.04	-0.05	<b>0.26</b>

YER143W	DDI1	B	20	0.07	0.07	0.08	0.08	0	0	0
YER145C	FTR1	B	20	0.07	0.07	0.1	0.15	0	0	0.1
YER146W		B	20	0.12	0.07	0.07	0.13	0	0	0.03
YER148W	SPT15	A-D	624	0.28	0.18	0.26	0.24	-0.02	0	0.02
YER150W		B	20	5.59	3.51	4.4	8.47	<b>-0.2</b>	-0.09	0.19
YER151C	UBP3	B	20	0.07	0.07	0.07	0.06	0	0	0
YER152C		B	21	0.2	0.16	0.18	0.21	-0.1	-0.03	-0.06
YER154W	OXA1	B	20	0.38	0.31	0.38	0.51	0.03	0	<b>0.2</b>
YER155C	BEM2	B	20	0.08	0.07	0.08	0.11	0	0	0
YER156C		B	20	0.16	0.18	0.22	0.14	0.07	<b>0.31</b>	-0.1
YER157W		B	21	0.07	0.07	0.07	0.06	0	0	-0.16
YER158C		B	20	0.07	0.15	0.08	0.22	0	0	0.04
YER159C	BUR6	B	21	0.09	0.07	0.07	0.06	0	0	-0.14
YER160C		B	40	0.12	0.11	0.2	0.39	0	0	<b>0.39</b>
YER163C		B	20	0.2	0.18	0.19	0.42	-0.01	0	<b>0.25</b>
YER164W	CHD1	B	21	0.07	0.07	0.07	0.05	-0	0	0
YER165W	PAB1	B	20	0.28	0.43	0.11	0.28	0.06	<b>-0.2</b>	0.03
YER166W		B	20	0.07	0.07	0.07	0.06	0	0	0
YER167W	BCK2	B	20	0.07	0.07	0.07	0.08	0	0	-0.14
YER170W	ADK2	B	21	0.07	0.07	0.07	0.05	0	0	0
YER174C		B	21	0.17	0.11	0.23	0.2	0	0.07	-0.15
YER175C		B	20	0.07	0.07	0.09	0.08	0	0	-0.14
YER176W	ECM32	B	21	0.07	0.08	0.07	0.06	0	0	0
YER177W	RPL23B	B	20	4.58	2.63	6.59	6.89	-0.22	-0.02	0.08
YER178W	PDA1	B	20	1.88	1.91	0.32	2.46	0.05	<b>-0.54</b>	0.12
YER183C		B	21	0.07	0.09	0.1	0.1	0	0.04	0.06
YER185W		B	20	0.07	0.07	0.07	0.06	0	0	0
YER186C		B	21	0.07	0.07	0.08	0.08	0	0	0
YER190W		B	20	0.73	0.39	0.1	0.91	-0.05	<b>-0.7</b>	0.12
YFL-TYA		B	20	0.07	0.07	0.07	0.06	0	0	0
YFL-TYB		B	20	0.07	0.07	0.08	0.05	0	0	0
YFL002C	SPB4	B	20	0.1	0.08	0.07	0.1	0	0	0
YFL005W	SEC4	B	21	0.14	0.14	0.19	0.15	0	0	0
YFL006W		B	20	0.1	0.12	0.08	0.14	0	0	0.04
YFL007W		B	21	0.07	0.07	0.07	0.07	0	0	-0.15
YFL009W	CDC4	B	20	0.09	0.09	0.07	0.13	0	0	0
YFL010C		B	20	1.22	0.76	1.01	1.45	-0.15	-0.05	0.1
YFL011W-A	AUA1	B	21	0.11	0.07	0.07	0.05	-0.01	-0.1	0
YFL013C		B	21	0.07	0.07	0.07	0.05	0	0	0
YFL014W	HSP12	B	20	2.53	1.62	2.65	16.82	-0.05	0.19	<b>0.89</b>
YFL016C	MDJ1	B	20	0.11	0.08	0.1	0.17	0	0	0.01
YFL017C		B	20	0.14	0.13	0.15	0.1	0	0	0
YFL018C	LPD1	B	20	0.44	0.53	0.9	0.69	-0.02	<b>0.27</b>	0.07
YFL018W-A	SNP2	B	21	0.22	0.23	0.24	0.25	0	0.17	-0.04
YFL019C		B	21	0.07	0.08	0.07	0.05	0	0	0
YFL020C	PAU5	B	20	0.12	0.12	0.1	0.14	0	0	0
YFL021W	GAT1	B	20	0.17	0.14	0.07	0.22	0	<b>-0.3</b>	-0.01
YFL022C	FRS2	B	20	0.56	0.64	0.39	1	0.11	0.03	<b>0.23</b>
YFL026W	STE2	B	20	0.57	0.07	0.69	1.21	<b>-0.8</b>	0.06	<b>0.29</b>
YFL027C		B	21	0.07	0.07	0.07	0.05	0	0	0
YFL028C	CAF16	B	20	0.13	0.11	0.25	0.16	0	0.09	-0.06
YFL030W		B	21	0.14	0.09	0.69	0.31	0	0.32	0.14
YFL031W	HAC1	B	21	1.89	1.74	1.18	2.07	-0.04	<b>-0.2</b>	0.05
YFL034W		B	21	0.07	0.07	0.07	0.06	0	0	0
YFL035C-A		B	20	0.08	0.07	0.07	0.06	0	0	0

YFL035C-B		B	20	0.15	0.26	0.22	0.36	0.1	0.02	<b>0.37</b>
YFL037W	TUB2	B	21	0.48	0.6	0.75	0.54	0.01	0	-0.05
YFL038C	YPT1	B	20	0.74	0.74	1.07	1.14	-0.01	0.06	0.16
YFL039C	ACT1	A-D	629	3.67	3.35	3.59	4.14	-0.04	-0.06	0.05
YFL041W	FET5	B	21	0.15	0.14	0.15	0.14	0	0	0.02
YFL043C		B	20	0.07	0.07	0.07	0.08	0	0	-0.08
YFL044C		B	20	0.07	0.07	0.07	0.06	0	0	0
YFL045C	SEC53	B	21	1.25	1.49	0.29	1.42	0.09	<b>-0.71</b>	-0.14
YFL048C	EMP47	B	21	0.12	0.09	0.07	0.19	0	0	0.18
YFL054C		B	21	0.08	0.07	0.07	0.08	0	-0.1	0
YFL057C		B	25	0.15	0.25	0.21	0.34	0	0	-0.05
YFL058W	THI5	B	20	0.07	0.07	0.07	0.07	0	0	0
YFL059W	SNZ3	B	20	0.1	0.07	0.07	0.07	-0	0	0
YFL062W	COS4	B	20	0.58	0.47	0.61	0.93	-0	0.06	0.17
YFL066C		B	23	0.12	0.07	0.07	0.08	0.01	-0.1	0
YFR001W		B	20	0.07	0.07	0.07	0.05	0	0	0
YFR003C		B	20	0.09	0.07	0.07	0.08	0	0	0
YFR004W	RPN11	B	20	0.26	0.27	0.42	0.73	0	0.12	<b>0.25</b>
YFR006W		B	20	0.13	0.07	0.14	0.12	0	0	-0.06
YFR007W		B	21	0.07	0.07	0.07	0.07	0	0	-0.08
YFR009W	GCN20	B	20	0.17	0.26	0.2	0.27	0.08	0	0.05
YFR010W		B	20	0.15	0.12	0.17	0.22	0	0	0.01
YFR011C		B	21	0.08	0.07	0.16	0.07	0	0	-0.05
YFR015C	GSY1	B	21	0.16	0.07	0.07	0.05	<b>-0.21</b>	-0.2	<b>-0.5</b>
YFR017C		B	21	0.23	0.31	0.36	0.47	-0.09	0.18	0.14
YFR018C		B	20	0.27	0.18	0.17	0.16	0	0	-0.14
YFR020W		B	21	0.07	0.1	0.07	0.14	0	0	-0.04
YFR021W		B	21	0.07	0.07	0.07	0.07	0	0	0
YFR022W		B	20	0.08	0.07	0.09	0.36	0	0	0.27
YFR024C		B	20	0.27	0.26	0.07	0.47	0	<b>-0.5</b>	0.02
YFR024C-A		B	26	0.14	0.08	0.1	0.15	-0.1	-0.1	0.1
YFR025C	HIS2	B	20	0.07	0.07	0.07	0.07	0	0	0
YFR026C		B	21	0.07	0.07	0.12	0.05	0	0	0
YFR028C	CDC14	B	20	0.09	0.07	0.07	0.09	0	0	-0.06
YFR030W	MET10	B	20	0.07	0.07	0.07	0.11	0	0	0.07
YFR031C	SMC2	B	21	0.07	0.07	0.07	0.06	0	0	0
YFR031C-A	RPL2A	B	52	2.22	5.11	5.37	2.57	<b>0.22</b>	0.14	0.01
YFR033C	QCR6	B	20	0.37	0.35	0.32	0.26	0	0	-0.14
YFR034C	PHO4	B	21	0.08	0.07	0.07	0.12	0	0	-0.07
YFR036W	CDC26	B	20	0.07	0.07	0.08	0.07	0	0	0
YFR037C	RSC8	B	20	0.13	0.1	0.15	0.24	0	0	0
YFR041C		B	21	0.07	0.07	0.08	0.07	0	0	0
YFR042W		B	20	0.07	0.08	0.07	0.15	0	0	0
YFR044C		B	21	0.72	0.86	1.03	1.57	0	0.11	<b>0.25</b>
YFR045W		B	21	0.07	0.07	0.07	0.11	0	0	0.07
YFR047C		B	21	0.43	0.53	0.95	1.28	-0.01	<b>0.3</b>	<b>0.39</b>
YFR048W		B	21	0.07	0.07	0.07	0.08	0	0	0
YFR049W	YMR31	B	21	0.23	0.29	0.83	0.41	0.04	<b>0.23</b>	0
YFR050C	PRE4	B	20	0.45	0.57	0.52	0.98	-0.01	0	0.17
YFR051C	RET2	B	20	0.55	1.02	0.16	0.99	0.1	<b>-0.43</b>	<b>0.21</b>
YFR052W	RPN12	B	20	0.07	0.13	0.09	0.29	0	0	0.18
YFR053C	HXK1	B	21	2.94	2.87	6.72	5	<b>-0.29</b>	0.1	0.03
YGL001C		B	20	0.31	0.2	0.2	0.41	-0.03	0	0.12
YGL002W		B	20	0.1	0.09	0.13	0.15	0	0	-0.07
YGL003C	CDH1	B	20	0.07	0.07	0.07	0.09	0	0	0

YGL004C		B	20	0.08	0.07	0.07	0.06	0	0	0
YGL006W	PMC1	B	20	0.07	0.08	0.08	0.09	0	0	-0
YGL008C	PMA1	B	20	6.06	5.38	7.72	8.74	0.05	0.14	0.17
YGL009C	LEU1	B	21	0.42	0.53	0.76	0.65	0.09	0.19	0.19
YGL010W		B	21	0.15	0.18	0.16	0.24	0	0	0.08
YGL011C	SCL1	B	21	0.39	0.3	0.67	0.54	0.03	<b>0.23</b>	<b>0.24</b>
YGL012W	ERG4	B	20	0.69	0.82	0.78	0.87	0.07	0	0.03
YGL013C	PDR1	B	21	0.07	0.07	0.07	0.12	0	0	-0.06
YGL019W	CKB1	B	20	0.17	0.18	0.19	0.31	-0	0	0.02
YGL020C		B	20	0.25	0.18	0.25	0.3	0	0.06	0.12
YGL021W	ALK1	B	20	0.07	0.07	0.07	0.05	0	0	0
YGL022W	STT3	B	21	0.21	0.21	0.13	0.2	0.03	0	0.16
YGL023C		B	20	0.07	0.08	0.07	0.09	0	0	0.05
YGL024W		B	20	0.07	0.07	0.07	0.07	0	0	0
YGL026C	TRP5	B	21	0.97	1.08	1.26	1.04	0	0.02	0.01
YGL028C		B	20	0.16	0.17	0.17	0.4	0	0.07	<b>0.25</b>
YGL029W		B	20	0.09	0.08	0.07	0.09	0	0	-0.11
YGL030W	RPL30	B	21	4.86	9.72	0.89	5.39	<b>0.32</b>	<b>-0.73</b>	0.03
YGL031C	RPL24A	B	20	2.6	2.56	2.74	3.71	-0.1	-0.05	0.09
YGL032C	AGA2	B	20	0.6	0.07	0.53	1.09	<b>-0.9</b>	0	0.13
YGL035C	MIG1	B	20	0.07	0.07	0.07	0.07	0	0	-0.12
YGL036W	MTC2	B	20	0.07	0.07	0.07	0.08	0	0	0.04
YGL037C		B	21	1.34	1.59	1.91	4.48	<b>-0.21</b>	0.08	<b>0.26</b>
YGL038C	OCH1	B	20	0.1	0.14	0.11	0.14	0	-0.01	0
YGL039W		B	20	0.16	0.16	0.08	0.27	0	0	0.12
YGL040C	HEM2	B	20	0.77	0.54	0.44	0.82	0	-0.05	0.09
YGL044C	RNA15	B	20	0.07	0.07	0.07	0.08	0	0	0
YGL045W		B	20	0.07	0.07	0.07	0.08	0	0	-0.11
YGL047W		B	20	0.07	0.07	0.07	0.14	0	0	0.03
YGL048C	RPT6	B	21	0.27	0.4	0.49	0.77	0.06	0.03	<b>0.31</b>
YGL051W		B	20	0.07	0.07	0.07	0.07	0	0	0
YGL053W		B	20	0.07	0.07	0.07	0.11	0	0	-0.02
YGL054C		B	20	0.78	0.5	0.43	0.6	-0.01	0	0.05
YGL055W	OLE1	B	20	0.65	1.19	2.44	3.08	<b>0.22</b>	<b>0.51</b>	<b>0.62</b>
YGL056C		B	20	0.07	0.11	0.07	0.1	0.08	0	0
YGL057C		B	20	0.07	0.07	0.08	0.07	0	0	0
YGL058W	RAD6	B	21	0.07	0.07	0.11	0.12	0	0.03	0.03
YGL062W	PYC1	B	21	0.08	0.11	0.16	0.22	0	0.03	0.09
YGL067W		B	21	0.25	0.18	0.28	0.34	-0.09	0.12	0.11
YGL068W		B	20	0.14	0.2	0.2	0.26	0	0.18	0.17
YGL070C	RPB9	B	20	0.07	0.14	0.11	0.17	0	0	0.11
YGL076C	RPL7A	B	41	3.81	4.11	4.26	2.99	0.06	0.01	-0.17
YGL077C	HNM1	B	20	1.04	0.97	0.77	1.03	0	-0.04	-0.06
YGL078C	DBP3	B	20	0.15	0.16	0.12	0.16	0	-0.02	0
YGL079W		B	20	0.1	0.07	0.07	0.06	0	0	0
YGL080W		B	20	0.21	0.24	0.28	0.29	-0.03	0.03	0.02
YGL081W		B	20	0.07	0.07	0.07	0.05	0	0	0
YGL082W		B	20	0.07	0.07	0.07	0.06	0	0	0
YGL084C		B	20	0.09	0.07	0.1	0.1	-0	0	-0.02
YGL087C	MMS2	B	20	0.18	0.11	0.21	0.2	0	0.11	0.07
YGL088W		B	20	0.07	0.09	0.07	0.1	0	0	-0.03
YGL089C	MFo2	B	21	0.07	3.67	0.07	0.05	<b>1.22</b>	0	0
YGL091C	NBP35	B	20	0.07	0.07	0.08	0.12	0	0	-0.02
YGL096W		B	21	0.09	0.07	0.07	0.07	0	0	-0.15
YGL097W	SRM1	B	20	0.07	0.07	0.07	0.07	0	0	-0.1

YGL099W		B	20	0.09	0.1	0.07	0.08	0	-0	0
YGL100W	SEH1	B	21	0.11	0.09	0.13	0.09	0	0	-0.05
YGL101W		B	20	0.08	0.09	0.08	0.05	0	0	0
YGL102C		B	20	0.08	0.08	0.07	0.05	0	0	0
YGL103W	RPL28	B	41	3.2	4.77	5.05	4.78	0.04	0.09	0.02
YGL104C		B	21	0.12	0.1	0.08	0.14	-0.04	-0.09	0
YGL105W	ARC1	B	21	0.65	0.84	0.67	0.99	-0.05	0	0.05
YGL106W	MLC1	B	20	0.16	0.51	0.07	0.46	<b>0.35</b>	<b>-0.22</b>	<b>0.33</b>
YGL107C		B	21	0.07	0.07	0.07	0.05	0	0	0
YGL111W		B	20	0.08	0.07	0.07	0.1	0	0	-0.02
YGL112C	TAF60	B	20	0.12	0.08	0.12	0.11	0	0	0
YGL114W		B	21	0.09	0.08	0.11	0.1	0	0	-0.07
YGL115W	SNF4	B	21	0.27	0.13	0.3	0.31	0	-0.01	-0.05
YGL117W		B	20	0.08	0.07	0.28	0.09	0	<b>0.34</b>	0
YGL119W	ABC1	B	20	0.07	0.07	0.07	0.1	0	0	0.16
YGL121C		B	20	0.15	0.13	0.43	1.53	-0.07	<b>0.44</b>	<b>0.82</b>
YGL122C	NAB2	B	20	0.07	0.08	0.12	0.14	0	0	0
YGL123W	RPS2	B	21	4.64	7.09	5.63	7.69	0.18	0.08	0.12
YGL124C		B	20	0.07	0.07	0.07	0.06	0	0	0
YGL125W	MET13	B	21	0.1	0.21	0.16	0.25	0.1	0	0.07
YGL126W	SCS3	B	21	0.31	0.25	0.81	0.43	0	<b>0.39</b>	0.1
YGL127C	SOH1	B	20	0.17	0.17	0.2	0.26	0	0.15	-0.03
YGL128C		B	21	0.07	0.07	0.07	0.07	0	0	0
YGL130W	CEG1	B	21	0.07	0.07	0.07	0.06	0	0	0
YGL134W	PCL10	B	21	0.07	0.07	0.11	0.07	0	0.19	0
YGL135W	RPL1B	B	20	7.5	7.35	8.23	10.97	-0.02	0.01	0.07
YGL137W	SEC27	B	20	0.14	0.17	0.23	0.22	0	0.08	0.04
YGL141W		B	21	0.07	0.07	0.07	0.07	0	0	-0.11
YGL142C	GPI10	B	21	0.07	0.07	0.07	0.07	0	0	0
YGL143C	MRF1	B	20	0.07	0.07	0.07	0.08	0	0	0
YGL147C	RPL9A	B	26	1.35	2.2	0.73	1.46	0.13	0.14	-0.03
YGL148W	ARO2	B	21	0.9	0.74	0.83	0.84	0	0.12	0.03
YGL151W	NUT1	B	20	0.07	0.07	0.07	0.05	0	0	0
YGL153W	PEX14	B	21	0.07	0.07	0.08	0.08	0	0	0
YGL154C	LYS5	B	21	0.1	0.07	0.11	0.15	0	0	0.01
YGL155W	CDC43	B	20	0.07	0.07	0.07	0.1	0	0	0
YGL156W	AMS1	B	21	0.12	0.07	0.08	0.2	0	0	0.07
YGL157W		B	20	0.26	0.23	0.07	0.4	0	<b>-0.3</b>	0.13
YGL159W		B	20	0.07	0.07	0.08	0.05	0	0	0
YGL160W		B	21	0.07	0.07	0.07	0.07	0	0	0.03
YGL161C		B	20	0.64	0.43	0.54	0.76	-0.08	0.02	0.12
YGL162W	SUT1	B	20	0.08	0.07	0.08	0.09	0	0	0
YGL166W	CUP2	B	21	0.1	0.09	0.11	0.14	0	0	0.03
YGL167C	PMR1	B	21	0.12	0.16	0.2	0.18	0.09	0	0.16
YGL172W	NUP49	B	21	0.07	0.1	0.07	0.09	0	0	0
YGL173C	KEM1	B	20	0.08	0.09	0.1	0.16	0	0	0
YGL178W	MPT5	B	21	0.07	0.07	0.07	0.12	0	0	0.05
YGL179C		B	20	0.1	0.08	0.18	0.18	0	0.04	<b>0.14</b>
YGL181W	GTS1	B	20	0.39	0.23	0.22	0.35	-0.1	-0.09	0.04
YGL184C		B	20	0.07	0.07	0.07	0.1	0	0	0.16
YGL186C		B	20	0.13	0.12	0.16	0.31	0	0	<b>0.28</b>
YGL187C	COX4	B	21	0.88	0.81	1.94	1.2	0	<b>0.37</b>	0.02
YGL188C		B	20	0.08	0.07	0.1	0.06	0	0	0
YGL189C	RPS26A	B	19	14.83	22.84	1.19	14.56	0.03	-0.89	-0.16
YGL191W	COX13	B	21	0.19	0.36	1.31	0.36	0	0.27	-0.04

YGL193C		B	21	0.33	0.17	0.17	0.18	0	-0.03	0
YGL195W	GCN1	B	21	0.09	0.07	0.1	0.12	0	0	-0.06
YGL196W		B	20	0.31	0.32	0.55	0.96	-0.03	0.14	<b>0.48</b>
YGL197W	MDS3	B	21	0.07	0.07	0.07	0.05	0	0	-0.17
YGL198W		B	21	0.21	0.82	0.12	0.34	0.2	-0.02	<b>0.22</b>
YGL199C		B	21	0.14	0.07	0.07	0.08	-0.05	-0.03	0
YGL200C	EMP24	B	21	1.24	1.12	2.5	2.29	0.07	0.21	0.1
YGL202W	ARO8	B	20	1.03	1.05	1.58	1.33	-0	0.12	-0.06
YGL203C	KEX1	B	21	0.07	0.07	0.07	0.1	0	0	-0.07
YGL206C	CHC1	B	20	0.17	0.17	0.23	0.23	0	0.05	0
YGL207W	SPT16	B	20	0.07	0.08	0.07	0.05	0	0	0
YGL208W	SIP2	B	21	0.07	0.07	0.07	0.06	0	0	0
YGL209W	MIG2	B	20	0.21	0.25	0.08	0.28	0	<b>-0.3</b>	-0.05
YGL210W	YPT32	B	20	0.07	0.07	0.07	0.07	0	0	0
YGL213C	SKI8	B	20	0.11	0.07	0.09	0.1	0	0	0
YGL215W	CLG1	B	21	0.09	0.09	0.11	0.16	0	0	-0.02
YGL216W	KIP3	B	21	0.07	0.07	0.09	0.05	0	0	0
YGL219C		B	20	0.07	0.07	0.07	0.05	0	0	0
YGL220W		B	20	1.03	0.85	1.06	1.14	0	0.16	0.03
YGL221C	NIF3	B	21	0.4	0.29	0.4	0.61	0.01	0.04	0.06
YGL223C		B	20	0.07	0.07	0.07	0.08	0	0	-0
YGL224C		B	20	0.07	0.09	0.07	0.05	0.05	0	0
YGL225W	GOG5	B	20	1.24	1.22	1.77	1.21	0	0.02	0
YGL231C		B	21	0.15	0.18	0.17	0.21	0	0.16	0.11
YGL234W	ADE5,7	B	20	0.09	0.09	0.09	0.09	0	0	0
YGL236C		B	21	0.07	0.07	0.07	0.07	0	0	0
YGL238W	CSE1	B	20	0.07	0.07	0.07	0.09	0	0	0
YGL242C		B	20	0.08	0.07	0.09	0.16	0	0	0.02
YGL244W	RTF1	B	20	0.07	0.07	0.07	0.06	0	0	0
YGL245W		B	20	0.74	0.45	0.57	0.77	-0.14	-0.1	-0.04
YGL247W		B	21	0.07	0.07	0.08	0.09	0	0	0
YGL248W	PDE1	B	20	0.17	0.14	0.19	0.36	-0.06	0.06	0.21
YGL252C	RTG2	B	20	0.07	0.07	0.1	0.08	0	0	-0.04
YGL253W	HXK2	B	21	1.57	2.17	0.79	2.01	0	-0.02	-0.18
YGL255W	ZRT1	B	20	4.53	4.95	3.95	1.99	0.05	0.01	<b>-0.34</b>
YGL256W	ADH4	B	20	2.66	3.48	0.52	0.99	0.05	<b>-0.39</b>	<b>-0.38</b>
YGL261C		B	20	0.22	0.1	0.19	0.3	-0.1	0	-0.08
YGR001C		B	40	0.07	0.07	0.07	0.07	0	0	0
YGR004W		B	21	0.07	0.07	0.07	0.06	0	0	0
YGR007W	MUQ1	B	20	0.15	0.15	0.11	0.24	0	0	-0.06
YGR008C	STF2	B	20	1.26	0.66	1.79	1.42	<b>-0.2</b>	<b>0.33</b>	0.12
YGR009C	SEC9	B	21	0.07	0.07	0.07	0.08	0	0	0
YGR010W		B	20	0.07	0.07	0.09	0.05	0	0	0
YGR011W		B	20	0.07	0.07	0.07	0.06	0	0	0
YGR014W	MSB2	B	20	0.12	0.07	0.1	0.07	0	0	0
YGR015C		B	21	0.09	0.07	0.07	0.06	0	0	0
YGR017W		B	20	0.07	0.07	0.07	0.05	0	0	0
YGR019W	UGA1	B	20	0.33	0.33	0.49	1.37	-0	0	<b>0.37</b>
YGR020C	VMA7	B	20	0.52	0.47	0.68	0.44	0	0	0
YGR021W		B	21	0.07	0.07	0.07	0.06	0	0	0
YGR023W		B	20	0.07	0.07	0.07	0.08	0	0	0
YGR024C		B	20	0.13	0.2	0.12	0.22	0.07	0	0.09
YGR026W		B	20	0.52	0.34	0.53	0.93	-0.01	0.1	<b>0.2</b>
YGR027C	RPS25A	B	20	0.81	0.9	0.89	0.81	-0.03	0.09	-0.11
YGR028W	MSP1	B	21	0.07	0.07	0.09	0.05	0	0.03	0

YGR029W	ERV1	B	20	0.15	0.14	0.22	0.14	-0.08	0.1	<i>0.01</i>
YGR031W		B	21	<i>0.07</i>	<i>0.07</i>	0.09	0.13	<i>0</i>	<i>0</i>	-0.02
YGR032W	GSC2	B	20	0.22	0.25	0.48	0.44	<i>0</i>	0.19	<i>0.1</i>
YGR033C		B	20	0.09	<i>0.07</i>	<i>0.07</i>	0.09	<i>0</i>	<i>0</i>	<i>0</i>
YGR034W	RPL26B	B	17	3.2	3.19	3.23	2.08	-0.04	-0.13	-0.19
YGR036C	CWH8	B	20	<i>0.08</i>	<i>0.07</i>	0.09	0.16	<i>0</i>	<i>0</i>	0.05
YGR037C	ACB1	B	21	2.26	2.95	6.31	2.21	0.05	<b>0.33</b>	0.09
YGR038W	ORM1	B	21	0.17	0.3	<i>0.07</i>	0.32	<b>0.35</b>	<b>-0.24</b>	<b>0.37</b>
YGR041W	BUD9	B	20	<i>0.07</i>	<i>0.07</i>	<i>0.07</i>	0.06	<i>0</i>	<i>0</i>	<i>0</i>
YGR043C		B	20	<i>0.07</i>	<i>0.07</i>	<i>0.07</i>	0.37	<i>0</i>	<i>0</i>	<b>0.41</b>
YGR044C	RME1	B	20	0.29	0.18	0.22	0.3	-0.12	0.04	<b>0.22</b>
YGR049W	SCM4	B	21	0.1	0.09	0.12	0.21	<i>0</i>	<i>0</i>	0.17
YGR050C		B	20	0.09	<i>0.07</i>	0.08	0.09	<i>-0</i>	<i>0</i>	<i>0</i>
YGR052W		B	21	0.16	0.11	<i>0.07</i>	0.33	-0.05	-0.04	<b>0.27</b>
YGR054W		B	20	<i>0.08</i>	<i>0.08</i>	<i>0.07</i>	0.11	<i>0</i>	<i>0</i>	<i>0</i>
YGR055W	MUP1	B	20	0.43	0.49	0.65	0.57	<i>0</i>	0.12	<b>0.22</b>
YGR060W	ERG25	B	20	1.96	2.6	1.84	2.88	0.14	0.02	<b>0.29</b>
YGR061C	ADE6	B	21	0.2	0.37	0.14	0.33	0.05	-0.16	0.05
YGR062C	COX18	B	21	0.18	0.08	0.18	0.2	<i>-0.1</i>	<i>0</i>	<i>0</i>
YGR063C	SPT4	B	20	0.65	0.57	0.67	0.7	<i>0</i>	0.01	-0.02
YGR065C		B	20	<i>0.07</i>	<i>0.07</i>	0.1	0.09	<i>0</i>	<i>0</i>	<i>0</i>
YGR069W		B	20	<i>0.07</i>	<i>0.07</i>	<i>0.07</i>	0.05	<i>0</i>	<i>0</i>	<i>0</i>
YGR073C		B	20	0.11	<i>0.07</i>	<i>0.07</i>	0.09	<i>0</i>	<i>0</i>	<i>0</i>
YGR074W	SMD1	B	20	0.1	0.08	0.15	0.09	<i>0</i>	<i>0</i>	<i>0</i>
YGR075C	PRP38	B	21	<i>0.07</i>	<i>0.07</i>	<i>0.07</i>	0.07	<i>0</i>	<i>0</i>	<i>0</i>
YGR076C	MRPL25	B	20	<i>0.07</i>	0.08	<i>0.07</i>	0.07	<i>0</i>	<i>0</i>	<i>0</i>
YGR077C	PEX8	B	20	0.21	0.15	0.15	0.3	-0.03	<i>0</i>	0.19
YGR078C	PAC10	B	20	<i>0.07</i>	<i>0.07</i>	0.08	0.1	<i>0</i>	<i>0</i>	-0.04
YGR079W		B	20	<i>0.07</i>	<i>0.07</i>	<i>0.07</i>	0.06	<i>0</i>	<i>0</i>	<i>0</i>
YGR080W	TWF1	B	20	<i>0.07</i>	<i>0.07</i>	0.08	0.08	<i>0</i>	<i>0</i>	<i>0</i>
YGR082W	TOM20	B	21	0.3	0.54	0.47	0.69	0.06	-0.01	0.16
YGR083C	GCD2	B	20	<i>0.07</i>	<i>0.07</i>	<i>0.07</i>	0.09	<i>0</i>	<i>0</i>	-0.07
YGR084C	MRP13	B	20	<i>0.07</i>	0.08	<i>0.07</i>	0.07	<i>0</i>	<i>0</i>	<i>0</i>
YGR085C	RPL11B	B	32	3.17	7.72	5.4	5.16	0.17	<b>0.2</b>	0.05
YGR086C		B	20	0.22	0.3	0.27	0.34	<i>0</i>	<i>0</i>	<i>0</i>
YGR088W	CTT1	B	21	0.11	0.08	<i>0.07</i>	0.67	<i>0</i>	<i>0</i>	<b>0.44</b>
YGR090W		B	20	<i>0.07</i>	<i>0.07</i>	<i>0.07</i>	0.09	<i>0</i>	<i>0</i>	<i>0</i>
YGR094W	VAS1	B	20	0.19	0.19	0.26	0.2	<i>0</i>	0.05	-0.04
YGR095C		B	21	0.2	0.16	0.19	0.35	<i>0</i>	<i>0</i>	0.02
YGR097W	ASK10	B	20	<i>0.08</i>	0.1	0.09	0.19	<i>0</i>	<i>0</i>	-0.06
YGR101W		B	21	0.23	0.18	0.17	0.31	-0.08	-0.06	-0.16
YGR102C		B	20	0.09	0.09	0.1	0.12	<i>0</i>	<i>0</i>	-0.07
YGR105W	VMA21	B	20	0.09	0.1	0.17	0.11	<i>0</i>	0.1	-0.05
YGR106C		B	20	0.7	0.82	1.01	0.74	0.04	<i>0</i>	0.06
YGR108W	CLB1	B	20	0.11	0.12	<i>0.07</i>	0.08	<i>0</i>	<i>0</i>	<i>0</i>
YGR110W		B	20	<i>0.07</i>	<i>0.07</i>	0.14	0.11	<i>0</i>	0.02	0.03
YGR111W		B	20	<i>0.07</i>	<i>0.07</i>	0.08	0.09	<i>0</i>	<i>0</i>	0.1
YGR118W	RPS23A	B	80	1.4	1.92	1.71	1.33	0.12	0.13	-0.07
YGR121C	MEP1	B	21	<i>0.07</i>	0.08	0.14	0.09	<i>0</i>	<i>0</i>	-0.11
YGR124W	ASN2	B	21	0.25	0.25	0.22	0.42	0.2	-0.01	0.19
YGR125W		B	21	<i>0.07</i>	<i>0.07</i>	0.07	0.09	<i>0</i>	<i>0</i>	-0.06
YGR126W		B	20	<i>0.07</i>	<i>0.07</i>	<i>0.07</i>	0.06	<i>0</i>	<i>0</i>	<i>0</i>
YGR127W		B	20	0.13	0.09	0.13	0.21	<i>0</i>	<i>0</i>	<b>0.14</b>
YGR132C	PHB1	B	20	<i>0.08</i>	0.12	0.18	0.17	<i>0</i>	0.07	0.01
YGR133W	PEX4	B	20	0.08	<i>0.07</i>	0.08	0.07	<i>0</i>	<i>0</i>	<i>0</i>

YGR135W	PRE9	B	20	0.4	0.56	0.28	0.94	0.1	-0.1	<b>0.27</b>
YGR136W		B	20	0.12	0.07	0.08	0.46	0	0	0.31
YGR137W		B	21	0.1	0.08	0.1	0.2	-0	0	<b>0.25</b>
YGR138C		B	21	0.6	0.38	0.69	1.35	-0.14	-0.02	<b>0.3</b>
YGR141W		B	20	0.07	0.07	0.07	0.07	0	0	0
YGR143W	SKN1	B	21	0.15	0.09	0.1	0.15	-0.05	-0.06	-0.04
YGR144W	THI4	B	21	0.2	0.16	0.17	0.2	-0.06	-0.03	-0.07
YGR146C		B	20	0.16	0.11	0.16	0.27	0	0.05	<b>0.22</b>
YGR147C	NAT2	B	20	0.07	0.1	0.09	0.1	0	0	0
YGR148C	RPL24B	B	19	1.23	1.66	0.93	1.35	0	-0.09	0.12
YGR149W		B	21	0.46	0.24	0.51	0.77	-0.16	0.11	0.19
YGR155W	CYS4	B	21	0.68	0.59	0.86	1.15	0.08	<b>0.21</b>	<b>0.21</b>
YGR157W	CHO2	B	20	0.45	0.65	0.7	0.97	0.06	0.1	0.01
YGR159C	NSR1	B	20	0.21	0.48	0.3	0.44	<b>0.31</b>	0	<b>0.25</b>
YGR161C		B	21	0.17	0.1	0.21	0.21	-0.1	0.04	0.01
YGR162W	TIF4631	B	20	0.09	0.08	0.07	0.11	0	0	0
YGR163W		B	20	0.07	0.07	0.07	0.08	0	0	-0.07
YGR165W		B	20	0.07	0.07	0.07	0.05	0	0	0
YGR167W	CLC1	B	20	0.13	0.15	0.19	0.2	0	0.03	0.06
YGR169C		B	20	0.08	0.07	0.07	0.05	0	0	0
YGR172C	YIP1	B	21	0.18	0.25	0.12	0.11	0.02	0	0
YGR173W		B	21	0.07	0.07	0.07	0.08	0	0	0
YGR174C	CBP4	B	20	0.07	0.07	0.08	0.07	0	0	0
YGR175C	ERG1	B	20	0.66	0.78	0.43	0.73	-0.02	0.04	0.14
YGR178C	PBP1	B	21	0.24	0.16	0.13	0.24	-0.12	-0.13	-0.02
YGR180C	RNR4	B	20	0.9	1.29	0.98	0.96	0	0.1	-0.13
YGR181W		B	21	0.64	0.75	1.07	0.97	0.05	0.09	0.11
YGR182C		B	20	0.4	0.27	0.49	0.2	0	0	0
YGR183C	QCR9	B	21	1.45	1.09	3.17	0.85	-0.11	<b>0.34</b>	-0.07
YGR184C	UBR1	B	21	0.07	0.07	0.07	0.07	0	0	-0.14
YGR185C	TYS1	B	20	0.17	0.22	0.1	0.17	0.04	-0.11	0.07
YGR189C		B	21	0.62	0.47	0.87	0.8	0	0.03	0.19
YGR191W	HIP1	B	20	0.24	0.29	0.46	0.46	0	0	<b>0.22</b>
YGR192C	TDH3	B	20	22.18	6.67	29.62	29.71	-0.05	0.19	0.1
YGR193C	PDX1	B	20	0.09	0.07	0.07	0.07	0	0	0
YGR194C		B	20	0.24	0.07	0.08	0.07	-0.1	0	0
YGR195W	SKI6	B	21	0.13	0.16	0.16	0.2	0	0	0.02
YGR197C	SNG1	B	20	0.1	0.07	0.07	0.06	0	0	0
YGR199W		B	21	0.07	0.07	0.07	0.11	0	0	0.07
YGR200C		B	21	0.07	0.07	0.07	0.05	0	0	-0.12
YGR201C		B	20	0.07	0.07	0.12	0.3	0	0	0.21
YGR203W		B	21	0.13	0.07	0.1	0.08	0	0	0
YGR204W	ADE3	B	21	0.38	0.35	0.44	0.78	-0.03	0	0.17
YGR206W		B	20	0.07	0.07	0.07	0.06	0	0	0
YGR207C		B	20	0.08	0.07	0.08	0.07	0	0	0
YGR209C	TRX2	B	21	2.07	1.93	1.6	2.79	0	0.15	0.23
YGR210C		B	21	0.2	0.25	0.22	0.24	0.03	0	-0.03
YGR211W		B	21	0.07	0.11	0.07	0.07	0.02	0	-0.16
YGR214W	RPS0A	B	41	1.38	1.64	2.3	1.27	0.09	0.14	-0.04
YGR215W		B	20	0.07	0.07	0.07	0.05	0	0	0
YGR216C	GPI1	B	20	0.07	0.07	0.07	0.09	0	0	-0.1
YGR217W	CCH1	B	20	0.08	0.07	0.07	0.05	0	0	0
YGR218W	CRM1	B	20	0.07	0.07	0.07	0.07	0	0	-0.13
YGR220C	MRPL9	B	20	0.12	0.12	0.12	0.15	0	0.03	-0.08
YGR222W	PET54	B	21	0.07	0.07	0.07	0.06	0	0	0

YGR224W		B	21	0.07	0.07	0.07	0.07	0	0	0
YGR227W	DIE2	B	20	0.09	0.08	0.07	0.13	0	0	-0.03
YGR229C	SMI1	B	20	0.09	0.07	0.12	0.12	0	0	-0.08
YGR231C	PHB2	B	20	0.17	0.14	0.2	0.22	0	0.05	0.09
YGR232W		B	20	0.19	0.54	0.56	0.6	0.26	<b>0.42</b>	<b>0.39</b>
YGR234W	YHB1	B	20	0.37	0.59	1.38	0.11	0.05	<b>0.41</b>	<b>-0.6</b>
YGR235C		B	21	0.07	0.16	0.22	0.13	0	0.1	0.1
YGR240C	PKF1	B	20	0.67	0.56	0.87	1.18	0	0.06	<b>0.28</b>
YGR241C	YAP1802	B	21	0.1	0.07	0.07	0.08	0	0	0
YGR243W		B	21	0.07	0.07	0.12	0.05	0	0	0
YGR244C		B	20	0.17	0.11	0.53	0.22	0	<b>0.48</b>	0.02
YGR246C	BRF1	B	20	0.07	0.08	0.07	0.07	0	0	0
YGR248W	SOL4	B	21	0.23	0.14	0.19	0.72	<b>-0.2</b>	-0.14	<b>0.35</b>
YGR250C		B	20	0.07	0.07	0.1	0.52	0	0.11	<b>0.59</b>
YGR252W	GCN5	B	21	0.07	0.07	0.07	0.05	0	0	0
YGR253C	PUP2	B	20	0.21	0.17	0.22	0.29	0.06	<b>0.21</b>	<b>0.28</b>
YGR254W	ENO1	B	20	7.04	5.36	5.52	18.48	0	0.05	<b>0.3</b>
YGR255C	COQ6	B	20	0.23	0.21	0.31	0.27	0	0.1	0.06
YGR256W	GND2	B	20	0.08	0.08	0.13	0.53	0	0.04	<b>0.75</b>
YGR257C		B	20	0.1	0.08	0.1	0.09	0	0	0
YGR258C	RAD2	B	20	0.07	0.07	0.08	0.05	0	0	0
YGR260W		B	20	0.3	0.26	0.44	0.36	0	0.05	0
YGR262C		B	20	0.17	0.23	0.2	0.16	0.11	0.05	-0.04
YGR263C		B	21	0.12	0.22	0.13	0.26	0	0	0.09
YGR264C	MES1	B	20	0.07	0.08	0.09	0.14	0	0	0.15
YGR267C	FOL2	B	20	0.14	0.11	0.15	0.19	0	0.01	0.07
YGR268C		B	20	0.2	0.14	0.3	0.36	-0.07	0.1	0.16
YGR270W	YTA7	B	20	0.07	0.07	0.07	0.08	0	0	0
YGR275W		B	20	0.1	0.19	0.11	0.15	0.09	0	0.04
YGR277C		B	20	0.09	0.08	0.1	0.11	0	0	0.07
YGR279C		B	20	3.4	2.96	4.15	2.65	0	0.13	-0.04
YGR281W	YOR1	B	20	0.08	0.07	0.07	0.1	0	0	0.06
YGR282C	BGL2	B	21	1.89	1.66	1.81	2.69	0.18	0.14	<b>0.29</b>
YGR284C		B	20	0.27	0.32	0.65	0.53	-0.01	0.19	0.12
YGR285C	ZUO1	B	21	0.88	1.37	1.32	1.06	0.12	0	0.03
YGR286C	BIO2	B	20	0.07	0.08	0.17	0.05	0	<b>0.3</b>	0
YGR294W		B	20	0.24	0.15	0.12	0.3	0	0	0
YGR295C	COS6	B	20	1.27	0.77	0.52	0.65	-0.1	-0.17	-0.04
YGR296W		B	20	0.37	0.45	0.62	0.59	0.03	0.08	0.12
YHL001W	RPL14B	B	63	3.27	3.71	3.21	2.67	0.1	0.09	0
YHL002W		B	20	0.07	0.08	0.08	0.1	0	0	0
YHL003C	LAG1	B	20	0.14	0.15	0.11	0.12	0	0	0.02
YHL004W	MRP4	B	20	0.07	0.12	0.15	0.14	0	0.1	0.05
YHL006C		B	21	0.07	0.07	0.07	0.07	0	0	-0.16
YHL008C		B	20	0.15	0.07	0.18	0.16	-0.05	0	-0.09
YHL011C	PRS3	B	20	0.11	0.19	0.21	0.24	0.09	0.12	0.15
YHL015W	RPS20	B	20	3.39	5.46	3.79	3.35	0.1	0.09	<b>-0.25</b>
YHL017W		B	20	0.15	0.18	0.23	0.19	0	0	0
YHL019C	APM2	B	20	0.07	0.07	0.07	0.05	0	0	0
YHL020C	OPI1	B	21	0.2	0.26	0.32	0.38	0	0	-0.03
YHL021C		B	21	0.16	0.07	0.27	0.25	-0.06	-0.02	0.01
YHL024W		B	20	0.07	0.07	0.07	0.06	0	0	0
YHL025W	SNF6	B	20	0.19	0.15	0.17	0.17	-0.1	-0.04	0
YHL026C		B	21	0.08	0.11	0.09	0.22	0	0	0.15
YHL027W	RIM101	B	20	0.09	0.07	0.07	0.14	0	0	-0.14

YHL028W	WSC4	B	21	0.09	0.1	0.07	0.05	0	-0.05	0
YHL029C		B	20	0.07	0.07	0.07	0.08	0	0	0
YHL031C	GOS1	B	20	0.07	0.07	0.07	0.08	0	0	0
YHL032C	GUT1	B	20	0.07	0.07	0.29	0.16	0	0.09	0.11
YHL033C	RPL8A	B	20	1.4	1.72	1.64	1.49	0.06	0.09	0.03
YHL034C	SBP1	B	20	0.53	0.52	1.1	0.95	-0.02	0.18	<b>0.29</b>
YHL035C		B	20	0.07	0.07	0.07	0.06	0	0	0
YHL039W		B	21	0.07	0.11	0.09	0.07	0	0.04	-0.15
YHL040C		B	20	0.09	0.07	0.07	0.07	0	0	0
YHL044W		B	20	0.07	0.07	0.07	0.09	0	0	0
YHL046C		B	20	0.1	0.1	0.14	0.19	0	0	0
YHL048W	COS8	B	21	0.24	0.38	0.33	0.48	0	-0.01	0.03
YHL049C		B	10	0.16	0.21	0.13	0.07	0	-0.12	<b>-0.2</b>
YHL050C		B	40	0.23	0.15	0.21	0.23	0	0	-0.04
YHR001W		B	20	0.08	0.08	0.07	0.1	0	0	0
YHR001W-A	QCR10	B	21	0.81	0.73	2.1	0.56	0.09	<b>0.35</b>	-0.11
YHR003C		B	20	0.07	0.08	0.07	0.06	0	0	-0.1
YHR004C		B	20	0.07	0.07	0.07	0.05	0	0	0
YHR005C	GPA1	B	20	0.07	0.08	0.07	0.08	0	0	-0
YHR007C	ERG11	B	20	1.02	1.3	0.71	2.6	0.02	-0.03	<b>0.47</b>
YHR008C	SOD2	B	21	0.62	0.4	1.24	1.05	-0.2	<b>0.34</b>	<b>0.28</b>
YHR009C		B	20	0.24	0.17	0.22	0.22	-0	0	-0.04
YHR010W	RPL27A	B	20	3.58	2.94	5.14	2.49	0.04	0.16	-0.02
YHR012W	VPS29	B	41	0.07	0.07	0.07	0.07	0	0	-0.12
YHR013C	ARD1	B	20	0.07	0.1	0.12	0.09	0.05	0.11	0
YHR016C	YSC84	B	38	0.07	0.07	0.07	0.06	0	0	0
YHR017W	YSC83	B	21	0.07	0.07	0.07	0.07	0	0	0
YHR018C	ARG4	B	20	1.11	0.61	2.01	1.33	-0.08	<b>0.35</b>	0.08
YHR019C	DED81	B	21	0.35	0.39	0.68	0.6	0	0.14	0.11
YHR020W		B	21	0.24	0.19	0.22	0.38	0	0	0.08
YHR021C	RPS27B	B	20	12.82	13.16	10.02	10.05	0.03	-0.05	-0.12
YHR022C		B	20	0.07	0.07	0.07	0.12	0	0	0.08
YHR024C	MAS2	B	20	0.08	0.11	0.14	0.16	0	0	0.01
YHR025W	THR1	B	21	1.54	2.18	2.38	1.38	0.12	0.11	-0.07
YHR026W	PPA1	B	20	6.83	6.49	7.25	4.63	0.17	0.05	-0.09
YHR027C	RPN1	B	21	0.13	0.17	0.2	0.24	0.05	0.06	0.13
YHR028C	DAP2	B	21	0.09	0.19	0.14	0.17	0	0	0.17
YHR030C	SLT2	B	20	0.07	0.07	0.07	0.09	0	0	0.13
YHR032W		B	21	0.16	0.15	0.12	0.17	0	0	0.12
YHR033W		B	20	0.21	0.07	0.65	0.05	-0.2	<b>0.5</b>	<b>-0.22</b>
YHR034C		B	20	0.07	0.07	0.09	0.05	0	0	0
YHR037W	PUT2	B	21	0.1	0.07	0.17	0.12	-0.07	0.06	-0.01
YHR039BC	VMA10	B	21	0.71	1.09	1.17	0.98	0.02	<b>0.22</b>	0
YHR039C		B	21	0.2	0.18	0.17	0.14	0	0	-0.13
YHR041C	SRB2	B	21	0.41	1.08	0.46	0.64	0.16	0	-0.09
YHR042W	NCP1	B	20	0.33	0.5	0.34	0.7	0	0	0.1
YHR043C	DOG2	B	20	0.11	0.07	0.2	0.07	-0.1	<b>0.22</b>	0
YHR045W		B	21	0.13	0.11	0.11	0.14	0	0	-0.13
YHR046C		B	21	0.07	0.07	0.07	0.11	0	0	0.13
YHR049W		B	21	0.28	0.54	0.55	0.25	0.06	0.18	-0.19
YHR050W	SMF2	B	20	0.18	0.19	0.18	0.14	0	0	0
YHR051W	COX6	B	21	0.56	0.66	2.02	0.85	0	<b>0.33</b>	0.06
YHR052W		B	20	0.07	0.07	0.07	0.06	0	0	0
YHR053C	CUP1	B	20	5.96	17.01	5.98	16.67	<b>0.4</b>	0.02	<b>0.34</b>
YHR054C		B	21	0.07	0.07	0.07	0.06	0	0	0

YHR055C	CUP1	B	20	6.8	6.52	4.94	15.95	0.05	-0.05	<b>0.43</b>
YHR056C		B	20	0.08	0.07	0.07	0.08	0	0	-0.13
YHR057C	CYP2	B	21	0.11	0.15	0.51	0.43	0.06	<b>0.35</b>	<b>0.32</b>
YHR062C	RPP1	B	21	0.07	0.09	0.07	0.05	0.09	0	0
YHR063C		B	21	0.18	0.17	0.26	0.1	0	0.1	-0.16
YHR064C	PDR13	B	20	0.94	1.16	1.05	0.87	0.06	0	-0.05
YHR065C	RRP3	B	20	0.07	0.07	0.09	0.05	0	0	0
YHR067W		B	20	0.07	0.07	0.08	0.05	0	0.05	0
YHR068W	DYS1	B	20	0.23	0.32	0.19	0.29	0	0	-0.03
YHR069C	RRP4	B	20	0.07	0.07	0.08	0.13	0	0	0
YHR070W		B	21	0.09	0.14	0.21	0.22	0	0	0.01
YHR071W	PCL5	B	20	0.07	0.07	0.18	0.08	0	<b>0.32</b>	-0
YHR072W	ERG7	B	20	0.07	0.09	0.14	0.12	0	0	0
YHR074W		B	21	0.11	0.15	0.19	0.15	0	0.06	0
YHR076W		B	21	0.12	0.08	0.14	0.09	-0.1	0	0
YHR078W		B	20	0.13	0.1	0.08	0.1	0	0	-0.12
YHR082C	KSP1	B	20	0.07	0.07	0.07	0.06	0	0	0
YHR083W		B	20	0.2	0.25	0.35	0.3	0.05	0.18	0.04
YHR084W	STE12	B	20	0.07	0.07	0.07	0.06	0	0	0
YHR086W	NAM8	B	20	0.19	0.25	0.22	0.11	0	0	0
YHR087W		B	20	0.82	0.7	0.88	0.52	-0.11	-0.09	0
YHR089C	GAR1	B	20	0.55	0.65	0.4	0.24	0.03	-0.05	<b>-0.21</b>
YHR091C	MSR1	B	20	0.08	0.07	0.09	0.07	0	0	-0.12
YHR092C	HXT4	B	20	0.76	0.41	0.12	0.61	-0.02	<b>-0.5</b>	-0.13
YHR094C	HXT1	B	20	0.84	1.34	0.07	1.57	0.06	<b>-0.8</b>	0.14
YHR096C	HXT5	B	20	0.07	0.07	0.07	0.16	0	0	0.16
YHR097C		B	40	0.12	0.07	0.08	0.07	-0.1	0	0
YHR098C		B	21	0.1	0.11	0.11	0.09	0	0	0
YHR100C		B	20	0.07	0.07	0.08	0.05	0	0	0
YHR104W	GRE3	B	20	0.43	0.19	0.78	1.63	-0.12	0.14	<b>0.57</b>
YHR106W	TRR2	B	20	0.13	0.11	0.1	0.18	0	0	-0.02
YHR107C	CDC12	B	20	0.12	0.11	0.09	0.09	0	0	0
YHR108W		B	20	0.07	0.1	0.12	0.06	0	0	0
YHR110W		B	20	0.2	0.14	0.25	0.11	0	0.03	<b>-0.2</b>
YHR112C		B	20	0.14	0.1	0.15	0.2	0	0	0.04
YHR113W		B	20	0.27	0.19	0.21	0.22	-0.02	0	-0.04
YHR114W		B	20	0.07	0.07	0.07	0.05	0	0	0
YHR115C		B	21	0.1	0.11	0.16	0.14	0	0	0
YHR116W		B	20	0.07	0.08	0.07	0.07	0	0	0
YHR123W	EPT1	B	41	0.14	0.14	0.13	0.05	0	0	<b>-0.22</b>
YHR128W	FUR1	B	21	0.44	1.09	0.48	0.69	<b>0.38</b>	0.14	0.15
YHR132C	ECM14	B	21	0.14	0.18	0.33	0.16	0.16	<b>0.21</b>	0
YHR133C		B	20	0.42	0.69	0.7	0.23	0.02	0.01	0
YHR135C	YCK1	B	20	0.11	0.09	0.07	0.11	0	0	0
YHR138C		B	20	0.35	0.33	0.51	0.51	-0.17	0.14	0.07
YHR139C	SPS100	B	20	0.07	0.07	0.08	0.07	0	0	0
YHR140W		B	20	0.07	0.07	0.08	0.05	0	0	0
YHR141C	RPL42B	B	20	1.03	1.98	2.78	1.45	<b>0.35</b>	<b>0.33</b>	0.04
YHR142W		B	20	0.27	0.27	0.39	0.37	-0.07	0.04	0.08
YHR143W		B	20	0.48	0.54	0.89	0.57	0.05	<b>0.24</b>	0.05
YHR143W-A	RPB12	B	20	0.12	0.23	0.32	0.16	0.1	<b>0.25</b>	0
YHR145C		B	21	0.1	0.07	0.07	0.05	0	0	0
YHR146W		B	20	0.07	0.07	0.14	0.06	0	0.15	0
YHR147C	MRPL6	B	20	0.11	0.14	0.08	0.12	0	0	0
YHR161C	YAP1801	B	20	0.09	0.08	0.1	0.08	0	0	0

YHR162W		B	20	1.38	2.26	1.85	1.21	0.13	0.19	-0.11
YHR163W	SOL3	B	20	0.47	0.59	0.84	0.7	0	0.14	-0.01
YHR170W	NMD3	B	21	0.07	0.15	0.09	0.09	0.02	0	0
YHR171W		B	20	0.09	0.07	0.07	0.05	0	0	0
YHR174W	ENO2	B	20	15.27	25.96	21.33	13.1	0.04	-0.07	-0.13
YHR175W	CTR2	B	20	0.4	0.55	0.7	0.24	0.11	<b>0.26</b>	<b>-0.2</b>
YHR176W		B	20	0.12	0.07	0.07	0.05	0	-0	0
YHR179W	OYE2	B	20	0.78	0.66	1.1	1.42	0	<b>0.35</b>	<b>0.33</b>
YHR180W		B	20	0.07	0.07	0.07	0.06	0	0	0
YHR181W		B	21	0.35	0.71	0.5	0.41	0.13	0.15	0.04
YHR183W	GND1	B	20	1.99	2.73	3.45	1.46	0.07	<b>0.31</b>	-0.09
YHR187W	IKI1	B	21	0.09	0.07	0.11	0.08	0	0	-0.14
YHR188C		B	20	0.3	0.31	0.33	0.3	-0.04	0.01	-0.07
YHR190W	ERG9	B	21	0.54	0.69	0.76	0.51	0.03	0.09	0.02
YHR191C	CTF8	B	21	0.07	0.09	0.08	0.06	0	0	0
YHR192W		B	20	0.07	0.07	0.08	0.11	0	0	-0.04
YHR193C	EGD2	B	21	1.12	2.16	2.79	2.23	0.19	<b>0.38</b>	0.15
YHR194W		B	21	0.07	0.1	0.11	0.08	0	0	-0.11
YHR195W		B	21	0.07	0.07	0.07	0.06	0	0	0
YHR198C		B	21	0.11	0.07	0.1	0.07	0	0	0
YHR199C		B	21	0.36	0.29	0.33	0.27	-0.02	-0	-0.05
YHR200W	RPN10	B	21	0.31	0.44	0.5	0.42	0.06	0.07	0.17
YHR201C	PPX1	B	21	0.07	0.07	0.08	0.06	0	0	0
YHR202W		B	20	0.07	0.07	0.09	0.06	0	0	-0.16
YHR203C	RPS4B	B	20	4.69	7.32	9.08	4.42	0.13	0.19	-0.14
YHR205W	SCH9	B	20	0.13	0.07	0.07	0.09	0	0	-0
YHR206W	SKN7	B	21	0.07	0.08	0.08	0.09	0	0	0
YHR208W	BAT1	B	20	0.47	0.89	1.18	0.57	0.04	0.11	0
YHR214C-B		B	40	0.23	0.19	0.28	0.63	0.08	0.09	0.21
YHR215W	PHO12	B	20	0.07	0.07	0.07	0.07	0	0	0
YHR217C		B	10	0.26	0.19	0.16	0.06	-0.11	-0.15	0
YHR219W		B	20	0.35	0.47	0.69	0.57	0	0.18	0.01
YIL001W		B	21	0.07	0.07	0.08	0.05	0	0	0
YIL007C		B	20	0.07	0.07	0.07	0.06	0	0	-0.15
YIL008W		B	21	0.07	0.11	0.07	0.05	0.04	0	0
YIL009W	FAA3	B	20	0.07	0.07	0.07	0.07	0	0	0
YIL010W	DOT5	B	20	0.08	0.09	0.2	0.13	0	0.1	0.02
YIL011W		B	21	0.64	0.49	0.33	0.34	0	-0.11	-0.19
YIL014W		B	21	0.07	0.07	0.07	0.07	0	0	-0.14
YIL015C-A		B	20	0.07	0.08	0.08	0.07	0	0	0
YIL015W	BAR1	B	20	0.45	0.07	0.42	0.64	<b>-0.7</b>	-0	0.11
YIL018W	RPL2B	B	26	8.69	15.94	13.08	7.97	<b>0.2</b>	0.05	-0.14
YIL020C	HIS6	B	20	0.07	0.11	0.08	0.09	0	0	0.01
YIL021W	RPB3	B	20	0.12	0.11	0.14	0.17	0	0	0.01
YIL022W	TIM44	B	20	0.07	0.09	0.08	0.12	0	0	0
YIL023C		B	20	0.26	0.13	0.21	0.23	-0.14	0	-0.1
YIL027C		B	20	0.07	0.08	0.14	0.07	0	0.12	0
YIL030C	SSM4	B	20	0.14	0.12	0.14	0.09	0	0.01	0
YIL033C	SRA1	B	21	0.38	0.36	0.52	0.59	-0.02	0	0.12
YIL034C	CAP2	B	20	0.62	0.51	0.52	1.26	-0.08	0	0.15
YIL036W		B	20	0.07	0.07	0.07	0.06	0	0	0
YIL038C	NOT3	B	20	0.09	0.07	0.12	0.07	0	0.02	0
YIL039W		B	21	0.13	0.25	0.34	0.15	0	0	0
YIL040W		B	20	0.31	0.38	0.61	0.24	0	0.19	0
YIL041W		B	20	0.81	1.1	1.22	0.8	0.09	0.17	0.04

YIL042C		B	21	0.12	0.07	0.11	0.09	-0.02	0	0
YIL043C	CBR1	B	20	2.69	2.41	2.93	1.48	0	0.04	0
YIL044C		B	20	0.07	0.07	0.07	0.08	0	0.03	0.06
YIL045W	PIG2	B	20	0.09	0.07	0.07	0.05	0	-0.1	0
YIL046W	MET30	B	21	0.09	0.08	0.07	0.19	0	0	0
YIL047C	SYG1	B	20	0.14	0.19	0.13	0.22	0	0	0.14
YIL048W	NEO1	B	21	0.17	0.15	0.19	0.16	0	-0.03	-0.09
YIL049W	DFG10	B	20	0.12	0.13	0.16	0.09	0	0.06	0
YIL050W	PCL7	B	20	0.1	0.1	0.29	0.12	0	<b>0.34</b>	0
YIL051C	MMD1	B	21	2.45	3.98	4.11	3.06	0.17	0.12	0.02
YIL052C	RPL34B	B	20	2.34	4.11	5.06	1.76	<b>0.28</b>	<b>0.24</b>	-0.25
YIL053W	RHR2	B	20	2.53	3.14	4.93	3.29	0.05	0.19	0.04
YIL056W		B	20	0.07	0.07	0.07	0.06	0	0	0
YIL059C		B	21	0.07	0.12	0.13	0.09	0	0	-0.15
YIL062C	ARC15	B	20	0.73	1.21	1.28	1.19	0.02	<b>0.21</b>	0.16
YIL064W		B	20	0.07	0.1	0.08	0.05	0.05	0	0
YIL065C		B	20	0.08	0.08	0.15	0.12	0	0.14	0.03
YIL066C	RNR3	B	21	0.07	0.14	0.1	0.06	0	0	0
YIL067C		B	21	0.07	0.07	0.09	0.08	0	0	-0.07
YIL069C	RPS24B	B	44	0.45	0.93	0.74	0.48	<b>0.2</b>	0.1	0.01
YIL070C		B	20	0.27	0.23	0.31	0.29	0	0	-0.02
YIL074C		B	20	0.12	0.12	0.11	0.2	0	0	0.07
YIL075C	RPN2	B	21	0.16	0.13	0.19	0.2	-0.1	0	-0.12
YIL076W	SEC28	B	20	0.1	0.13	0.28	0.14	0.1	<b>0.29</b>	-0.03
YIL077C		B	20	0.09	0.07	0.07	0.05	-0.1	-0.1	0
YIL078W	THS1	B	20	0.8	1.46	0.94	0.65	0.04	0.05	0
YIL083C		B	20	0.26	0.39	0.39	0.54	0.05	0.09	0.05
YIL085C	KTR7	B	20	0.07	0.07	0.07	0.08	0	0	0
YIL087C		B	21	0.37	0.34	0.54	0.33	-0.06	0.14	-0.07
YIL088C		B	21	0.26	0.16	0.26	0.1	0	0.03	-0.14
YIL090W		B	20	0.11	0.1	0.12	0.08	0	0	0
YIL093C		B	21	0.07	0.07	0.08	0.05	0	0.03	0
YIL094C		B	21	0.85	0.98	1.97	0.86	-0.09	<b>0.2</b>	-0.05
YIL098C	FMC1	B	21	0.07	0.07	0.08	0.06	0	0	0
YIL099W	SGA1	B	20	0.09	0.07	0.07	0.05	0	0	0
YIL101C	XBP1	B	20	0.12	0.08	0.22	0.06	0	0	0
YIL104C		B	21	0.07	0.07	0.08	0.11	0	0	-0.14
YIL106W	MOB1	B	20	0.11	0.13	0.12	0.07	0	0	-0.12
YIL108W		B	20	0.1	0.12	0.11	0.15	0	0	0.02
YIL109C	SEC24	B	20	0.37	0.36	0.47	0.38	-0.03	0.13	0.01
YIL111W	COX5B	B	20	0.23	0.13	0.2	0.33	<b>-0.2</b>	0	0.21
YIL113W		B	20	0.07	0.07	0.07	0.06	0	0	0
YIL114C	POR2	B	21	0.16	0.15	0.22	0.11	0	0	0
YIL115C	NUP159	B	20	0.08	0.07	0.08	0.05	0	0	0
YIL116W	HIS5	B	21	0.08	0.07	0.1	0.08	0	-0.01	0
YIL117C		B	20	0.07	0.07	0.07	0.16	0	0	0.15
YIL118W	RHO3	B	21	0.08	0.07	0.1	0.08	0	0.03	-0.15
YIL119C	RPI1	B	20	0.07	0.08	0.07	0.1	0	0	-0.09
YIL121W		B	20	0.16	0.2	0.21	0.14	<i>0.11</i>	0.08	0
YIL123W	SIM1	B	21	0.68	1.15	1.03	1.1	0.12	0.04	0.07
YIL124W		B	20	0.69	0.69	0.65	1.08	0	0.2	0.19
YIL125W	KGD1	B	20	0.15	0.1	0.27	0.08	-0.03	<b>0.24</b>	0
YIL129C		B	20	0.12	0.13	0.15	0.15	0	0	-0.04
YIL131C	FKH1	B	21	0.07	0.1	0.07	0.06	0	0	0
YIL133C	RPL16A	B	20	4.77	8.84	5.2	3.77	<b>0.26</b>	0.11	-0.09

YIL134W	FLX1	B	21	0.07	0.07	0.07	0.06	0	0	-0.14
YIL135C		B	20	0.13	0.18	0.1	0.24	0	0	0.04
YIL136W	OM45	B	21	0.15	0.09	0.23	0.37	-0.1	0.11	0.12
YIL137C		B	21	0.07	0.07	0.07	0.06	0	0	-0.12
YIL140W	SRO4	B	21	0.09	0.1	0.08	0.06	0	0	0
YIL142W	CCT2	B	21	0.11	0.19	0.23	0.21	0	0.11	0.01
YIL145C		B	20	0.21	0.23	0.31	0.22	0	0.08	0
YIL148W	RPL40A	B	32	3.68	4.12	3.82	2.64	0.02	-0.02	-0.11
YIL152W		B	20	0.11	0.07	0.14	0.05	0	0	0
YIL154C	IMP2'	B	21	0.27	0.22	0.31	0.4	-0.13	0	0.03
YIL155C	GUT2	B	21	0.07	0.07	0.15	0.08	0	0.2	0
YIL156W	UBP7	B	20	0.07	0.07	0.07	0.06	0	0	0
YIL157C		B	20	0.89	0.39	0.55	0.73	-0.06	0.01	0
YIL158W		B	21	0.15	0.19	0.16	0.05	0.02	0	0
YIL160C	POT1	B	20	0.08	0.07	0.07	0.05	0	0	0
YIL162W	SUC2	B	20	0.08	0.09	0.13	0.06	0	0	0
YIL164C	NIT1	B	21	0.07	0.07	0.11	0.05	0	0	0
YIL165C		B	21	0.1	0.07	0.18	0.08	0	0.14	-0.11
YIL169C		B	20	0.07	0.07	0.07	0.07	0	0	0
YIL170W	HXT12	B	23	0.08	0.07	0.07	0.05	0	0	0
YIL176C		B	20	0.28	0.24	0.22	0.21	0	0	0
YIL177C		B	40	0.1	0.09	0.07	0.07	0	0	0
YIR003W		B	20	0.07	0.12	0.09	0.14	0	0	0
YIR006C	PAN1	B	20	0.14	0.17	0.34	0.33	0	0.03	0.01
YIR007W		B	21	0.07	0.07	0.07	0.07	0	0	-0.1
YIR011C	STS1	B	21	0.18	0.2	0.18	0.28	0.01	0	-0.01
YIR012W	SQT1	B	21	0.07	0.09	0.13	0.15	0.02	0.01	<b>0.23</b>
YIR013C		B	21	0.08	0.07	0.07	0.05	0	0	0
YIR016W		B	20	0.34	0.2	0.38	0.23	-0.1	0.1	<b>-0.21</b>
YIR018W	YAP5	B	21	0.09	0.07	0.07	0.05	0	0	0
YIR019C	MUC1	B	21	0.07	0.07	0.07	0.07	0	0	-0.16
YIR021W	MRS1	B	21	0.13	0.14	0.13	0.09	0	0	0
YIR022W	SEC11	B	20	0.8	1.03	1.51	0.96	-0.1	0.03	0
YIR024C	GIF1	B	21	0.07	0.07	0.07	0.07	0	0	0
YIR026C	YVH1	B	20	0.08	0.12	0.07	0.08	0	0	0
YIR028W	DAL4	B	20	0.07	0.07	0.07	0.07	0	0	0
YIR034C	LYS1	B	20	4.01	3.18	4.66	2.33	<b>-0.25</b>	0.07	<b>-0.4</b>
YIR035C		B	21	0.31	0.6	0.42	1.16	0.16	0.04	<b>0.31</b>
YIR036C		B	20	0.36	0.23	0.33	0.46	-0.05	0	0.13
YIR037W	HYR1	B	20	2.43	3.06	2.8	4.8	-0.05	-0.01	0.21
YIR038C		B	20	0.66	0.38	0.93	1.67	-0.14	0.13	<b>0.41</b>
YIR041W		B	20	0.11	0.13	0.17	0.16	0	0	0
YIR043C		B	26	0.09	0.07	0.07	0.08	0	0	0
YIR044C		B	20	0.25	0.41	0.41	0.34	0.1	0	0
YJL001W	PRE3	B	29	0.39	0.61	0.66	0.98	0.12	0.14	<b>0.27</b>
YJL002C	OST1	B	20	0.57	0.96	0.4	0.6	0.09	0	-0.01
YJL004C	SYS1	B	20	0.21	0.25	0.29	0.18	0.03	0.07	-0.05
YJL008C	CCT8	B	20	0.09	0.12	0.19	0.1	0	0	0
YJL011C		B	21	0.09	0.07	0.07	0.05	0	-0.1	0
YJL012C		B	20	0.14	0.2	0.12	0.15	0	-0.11	-0.13
YJL014W	CCT3	B	20	0.23	0.23	0.29	0.18	0.08	0.04	-0.08
YJL015C		B	21	0.07	0.07	0.07	0.05	0	0	0
YJL016W		B	21	0.12	0.11	0.13	0.35	0	-0.01	<b>0.36</b>
YJL017W		B	21	0.09	0.07	0.1	0.17	0	0	-0.05
YJL020C		B	21	0.09	0.07	0.07	0.07	0	0	0

YJL021C		B	20	0.07	0.07	0.07	0.05	0	0	0
YJL026W	RNR2	B	20	0.39	0.88	0.72	0.25	0	0.02	0
YJL027C		B	21	0.11	0.07	0.07	0.06	0	0	0
YJL030W	MAD2	B	20	0.07	0.07	0.07	0.09	0	0	0
YJL032W		B	20	0.07	0.07	0.07	0.06	0	0	0
YJL034W	KAR2	B	21	1.13	0.99	2.07	1.16	-0.09	<b>0.2</b>	0.09
YJL041W	NSP1	B	20	0.07	0.07	0.1	0.1	0	0	0
YJL042W	MHP1	B	20	0.09	0.14	0.2	0.17	0	0	-0.01
YJL044C	GYP6	B	20	0.09	0.07	0.09	0.06	0	0	0
YJL045W		B	21	0.07	0.07	0.07	0.1	0	0	-0.11
YJL048C		B	20	0.19	0.07	0.23	0.22	<b>-0.29</b>	0	0.05
YJL052W	TDH1	B	21	9.02	8.02	6.58	0.05	-0.01	-0.15	<b>-1.7</b>
YJL053W	PEP8	B	20	0.23	0.17	0.18	0.21	-0	0	-0.03
YJL055W		B	21	0.51	0.55	0.57	0.77	0.01	0.13	0.12
YJL057C	IKS1	B	20	0.12	0.07	0.07	0.05	-0.2	0	0
YJL060W		B	20	0.1	0.07	0.07	0.08	-0	0	0
YJL061W	NUP82	B	20	0.1	0.07	0.07	0.08	-0.1	-0.1	0
YJL062W		B	21	0.26	0.08	0.09	0.06	-0.06	-0.16	0
YJL063C	MRPL8	B	21	0.25	0.2	0.11	0.17	0	-0.06	-0.16
YJL065C		B	21	0.19	0.16	0.15	0.21	-0.05	-0.05	-0.08
YJL066C		B	20	0.09	0.09	0.11	0.17	0	0	0.09
YJL068C		B	21	0.5	0.36	0.57	0.61	-0.13	-0.03	0.14
YJL078C	PRY3	B	21	0.08	0.07	0.08	0.1	0	0	0
YJL079C	PRY1	B	21	1.44	0.61	2.1	1.78	-0.14	0.19	-0.1
YJL080C	SCP160	B	20	0.27	0.2	0.23	0.19	0	0	-0.17
YJL081C	ARP4	B	21	0.09	0.07	0.07	0.05	-0.02	0	0
YJL082W		B	20	0.12	0.07	0.08	0.11	0	0	-0.15
YJL083W		B	21	0.12	0.07	0.09	0.07	0	0	0
YJL088W	ARG3	B	20	0.28	0.14	0.23	0.1	<b>-0.26</b>	0	<b>-0.29</b>
YJL091C		C	20	0.35	0.11	0.26	0.24	0	0	0
YJL097W		C	20	0.5	0.54	0.39	0.89	-0.05	0	0
YJL111W	CCT7	C	20	0.35	0.1	0.26	0.24	0	0	0
YJL116C	NCA3	C	20	0.35	0.1	0.26	0.45	0	0	0.1
YJL117W	PHO86	C	20	0.35	0.17	0.26	0.29	0	0	0
YJL121C	RPE1	C	21	0.84	0.74	0.45	0.61	-0.06	0	-0.12
YJL124C	SPB8	C	21	0.35	0.12	0.26	0.24	0	0	0
YJL130C	URA2	C	21	0.35	0.55	0.4	0.56	0.01	0	0.07
YJL133W	MRS3	C	20	0.35	0.1	0.26	0.24	0	0	0
YJL134W	LCB3	C	20	0.35	0.21	0.26	0.3	0	0	0
YJL136C	RPS21B	C	20	5.56	7.42	1.81	7.58	-0.02	<b>-0.25</b>	-0.07
YJL138C	TIF2	C	20	2.78	2.74	1.89	2.45	-0.09	0	-0.1
YJL143W	TIM17	C	21	0.42	0.56	0.26	0.66	-0.11	-0.16	-0.07
YJL151C		C	21	2.34	2	2.44	3.2	-0.05	0	0.1
YJL152W		C	21	0.35	0.11	0.26	0.24	0	0	0
YJL153C	INO1	C	20	0.35	1.25	1.27	0.4	0.22	0.24	0
YJL157C	FAR1	C	20	0.36	0.16	0.26	0.24	0	0	0
YJL158C	CIS3	C	20	9.57	6.6	3.2	4.62	-0.13	<b>-0.36</b>	<b>-0.33</b>
YJL159W		C	21	2.11	1.73	1.97	3.38	<b>-0.24</b>	<b>-0.2</b>	0.14
YJL164C	SRA3	C	21	0.47	0.15	0.26	0.44	<b>-0.56</b>	0	0
YJL166W	QCR8	C	20	0.37	0.35	0.37	0.52	0	0	0.05
YJL167W	ERG20	C	20	0.57	0.56	0.26	0.82	-0.04	<b>-0.3</b>	0.09
YJL171C		C	20	0.55	0.19	0.27	0.36	0	-0.2	0
YJL173C	RFA3	C	20	0.43	0.16	0.36	0.27	0	0	0
YJL174W	KRE9	C	20	0.5	0.42	0.41	0.6	0	0	0.05
YJL177W	RPL17B	C	38	4.7	4.6	2.6	3.03	0.01	-0.17	-0.1

YJL178C		C	20	0.35	0.17	0.28	0.26	0	0	0
YJL189W	RPL39	C	20	5.75	4.06	2.91	3.81	-0.06	-0.18	-0.14
YJL190C	RPS22A	C	20	19.08	8.49	3.19	6.52	-0.13	<b>-0.44</b>	<b>-0.29</b>
YJL191W	RPS14B	C	20	2.33	1.56	0.94	4.33	-0.04	<b>-0.39</b>	<b>0.2</b>
YJL192C		C	21	0.37	0.3	0.26	0.38	0	0	0
YJL196C	ELO1	C	20	1.02	0.67	0.43	0.81	-0.09	<b>-0.3</b>	-0.14
YJL199C		C	21	0.35	0.11	0.26	0.24	0	0	0
YJL206C-A	NCE101	C	20	0.35	0.39	0.26	0.48	0	0	0.09
YJL210W	PEX2	C	21	0.6	0.26	0.26	0.34	<b>-0.38</b>	-0.19	0
YJL217W		C	20	0.35	0.3	0.26	0.47	0	0	0
YJR001W		C	21	0.35	0.19	0.26	0.24	<b>-0.27</b>	0	0
YJR004C	SAG1	C	21	0.35	1.74	0.26	0.24	<b>0.48</b>	0	0
YJR007W	SUI2	C	20	0.35	0.17	0.26	0.37	0	0	0
YJR008W		C	20	0.35	0.1	0.26	0.24	0	0	0
YJR009C	TDH2	C	20	7.93	10.33	3.96	10.44	-0.03	<b>-0.35</b>	0.03
YJR010C-A	SPC1	C	21	0.35	0.21	0.26	0.24	0	0	0
YJR014W		C	21	0.35	0.14	0.26	0.24	0	0	0
YJR015W		C	21	0.35	0.3	0.26	0.54	-0.16	0	0.09
YJR016C	ILV3	C	21	0.52	0.34	0.42	0.36	0	0	0
YJR017C	ESS1	C	21	0.4	0.28	0.26	0.53	0	0	0.03
YJR019C	TES1	C	21	0.35	0.21	0.26	0.3	0	0	-0.16
YJR024C		C	21	0.46	0.35	0.39	0.54	-0.17	0	-0.12
YJR025C	BNA1	C	20	0.66	0.53	0.86	1.09	<b>-0.2</b>	-0.1	0.08
YJR026W		C	20	0.35	0.09	0.26	0.67	0	0	<b>0.28</b>
YJR027W		C	40	0.35	0.21	0.26	0.57	0	0	0.18
YJR028W		C	20	0.35	0.11	0.26	0.53	0	0	0.19
YJR029W		C	40	0.35	0.18	0.26	0.44	0	0	0.08
YJR044C		C	20	0.49	0.7	0.44	1.1	-0.03	0	<b>0.26</b>
YJR045C	SSC1	C	20	0.48	0.54	0.34	1.1	-0.13	-0.2	0.1
YJR048W	CYC1	C	20	0.35	0.27	0.49	0.24	0	0	0
YJR058C	APS2	C	20	0.45	0.4	0.27	0.45	0	0	0
YJR059W	PTK2	C	21	0.35	0.09	0.26	0.24	0	0	0
YJR063W	RPA12	C	20	0.35	0.32	0.26	0.31	0	0	0
YJR064W	CCT5	C	20	0.35	0.25	0.26	0.47	0	0	0.01
YJR065C	ARP3	C	21	0.56	0.56	0.6	1.57	-0.18	0	0.24
YJR069C	HAM1	C	20	0.35	0.21	0.26	0.24	0	0	0
YJR070C		C	21	0.35	0.43	0.26	0.24	0.09	0	0
YJR073C	OPI3	C	20	14.51	12.48	4.73	9.55	-0.07	<b>-0.47</b>	<b>-0.26</b>
YJR074W		C	21	0.35	0.23	0.31	0.42	0	0	0.06
YJR075W	HOC1	C	21	0.35	0.14	0.26	0.24	0	0	0
YJR076C	CDC11	C	20	0.35	0.14	0.26	0.24	0	0	0
YJR077C	MIR1	C	20	2.68	2.67	3.01	3.73	-0.04	-0.02	0.09
YJR080C		C	21	0.35	0.1	0.26	0.24	0	0	0
YJR084W		C	20	0.35	0.11	0.26	0.24	0	0	0
YJR085C		C	20	1.62	1.82	1.05	2.57	-0.01	-0.2	0.08
YJR086W	STE18	C	21	0.35	0.11	0.26	0.24	<b>-0.51</b>	0	0
YJR094W-A	RPL43B	C	20	3.91	5.68	1.9	5.1	0.14	<b>-0.33</b>	0.04
YJR096W		C	21	0.35	0.09	0.26	0.52	0	0	0.17
YJR101W		C	21	0.35	0.31	0.26	0.31	0	0	0
YJR103W	URA8	C	21	0.35	0.17	0.26	0.39	<b>-0.36</b>	0	0
YJR104C	SOD1	C	21	5.06	3.61	4.83	6.49	<b>-0.21</b>	-0.19	0.01
YJR105W		C	20	1.17	0.98	0.61	1.32	0	<b>-0.24</b>	-0
YJR113C		C	20	0.35	0.27	0.37	0.68	0	0	-0.06
YJR115W		C	21	0.35	0.28	0.26	0.47	-0.22	0	0
YJR116W		C	20	0.35	0.28	0.26	0.44	0	0	0

YJR117W	STE24	C	20	0.35	0.1	0.26	0.37	0	0	-0.13
YJR118C		C	20	0.35	0.17	0.26	0.24	0	0	0
YJR121W	ATP2	C	21	0.8	1.3	0.7	1.16	0.05	0	-0.06
YJR123W	RPS5	C	20	5.23	7.14	1.26	3.89	0.07	<b>-0.3</b>	0
YJR125C		C	20	0.35	0.12	0.26	0.24	0	0	0
YJR126C		C	20	0.35	0.15	0.26	0.24	0	0	0
YJR127C	ZMS1	C	20	0.35	0.14	0.26	0.44	0	0	0.07
YJR133W		C	21	0.46	0.63	0.63	0.83	0.03	0	-0.01
YJR139C	HOM6	C	21	1.05	1.09	1	1.55	0.03	-0.1	0.05
YJR143C	PMT4	C	20	0.49	0.35	0.26	0.4	0	<b>-0.3</b>	0
YJR145C	RPS4A	C	20	2.08	3.91	1.25	2.76	<b>0.26</b>	-0.19	0.07
YJR148W	BAT2	C	20	0.35	0.09	0.26	0.25	0	0	0
YJR161C	C0S5	C	20	0.35	0.23	0.26	0.3	0	0	0
YKL001C	MET14	C	20	0.35	0.11	0.26	0.29	0	0	0
YKL002W		C	20	0.35	0.19	0.26	0.24	0	0	0
YKL003C	MRP17	C	20	0.35	0.17	0.26	0.32	0	0	0
YKL004W	AUR1	C	20	0.72	0.42	0.29	0.81	0	0	0.08
YKL006W	RPL14A	C	59	5.69	3.42	2.67	3.55	-0.26	-0.21	0
YKL007W	CAP1	C	21	0.35	0.13	0.26	0.26	0	0	0
YKL008C		C	20	0.35	0.31	0.26	0.37	0	0	0
YKL009W	MRT4	C	20	0.35	0.17	0.26	0.24	0	0	0
YKL010C	UFD4	C	21	0.35	0.09	0.26	0.25	0	0	0
YKL013C	ARC19	C	21	0.35	0.4	0.26	0.48	-0.06	0	-0.03
YKL016C	ATP7	C	21	0.4	0.51	0.55	0.85	-0.02	0.16	0.03
YKL018W		C	21	0.35	0.14	0.26	0.24	0	0	0
YKL019W	RAM2	C	20	0.35	0.1	0.26	0.26	0	0	0
YKL024C	URA6	C	21	0.35	0.29	0.26	0.43	-0.08	0	0.08
YKL028W	TFA1	C	20	0.35	0.11	0.26	0.28	0	0	0
YKL029C		C	21	0.35	0.12	0.26	0.4	0	0	-0.06
YKL034W		C	21	0.35	0.14	0.26	0.24	0	0	0
YKL035W		C	20	2.32	2.48	0.81	3.08	-0.09	<b>-0.42</b>	0.14
YKL039W	PTM1	C	21	0.35	0.35	0.26	0.69	-0.17	0	0.17
YKL043W	PHD1	C	20	0.53	0.09	0.26	0.24	0	0	0
YKL046C		C	21	0.35	0.32	0.26	0.52	0	0	0.02
YKL051W		C	21	0.35	0.11	0.26	0.24	0	0	0
YKL053W		C	21	0.35	0.09	0.26	0.24	0	0	0
YKL054C		C	20	0.35	0.21	0.26	0.36	0	0	0
YKL056C		C	20	10.71	10.33	5.08	8.56	0.03	-0.17	-0.06
YKL058W	TOA2	C	20	0.35	0.29	0.26	0.45	0	0	0
YKL060C	FBA1	C	20	11.55	22.12	8.98	25.53	0.02	-0.17	0.05
YKL062W	MSN4	C	20	0.35	0.19	0.26	0.51	0	0	0.01
YKL065C	YET1	C	20	0.53	0.68	0.46	1.2	-0.11	0	<b>0.2</b>
YKL066W		C	21	0.35	0.13	0.26	0.24	<b>-0.43</b>	0	0
YKL067W	YNK1	C	20	0.78	0.78	0.9	1.91	-0.11	0	<b>0.24</b>
YKL077W		C	20	0.35	0.32	0.26	0.48	-0.08	0	0.04
YKL080W	VMA5	C	20	1.29	0.8	1.11	1.24	<b>-0.32</b>	<b>-0.22</b>	-0.02
YKL081W	TEF4	C	40	0.51	0.84	0.34	0.37	0.05	-0.18	0
YKL084W		C	20	0.35	0.19	0.26	0.24	0	0	0
YKL085W	MDH1	C	21	1.47	0.86	1.04	1.45	<b>-0.21</b>	0	0
YKL086W		C	21	0.35	0.12	0.26	0.26	0	0	0
YKL087C	CYT2	C	20	0.35	0.2	0.28	0.47	0	0	0
YKL091C		C	20	0.35	0.1	0.26	0.27	0	0	0
YKL094W	YJU3	C	20	0.35	0.21	0.26	0.46	0	0	0.07
YKL096W	CWP1	C	21	4.38	5.54	1.36	9.13	0.01	<b>-0.47</b>	<b>0.31</b>
YKL097W-A	CWP2	C	20	40.86	25.7	15.05	33.07	-0.18	<b>-0.29</b>	-0.12

YKL100C		C	21	0.35	0.12	0.26	0.24	0	0	0
YKL103C	LAP4	C	21	0.35	0.25	0.26	1	<b>-0.29</b>	0	0.17
YKL104C	GFA1	C	20	0.35	0.36	0.28	0.46	-0.05	0	0
YKL117W	SBA1	C	20	0.42	0.33	0.45	1.51	<b>-0.26</b>	0	<b>0.28</b>
YKL120W		C	20	0.35	0.14	0.26	0.25	0	0	0
YKL122C	SRP21	C	20	0.35	0.11	0.26	0.25	0	0	0
YKL126W	YPK1	C	20	0.45	0.24	0.27	0.28	0	0	0
YKL127W	PGM1	C	21	0.35	0.21	0.26	0.24	-0.28	0	0
YKL128C	PMU1	C	21	0.35	0.15	0.26	0.24	<b>-0.44</b>	0	0
YKL140W	TGL1	C	20	0.35	0.16	0.26	0.39	0	0	0
YKL141W	SDH3	C	20	0.6	0.42	0.82	0.59	-0.12	0.02	-0.07
YKL142W	MRP8	C	20	0.37	0.2	0.37	0.64	0	0	0.13
YKL144C	RPC25	C	20	0.35	0.09	0.26	0.24	0	0	0
YKL145W	RPT1	C	20	0.56	0.53	0.44	0.82	-0.03	0	0.11
YKL146W		C	20	0.38	0.35	0.27	0.37	-0.17	0	0
YKL148C	SDH1	C	20	0.51	0.15	0.36	0.24	0	0	0
YKL150W	MCR1	C	20	0.62	0.43	0.92	1.02	0	0.14	<b>0.27</b>
YKL151C		C	20	0.35	0.16	0.26	0.9	0	0	0.35
YKL152C	GPM1	C	20	8.38	7.69	4.91	9.57	0	-0.14	0.1
YKL156W	RPS27A	C	20	2.36	1.5	2.3	3.31	-0.17	0.07	0.15
YKL157W	APE2	C	20	0.35	0.24	0.26	0.43	<b>-0.3</b>	0	0
YKL160W		C	20	0.35	0.17	0.29	0.24	0	0	0
YKL163W	PIR3	C	20	1.28	0.88	1.3	9.38	0	0.01	<b>0.49</b>
YKL164C	PIR1	C	21	5.07	5.54	2.62	7.47	0.03	<b>-0.28</b>	<b>0.21</b>
YKL165C	MCD4	C	20	0.35	0.17	0.47	0.24	0	0	0
YKL167C	MRP49	C	20	0.35	0.14	0.26	0.29	0	0	0
YKL170W	MRPL38	C	21	0.35	0.12	0.26	0.24	<b>-0.47</b>	0	0
YKL172W		C	20	0.35	0.11	0.26	0.24	0	0	0
YKL174C		C	20	0.35	0.16	0.26	0.41	0	0	0.05
YKL175W		C	21	0.65	1.27	0.32	0.53	0	0	0
YKL178C	STE3	C	20	0.35	0.43	0.26	0.24	0.09	0	0
YKL180W	RPL17A	C	43	11.66	11.93	8.58	9.2	-0.02	-0.11	-0.1
YKL181W	PRS1	C	21	0.44	0.37	0.45	0.65	-0.26	0	-0.02
YKL182W	FAS1	C	20	0.77	1.43	0.59	1.36	0.12	0	0.15
YKL184W	SPE1	C	21	0.35	0.52	0.26	0.34	0.05	0	0
YKL185W	ASH1	C	20	0.35	0.3	0.28	0.3	0	0	0
YKL186C	MTR2	C	20	0.35	0.16	0.26	0.24	0	0	0
YKL190W	CNB1	C	41	0.35	0.25	0.3	0.52	0	0	-0.07
YKL191W	DPH2	C	20	0.35	0.34	0.31	0.44	0	0	0.01
YKL192C		C	20	2.87	3.42	2.83	5.54	-0.07	0	0.23
YKL196C	YKT6	C	21	0.35	0.16	0.26	0.24	<b>-0.34</b>	0	0
YKL199C	YKT9	C	21	0.35	0.21	0.26	0.24	<b>-0.31</b>	0	0
YKL207W		C	21	0.35	0.56	0.26	0.52	0	0	-0.01
YKL210W	UBA1	C	21	0.35	0.22	0.26	0.26	0	0	0
YKL211C	TRP3	C	20	0.35	0.35	0.37	0.46	0	0	0
YKL212W	SAC1	C	20	0.35	0.2	0.26	0.42	0	0	-0.03
YKL213C	DOA1	C	21	0.35	0.12	0.26	0.3	0	0	0
YKL214C		C	21	0.35	0.14	0.26	0.24	<b>-0.48</b>	0	0
YKL216W	URA1	C	20	0.35	0.21	0.3	0.24	0	0	0
YKR004C	ECM9	C	20	0.35	0.13	0.26	0.24	0	0	0
YKR006C	MRPL13	C	20	0.35	0.16	0.26	0.26	0	0	0
YKR013W	PRY2	C	21	1.31	1.85	1.08	2.67	0.12	-0.06	<b>0.2</b>
YKR018C		C	21	0.35	0.19	0.26	0.4	<b>-0.49</b>	0	-0.11
YKR025W		C	20	0.35	0.13	0.26	0.24	0	0	0
YKR026C	GCN3	C	20	0.35	0.15	0.26	0.24	0	0	0

YKR030W		C	20	0.35	0.19	0.26	0.34	0	0	0
YKR038C		C	21	0.35	0.1	0.26	0.24	0	0	0
YKR039W	GAP1	C	20	0.49	0.2	0.26	0.44	0	0	0
YKR042W	UTH1	C	21	4.61	6.54	2.7	7.27	0.1	<b>-0.23</b>	0.08
YKR043C		C	21	0.36	0.65	0.57	0.8	0	0	-0.01
YKR046C		C	21	0.35	0.16	0.29	1.21	0	0	<b>0.32</b>
YKR048C	NAP1	C	21	0.38	0.29	0.26	0.4	-0.12	0	0.05
YKR049C		C	21	0.35	0.2	0.26	0.53	0	0	0.18
YKR056W	RNC1	C	20	0.35	0.09	0.26	0.24	0	0	0
YKR057W	RPS21A	C	29	2.86	8.27	4.07	5.08	0.17	-0.12	-0.09
YKR059W	TIF1	C	20	1.57	4.14	1.34	2.32	0.14	0	0
YKR062W	TFA2	C	21	0.35	0.1	0.26	0.24	0	0	0
YKR065C		C	20	0.92	0.88	0.61	1.22	-0.08	0	0.1
YKR066C	CCP1	C	20	1.09	1.22	0.63	3.07	-0.13	0	<b>0.22</b>
YKR067W		C	20	0.35	0.1	0.26	0.28	0	0	0
YKR068C	BET3	C	21	0.47	0.39	0.29	0.54	-0.03	0	0.11
YKR070W		C	20	0.35	0.15	0.26	0.29	0	0	0
YKR071C		C	21	0.35	0.11	0.26	0.24	<b>-0.53</b>	0	0
YKR074W		C	20	0.35	0.36	0.26	0.38	0	0	-0.01
YKR076W	ECM4	C	21	0.35	0.11	0.26	0.27	0	0	0
YKR080W	MTD1	C	20	0.35	0.15	0.26	0.3	0	0	0
YKR088C		C	20	0.35	0.15	0.26	0.25	0	0	0
YKR093W	PTR2	C	20	0.35	0.33	0.26	0.43	0	0	-0.13
YKR094C	RPL40B	C	29	1.16	1.48	1.19	0.98	0.14	-0.08	-0.05
YKR100C		C	20	0.35	0.1	0.26	0.24	0	0	0
YLL009C	COX17	C	21	0.35	0.12	0.26	0.26	0	0	0
YLL010C		C	20	0.35	0.1	0.26	0.24	0	0	0
YLL014W		C	21	0.77	1.1	0.49	0.86	0.05	0	-0.09
YLL018C	DPS1	C	20	0.36	0.81	0.3	0.76	0	0	0.09
YLL020C		C	24	0.35	0.34	0.26	0.63	0	0	<b>0.22</b>
YLL022C	HIF1	C	20	0.35	0.1	0.26	0.24	0	0	0
YLL023C		C	21	1.04	0.93	0.28	1.53	0	0	0.01
YLL024C	SSA2	C	20	2.07	3.05	0.76	4.73	0.17	<b>-0.46</b>	<b>0.26</b>
YLL025W		C	22	0.35	0.27	0.36	0.42	0	0	0
YLL026W	HSP104	C	20	0.47	0.25	0.4	1.25	0	0	<b>0.27</b>
YLL027W		C	21	0.35	0.24	0.26	0.24	-0.23	0	0
YLL028W		C	21	0.35	0.26	0.26	0.37	-0.21	0	0
YLL031C		C	20	0.35	0.17	0.26	0.24	<b>-0.49</b>	0	0
YLL039C	UBI4	C	20	0.35	0.43	0.71	2.2	-0.19	0	<b>0.57</b>
YLL040C	VPS13	C	20	0.35	0.11	0.26	0.24	<b>-0.55</b>	0	0
YLL041C	SDH2	C	21	1.13	0.79	1.73	1.32	<b>-0.26</b>	0.05	-0.04
YLL043W	FPS1	C	20	0.35	0.19	0.26	0.24	0	0	0
YLL044W		C	20	0.35	0.12	0.26	0.24	0	0	0
YLL045C	RPL8B	C	20	1.68	3.2	0.74	2.01	0.12	<b>-0.34</b>	0
YLL048C	YBT1	C	20	0.35	0.16	0.26	0.24	0	0	0
YLL049W		C	20	0.35	0.1	0.26	0.24	0	0	0
YLL050C	COF1	C	21	1.14	2.89	1.57	3.83	0.18	-0.03	<b>0.3</b>
YLL051C	FRE6	C	20	0.35	0.09	0.26	0.24	0	0	0
YLL053C		C	20	0.35	0.25	0.26	0.31	0	0	0
YLL056C		C	21	0.35	0.09	0.26	0.26	0	0	0
YLL058W		C	21	0.35	0.15	0.26	0.24	0	0	0
YLL064C		C	20	0.37	0.33	0.52	0.42	0	0	0
YLL066C		C	40	0.35	0.16	0.26	0.32	0	0	0
YLL067C		C	45	0.35	0.19	0.26	0.43	0	0	-0.16
YLR001C		C	21	0.35	0.09	0.26	0.33	0	0	-0.05

YLR005W	SSL1	C	20	0.35	0.14	0.26	0.24	0	0	0
YLR008C		C	20	0.35	0.2	0.26	0.36	0	0	0
YLR017W	MEU1	C	20	0.35	0.63	0.36	0.82	0.09	0	0.14
YLR018C		C	20	0.35	0.15	0.26	0.24	0	0	0
YLR019W		C	21	0.35	0.14	0.26	0.24	0	0	0
YLR023C		C	20	0.35	0.13	0.27	0.35	0	0	0
YLR025W	SNF7	C	21	0.35	0.09	0.26	0.24	0	0	0
YLR027C	AAT2	C	21	0.84	0.97	0.99	1.5	-0.13	-0.06	0.05
YLR028C	ADE16	C	21	0.35	0.23	0.26	0.36	<b>-0.34</b>	0	-0.07
YLR029C	RPL15A	C	21	0.97	2.84	0.88	1.24	<b>0.32</b>	-0.14	-0.1
YLR034C		C	20	0.53	0.6	0.26	1.24	0	0	<b>0.26</b>
YLR037C		C	20	0.44	0.34	0.52	0.46	-0.15	0	-0.14
YLR038C	COX12	C	20	0.6	0.64	1.16	0.72	-0.1	0.05	-0.05
YLR040C		C	20	0.35	1	0.26	0.24	0.42	0	0
YLR042C		C	20	0.35	0.1	0.26	0.24	0	0	0
YLR043C	TRX1	C	21	2.64	5.22	2.07	5.41	0.1	<b>-0.3</b>	0.07
YLR044C	PDC1	C	20	11.63	13.96	6.64	15.05	0.09	<b>-0.26</b>	0.03
YLR048W	RPS0B	C	41	2.25	3.36	1.27	2.04	0.15	-0.19	-0.05
YLR050C		C	20	0.4	0.32	0.28	0.57	0	0	0.05
YLR056W	ERG3	C	20	0.65	1.53	0.63	1.57	<b>0.28</b>	0	<b>0.23</b>
YLR058C	SHM2	C	21	1.52	3.52	1.05	6.78	0.08	0	<b>0.59</b>
YLR059C	YNT20	C	20	0.35	0.19	0.26	0.24	0	0	0
YLR060W	FRS1	C	20	0.4	0.55	0.31	0.62	-0.09	0	0
YLR061W	RPL22A	C	20	7.13	9.29	3.06	6.95	0.02	<b>-0.3</b>	-0.02
YLR064W		C	20	0.35	0.21	0.26	0.46	0	0	0
YLR065C		C	20	0.35	0.48	0.28	0.25	0.05	0	0
YLR066W	SPC3	C	20	0.35	0.13	0.26	0.24	0	0	0
YLR069C	MEF1	C	20	0.35	0.12	0.26	0.24	0	0	0
YLR073C		C	21	0.35	0.22	0.26	0.41	0	0	0.01
YLR074C		C	21	0.35	0.16	0.26	0.45	0	0	0.01
YLR075W	RPL10	C	21	5.4	8.55	3.96	6.55	0.02	-0.19	0
YLR076C		C	20	0.5	0.19	0.29	0.37	0	0	0
YLR078C	BOS1	C	20	0.35	0.11	0.26	0.24	0	0	0
YLR079W	SIC1	C	21	0.35	0.21	0.26	0.3	0	0	0
YLR081W	GAL2	C	21	0.35	0.09	2.84	0.24	0	<b>0.91</b>	0
YLR083C	EMP70	C	21	0.35	0.18	0.26	0.24	<b>-0.31</b>	0	0
YLR088W	GAA1	C	20	0.35	0.12	0.26	0.24	0	0	0
YLR089C		C	20	0.35	0.15	0.26	0.24	0	0	0
YLR093C		C	20	0.35	0.11	0.26	0.24	0	0	0
YLR095C		C	20	0.35	0.16	0.26	0.24	0	0	0
YLR099C		C	20	0.35	0.27	0.43	0.3	-0.28	0	0
YLR100W		C	20	0.35	0.27	0.26	0.44	0	0	0
YLR104W		C	20	0.35	0.18	0.26	0.38	0	0	-0.09
YLR109W		C	21	3.58	9.66	1.96	8.52	0.1	<b>-0.31</b>	<b>0.34</b>
YLR110C		C	20	13.2	35.7	17.05	34.4	0.08	-0.07	0.09
YLR112W		C	21	0.35	0.11	0.26	0.24	0	0	0
YLR113W	HOG1	C	21	0.41	0.57	0.26	0.71	0.06	0	<b>0.22</b>
YLR118C		C	20	0.35	0.26	0.28	0.68	<b>-0.22</b>	0	0.26
YLR120C	YPS1	C	20	0.57	0.53	0.57	1.34	-0.13	0	0.17
YLR121C	YPS3	C	20	0.35	0.1	0.26	0.42	0	0	0.08
YLR129W	DIP2	C	20	0.35	0.13	0.26	0.24	0	0	0
YLR130C	ZRT2	C	21	0.35	0.33	0.26	0.6	-0.08	0	0.1
YLR132C		C	20	0.35	0.16	0.26	0.24	0	0	0
YLR133W	CKI1	C	20	0.35	0.12	0.26	0.24	0	0	0
YLR134W	PDC5	C	20	0.35	0.14	0.26	0.24	0	0	0

YLR146C	SPE4	C	20	0.35	0.22	0.26	0.24	0	0	0
YLR150W	MPT4	C	21	0.77	1.74	1.09	1.29	0.25	0.14	0.06
YLR153C	ACS2	C	20	0.47	0.8	0.28	0.55	0.07	0	-0.03
YLR154C		C	21	0.35	0.14	0.26	0.24	0	0	0
YLR155C	ASP3	C	20	0.35	0.09	0.26	0.38	0	0	0
YLR157C	ASP3	C	20	0.35	0.09	0.26	0.26	0	0	0
YLR160C	ASP3	C	20	0.35	0.15	0.26	0.45	0	0	0
YLR167W	RPS31	C	20	4.08	7.94	3.51	3.94	0.18	<b>-0.24</b>	-0.1
YLR172C	DPH5	C	21	0.36	0.44	0.32	0.42	0.02	0	0.02
YLR175W	CBF5	C	20	0.35	0.34	0.36	0.44	0	0	0.1
YLR177W		C	20	0.35	0.13	0.26	0.24	0	0	0
YLR178C	TFS1	C	21	0.39	0.47	0.31	3.31	0	0	<b>0.65</b>
YLR179C		C	21	0.83	1.58	0.63	1.38	0.14	-0.14	0.07
YLR180W	SAM1	C	20	0.6	1.41	0.33	1.28	0.1	0	<b>0.23</b>
YLR185W	RPL37A	C	21	4.65	5.62	2.88	5.18	0.08	<b>-0.22</b>	-0.08
YLR186W		C	20	0.35	0.24	0.28	0.33	0	0	0
YLR192C		C	21	0.35	0.32	0.26	0.27	-0.11	0	0
YLR194C		C	20	0.35	0.49	0.78	1.01	0	0.04	0.15
YLR195C	NMT1	C	21	0.35	0.11	0.26	0.24	0	0	0
YLR197W	SIK1	C	20	0.35	0.22	0.26	0.25	0	0	0
YLR199C		C	20	0.35	0.26	0.27	0.59	0	0	0.08
YLR201C		C	20	0.35	0.38	0.46	0.65	0	0	0.09
YLR202C		C	18	0.35	0.15	0.26	0.3	0	0	0
YLR203C	MSS51	C	21	0.45	0.67	0.26	0.6	0	-0.14	0.1
YLR204W	QRIS	C	20	0.35	0.18	0.26	0.24	0	0	0
YLR206W		C	20	0.35	0.26	0.28	0.3	0	0	0
YLR208W	SEC13	C	21	0.94	0.91	0.7	1.46	-0.1	0	0.03
YLR209C		C	21	0.35	0.4	0.26	0.41	0	0	0
YLR212C	TUB4	C	20	0.35	0.09	0.26	0.24	0	0	0
YLR216C	CPR6	C	21	0.35	0.43	0.26	1.4	0	0	<b>0.53</b>
YLR220W	CCC1	C	20	0.35	0.41	0.26	0.55	0	0	0
YLR222C		C	20	0.35	0.12	0.26	0.24	0	0	0
YLR224W		C	21	0.35	0.16	0.26	0.33	0	0	0
YLR229C	CDC42	C	20	0.72	1.6	0.41	1.89	<b>0.26</b>	0	<b>0.22</b>
YLR231C		C	20	0.35	0.3	0.26	0.39	0	0	0
YLR237W	THI7	C	21	0.35	0.12	0.26	0.24	0	0	0
YLR241W		C	21	0.35	0.16	0.26	0.3	0	0	-0.11
YLR244C	MAP1	C	20	0.35	0.44	0.26	0.57	-0.12	0	-0.11
YLR248W	RCK2	C	20	0.43	0.31	0.28	0.33	-0.22	0	0
YLR249W	YEF3	C	20	1.04	1.8	0.83	1.68	0.19	-0.18	0.14
YLR250W	SSP120	C	20	0.35	0.16	0.26	0.27	0	0	0
YLR251W		C	20	0.36	0.22	0.34	0.59	<b>-0.29</b>	0	0.18
YLR252W		C	20	0.35	0.22	0.26	0.47	0	0	0.11
YLR253W		C	21	0.35	0.09	0.26	0.24	0	0	0
YLR256W	HAP1	C	20	0.35	0.09	0.26	0.29	0	0	0
YLR257W		C	21	0.35	0.11	0.26	0.24	0	0	0
YLR258W	GSY2	C	21	0.35	0.48	0.42	0.58	-0.19	-0.11	0.04
YLR259C	HSP60	C	21	0.98	1.19	0.81	3.58	0.03	0	<b>0.32</b>
YLR264W	RPS28B	C	20	2.16	3.08	0.52	2.38	0.07	<b>-0.29</b>	-0.06
YLR268W	SEC22	C	21	0.35	0.21	0.26	0.34	0	0	0
YLR270W		C	20	0.35	0.15	0.26	0.3	0	0	0
YLR285W		C	21	0.35	0.15	0.26	0.24	0	0	0
YLR286C	CTS1	C	20	1.1	1.61	0.79	1.21	0.19	0	0.14
YLR287C-A	RPS30A	C	40	3.45	4.59	2.83	3.33	-0.01	0	0
YLR290C		C	20	0.35	0.09	0.26	0.25	0	0	0

YLR291C	GCD7	C	20	0.35	0.21	0.26	0.44	0	0	0.06
YLR292C	SEC72	C	21	0.35	0.12	0.26	0.24	0	0	0
YLR293C	GSP1	C	20	1.16	2.37	0.72	2.02	<b>0.24</b>	<b>-0.23</b>	0.17
YLR294C		C	20	0.45	1.1	1.05	1.06	0.12	<b>0.2</b>	<b>0.27</b>
YLR295C	ATP14	C	20	0.35	0.53	0.62	0.33	0	0.09	0
YLR297W		C	21	0.5	0.57	0.4	1.2	0.05	0	0.19
YLR300W	EXG1	C	21	6.8	4.85	2.29	8.56	0.03	<b>-0.21</b>	0.08
YLR301W		C	20	0.35	0.29	0.26	0.31	0	0	0
YLR303W	MET17	C	21	0.39	0.51	0.81	3.15	0.01	0.12	<b>0.77</b>
YLR304C	ACO1	C	20	0.54	0.44	0.52	0.98	-0.05	0	0.09
YLR317W		C	20	0.35	0.16	0.26	0.25	0	0	0
YLR325C	RPL38	C	20	1.24	2.24	1.16	2.24	0.12	-0.19	0.01
YLR327C		C	21	0.35	0.18	0.42	0.6	<b>-0.31</b>	-0.02	0.03
YLR328W		C	20	0.35	0.11	0.26	0.26	0	0	0
YLR330W		C	20	0.35	0.13	0.26	0.24	0	0	0
YLR333C	RPS25B	C	28	1.58	2.59	0.72	1.71	<b>0.21</b>	-0.19	0.09
YLR335W	NUP2	C	20	0.35	0.13	0.26	0.24	0	0	0
YLR340W	RPP0	C	20	8.13	9.17	3.54	4.96	0.04	<b>-0.25</b>	-0.19
YLR342W	FKS1	C	20	0.4	0.47	0.26	0.64	0.02	0	0.12
YLR344W	RPL26A	C	30	0.58	0.45	0.26	0.4	-0.15	0	0
YLR347C	KAP95	C	20	0.35	0.17	0.26	0.24	0	0	0
YLR348C	DIC1	C	20	0.36	0.59	0.26	0.55	0	0	-0.09
YLR350W		C	21	1.57	1.94	1.86	2.09	0.05	-0.02	0.16
YLR351C	NIT3	C	21	0.45	0.4	0.29	0.47	<b>-0.24</b>	0	0
YLR354C	TAL1	C	20	1.04	1.35	0.83	1.8	0.03	-0.08	0.2
YLR355C	ILV5	C	20	1.09	2.59	1.31	2.74	<b>0.33</b>	-0.03	<b>0.29</b>
YLR356W		C	20	0.48	0.29	0.39	1.13	<b>-0.26</b>	0	<b>0.32</b>
YLR359W	ADE13	C	20	0.51	0.44	0.33	0.53	-0.02	0	0.1
YLR364W		C	21	0.35	0.1	0.26	0.24	0	0	0
YLR367W	RPS22B	C	90	0.67	0.97	0.73	0.79	0.07	-0.04	-0.03
YLR370C	ARC18	C	20	0.58	0.83	0.42	0.87	0.04	0	0.11
YLR372W	SUR4	C	20	1.33	2.24	0.68	1.53	0.12	<b>-0.23</b>	0.02
YLR375W	STP3	C	20	0.76	0.93	0.57	2.35	0.05	0	<b>0.39</b>
YLR378C	SEC61	C	21	0.85	1.03	0.59	1.14	-0.05	0	0.06
YLR380W		C	20	0.35	0.24	0.26	0.26	0	0	0
YLR384C	IKI3	C	20	0.35	0.11	0.26	0.24	0	0	0
YLR388W	RPS29A	C	21	5.94	10.34	2.44	6.05	0.14	<b>-0.26</b>	-0.08
YLR390W	ECM19	C	20	0.35	0.2	0.26	0.36	0	0	0
YLR391W		C	21	2.73	4.58	2.53	6.49	-0.05	-0.17	0.16
YLR395C	COX8	C	20	1.2	1.6	0.95	1.23	-0.01	0	-0.11
YLR404W		C	20	0.35	0.1	0.26	0.24	0	0	0
YLR405W		C	20	0.35	0.12	0.26	0.24	0	0	0
YLR406C	RPL31B	C	55	1.33	2.85	1.27	2.5	0.08	0	0.1
YLR412W		C	21	0.35	0.1	0.26	0.24	0	0	0
YLR413W		C	20	0.35	0.15	0.26	0.37	0	0	0.02
YLR414C		C	20	0.67	0.61	0.53	1.1	0	0	0.15
YLR420W	URA4	C	20	0.35	0.15	0.26	0.24	0	0	0
YLR421C		C	20	0.35	0.49	0.26	0.52	0	0	0.01
YLR426W		C	41	0.35	0.12	0.26	0.24	0	0	0
YLR429W	CRN1	C	20	0.35	0.15	0.26	0.24	0	0	0
YLR432W		C	20	0.35	0.59	0.26	0.42	0.09	0	0
YLR437C		C	20	0.35	0.21	0.26	0.24	0	0	0
YLR438W	CAR2	C	21	0.35	0.22	0.26	0.68	<b>-0.32</b>	0	<b>0.29</b>
YLR439W	MRPL4	C	21	0.35	0.14	0.26	0.24	0	0	0
YLR441C	RPS1A	C	29	2.69	3.96	1.15	2.87	0.02	0	-0.01

YLR447C	VMA6	C	20	0.58	1.07	0.43	0.85	0.1	0	0.09
YLR448W	RPL6B	C	20	4.37	6.39	3.19	3.25	0.15	<b>-0.26</b>	-0.1
YLR449W	FPR4	C	21	0.35	0.13	0.26	0.24	0	0	0
YLR459W	CDC91	C	20	0.35	0.15	0.26	0.26	0	0	0
YLR461W	PAU4	C	20	0.35	0.16	0.28	0.24	0	0	0
YLR466W		C	20	0.75	0.55	0.57	1.03	<b>-0.24</b>	-0.05	0.17
YLR467W		C	20	0.6	0.58	0.54	1.18	0	0	0.2
YML001W	YPT7	C	20	0.36	0.32	0.34	0.53	0	0	0.03
YML004C	GLO1	C	21	0.35	0.33	0.26	0.64	0	0	0.13
YML008C	ERG6	C	20	0.4	0.42	0.26	0.39	-0.05	0	0
YML009C	MRPL39	C	21	0.35	0.34	0.31	0.54	0	-0.11	0
YML010W		C	20	0.35	0.11	0.26	0.24	0	0	0
YML010W-A	SPT5	C	20	0.37	0.26	0.26	0.52	0	0	0
YML010W-B		C	41	0.35	0.09	0.26	0.24	0	0	0
YML012W	ERV25	C	20	1.59	2.25	1.25	2.25	0.08	0	0.07
YML014W		C	20	0.35	0.1	0.26	0.24	0	0	0
YML018C		C	21	0.35	0.1	0.26	0.24	0	0	0
YML019W	OST6	C	20	0.35	0.15	0.27	0.34	0	0	0
YML022W	APT1	C	20	0.76	0.81	0.39	0.82	-0.11	<b>-0.1</b>	0.03
YML024W	RPS17A	C	20	3.63	4.98	1.43	3.27	0.14	<b>-0.2</b>	-0.09
YML025C		C	21	0.35	0.15	0.26	0.24	0	0	0
YML026C	RPS18B	C	19	0.84	2.28	0.97	1.38	0.14	-0.06	-0.02
YML027W	YOX1	C	21	0.35	0.15	0.26	0.24	<b>-0.5</b>	0	0
YML028W	TSA1	C	21	4.04	7.95	6.35	6.44	0.1	0.08	0.14
YML029W		C	21	0.35	0.1	0.26	0.24	0	0	0
YML030W		C	20	0.35	0.23	0.26	0.3	0	0	0
YML031W	NDC1	C	21	0.35	0.15	0.26	0.29	0	0	-0.13
YML039W		C	40	0.35	0.19	0.26	0.53	0	0	0.04
YML040W		C	20	0.35	0.13	0.26	0.55	0	0	<b>0.2</b>
YML045W		C	40	0.35	0.15	0.26	0.55	0	0	0.11
YML048W	GSF2	C	20	0.35	0.3	0.26	0.43	0	0	0.03
YML051W	GAL80	C	21	0.35	0.19	0.61	0.35	0	0.17	0
YML052W	SUR7	C	21	0.88	1.32	0.29	0.89	0	<b>-0.3</b>	0
YML055W	SPC2	C	20	0.35	0.21	0.26	0.24	0	0	0
YML056C		C	41	0.41	0.58	0.36	0.6	0.06	0	0.02
YML057W	CMP2	C	20	0.35	0.11	0.26	0.74	0	0	0.12
YML058W		C	20	1.15	2.37	0.85	2.24	0.17	<b>-0.23</b>	0.16
YML063W	RPS1B	C	20	0.39	0.45	0.26	0.24	0	0	0
YML064C	TEM1	C	21	0.35	0.13	0.26	0.24	0	0	0
YML067C		C	20	0.46	0.33	0.26	0.75	-0.2	0	0.07
YML070W	DAK1	C	20	0.42	0.26	0.26	0.94	0	-0.2	<b>0.37</b>
YML072C		C	21	0.35	0.41	0.26	0.35	-0.02	0	-0.16
YML073C	RPL6A	C	20	3.12	4.4	1.66	1.81	0.11	<b>-0.35</b>	<b>-0.25</b>
YML074C	NPI46	C	20	0.35	0.37	0.29	0.36	0	0	0
YML075C	HMG1	C	21	0.35	0.17	0.26	0.24	<b>-0.38</b>	0	0
YML078W	CPR3	C	21	1.42	1.64	0.83	2.07	0	-0.19	0.07
YML079W		C	21	0.35	0.1	0.26	0.24	0	0	0
YML085C	TUB1	C	20	0.44	0.7	0.26	0.26	0.04	0	0
YML086C	ALO1	C	21	0.39	0.69	0.4	0.54	0.08	0	0
YML092C	PRE8	C	20	0.56	0.95	0.48	2.15	0.09	-0.2	<b>0.39</b>
YML100W	TSL1	C	21	1.12	0.67	0.51	1.58	<b>-0.25</b>	<b>-0.2</b>	<b>0.2</b>
YML101C		C	21	0.35	0.58	0.33	0.32	0.1	0	0
YML105C	SEC65	C	20	0.35	0.28	0.26	0.33	0	0	0
YML106W	URA5	C	20	2.55	4.41	1.56	3.48	0.15	<b>-0.29</b>	0.08
YML110C	DBI56	C	20	0.62	0.49	0.31	1.05	-0.09	-0.2	0.19

YML112W	CTK3	C	21	0.35	0.09	0.26	0.24	0	0	0
YML113W	DAT1	C	20	0.35	0.16	0.26	0.35	0	0	0
YML114C		C	21	0.35	0.09	0.26	0.29	0	0	0
YML116W	ATR1	C	21	0.35	0.17	0.26	0.27	0	0	0
YML117W-A		C	20	0.35	0.27	0.26	0.85	<b>-0.26</b>	0	<b>0.3</b>
YML121W	GTR1	C	20	0.35	0.1	0.26	0.25	0	0	0
YML123C	PHO84	C	21	0.35	0.56	0.26	0.68	0.14	0	-0.06
YML124C	TUB3	C	21	0.37	0.53	0.42	0.5	-0.1	0	-0.09
YML125C		C	20	0.46	0.41	0.26	0.52	0	0	0.06
YML126C	HMGS	C	20	1.23	1.35	0.99	1.63	0.03	0	0.08
YML127W		C	20	0.53	0.4	0.26	0.67	0	-0.14	-0.09
YML128C		C	20	0.35	0.21	0.26	1.06	0	0	<b>0.47</b>
YML129C	COX14	C	20	0.35	0.15	0.26	0.43	0	0	0
YML130C	ERO1	C	21	0.35	0.09	0.26	0.31	0	0	0
YML131W		C	20	0.35	0.18	0.26	0.24	0	0	0
YML132W	COS3	C	20	0.82	0.88	0.51	0.96	-0.11	0	0.01
YML133C		C	40	0.35	0.24	0.26	0.27	<b>-0.32</b>	0	0
YMR002W		C	21	1.24	1.96	1.43	2.02	0.02	-0.03	0.03
YMR003W		C	21	0.35	0.13	0.26	0.24	<b>-0.44</b>	0	0
YMR005W	MPT1	C	21	0.35	0.16	0.26	0.31	0	0	-0.09
YMR006C		C	21	0.35	0.11	0.26	0.24	0	0	0
YMR008C	PLB1	C	21	0.92	0.65	0.76	1.73	<b>-0.22</b>	0	0.14
YMR009W		C	21	0.35	0.12	0.26	0.42	0	0	0.08
YMR010W		C	21	0.35	0.11	0.26	0.24	0	0	0
YMR011W	HXT2	C	20	0.35	0.17	0.26	0.24	0	0	0
YMR012W	CLU1	C	20	0.35	0.26	0.26	0.26	0	0	0
YMR015C	ERG5	C	20	0.35	0.17	0.26	0.24	0	0	0
YMR022W	QRI8	C	20	0.5	0.43	0.26	0.94	-0.13	0	<b>0.22</b>
YMR024W		C	21	0.35	0.14	0.26	0.24	0	0	0
YMR027W	HRT2	C	21	0.35	0.11	0.26	0.25	0	0	0
YMR035W	IMP2	C	20	0.35	0.22	0.26	0.31	0	0	0
YMR038C	LYS7	C	21	0.35	0.22	0.26	0.24	<b>-0.34</b>	0	0
YMR042W	ARG80	C	21	0.35	0.14	0.26	0.24	<b>-0.5</b>	0	0
YMR043W	MCM1	C	20	0.52	0.41	0.54	0.97	<b>-0.28</b>	0	0
YMR047C	NUP116	C	21	0.35	0.15	0.26	0.24	<b>-0.5</b>	0	0
YMR049C		C	21	0.35	0.25	0.26	0.3	-0.19	0	0
YMR050C		C	40	0.35	0.21	0.26	0.43	0	0	0.05
YMR051C		C	20	0.35	0.15	0.26	0.59	0	0	<b>0.23</b>
YMR054W	STV1	C	21	0.35	0.15	0.26	0.24	0	0	0
YMR055C	BUB2	C	20	0.35	0.12	0.26	0.24	0	0	0
YMR056C	AAC1	C	20	0.35	0.17	0.29	0.58	0	0	0
YMR058W	FET3	C	20	0.36	0.2	0.26	0.43	0	0	-0
YMR062C	ECM40	C	20	0.35	0.22	0.26	0.24	0	0	0
YMR067C		C	20	0.35	0.13	0.26	0.24	0	0	0
YMR071C		C	20	0.41	0.4	0.27	0.79	-0.12	0	<b>0.31</b>
YMR072W	ABF2	C	20	0.35	0.26	0.26	0.29	0	0	0
YMR073C		C	21	0.35	0.13	0.26	0.29	0	0	-0.12
YMR074C		C	21	0.35	0.3	0.26	0.35	-0.23	0	0
YMR079W	SEC14	C	21	0.35	0.44	0.27	0.24	-0.13	0	0
YMR081C	ISF1	C	21	0.35	0.09	0.6	0.24	0	0.05	0
YMR083W	ADH3	C	20	2.24	1.96	1.42	4.37	-0.09	-0.1	<b>0.27</b>
YMR087W		C	20	0.35	0.12	0.26	0.24	0	0	0
YMR088C		C	20	0.35	0.11	0.26	0.24	0	0	0
YMR089C	YTA12	C	21	0.35	0.27	0.26	0.26	0	0	0
YMR090W		C	20	0.35	0.21	0.3	0.83	<b>-0.39</b>	0	<b>0.35</b>

YMR091C	NPL6	C	20	0.35	0.1	0.26	0.24	0	0	0
YMR092C	AIP1	C	21	0.35	0.18	0.26	0.67	0	0	0.02
YMR099C		C	20	0.35	0.26	0.26	0.33	0	0	0
YMR105C	PGM2	C	20	0.35	0.17	0.38	0.58	0	0	0.1
YMR108W	ILV2	C	21	0.35	0.37	0.47	0.91	-0.13	-0.1	0.09
YMR110C		C	21	0.35	0.17	0.26	0.32	0	0	0
YMR113W		C	21	0.35	0.11	0.26	0.24	0	0	0
YMR116C	BEL1	C	40	9.06	8.98	3.58	7.36	0.03	<b>-0.29</b>	-0.1
YMR119W		C	20	0.35	0.14	0.26	0.35	<b>-0.47</b>	0	0
YMR119W-A		C	20	0.35	0.1	0.26	0.24	0	0	0
YMR120C	ADE17	C	20	0.35	0.18	0.26	0.71	0	0	0
YMR121C	RPL15B	C	20	0.35	0.27	0.26	0.52	0	0	-0.07
YMR123W		C	20	0.85	1.03	0.56	0.56	0	0	-0.13
YMR128W	ECM16	C	20	0.35	0.1	0.26	0.24	0	0	0
YMR131C		C	20	0.35	0.16	0.26	0.24	0	0	0
YMR135C		C	20	0.35	0.12	0.26	0.59	0	0	0
YMR136W		C	20	0.35	0.34	0.26	0.37	<b>-0.3</b>	0	0
YMR142C	RPL13B	C	20	1.95	2.96	1.08	1.69	0.11	<b>-0.23</b>	-0.07
YMR143W	RPS16A	C	33	2.01	2.16	0.86	1.55	-0.01	<b>-0.25</b>	-0.12
YMR145C		C	20	0.69	0.91	0.94	0.98	0	0.1	0.12
YMR146C	TIF34	C	21	0.36	0.88	0.42	0.87	0.16	0	0.12
YMR148W		C	20	0.4	0.5	0.36	0.71	0	0	-0.13
YMR149W	SWP1	C	20	0.71	0.69	0.44	0.86	0.05	0	0.01
YMR150C	IMP1	C	21	0.35	0.17	0.26	0.24	0	0	0
YMR152W		C	20	0.35	0.14	0.26	0.29	0	0	0
YMR157C		C	20	0.35	0.1	0.26	0.25	0	0	0
YMR161W	HLJ1	C	20	0.35	0.16	0.26	0.27	0	0	0
YMR169C	ALD3	C	21	0.35	0.09	0.26	0.6	0	0	0.24
YMR171C		C	20	0.35	0.09	0.26	0.24	0	0	0
YMR173W	DDR48	C	20	0.35	0.13	0.26	0.25	0	0	0
YMR173W-A		C	21	11.18	7.89	5.6	14.76	-0.08	0	0.18
YMR174C	PAI3	C	20	0.35	0.09	0.28	1.45	0	0	<b>0.51</b>
YMR175W	SIP18	C	20	0.35	0.09	0.26	1.33	0	0	0.5
YMR177W	MMT1	C	21	0.35	0.11	0.26	0.24	0	0	0
YMR181C		C	21	0.35	0.25	0.26	0.57	<b>-0.23</b>	0	0.16
YMR184W		C	21	0.35	0.2	0.55	0.47	<b>-0.34</b>	-0.06	-0.09
YMR186W	HSC82	C	20	0.48	0.41	0.51	0.86	<b>-0.22</b>	0	0.03
YMR189W	GCV2	C	20	0.35	0.21	0.26	0.72	0	0	0.24
YMR191W		C	21	0.35	0.11	0.26	0.24	0	0	0
YMR194W	RPL36A	C	19	5.47	4.55	4.29	4.64	0.06	0	0
YMR195W		C	21	0.98	0.97	0.64	2.27	0.03	-0.13	<b>0.2</b>
YMR200W	ROT1	C	20	0.35	0.21	0.26	0.37	0	0	0
YMR202W	ERG2	C	20	1.87	2.57	1.39	2.24	0.07	0	0
YMR203W	TOM40	C	21	0.4	0.39	0.26	0.58	0.01	0	0.01
YMR205C	PKF2	C	20	0.8	0.75	0.43	1.33	-0.06	-0.14	0.13
YMR208W	ERG12	C	21	0.35	0.12	0.26	0.24	0	0	0
YMR211W		C	21	0.35	0.09	0.26	0.24	0	0	0
YMR215W		C	21	0.92	1.29	0.68	0.44	0.16	0	0
YMR216C	SKY1	C	21	0.35	0.09	0.26	0.24	0	0	0
YMR217W	GUA1	C	21	0.35	0.61	0.27	0.3	0.18	0	0
YMR221C		C	21	0.35	0.18	0.26	0.24	0	0	0
YMR222C		C	21	0.42	0.23	0.26	0.36	0	0	-0.1
YMR224C	MRE11	C	20	0.35	0.09	0.26	0.28	0	0	0
YMR226C		C	21	1.5	1.42	1.04	2.48	-0.17	0	0.17
YMR230W	RPS10B	C	23	0.61	0.76	0.56	0.45	-0.02	0	-0.15

YMR234W	RNH1	D	20	0.11	0.08	0.06	0.04	0	0	0
YMR235C	RNA1	D	20	0.19	0.16	0.25	0.28	0	0.13	0.08
YMR236W	TAF17	D	21	0.23	0.47	0.43	0.75	0.17	0.12	<b>0.29</b>
YMR237W		D	21	0.11	0.08	0.2	0.16	0	-0.07	0.03
YMR238W	DFG5	D	21	0.25	0.33	0.26	0.46	0.07	-0.02	<b>0.22</b>
YMR239C	RNT1	D	20	0.11	0.08	0.04	0.06	0	0	0
YMR240C	CUS1	D	21	0.11	0.08	0.04	0.06	0	0	<b>-0.29</b>
YMR241W		D	21	0.94	1.18	1.16	0.86	0.02	0	-0.12
YMR242C	RPL20A	D	17	0.58	1.15	0.85	0.7	0.12	0.06	-0.08
YMR243C	ZRC1	D	21	0.75	0.75	0.69	0.81	0.13	-0.06	0.16
YMR244C-A		D	20	0.11	0.16	0.22	0.27	0	0.14	<b>0.26</b>
YMR244W		D	21	0.11	0.08	0.04	0.06	0	0	0
YMR245W		D	20	0.11	0.08	0.04	0.06	0	0	0
YMR246W	FAA4	D	20	0.2	0.28	0.3	0.65	0.08	0.09	<b>0.47</b>
YMR247C		D	20	0.11	0.08	0.05	0.06	0	0	0
YMR250W		D	20	0.65	0.46	0.67	1.3	0	-0.03	<b>0.29</b>
YMR251W-A	HOR7	D	20	10.08	12.08	12.88	7.72	-0.02	-0.05	-0.01
YMR252C		D	20	0.2	0.22	0.32	0.34	0	0.03	0.11
YMR253C		D	20	0.11	0.08	0.06	0.14	0	0	0.06
YMR255W		D	21	0.11	0.09	0.07	0.08	0	0	0
YMR256C	COX7	D	21	0.54	0.58	2.43	0.87	0.08	<b>0.45</b>	0.07
YMR257C	PET111	D	20	0.11	0.08	0.08	0.07	0	0	0
YMR258C		D	21	0.11	0.08	0.06	0.08	0	<b>-0.26</b>	0
YMR259C		D	20	0.11	0.08	0.06	0.06	0	0	0
YMR260C	TIF11	D	20	0.27	0.38	0.46	0.28	0.12	<b>0.21</b>	-0.04
YMR261C	TPS3	D	21	0.13	0.21	0.17	0.21	-0.02	-0.1	0
YMR262W		D	20	0.11	0.08	0.04	0.06	0	0	0
YMR263W		D	20	0.11	0.08	0.11	0.11	0	-0.14	-0.16
YMR264W	CUE1	D	21	0.42	0.43	0.49	0.7	0.15	0.17	<b>0.37</b>
YMR266W		D	21	0.11	0.08	0.13	0.2	0	-0.04	0.19
YMR267W	PPA2	D	20	0.11	0.1	0.09	0.07	0	0	0
YMR269W		D	20	0.11	0.08	0.05	0.05	0	0	0
YMR271C	URA10	D	21	0.11	0.08	0.04	0.11	0	0	0.01
YMR272C	SCS7	D	20	0.72	0.84	0.84	0.76	-0.11	0	0.03
YMR274C	RCE1	D	20	0.11	0.2	0.19	0.14	0	-0.04	-0.09
YMR275C	BUL1	D	21	0.11	0.08	0.05	0.04	0	0	0
YMR276W	DSK2	D	21	0.54	0.64	0.51	1.2	0.21	0.01	<b>0.43</b>
YMR278W		D	20	0.11	0.08	0.09	0.09	0	0	0
YMR281W		D	20	0.11	0.11	0.16	0.24	0	0.02	<b>0.14</b>
YMR283C	RIT1	D	21	0.11	0.09	0.08	0.06	0	-0.17	<b>-0.34</b>
YMR286W	MRPL33	D	20	0.29	0.42	0.29	0.43	0.11	0.02	0.16
YMR289W		D	20	0.11	0.08	0.05	0.13	0	0	<b>0.05</b>
YMR290C	HAS1	D	20	0.11	0.11	0.04	0.06	0	0	0
YMR290W-A		D	20	0.11	0.08	0.04	0.07	0	0	0
YMR291W		D	20	0.18	0.16	0.34	0.39	0	0.15	0.13
YMR292W		D	20	0.48	0.86	0.68	0.6	<b>0.23</b>	0.14	-0.04
YMR293C		D	21	0.11	0.1	0.14	0.08	0	0.02	0
YMR294W-A		D	21	0.13	0.09	0.12	0.07	0	-0.17	0
YMR295C		D	20	1.83	1.7	1.94	2.39	0.09	0.09	0.07
YMR296C	LCB1	D	20	0.41	0.53	0.34	0.61	0	-0.08	0.1
YMR297W	PRC1	D	20	1.65	2.6	2.59	2.87	0.14	0.13	<b>0.24</b>
YMR298W		D	21	0.5	0.63	0.65	0.91	0.15	0.02	0.14
YMR299C		D	20	0.11	0.08	0.04	0.05	0	0	0
YMR300C	ADE4	D	20	0.11	0.12	0.1	0.11	0.06	0	0
YMR301C	ATM1	D	20	0.11	0.08	0.08	0.07	0	0	0

YMR302C	PRP12	D	20	0.11	0.1	0.11	0.17	0	-0.09	0.1
YMR303C	ADH2	D	20	0.15	0.27	0.34	0.36	0.02	0.18	0.12
YMR304C-A		D	20	0.11	0.08	0.15	0.07	0	0	0
YMR304W		D	21	0.11	0.08	0.06	0.04	0	0	0
YMR305C		D	20	0.75	1.37	1.02	0.95	0.1	0.05	0.05
YMR308C	PSE1	D	20	0.29	0.24	0.35	0.6	0.08	0.09	<b>0.27</b>
YMR309C	NIP1	D	21	0.11	0.08	0.07	0.08	0	0	0
YMR310C		D	20	0.12	0.21	0.3	0.29	0.13	0.14	<b>0.24</b>
YMR311C	GLC8	D	20	0.11	0.09	0.11	0.15	0	0	0.16
YMR312W		D	20	0.13	0.16	0.08	0.09	0	0	0
YMR314W	PRE5	D	20	0.31	0.31	0.43	0.6	0.02	0.1	0.18
YMR315W		D	20	0.82	0.57	1.35	1.33	0	<b>0.28</b>	<b>0.26</b>
YMR316C-A		D	20	0.11	0.08	0.05	0.06	0	0	0
YMR316W		D	21	0.11	0.08	0.16	0.15	0	0	0.04
YMR318C		D	20	0.37	0.56	1.89	0.93	0.11	<b>0.6</b>	<b>0.2</b>
YMR319C	FET4	D	20	0.15	0.14	0.05	0.09	0	0	-0.18
YMR321C		D	21	0.46	0.63	0.7	0.33	<b>0.2</b>	<b>0.2</b>	-0.13
YMR322C		D	20	0.11	0.08	0.05	0.07	0	0	0
YMR323W		D	20	0.11	0.08	0.04	0.06	0	0	0
YMR325W		D	20	0.11	0.12	0.04	0.09	0	0	0
YNL001W	DOM34	D	20	0.11	0.08	0.04	0.05	0	0	0
YNL002C	RLP7	D	20	0.11	0.12	0.1	0.09	0.05	0	0
YNL003C	PET8	D	20	0.22	0.18	0.32	0.35	0.03	-0.02	0.06
YNL004W	HRB1	D	21	0.11	0.09	0.05	0.06	0	0	0
YNL005C	MRP7	D	21	0.11	0.09	0.11	0.1	0	0	0
YNL006W	LST8	D	21	0.22	0.3	0.24	0.14	0	0.01	0.04
YNL007C	SIS1	D	20	1.29	1.28	1.37	1.83	-0.06	-0.05	0.09
YNL008C		D	20	0.11	0.18	0.16	0.18	0.03	0.03	0.12
YNL009W	IDP3	D	20	0.11	0.08	0.04	0.09	0	0	0
YNL010W		D	21	0.23	0.37	0.56	0.49	0.12	<b>0.26</b>	0.12
YNL011C		D	20	0.11	0.08	0.07	0.05	0	0	0
YNL013C		D	20	0.11	0.08	0.04	0.09	0	0	0
YNL015W	PBI2	D	20	0.95	0.47	3.03	2.58	-0.09	<b>0.59</b>	<b>0.38</b>
YNL016W	PUB1	D	20	0.14	0.17	0.22	0.25	0	0.18	0.05
YNL021W	HDA1	D	20	0.11	0.08	0.05	0.06	0	0	0
YNL022C		D	21	0.11	0.08	0.06	0.15	0	0	0.09
YNL023C		D	20	0.11	0.08	0.07	0.06	0	0	0
YNL025C	SSN8	D	21	0.11	0.08	0.04	0.04	0	0	0
YNL026W		D	20	0.11	0.08	0.07	0.07	0	0	0
YNL029C	KTR5	D	21	0.11	0.08	0.05	0.11	0	0	0.02
YNL030W	HHF2	D	20	2.55	1.8	3.38	1.03	0.04	0.1	<b>-0.39</b>
YNL031C	HHT2	D	20	5.59	7.11	11.01	5.71	0.01	0.13	0
YNL032W	SIW14	D	21	0.11	0.08	0.11	0.07	0	-0.04	0
YNL035C		D	20	0.11	0.08	0.05	0.04	0	0	0
YNL036W	NCE103	D	20	0.11	0.08	0.12	0.05	0	0.02	0
YNL037C	IDH1	D	21	0.36	0.21	0.78	0.85	-0.09	0.18	0.17
YNL038W		D	21	0.11	0.08	0.07	0.06	0	0	0
YNL039W	TFC5	D	20	0.11	0.08	0.04	0.08	0	0	0
YNL040W		D	21	0.11	0.1	0.04	0.12	0	0	0.05
YNL042W		D	20	0.11	0.08	0.04	0.11	0	0	0.01
YNL043C		D	20	0.12	0.15	0.09	0.11	0	0	<b>-0.21</b>
YNL044W		D	20	2.07	1.62	2.68	1.55	-0.03	0.1	-0.09
YNL045W		D	20	0.11	0.16	0.29	0.41	0	-0.11	0.13
YNL046W		D	21	0.51	0.56	0.63	0.37	0.08	0.02	-0.13
YNL048W	ALG11	D	20	0.11	0.08	0.11	0.11	0	0	0

YNL050C		D	20	0.11	0.1	0.08	0.05	-0.1	-0.19	0
YNL051W		D	21	0.11	0.08	0.05	0.05	0	0	0
YNL052W	COX5A	D	20	1.09	0.9	2.69	1.08	0.04	<b>0.47</b>	-0.03
YNL053W	MSG5	D	20	0.11	0.08	0.15	0.17	0	0.05	0.16
YNL054W	VAC7	D	21	0.11	0.08	0.05	0.04	0	<b>-0.37</b>	0
YNL055C	POR1	D	21	6.5	5.85	8.2	8.19	0.02	<b>0.24</b>	0.18
YNL056W		D	21	0.14	0.21	0.15	0.14	-0.03	-0.05	0
YNL058C		D	20	0.11	0.2	0.12	0.17	0.03	0	0.1
YNL061W	NOP2	D	20	0.11	0.1	0.05	0.06	0	0	0
YNL062C	GCD10	D	20	0.11	0.11	0.12	0.05	0.01	-0	0
YNL063W		D	20	0.11	0.08	0.07	0.15	0	0	0.06
YNL064C	YDJ1	D	20	0.49	0.72	0.86	1.54	0.16	0.17	<b>0.34</b>
YNL065W		D	20	0.11	0.08	0.04	0.09	0	0	0
YNL066W	SUN4	D	20	0.32	0.42	0.35	0.63	0.11	0.07	<b>0.26</b>
YNL067W	RPL9B	D	34	1.48	1.54	2.52	1.93	0.16	<b>0.27</b>	<b>0.22</b>
YNL069C	RPL16B	D	20	5	7.52	3.46	4.06	0.07	-0.11	-0.12
YNL070W	TOM7	D	20	0.35	0.54	0.56	0.94	0.08	0.05	0.13
YNL071W	LAT1	D	21	0.8	0.81	0.71	1.04	0	-0.07	0.05
YNL072W	RNH35	D	20	0.11	0.08	0.06	0.04	0	0	0
YNL073W	MSK1	D	20	0.11	0.08	0.15	0.08	0	0.15	0
YNL074C	YMK1	D	20	0.11	0.08	0.15	0.12	0	0.1	-0.04
YNL075W		D	20	0.11	0.16	0.1	0.08	0.13	0	0
YNL076W	MKS1	D	20	0.11	0.08	0.06	0.04	0	0	0
YNL078W		D	20	0.2	0.29	0.15	0.29	0.08	0	0.14
YNL079C	TPM1	D	21	0.19	0.29	0.45	0.44	0.03	<b>0.2</b>	0.18
YNL080C		D	20	0.13	0.22	0.24	0.33	0	0.02	<b>0.23</b>
YNL081C		D	21	0.13	0.11	0.21	0.19	-0.09	0.07	0.14
YNL084C	END3	D	21	0.11	0.09	0.07	0.08	0	<b>-0.31</b>	0
YNL085W	MKT1	D	21	0.11	0.08	0.09	0.11	0	0	0
YNL086W		D	21	0.13	0.18	0.21	0.22	0.05	0.11	0.07
YNL087W		D	20	0.11	0.08	0.06	0.08	0	<b>-0.27</b>	<b>-0.23</b>
YNL088W	TOP2	D	21	0.11	0.08	0.05	0.04	0	0	0
YNL090W	RHO2	D	20	0.11	0.16	0.17	0.14	0	0.1	0
YNL091W		D	20	0.11	0.08	0.07	0.1	0	0	0
YNL092W		D	20	0.11	0.08	0.04	0.14	0	0	0
YNL093W	YPT53	D	20	0.11	0.08	0.04	0.05	0	0	0
YNL094W		D	20	0.11	0.09	0.09	0.16	0	0	0.12
YNL096C	RPS7B	D	42	0.82	1.58	1.07	1.4	0.16	0.02	0.14
YNL097C	PHO23	D	20	0.11	0.12	0.06	0.09	0	0	0
YNL098C	RAS2	D	20	0.16	0.15	0.16	0.21	-0.07	-0.04	0.14
YNL099C		D	21	0.11	0.24	0.17	0.22	0.13	-0.03	0.09
YNL100W		D	20	0.19	0.16	0.35	0.24	0.02	<b>0.22</b>	0.02
YNL101W		D	21	0.11	0.17	0.13	0.19	0.09	0.1	0.22
YNL103W	MET4	D	20	0.11	0.08	0.06	0.12	0	0	0
YNL104C	LEU4	D	21	1.2	0.85	1.98	1.85	0.02	<b>0.35</b>	<b>0.22</b>
YNL107W		D	20	0.11	0.08	0.07	0.05	0	0	0
YNL108C		D	20	0.16	0.16	0.14	0.23	0.02	-0.11	0.05
YNL110C		D	20	0.11	0.09	0.1	0.08	0	0	0
YNL111C	CYB5	D	20	0.11	0.19	0.17	0.26	0	0.1	0.12
YNL112W	DBP2	D	42	0.16	0.33	0.44	0.13	<b>0.27</b>	<b>0.35</b>	-0.15
YNL113W	RPC19	D	20	0.13	0.15	0.2	0.16	0	0.06	0.09
YNL114C		D	21	0.11	0.08	0.06	0.05	0	0	0
YNL115C		D	20	0.11	0.08	0.05	0.1	0	0	0
YNL116W		D	20	0.11	0.09	0.08	0.07	0	0	0
YNL117W	MLS1	D	21	0.11	0.08	0.04	0.05	0	0	<b>-0.36</b>

YNL118C	PSU1	D	21	0.11	0.08	0.06	0.07	0	0	-0.21
YNL121C	TOM70	D	20	0.11	0.1	0.07	0.09	0	0	0
YNL122C		D	20	0.11	0.08	0.05	0.06	0	0	0
YNL123W		D	21	0.11	0.08	0.08	0.1	0	0	0
YNL124W		D	21	0.11	0.13	0.18	0.19	0	-0.07	0.01
YNL125C	ESBP6	D	21	0.14	0.23	0.3	0.35	0	0.17	<b>0.29</b>
YNL129W		D	21	0.11	0.08	0.07	0.07	0	-0.21	0
YNL130C	CPT1	D	20	0.82	0.79	1.04	1.03	0.03	0.13	0.11
YNL131W	TOM22	D	21	0.46	0.59	0.71	0.75	0.08	0.08	0.12
YNL132W		D	20	0.11	0.11	0.08	0.08	0	0	0
YNL133C		D	20	0.11	0.08	0.05	0.05	0	0	0
YNL134C		D	20	2.28	2.07	3.28	2.58	0	0.17	0.12
YNL135C	FPR1	D	20	4.35	9.95	7.86	6.05	0.13	0.07	0
YNL136W		D	20	0.11	0.08	0.04	0.06	0	0	0
YNL137C	NAM9	D	20	0.11	0.08	0.14	0.04	0	0.03	0
YNL138W	SRV2	D	21	0.39	0.61	0.51	0.45	0.15	0.12	0.16
YNL141W	AAH1	D	21	0.11	0.18	0.14	0.09	0.16	0.03	<b>-0.22</b>
YNL142W	MEP2	D	21	0.13	0.12	0.12	0.13	0.05	-0.17	-0.1
YNL144C		D	20	0.11	0.08	0.13	0.04	0	0.04	0
YNL145W	MFA2	D	21	7.14	0.09	6.35	10.97	<b>-1.6</b>	0.04	0.14
YNL147W		D	20	0.11	0.13	0.16	0.12	0	0.1	0
YNL149C		D	21	0.11	0.14	0.18	0.12	0.1	0.08	0
YNL150W		D	20	0.11	0.08	0.05	0.08	0	0	<b>-0.22</b>
YNL151C	RPC31	D	21	0.11	0.11	0.06	0.11	-0.03	0	0
YNL153C	PFD4	D	21	0.11	0.18	0.14	0.15	-0.03	0.07	-0.07
YNL154C	YCK2	D	21	0.13	0.3	0.16	0.18	0.02	0	0.06
YNL155W		D	20	0.11	0.08	0.06	0.13	0	0	0.06
YNL156C		D	20	0.44	0.45	0.55	0.89	0.04	<b>0.2</b>	<b>0.32</b>
YNL157W		D	21	0.37	0.45	0.48	0.78	0.01	<b>0.2</b>	<b>0.27</b>
YNL158W		D	21	0.11	0.11	0.09	0.11	0	0	0
YNL159C		D	21	0.11	0.09	0.1	0.19	0	<b>-0.22</b>	0
YNL160W	YGP1	D	21	2.57	3.77	4.97	7.09	0.05	0.09	<b>0.27</b>
YNL162W	RPL42A	D	44	1.22	2.11	1.22	1.51	0.09	-0.11	-0.07
YNL163C		D	20	0.11	0.08	0.04	0.07	0	0	0
YNL165W		D	21	0.11	0.09	0.08	0.08	0	0	0
YNL166C		D	20	0.11	0.08	0.06	0.05	0	0	0
YNL167C	SKO1	D	20	0.11	0.08	0.05	0.05	0	0	0
YNL168C		D	20	0.21	0.25	0.4	0.31	0.06	0.09	0.18
YNL169C	PSD1	D	20	0.41	0.43	0.57	0.46	-0	0.15	-0.07
YNL170W		D	21	0.11	0.08	0.06	0.06	0	0	0
YNL173C	MDG1	D	20	0.11	0.08	0.12	0.09	0	0	0
YNL174W		D	20	0.11	0.08	0.06	0.04	0	0	0
YNL175C		D	20	0.11	0.1	0.04	0.04	0	0	0
YNL176C		D	20	0.11	0.08	0.06	0.04	0	0	0
YNL177C		D	21	0.11	0.08	0.07	0.04	0	0	0
YNL178W	RPS3	D	20	7.05	7.67	6.58	6.59	0.07	0.05	-0.12
YNL180C		D	20	0.19	0.25	0.25	0.23	0.01	0.01	0
YNL181W		D	20	0.11	0.08	0.09	0.11	0	0	0
YNL183C	NPR1	D	20	0.11	0.09	0.07	0.05	0	0	0
YNL184C		D	20	0.12	0.14	0.09	0.11	-0.03	0	-0.1
YNL185C		D	20	0.18	0.17	0.17	0.33	0.02	0	0.05
YNL186W	DOT4	D	20	0.11	0.08	0.06	0.13	0	0	0
YNL189W	SRP1	D	20	0.14	0.23	0.23	0.28	-0.01	0.13	0.11
YNL190W		D	20	1.14	1.61	1.95	2.99	0.13	<b>0.24</b>	<b>0.31</b>
YNL191W		D	21	0.11	0.08	0.04	0.15	0	0	0.12

YNL192W	CHS1	D	20	0.13	0.14	0.25	0.31	0	0.18	<b>0.27</b>
YNL193W		D	20	0.11	0.13	0.04	0.06	0	0	0
YNL194C		D	21	0.11	0.08	0.04	0.12	0	0	-0.02
YNL195C		D	20	0.11	0.08	0.05	0.16	0	0	0.08
YNL199C	GCR2	D	20	0.11	0.11	0.04	0.08	0	0	<b>-0.35</b>
YNL200C		D	20	0.31	0.29	0.36	0.48	0	-0.13	<b>0.22</b>
YNL201C		D	20	0.11	0.08	0.04	0.07	0	0	-0.18
YNL202W	SPS19	D	20	0.11	0.08	0.26	0.14	0	0.17	0
YNL206C		D	20	0.11	0.08	0.05	0.09	0	0	0
YNL208W		D	20	2.81	2.76	5.52	7	0.09	<b>0.26</b>	<b>0.3</b>
YNL209W	SSB2	D	20	2.31	3.13	2.16	2.51	0.17	0	-0.11
YNL211C		D	20	0.11	0.08	0.09	0.09	0	0	0
YNL213C		D	21	0.11	0.08	0.05	0.06	0	0	0
YNL216W	RAP1	D	20	0.11	0.09	0.06	0.11	0	0	0
YNL217W		D	21	0.11	0.09	0.18	0.1	0	0.09	0
YNL219C	ALG9	D	20	0.13	0.17	0.15	0.15	-0.01	-0.07	0
YNL220W	ADE12	D	20	0.22	0.22	0.2	0.33	0.07	0.03	0.14
YNL221C	POP1	D	20	0.11	0.08	0.04	0.08	0	0	0
YNL222W	SSU72	D	21	0.11	0.08	0.08	0.06	0	0	0
YNL223W		D	20	0.11	0.08	0.06	0.04	0	0	0
YNL229C	URE2	D	21	0.11	0.11	0.15	0.11	0.03	0.01	0.02
YNL230C		D	21	0.11	0.08	0.04	0.07	0	0	0
YNL231C		D	20	0.12	0.18	0.28	0.16	0.06	0.13	0.03
YNL232W		D	21	0.11	0.16	0.1	0.13	0.15	0	-0.05
YNL234W		D	20	0.11	0.08	0.04	0.07	0	0	0
YNL236W	SIN4	D	21	0.11	0.08	0.06	0.09	0	0	0
YNL237W	YTP1	D	20	0.11	0.08	0.09	0.14	0	<b>-0.27</b>	0
YNL238W	KEX2	D	21	0.11	0.11	0.06	0.13	0	0	0.07
YNL239W	LAP3	D	20	0.26	0.25	0.88	0.41	0.06	<b>0.41</b>	0.19
YNL240C		D	21	0.12	0.13	0.15	0.22	0.01	0.11	<b>0.21</b>
YNL241C	ZWF1	D	20	0.27	0.36	0.34	0.62	0.15	0.15	<b>0.33</b>
YNL243W	SLA2	D	21	0.13	0.16	0.18	0.15	0.04	-0.01	0.07
YNL244C	SUI1	D	20	0.88	0.81	1.14	1.12	0.11	<b>0.21</b>	0.18
YNL245C		D	20	0.11	0.08	0.1	0.12	0	0	0
YNL246W		D	20	0.18	0.17	0.13	0.15	0	-0.18	-0.04
YNL247W		D	20	0.11	0.17	0.17	0.15	0.07	0.08	0.02
YNL248C	RPA49	D	20	0.11	0.17	0.1	0.09	0.12	0	0
YNL249C	MPA43	D	20	0.11	0.08	0.1	0.11	0	0	-0.1
YNL251C	NRD1	D	20	0.11	0.19	0.07	0.08	0.05	0	0
YNL252C		D	20	0.11	0.12	0.11	0.11	0	0	0
YNL255C		D	21	0.25	0.51	0.4	0.37	<b>0.22</b>	0.17	<b>0.24</b>
YNL256W		D	20	0.11	0.08	0.05	0.05	0	0	0
YNL259C	ATX1	D	21	0.22	0.2	0.35	0.31	0	<b>0.32</b>	0.17
YNL261W	ORC5	D	21	0.11	0.1	0.06	0.1	0	0	0
YNL262W	POL2	D	21	0.11	0.08	0.05	0.05	0	0	0
YNL263C	YIF1	D	21	0.49	0.75	0.44	0.67	0.07	<b>-0.23</b>	-0.01
YNL264C		D	21	0.11	0.09	0.09	0.17	0	-0.18	0.07
YNL265C		D	20	0.11	0.09	0.04	0.07	0	0	0
YNL268W	LYP1	D	21	0.96	1.53	0.89	0.89	-0.02	-0.05	-0.13
YNL271C	BNI1	D	20	0.11	0.08	0.05	0.14	0	0	-0.04
YNL274C		D	21	0.19	0.32	0.64	0.75	0	0.07	<b>0.39</b>
YNL277W	MET2	D	20	0.11	0.08	0.04	0.06	0	0	0
YNL278W		D	21	0.11	0.08	0.1	0.11	0	0	0
YNL280C	ERG24	D	21	0.26	0.26	0.29	0.34	-0.05	-0.04	0.12
YNL281W		D	21	0.16	0.24	0.35	0.69	0.17	0.19	<b>0.51</b>

YNL283C	WSC2	D	21	0.23	0.35	0.29	0.29	0.1	-0.02	0.06
YNL284C	MRPL10	D	21	0.18	0.18	0.25	0.38	0	0.1	0.03
YNL287W	SEC21	D	20	0.17	0.19	0.2	0.21	-0.08	-0.02	0.02
YNL288W		D	20	0.23	0.3	0.22	0.32	0.05	0	0.09
YNL289W	PCL1	D	21	0.11	0.08	0.1	0.04	0	0	0
YNL290W	RFC3	D	20	0.11	0.08	0.04	0.11	0	0	0
YNL291C	MID1	D	21	0.11	0.18	0.13	0.11	0.02	0	0.02
YNL292W	PUS4	D	20	0.11	0.08	0.09	0.07	0	0	0
YNL293W	MSB3	D	20	0.11	0.08	0.05	0.05	0	0	0
YNL294C		D	21	0.11	0.08	0.09	0.2	0	0	0.01
YNL300W		D	21	3.3	1.49	1.98	1.34	0.06	0.08	-0.17
YNL301C	RPL18B	D	56	1.8	1.97	1.74	1.52	0.1	0.07	-0.01
YNL302C	RPS19B	D	40	2.55	2.95	2.83	2.03	0.04	0.03	-0.11
YNL303W		D	20	0.11	0.1	0.06	0.06	0	0	0
YNL304W		D	20	0.11	0.08	0.04	0.05	0	0	0
YNL305C		D	20	1.14	0.57	0.6	1.72	-0.2	-0.17	0.14
YNL306W		D	20	0.21	0.25	0.36	0.29	-0.05	0	0.03
YNL307C	MCK1	D	20	0.14	0.28	0.26	0.13	0.05	0.04	-0.02
YNL308C		D	20	0.11	0.08	0.09	0.1	0	0	0
YNL310C		D	20	0.11	0.08	0.07	0.06	0	-0.19	0
YNL312W	RFA2	D	21	0.28	0.65	0.51	0.41	0.15	0.1	0.03
YNL313C		D	20	0.11	0.08	0.05	0.07	0	0	0
YNL314W	DAL82	D	20	0.11	0.08	0.05	0.05	0	0	0
YNL315C	ATP11	D	21	0.11	0.08	0.1	0.17	0	0	0.08
YNL316C	PHA2	D	20	0.11	0.1	0.05	0.14	0	0	0.12
YNL317W		D	21	0.11	0.08	0.07	0.04	0	0	0
YNL320W		D	20	0.23	0.25	0.29	0.3	0	0.14	0.13
YNL321W		D	21	0.14	0.22	0.2	0.22	-0.1	-0.02	0.05
YNL322C	KRE1	D	20	1.45	1.29	1.97	1.41	0.1	0.01	0.09
YNL323W		D	21	0.11	0.17	0.08	0.11	0	0	0
YNL326C		D	20	0.11	0.09	0.08	0.09	0	0	-0.18
YNL327W	EGT2	D	21	1.57	2.13	2.34	2.31	0.17	0.15	0.19
YNL328C	MDJ2	D	20	0.11	0.08	0.09	0.07	0	0	0
YNL329C	PEX6	D	20	0.11	0.08	0.13	0.13	0	0	0
YNL330C	RPD3	D	20	0.16	0.15	0.16	0.25	0	-0.05	0.11
YNL331C		D	21	0.11	0.08	0.04	0.1	0	0	-0.07
YNL332W		D	20	0.11	0.08	0.1	0.04	0	0	0
YNL333W	SNZ2	D	20	0.11	0.08	0.16	0.06	0	0.11	0
YNL334C	SNO2	D	20	0.11	0.08	0.11	0.06	0	0	0
YNL336W	COS1	D	30	0.31	0.22	0.5	0.37	0	0.11	0.04
YNL337W		D	20	0.11	0.08	0.06	0.04	0	0	0
YNL339C		D	20	0.42	0.43	0.57	0.65	-0.06	0.12	0.09
YNR001C	CIT1	D	20	1.13	0.82	1.91	1.63	0	<b>0.2</b>	0.08
YNR002C	FUN34	D	20	0.12	0.12	0.24	0.14	0	<b>0.24</b>	0
YNR006W	VPS27	D	20	0.11	0.08	0.04	0.06	0	0	0
YNR007C	AUT1	D	21	0.11	0.08	0.09	0.09	0	<b>-0.25</b>	<b>-0.22</b>
YNR009W		D	21	0.11	0.11	0.07	0.04	-0.08	0	0
YNR010W	CSE2	D	21	0.11	0.08	0.04	0.06	0	0	0
YNR011C	PRP2	D	20	0.11	0.08	0.05	0.05	0	0	0
YNR012W	URK1	D	21	0.11	0.08	0.07	0.08	0	0	-0.18
YNR013C		D	20	0.11	0.13	0.09	0.17	0	0	0.04
YNR014W		D	20	0.49	0.19	0.1	0.33	0	0	0
YNR015W	SMM1	D	20	0.11	0.09	0.1	0.08	0	0	0
YNR016C	ACC1	D	20	0.41	0.5	0.6	0.64	0.12	0.13	0.16
YNR017W	MAS6	D	20	0.36	0.58	0.87	0.92	0.06	<b>0.21</b>	0.19

YNR018W		D	20	1.45	1.95	2.94	2.36	0.06	<b>0.28</b>	0.14
YNR019W	ARE2	D	21	0.11	0.08	0.04	0.11	0	0	0.01
YNR020C		D	20	0.11	0.08	0.06	0.07	0	0	0
YNR021W		D	20	0.59	0.61	0.59	0.72	0.03	0	0.05
YNR022C		D	21	0.11	0.08	0.09	0.07	0	-0.08	0
YNR025C		D	21	0.11	0.08	0.05	0.04	0	0	0
YNR026C	SEC12	D	20	0.11	0.08	0.05	0.05	0	0	0
YNR027W		D	20	0.11	0.08	0.07	0.13	0	0	0.02
YNR028W	CPR8	D	20	0.11	0.09	0.08	0.08	0	0	0
YNR029C		D	20	0.11	0.08	0.06	0.05	0	0	0
YNR030W	ECM39	D	20	0.14	0.16	0.2	0.18	0.03	0.03	0.07
YNR031C	SSK2	D	20	0.11	0.08	0.04	0.06	0	0	0
YNR032W	PPG1	D	20	0.11	0.11	0.1	0.1	0.02	0	0
YNR033W	ABZ1	D	21	0.11	0.08	0.11	0.07	0	0	0
YNR034W	SOL1	D	20	0.13	0.09	0.09	0.21	0	0	0.09
YNR035C	ARC35	D	20	0.16	0.26	0.29	0.36	0.08	0.01	0.23
YNR036C		D	20	0.96	0.94	1.07	0.87	0.03	0.06	0.14
YNR037C		D	20	0.18	0.18	0.18	0.21	0	0	0.1
YNR038W	DBP6	D	21	0.11	0.1	0.1	0.13	0	<b>-0.2</b>	0.07
YNR039C		D	20	0.12	0.14	0.24	0.19	0	0.14	0.14
YNR040W		D	20	0.11	0.08	0.11	0.16	0	0	0.07
YNR041C	COQ2	D	21	0.2	0.23	0.19	0.22	-0.03	0	0
YNR043W	MVD1	D	20	0.35	0.44	0.52	0.65	0.1	0.16	0.16
YNR044W	AGA1	D	20	0.18	0.28	0.12	0.44	0.16	<b>-0.22</b>	<b>0.2</b>
YNR046W		D	20	0.14	0.45	0.46	0.47	0.12	0.05	0.13
YNR047W		D	20	0.11	0.08	0.05	0.06	0	0	0
YNR048W		D	20	0.11	0.08	0.06	0.08	0	0	0
YNR049C	MSO1	D	20	0.11	0.08	0.07	0.08	0	0	0
YNR050C	LYS9	D	20	2.88	1.54	4.73	1.52	-0.16	<b>0.3</b>	<b>-0.21</b>
YNR051C		D	20	0.11	0.08	0.07	0.06	0	0	0
YNR052C	POP2	D	20	0.12	0.18	0.23	0.2	0.06	0	-0.01
YNR053C		D	41	0.11	0.14	0.14	0.14	0.09	0.02	-0.04
YNR054C		D	21	0.11	0.08	0.05	0.04	0	0	0
YNR055C	HOL1	D	21	0.31	0.39	0.39	0.52	0.01	0	0.08
YNR057C	BIO4	D	21	0.11	0.11	0.29	0.33	0	<b>0.26</b>	0.17
YNR058W	BIO3	D	21	0.11	0.08	0.19	0.09	0	0.19	-0.1
YNR061C		D	21	0.16	0.27	0.31	0.19	0.07	-0.06	-0.09
YNR065C		D	21	0.11	0.1	0.15	0.11	0	0.03	0
YNR067C		D	21	0.12	0.19	0.28	0.59	-0.02	0.12	<b>0.35</b>
YNR068C		D	20	0.11	0.08	0.04	0.05	0	0	0
YNR071C		D	21	0.11	0.08	0.06	0.04	0	0	0
YNR074C		D	20	0.11	0.08	0.1	0.16	0	0	0.1
YNR075W	COS10	D	20	0.11	0.08	0.04	0.06	0	0	0
YNR076W	PAU6	D	20	0.26	0.28	0.67	0.54	-0	0.11	0.08
YOL001W	PHO80	D	21	0.11	0.08	0.04	0.1	0	0	0
YOL002C		D	20	0.32	0.28	0.48	0.56	0.03	0.17	0.12
YOL003C		D	20	0.11	0.08	0.05	0.09	0	0	0
YOL004W	SIN3	D	20	0.11	0.09	0.08	0.1	0	0	0
YOL005C	RPB11	D	21	0.44	0.42	0.41	0.43	0	0.09	0.03
YOL007C	CSI2	D	21	0.11	0.08	0.11	0.04	0	-0.04	0
YOL008W		D	21	0.11	0.14	0.17	0.19	0	0.07	0.09
YOL009C	MDM12	D	21	0.11	0.1	0.15	0.13	0	0.01	0
YOL010W		D	20	0.11	0.1	0.05	0.11	0	0	-0
YOL011W		D	21	0.15	0.1	0.17	0.3	0	0	0.17
YOL012C	HTA3	D	20	0.5	0.6	0.8	0.43	0.1	0.01	-0.1

YOL013C	HRD1	D	20	0.11	0.08	0.05	0.08	0	0	0
YOL014W		D	20	0.14	0.23	0.05	0.04	0.11	0	0
YOL016C	CMK2	D	20	0.24	0.13	0.35	0.31	0	0.12	0.03
YOL019W		D	20	0.15	0.29	0.36	0.27	0.11	<b>0.21</b>	0.03
YOL020W	TAT2	D	21	0.11	0.15	0.17	0.13	0.05	0.17	0
YOL021C	DIS3	D	20	0.11	0.21	0.16	0.11	<b>0.21</b>	0.1	-0.02
YOL022C		D	21	0.11	0.14	0.06	0.08	-0.01	0	-0.14
YOL026C		D	20	0.36	0.34	0.27	0.68	0	-0.1	0.12
YOL027C		D	21	0.17	0.11	0.2	0.24	-0.1	0.07	0.07
YOL030W		D	20	1.07	0.98	1.31	0.83	0.06	0.11	-0.02
YOL031C		D	20	0.11	0.08	0.43	0.13	0	<b>0.45</b>	0
YOL032W		D	20	0.11	0.12	0.07	0.09	0	0	0
YOL033W	MSE1	D	20	0.11	0.08	0.08	0.05	0	0	0
YOL035C		D	20	0.11	0.1	0.04	0.04	0	0	0
YOL036W		D	20	0.11	0.08	0.06	0.07	0	0	0
YOL038W	PRE6	D	20	0.51	0.54	0.57	0.96	0.05	0.12	<b>0.3</b>
YOL039W	RPP2A	D	20	8.1	11.06	13.38	10.26	0.1	-0.09	-0.12
YOL040C	RPS15	D	20	10.86	20.6	12.74	8.63	<b>0.24</b>	0	-0.19
YOL042W		D	20	0.11	0.12	0.1	0.09	0.06	0	0
YOL043C	NTG2	D	20	0.11	0.08	0.06	0.06	0	0	0
YOL048C		D	20	0.17	0.17	0.24	0.24	0	0.12	0.1
YOL049W	GSH2	D	20	0.13	0.11	0.11	0.12	0	0	0
YOL051W	GAL11	D	20	0.11	0.08	0.07	0.04	0	0	0
YOL052C	SPE2	D	20	0.24	0.18	0.23	0.37	0	0.03	0.15
YOL053C-A	DDR2	D	20	5.4	5.24	8.5	16.53	-0.07	0.19	<b>0.44</b>
YOL053W		D	20	0.11	0.08	0.06	0.06	0	0	<b>-0.3</b>
YOL055C		D	21	0.11	0.09	0.09	0.07	0	0	0
YOL056W	GPM3	D	20	0.11	0.08	0.05	0.08	0	0	0
YOL057W		D	21	0.16	0.21	0.22	0.17	0.02	-0.06	-0.07
YOL058W	ARG1	D	20	0.65	0.22	1.99	0.38	<b>-0.35</b>	<b>0.53</b>	0
YOL059W	GPD2	D	21	0.43	0.5	0.97	0.67	0.03	<b>0.27</b>	0.19
YOL060C		D	21	0.11	0.14	0.15	0.16	0	0	-0.01
YOL061W	PRPS5	D	21	0.45	0.74	0.57	0.93	0.13	0.07	0.17
YOL062C	APM4	D	20	0.11	0.15	0.13	0.16	0	0	0.05
YOL063C		D	20	0.11	0.09	0.06	0.07	0	0	0
YOL064C	MET22	D	21	0.11	0.13	0.2	0.17	0	0.16	0.07
YOL065C	INP54	D	20	0.11	0.08	0.08	0.06	0	0	0
YOL066C	RIB2	D	20	0.11	0.08	0.06	0.04	0	0	0
YOL068C	HST1	D	20	0.11	0.12	0.16	0.19	0	0	0.03
YOL070C		D	20	0.11	0.08	0.04	0.06	0	0	0
YOL071W		D	21	0.11	0.1	0.13	0.23	-0.06	0	0.17
YOL072W		D	21	0.11	0.08	0.07	0.08	0	0	0
YOL073C		D	20	0.46	0.47	0.34	0.55	0.1	0	-0.03
YOL075C		D	20	0.11	0.08	0.05	0.06	0	0	0
YOL077C		D	20	0.11	0.18	0.19	0.13	<b>0.14</b>	0	-0.05
YOL080C		D	20	0.11	0.08	0.07	0.04	0	0	0
YOL081W	IRA2	D	21	0.11	0.09	0.08	0.21	0	0	0.2
YOL082W		D	21	0.11	0.12	0.15	0.19	0	0.04	0.16
YOL083W		D	20	0.11	0.11	0.14	0.22	0	-0.11	0.11
YOL084W		D	21	0.11	0.08	0.04	0.07	0	0	0
YOL086C	ADH1	D	20	7.45	8.52	12.76	12.09	0.11	0.11	0.12
YOL087C		D	20	0.11	0.08	0.06	0.04	0	0	0
YOL088C	MPD2	D	21	0.14	0.11	0.18	0.18	0	-0.06	-0.01
YOL090W	MSH2	D	20	0.11	0.08	0.04	0.06	0	0	0
YOL092W		D	20	0.39	0.62	0.54	0.45	0.17	0.06	-0.02

YOL094C	RFC4	D	20	0.11	0.17	0.17	0.17	0	0	0
YOL096C	COQ3	D	21	0.11	0.11	0.11	0.1	0	-0.18	-0.1
YOL097C		D	20	0.29	0.52	0.49	0.63	0.16	0.1	0.18
YOL098C		D	20	0.11	0.1	0.04	0.1	0	0	0
YOL101C		D	20	0.11	0.08	0.11	0.06	0	0	0
YOL102C	TPT1	D	20	0.11	0.08	0.11	0.07	0	0	0
YOL103W	ITR2	D	20	0.22	0.23	0.2	0.33	0	0	0.17
YOL106W		D	20	0.11	0.08	0.06	0.07	0	0	0
YOL107W		D	20	0.15	0.16	0.23	0.21	0.03	0.13	0
YOL108C	INO4	D	20	0.13	0.17	0.15	0.11	-0.04	-0	-0.18
YOL109W	ZEO1	D	20	1.59	1.89	2.5	2.26	0.16	<b>0.28</b>	0.15
YOL110W	SHR5	D	20	0.19	0.36	0.31	0.6	0.07	0.13	<b>0.26</b>
YOL111C		D	20	0.47	0.51	0.56	0.78	0.05	0.02	0.13
YOL112W	MSB4	D	20	0.11	0.08	0.06	0.06	0	0	0
YOL119C		D	20	0.11	0.08	0.07	0.08	0	0	0
YOL120C	RPL18A	D	40	7.79	6.78	8.19	7.15	0.1	0.11	-0.02
<i>YOL121C</i>	RPS19A	D	40	3.34	3.89	4.38	2.9	0.04	0.07	-0.11
YOL122C	SMF1	D	21	0.23	0.23	0.35	0.36	-0.06	<b>0.27</b>	<b>0.24</b>
YOL123W	HRP1	D	21	0.12	0.14	0.18	0.11	0.07	0.07	-0.19
YOL124C		D	20	0.11	0.08	0.09	0.07	0	0	0
YOL125W		D	20	0.11	0.09	0.06	0.06	0	0	0
YOL126C	MDH2	D	21	0.18	0.14	0.45	0.24	0	<b>0.2</b>	-0.06
YOL127W	RPL25	D	20	2.08	3.37	2.36	1.38	0.18	0.02	-0.13
YOL128C		D	21	0.11	0.08	0.05	0.05	0	0	0
YOL129W		D	21	1.56	1.5	1.61	2.13	0.04	0.13	0.07
YOL130W	ALR1	D	21	0.11	0.08	0.09	0.1	0	0	-0.17
YOL133W	HRT1	D	20	0.19	0.15	0.25	0.28	0	0.06	0.04
YOL135C	MED7	D	20	0.11	0.09	0.11	0.09	0	0	0
YOL136C	PKF27	D	20	0.14	0.15	0.19	0.26	0.11	0.03	<b>0.27</b>
YOL137W		D	20	0.11	0.08	0.13	0.1	0	0	0
YOL139C	CDC33	D	21	1.27	1.24	1.21	0.99	0.13	0.18	0.05
YOL140W	ARG8	D	20	0.11	0.11	0.13	0.1	0	0	0
YOL142W		D	20	0.14	0.24	0.28	0.25	0.09	0.13	0.04
YOL143C	RIB4	D	20	0.32	0.48	0.66	0.47	0.17	<b>0.34</b>	<b>0.23</b>
YOL146W		D	20	0.11	0.09	0.08	0.08	0	0	0
YOL147C	PEX11	D	20	0.79	0.81	0.77	0.48	0.05	0.01	-0.18
YOL148C	SPT20	D	21	0.11	0.08	0.04	0.08	0	0	0
YOL149W	DCP1	D	20	0.11	0.08	0.09	0.05	0	0	0
YOL151W	GRE2	D	20	0.64	0.42	0.8	0.79	0	0.17	<b>0.24</b>
YOL153C		D	21	0.17	0.15	0.2	0.24	0	-0.12	-0.04
YOL154W		D	21	1.89	1.48	0.17	0.08	0.18	<b>-0.78</b>	<b>-0.99</b>
YOL155C		D	20	0.13	0.13	0.21	0.28	0	0	0.01
YOL158C		D	21	0.11	0.09	0.05	0.1	0	<b>-0.33</b>	0
YOL159C		D	20	0.11	0.13	0.2	0.19	0	0.09	0.1
YOL162W		D	20	0.11	0.08	0.05	0.06	0	0	0
YOL164W		D	20	0.11	0.11	0.15	0.09	0	0.05	0
YOL165C		D	20	0.11	0.1	0.07	0.05	0	<b>-0.23</b>	0
YOR001W	RRP6	D	20	0.11	0.18	0.12	0.11	-0.04	-0.11	0
YOR002W	ALG6	D	20	0.18	0.13	0.18	0.14	0	-0.02	-0.19
YOR004W		D	21	0.11	0.08	0.07	0.09	0	0	-0.14
YOR006C		D	20	0.11	0.08	0.07	0.04	0	0	0
YOR007C	SGT2	D	20	0.71	0.54	1.09	1.86	0.01	0.19	<b>0.41</b>
YOR008C	SLG1	D	20	0.21	0.18	0.22	0.25	-0.09	-0.02	0.1
YOR009W		D	21	0.26	0.09	0.24	0.4	0	-0.17	-0.06
YOR010C	TIR2	D	20	1.16	1.62	1.59	0.81	0.13	0.11	-0.07

YOR013W		D	21	0.11	0.11	0.09	0.17	0	0	0.02
YOR014W	RTS1	D	21	0.11	0.08	0.08	0.07	0	0	0
YOR015W		D	20	0.11	0.15	0.16	0.23	0.05	0.01	0.16
YOR016C		D	20	0.18	0.35	0.32	0.27	0.13	-0.07	0
YOR018W	ROD1	D	21	0.11	0.08	0.05	0.05	0	0	0
YOR020C	HSP10	D	21	1.22	0.77	1.63	2.71	0.06	<b>0.24</b>	<b>0.42</b>
YOR021C		D	21	0.11	0.23	0.24	0.16	<b>0.2</b>	<b>0.22</b>	-0.05
YOR022C		D	20	0.11	0.12	0.08	0.07	0	0	0
YOR023C		D	21	0.11	0.16	0.06	0.17	0.08	0	0.12
YOR027W	STI1	D	21	0.3	0.21	0.41	0.89	0	0.01	<b>0.38</b>
YOR031W	CRS5	D	20	0.16	0.17	0.24	0.51	0	0	<b>0.34</b>
YOR034C	AKR2	D	20	0.11	0.1	0.08	0.11	0	0	0
YOR035C		D	20	0.11	0.09	0.04	0.05	0	0	0
YOR036W	PEP12	D	20	0.11	0.08	0.05	0.06	0	0	0
YOR039W	CKB2	D	20	0.2	0.18	0.25	0.27	-0.03	0.08	0.05
YOR040W	GLO4	D	20	0.11	0.08	0.08	0.12	0	0	0.07
YOR042W		D	21	0.11	0.13	0.13	0.28	-0.07	-0.06	0.18
YOR043W	WHI2	D	20	0.11	0.09	0.11	0.15	0	0	0
YOR044W		D	20	0.16	0.12	0.19	0.26	0	-0.09	<b>0.2</b>
YOR045W	TOM6	D	21	1.6	2.22	2.09	2.27	0.13	0.08	0.06
YOR046C	DBP5	D	20	0.14	0.18	0.26	0.25	0.11	0.05	0.09
YOR047C	STD1	D	21	0.11	0.1	0.05	0.11	0	0	0
YOR051C		D	21	0.11	0.12	0.04	0.09	0.05	0	-0.08
YOR052C		D	20	0.17	0.15	0.3	0.41	0	0.18	<b>0.28</b>
YOR053W		D	20	0.11	0.08	0.06	0.07	0	0	0
YOR054C		D	21	0.11	0.08	0.07	0.09	0	0	0
YOR056C		D	20	0.11	0.08	0.08	0.04	0	0	0
YOR057W	SGT1	D	20	0.11	0.08	0.04	0.06	0	0	0
YOR059C		D	21	0.14	0.13	0.16	0.19	-0.06	0	0.1
YOR061W	CKA2	D	20	0.13	0.18	0.15	0.17	0.05	0	0
YOR062C		D	20	0.11	0.15	0.11	0.11	0	<b>-0.27</b>	0
YOR063W	RPL3	D	20	4.77	6.58	5.5	4.18	0.09	0.03	-0.15
YOR064C		D	20	0.11	0.08	0.1	0.05	0	0	0
YOR065W	CYT1	D	20	0.28	0.23	0.92	0.28	0	0.17	-0.02
YOR066W		D	20	0.11	0.11	0.1	0.17	0	0	0.16
YOR067C	ALG8	D	21	0.18	0.16	0.21	0.18	0	0.02	0.01
YOR069W	VPS5	D	21	0.11	0.08	0.05	0.04	0	0	0
YOR071C		D	21	0.11	0.09	0.11	0.12	0	-0.05	-0.1
YOR072W		D	21	0.11	0.09	0.04	0.04	0	0	0
YOR074C	CDC21	D	45	0.11	0.08	0.04	0.05	0	0	0
YOR078W		D	20	0.11	0.09	0.09	0.06	0	0	0
YOR079C	ATX2	D	21	0.11	0.12	0.18	0.12	-0.07	0.05	0
YOR081C		D	21	0.11	0.09	0.12	0.11	0	0	<b>-0.31</b>
YOR084W		D	20	0.18	0.17	0.21	0.17	0	0.07	-0.19
YOR085W	OST3	D	20	0.25	0.23	0.31	0.2	0.1	0.09	-0.02
YOR086C		D	20	0.11	0.13	0.11	0.19	0	-0.1	0
YOR087W		D	20	0.11	0.08	0.05	0.04	0	0	0
YOR088W		D	20	0.11	0.08	0.07	0.13	0	0	0
YOR089C	VPS21	D	21	0.11	0.12	0.18	0.24	0.02	0.05	0.14
YOR090C		D	20	0.11	0.08	0.08	0.16	0	0	-0.04
YOR091W		D	20	0.11	0.15	0.08	0.08	0	0	0
YOR092W	ECM3	D	20	0.12	0.21	0.24	0.33	0.11	0.01	<b>0.23</b>
YOR094W	ARF3	D	20	0.11	0.08	0.06	0.07	0	0	0
YOR095C	RKI1	D	20	0.11	0.13	0.13	0.07	0.08	0.07	0
YOR096W	RPS7A	D	42	2.93	3.29	4.26	2.03	0.13	0.11	-0.1

YOR097C		D	20	0.14	0.19	0.18	0.18	0	0.04	0.11
YOR098C	NUP1	D	20	0.11	0.1	0.09	0.11	0	0	-0
YOR099W	KTR1	D	20	1.34	1.16	2.53	1.54	0.05	<b>0.23</b>	0.01
YOR101W	RAS1	D	20	0.11	0.09	0.1	0.05	0	0	0
YOR102W		D	20	0.11	0.08	0.04	0.06	0	0	0
YOR103C	OST2	D	20	0.37	0.32	0.71	0.42	-0.01	<b>0.26</b>	0.07
YOR104W		D	20	0.11	0.08	0.06	0.08	0	0	0
YOR106W	VAM3	D	21	0.11	0.11	0.11	0.1	0.01	-0.1	0
YOR107W		D	20	0.11	0.08	0.06	0.07	0	0	0
YOR108W		D	21	0.27	0.34	0.27	0.22	0.18	0.11	0
YOR109W	INP53	D	21	0.11	0.08	0.04	0.08	0	0	0
YOR110W		D	21	0.11	0.08	0.04	0.04	0	0	0
YOR112W		D	21	0.11	0.08	0.07	0.04	0	0	0
YOR115C		D	21	0.11	0.08	0.1	0.08	0	0	0
YOR116C	RPO31	D	20	0.11	0.08	0.04	0.05	0	0	0
YOR117W	RPT5	D	21	0.33	0.23	0.33	0.36	0	0	0.07
YOR119C	RIO1	D	20	0.11	0.08	0.1	0.05	0	0	0
YOR120W	GCY1	D	20	0.11	0.14	3.21	0.72	0	<b>1.09</b>	<b>0.48</b>
YOR121C		D	20	0.11	0.08	0.13	0.07	0	0	0
YOR122C	PFY1	D	21	2.73	4.46	4.22	3.77	0.12	0.09	0.07
YOR123C	LEO1	D	20	0.11	0.1	0.06	0.05	0	0	0
YOR124C	UBP2	D	20	0.11	0.08	0.06	0.09	0	0	0
YOR125C	CAT5	D	21	0.11	0.1	0.2	0.18	0	0.05	0.04
YOR126C	IAH1	D	20	0.11	0.08	0.19	0.14	0	0.01	0
YOR128C	ADE2	D	20	0.19	0.24	0.21	0.48	0.06	0.07	<b>0.33</b>
YOR129C		D	20	0.11	0.08	0.09	0.05	0	0	0
YOR130C	ARG11	D	21	0.11	0.12	0.16	0.06	-0.09	0.14	0
YOR131C		D	20	0.11	0.18	0.19	0.14	0.01	0.05	0.02
YOR132W	VPS17	D	20	0.11	0.1	0.1	0.21	0	-0.11	0.04
YOR133W	EFT1	D	20	2.91	3.52	3.39	2.87	0.14	0.07	0.02
YOR134W	BAG7	D	21	0.11	0.08	0.08	0.32	0	0	0.22
YOR135C		D	20	0.11	0.08	0.04	0.05	0	0	0
YOR136W	IDH2	D	20	1.42	0.88	3.46	2.03	-0.13	<b>0.28</b>	0.12
YOR137C		D	20	0.11	0.08	0.04	0.08	0	0	0
YOR138C		D	21	0.11	0.08	0.08	0.06	0	-0.13	0
YOR140W	SFL1	D	20	0.11	0.08	0.06	0.04	0	0	0
YOR141C	ARP8	D	20	0.11	0.08	0.07	0.06	0	0	0
YOR142W		D	20	0.52	0.49	0.74	0.53	0.01	0.14	-0.04
YOR143C	THI80	D	20	0.11	0.08	0.05	0.04	0	0	0
YOR145C		D	20	0.11	0.08	0.13	0.15	0	0	0.03
YOR147W		D	20	0.11	0.08	0.05	0.04	0	0	0
YOR149C	SMP3	D	21	0.11	0.08	0.07	0.09	0	0	-0.1
YOR150W		D	20	0.3	0.16	0.36	0.27	0	0.1	0.07
YOR151C	RPB2	D	20	0.11	0.18	0.18	0.24	0.09	0.07	0.1
YOR152C		D	20	0.11	0.1	0.08	0.06	0	0	0
YOR153W	PDR5	D	20	0.46	0.52	0.8	0.63	0.09	0.04	0.07
YOR154W		D	21	0.11	0.08	0.04	0.07	0	0	<b>-0.31</b>
YOR155C		D	20	0.11	0.08	0.08	0.15	0	0	0
YOR157C	PUP1	D	20	0.47	0.68	0.7	0.86	0.16	0.13	<b>0.21</b>
YOR158W	PET123	D	20	0.11	0.11	0.05	0.06	0	0	0
YOR159C	SME1	D	21	0.11	0.14	0.13	0.14	0	-0	0.01
YOR160W	MTR10	D	21	0.11	0.09	0.04	0.05	0	0	0
YOR161C		D	20	0.25	0.16	0.16	0.38	0	-0.17	0.13
YOR163W		D	21	0.11	0.08	0.12	0.12	0	-0.03	-0.05
YOR164C		D	20	0.17	0.17	0.19	0.2	-0.09	0.02	-0.1

YOR165W		D	20	0.12	0.08	0.1	0.08	0	-0.06	0
YOR166C		D	21	0.11	0.08	0.04	0.06	0	0	0
YOR167C	RPS28A	D	36	2.32	2.43	3.4	2.6	0.15	0.08	-0.14
YOR168W	GLN4	D	21	0.11	0.15	0.14	0.15	-0.02	-0.09	0.02
YOR172W		D	20	0.11	0.08	0.04	0.07	0	0	0
YOR173W		D	20	0.11	0.08	0.14	0.17	0	0	0.13
YOR174W	MED4	D	21	0.11	0.08	0.08	0.06	0	0	0
YOR175C		D	20	0.11	0.19	0.16	0.14	-0.02	-0	-0.02
YOR176W	HEM15	D	21	0.69	0.73	0.89	0.72	-0.04	0.07	-0.07
YOR178C	GAC1	D	20	0.11	0.08	0.22	0.08	0	<b>0.29</b>	-0.14
YOR179C		D	21	0.11	0.08	0.17	0.11	0	-0.01	-0.08
YOR180C	EHD2	D	20	0.11	0.08	0.07	0.05	0	0	0
YOR181W	LAS17	D	20	0.11	0.1	0.07	0.09	0	0	0
YOR182C	RPS30B	D	20	7	11.26	9.27	5.75	0.18	0.15	-0.08
YOR184W	SER1	D	20	0.17	0.22	0.24	0.31	0.06	0.03	0.16
YOR185C	GSP2	D	20	0.7	0.54	0.8	1.74	-0.1	0.06	<b>0.34</b>
YOR187W		D	21	1.03	0.97	1.26	1.51	-0.02	0.09	0.13
YOR189W		D	20	0.11	0.11	0.09	0.07	0	0	0
YOR191W	RIS1	D	20	0.11	0.08	0.06	0.04	0	0	0
YOR194C	TOA1	D	20	0.11	0.08	0.09	0.15	0	0	0
YOR196C	LIP5	D	20	0.11	0.09	0.24	0.16	0	0.18	0.06
YOR197W		D	20	0.17	0.26	0.27	0.24	-0.06	0.09	0.05
YOR198C	BFR1	D	20	0.18	0.18	0.55	0.32	-0.03	0.01	0
YOR200W		D	20	0.11	0.08	0.04	0.05	0	0	0
YOR201C	PET56	D	20	0.11	0.09	0.16	0.2	0	0.09	0.08
YOR202W	HIS3	D	20	0.23	0.27	0.69	0.67	-0.01	<b>0.33</b>	<b>0.32</b>
YOR203W		D	20	0.12	0.21	0.23	0.19	0.09	0.21	0.18
YOR204W	DED1	D	21	0.34	0.32	0.5	0.43	0.01	0.11	0.12
YOR205C		D	20	0.11	0.08	0.08	0.05	0	0	0
YOR206W		D	20	0.11	0.09	0.06	0.05	0	0	0
YOR207C	RET1	D	20	0.11	0.1	0.1	0.14	0	0	0
YOR208W	PTP2	D	20	0.11	0.08	0.08	0.11	0	0	-0.2
YOR209C	NPT1	D	21	0.24	0.21	0.53	0.46	0.06	<b>0.26</b>	<b>0.2</b>
YOR210W	RPB10	D	20	0.17	0.2	0.51	0.37	-0.04	0.21	0.1
YOR212W	STE4	D	21	0.11	0.14	0.23	0.17	0	0	0.02
YOR213C	SAS5	D	21	0.11	0.08	0.16	0.12	0	0.09	-0.01
YOR215C		D	20	0.18	0.1	0.24	0.16	-0.2	-0.01	0.02
YOR217W	RFC1	D	20	0.11	0.09	0.04	0.07	0	0	0
YOR218C		D	21	0.11	0.08	0.04	0.05	0	0	0
YOR219C	STE13	D	21	0.11	0.08	0.07	0.07	0	0	<b>-0.2</b>
YOR220W		D	20	0.32	0.22	0.75	0.54	0	0.15	0.17
YOR222W		D	20	0.24	0.29	0.42	0.2	0.06	0.14	-0.1
YOR223W		D	20	0.11	0.08	0.05	0.1	0	0	0
YOR224C	RPB8	D	21	1.35	1.63	1.3	1.36	0.07	0.07	0.12
YOR226C		D	20	0.19	0.23	0.31	0.26	-0.05	0.07	0.06
YOR227W		D	20	0.11	0.08	0.06	0.11	0	0	0
YOR228C		D	21	0.39	0.34	0.45	0.33	0	0.06	-0.07
YOR229W	WTM2	D	21	0.17	0.13	0.26	0.18	0	-0.01	0.02
YOR230W	WTM1	D	21	3.27	3.1	3.33	5.06	-0.08	-0.04	<b>0.2</b>
YOR231W	MKK1	D	20	0.11	0.11	0.07	0.13	0	0	0
YOR232W	MGE1	D	20	0.16	0.24	0.19	0.22	0.12	0.05	0.03
YOR233W	KIN4	D	20	0.11	0.08	0.04	0.06	0	0	0
YOR234C		D	64	1.87	2.69	2.54	2.07	0.06	0.06	-0.01
YOR236W	DFR1	D	21	0.11	0.11	0.13	0.06	0	0.09	0
YOR238W		D	21	0.11	0.1	0.08	0.07	0	-0.11	-0.17

YOR239W		D	20	0.11	0.14	0.12	0.14	0	0	-0.01
YOR240W		D	21	0.11	0.1	0.18	0.1	0	0.13	0
YOR241W		D	20	0.11	0.11	0.11	0.14	0	0	-0.04
YOR243C		D	20	0.11	0.08	0.04	0.08	0	0	0
YOR244W	ESA1	D	21	0.11	0.08	0.08	0.09	0	0	-0.19
YOR245C		D	20	0.11	0.11	0.19	0.24	0	0.04	0.15
YOR246C		D	20	0.27	0.42	0.32	0.32	0.1	-0.06	-0.02
YOR247W		D	20	3.99	5.53	4.21	3.89	<b>0.21</b>	0.08	0.05
YOR248W		D	22	1.59	2.18	2.03	1.14	0.11	0.11	-0.02
YOR249C	APC5	D	20	0.11	0.08	0.04	0.05	0	0	0
YOR250C	CLP1	D	21	0.11	0.08	0.16	0.11	0	0.13	-0.15
YOR251C		D	20	0.14	0.17	0.24	0.17	0.02	0.12	0.02
YOR253W		D	20	0.22	0.27	0.39	0.21	0	0.14	0
YOR254C	SEC63	D	20	0.11	0.2	0.23	0.23	0	0.14	0.05
YOR257W	CDC31	D	21	0.11	0.14	0.23	0.23	0.03	0.07	-0.05
YOR258W		D	21	0.11	0.08	0.05	0.04	0	0	0
YOR259C	RPT4	D	20	0.22	0.26	0.35	0.53	0.05	0.19	<b>0.34</b>
YOR260W	GCD1	D	20	0.29	0.4	0.33	0.49	0.15	0.1	<b>0.22</b>
YOR261C	RPN8	D	20	0.11	0.09	0.1	0.12	0	0	0
YOR262W		D	20	0.11	0.09	0.12	0.17	0	0	0.01
YOR264W		D	21	0.11	0.08	0.07	0.09	0	0	0
YOR265W	RBL2	D	20	0.21	0.18	0.31	0.22	-0.06	0.13	0.02
YOR266W	PNT1	D	20	0.11	0.08	0.08	0.06	0	0	0
YOR267C		D	20	0.61	0.55	0.8	1.16	0	0	0.15
YOR269W	PAC1	D	21	0.11	0.08	0.07	0.07	0	0	0
YOR270C	VPH1	D	21	1.73	2.15	1.38	2.54	0.1	-0.03	0.14
YOR271C		D	20	0.48	0.67	0.62	0.73	0.14	0.03	-0.02
YOR272W	YTM1	D	20	0.11	0.09	0.08	0.04	0	0	0
YOR273C		D	21	0.42	0.4	0.86	0.35	-0.07	0.16	-0.05
YOR275C		D	20	0.11	0.08	0.05	0.07	0	0	0
YOR276W	CAF20	D	20	0.65	0.75	0.74	0.58	0.13	0.08	-0.09
YOR278W	HEM4	D	21	0.11	0.08	0.07	0.1	0	0	-0.05
YOR280C		D	20	0.17	0.1	0.28	0.23	0	0.09	0.11
YOR281C		D	20	0.11	0.08	0.08	0.08	0	0	0
YOR283W		D	20	0.11	0.12	0.21	0.2	0.04	0.08	0.16
YOR284W		D	21	0.11	0.08	0.09	0.04	0	-0.12	0
YOR285W		D	20	3.41	1.68	4.63	6.73	-0.07	0.17	<b>0.22</b>
YOR286W		D	20	0.52	0.58	0.8	0.69	0.08	0.12	0.04
YOR288C	MPD1	D	21	0.18	0.18	0.53	0.25	-0.03	<b>0.36</b>	<b>0.21</b>
YOR289W		D	20	0.11	0.14	0.23	0.24	0	0.04	0.19
YOR290C	SNF2	D	21	0.11	0.1	0.07	0.06	-0.07	<b>-0.27</b>	<b>-0.27</b>
YOR291W		D	20	0.14	0.09	0.08	0.08	0	0	0
YOR292C		D	20	0.11	0.08	0.07	0.09	0	0	0
YOR293W	RPS10A	D	50	3.03	3.22	3.27	2.24	0.09	0.02	<b>-0.2</b>
YOR294W		D	20	0.11	0.08	0.06	0.06	0	0	0
YOR297C		D	20	0.19	0.17	0.27	0.2	0	-0.04	0
YOR299W	BUD7	D	20	0.11	0.08	0.06	0.08	0	0	0
YOR301W		D	21	0.11	0.13	0.12	0.12	-0.08	-0.19	<b>-0.2</b>
YOR302W		D	20	0.54	0.39	0.83	0.83	-0.09	0.14	0.16
YOR303W	CPA1	D	20	0.67	0.68	1.58	1.35	-0.02	<b>0.28</b>	<b>0.23</b>
YOR304C-A		D	20	0.11	0.08	0.06	0.04	0	0	0
YOR304W	ISW2	D	20	0.11	0.08	0.05	0.04	0	0	0
YOR305W		D	20	0.13	0.08	0.11	0.15	0	0	0
YOR306C		D	21	0.11	0.08	0.06	0.14	0	<b>-0.24</b>	0.13
YOR307C	SLY41	D	20	0.11	0.1	0.09	0.12	0	0	-0.11

YOR309C		D	34	0.41	0.93	0.99	0.62	<b>0.29</b>	<b>0.31</b>	0.12
YOR310C	NOP5	D	20	0.42	0.76	0.87	0.66	<b>0.21</b>	<b>0.22</b>	0.11
YOR311C		D	20	0.38	0.38	0.53	0.41	0	0.09	0.01
<i>YOR312C</i>	RPL20B	D	66	1.2	1.65	1.14	1.08	0.11	-0.11	-0.16
YOR315W		D	20	0.11	0.08	0.11	0.04	0	-0.1	0
YOR316C	COT1	D	21	0.11	0.15	0.19	0.26	-0.07	-0.07	<b>0.21</b>
YOR317W	FAA1	D	20	0.46	0.38	0.44	0.76	-0.13	-0.06	0.04
YOR318C		D	21	0.11	0.08	0.05	0.04	0	0	0
YOR319W	HSH49	D	20	0.11	0.08	0.06	0.06	0	0	0
YOR320C		D	21	0.11	0.11	0.07	0.08	0	0	0
YOR321W	PMT3	D	20	0.11	0.09	0.16	0.19	0	0.01	-0.07
YOR322C		D	20	0.11	0.08	0.08	0.08	0	0	0
YOR323C	PRO2	D	20	0.2	0.17	0.25	0.27	-0.07	0.03	0.11
YOR326W	MYO2	D	20	0.13	0.1	0.1	0.1	-0.1	0	0
YOR327C	SNC2	D	21	0.27	0.35	0.44	0.46	-0.04	0.12	0.13
YOR328W	PDR10	D	20	0.11	0.08	0.04	0.1	0	0	0
YOR329C	SCD5	D	20	0.11	0.1	0.09	0.1	0	0	0
YOR331C		D	21	0.11	0.08	0.05	0.04	0	0	0
YOR332W	VMA4	D	20	0.91	0.49	1.03	0.95	0	0.04	0.02
YOR335C	ALA1	D	20	0.35	0.43	0.56	0.41	0.01	0.17	0.05
YOR336W	KRE5	D	21	0.11	0.12	0.13	0.1	0	-0.1	0
YOR337W	TEA1	D	21	0.11	0.08	0.06	0.04	0	0	0
YOR338W		D	20	0.11	0.08	0.06	0.12	0	0	0
YOR340C	RPA43	D	20	0.11	0.08	0.1	0.07	0	0	0
YOR341W	RPA190	D	21	0.11	0.08	0.06	0.11	0	0	-0.09
YOR342C		D	21	0.11	0.08	0.07	0.1	0	0	-0.07
YOR343C		D	20	0.11	0.08	0.08	0.09	0	0	0
YOR344C	TYE7	D	20	0.21	0.17	0.53	0.38	0	0.13	0.07
YOR346W	REV1	D	21	0.11	0.08	0.04	0.05	0	0	0
YOR347C	PYK2	D	21	0.13	0.11	0.25	0.21	0	0.13	0.08
YOR348C	PUT4	D	20	0.11	0.08	0.06	0.04	0	0	0
YOR349W	CIN1	D	21	0.11	0.08	0.05	0.05	0	0	0
YOR352W		D	21	0.11	0.08	0.08	0.09	0	<b>-0.36</b>	0
YOR354C		D	20	0.11	0.1	0.08	0.07	0	0	0
YOR355W	GDS1	D	20	0.15	0.2	0.2	0.32	0.15	0.15	<b>0.23</b>
YOR356W		D	20	0.11	0.13	0.14	0.11	0	0.08	0
YOR357C	GRD19	D	20	0.11	0.1	0.12	0.13	0	0	0
YOR358W	HAP5	D	21	0.11	0.08	0.05	0.11	0	0	0
YOR359W		D	20	0.12	0.21	0.16	0.21	-0.03	0.02	0.07
YOR360C	PDE2	D	20	0.15	0.11	0.16	0.23	0	-0	0.1
YOR361C	PRT1	D	20	0.24	0.3	0.34	0.37	0.02	0.02	0.03
YOR362C	PRE10	D	20	0.23	0.26	0.56	0.66	0.07	0.14	<b>0.24</b>
YOR363C	PIP2	D	21	0.11	0.11	0.06	0.11	0	0	-0.02
YOR367W	SCP1	D	20	0.11	0.1	0.12	0.21	0	0	0.05
YOR369C	RPS12	D	21	3.54	3.26	5.34	4.02	0.05	0.06	-0.17
YOR370C	MRS6	D	20	0.12	0.15	0.17	0.25	0	0	0.12
YOR373W	NUD1	D	21	0.11	0.08	0.04	0.07	0	0	0
YOR374W	ALD7	D	20	0.88	0.48	1.58	1.55	<b>-0.21</b>	<b>0.23</b>	<b>0.23</b>
YOR375C	GDH1	D	20	1.18	1.05	2.05	0.93	0.01	<b>0.28</b>	-0.1
YOR377W	ATF1	D	20	0.11	0.08	0.05	0.06	0	<b>-0.35</b>	0
YOR380W		D	20	0.11	0.08	0.11	0.1	0	0	0
YOR382W		D	20	0.14	0.15	0.28	0.41	0.02	0.14	<b>0.24</b>
YOR383C		D	21	1.18	1.37	1.37	1.72	0.04	0.06	0.02
YOR385W		D	20	0.12	0.14	0.18	0.12	0	0.02	-0.11
YOR388C	FDH1	D	27	0.11	0.08	0.07	0.04	0	0	0

YOR389W		D	20	0.11	0.08	0.06	0.05	0	0	0	0
YOR390W		D	20	0.12	0.08	0.09	0.1	0	-0.18	<b>-0.23</b>	
YOR391C		D	20	0.11	0.08	0.05	0.09	0	0	0	0
YOR393W	ERR1	D	20	0.11	0.08	0.04	0.07	0	0	0	0
YOR394W		D	20	0.11	0.08	0.11	0.11	0	0	-0.09	
YPL001W	HAT1	D	20	0.11	0.08	0.04	0.07	0	0	0	0
YPL002C	SNF8	D	21	0.11	0.08	0.08	0.1	0	0	0	0
YPL003W	ULA1	D	20	0.12	0.11	0.12	0.11	0	-0.05	0	
YPL004C		D	21	1.47	1.1	1.71	1.76	-0.04	0.15	0.09	
YPL006W	NCR1	D	21	0.12	0.12	0.22	0.38	-0.09	0.13	<b>0.3</b>	
YPL007C		D	21	0.11	0.08	0.05	0.06	0	0	0	
YPL009C		D	20	0.11	0.09	0.12	0.12	0	0	0	
YPL010W	RET3	D	20	0.72	0.8	1.2	0.75	0	0.13	-0.02	
YPL011C	TAF47	D	20	0.11	0.09	0.11	0.12	0	0	0	
YPL012W		D	20	0.11	0.13	0.1	0.09	0.06	0	-0.11	
YPL013C		D	20	0.21	0.28	0.31	0.29	0.02	0.13	0.08	
YPL014W		D	20	0.26	0.33	0.57	0.65	0.04	0.17	<b>0.22</b>	
YPL015C	HST2	D	20	0.27	0.18	0.4	0.27	-0.04	0.09	-0.07	
YPL017C		D	21	0.11	0.08	0.04	0.06	0	0	0	
YPL018W	CTF19	D	21	0.11	0.08	0.04	0.06	0	0	0	
YPL019C		D	20	0.11	0.09	0.2	0.19	0	0.07	0	
YPL020C		D	20	0.11	0.08	0.06	0.1	0	0	0	
YPL023C	MET12	D	20	0.14	0.12	0.1	0.11	0	0	0	
YPL024W	NCE4	D	20	0.11	0.08	0.05	0.12	0	0	0	
YPL026C	SKS1	D	20	0.11	0.14	0.08	0.13	0	-0.19	-0.01	
YPL028W	ERG10	D	21	2.49	2.75	3.82	2.35	0.04	0.16	-0.06	
YPL030W		D	20	0.11	0.12	0.12	0.15	0	0	0.06	
YPL031C	PHO85	D	21	0.52	0.41	0.56	0.66	0.01	0.08	0.14	
YPL032C	SVL3	D	20	0.11	0.21	0.14	0.25	0.07	0	0.11	
YPL034W		D	21	0.11	0.08	0.1	0.08	0	-0.1	<b>-0.24</b>	
YPL036W	PMA2	D	21	0.11	0.08	0.04	0.11	0	0	-0.1	
YPL037C	EGD1	D	21	3.31	1.77	3.26	3.13	0.01	0.01	-0.06	
YPL039W	MET31	D	20	0.11	0.08	0.11	0.08	0	0	0	
YPL042C	SSN3	D	20	0.11	0.09	0.05	0.04	0	0	0	
YPL046C	ELC1	D	21	0.11	0.08	0.07	0.07	0	0	<b>-0.27</b>	
YPL047W		D	20	0.12	0.12	0.09	0.14	0	0	0.02	
YPL048W	CAM1	D	20	1.6	0.88	1.02	1.28	-0.06	0	-0.08	
YPL049C	DIG1	D	21	0.11	0.08	0.05	0.16	0	0	0	
YPL050C	MNN9	D	20	0.11	0.1	0.11	0.21	0	0	0.02	
YPL051W		D	20	0.11	0.08	0.07	0.04	0	0	0	
YPL052W		D	20	0.11	0.08	0.05	0.05	0	0	0	
YPL053C	KTR6	D	20	0.11	0.16	0.11	0.13	0.07	0	0.06	
YPL054W	LEE1	D	21	0.11	0.08	0.06	0.11	0	<b>-0.24</b>	-0.19	
YPL055C		D	20	0.11	0.09	0.11	0.12	0	0	0	
YPL056C		D	20	0.11	0.08	0.13	0.1	0	-0.09	0	
YPL057C	SUR1	D	20	0.25	0.32	0.49	0.44	-0.05	<b>0.2</b>	0.08	
YPL058C	PDR12	D	20	0.12	0.24	0.22	0.29	0.11	0.13	0.12	
YPL059W		D	20	0.37	0.32	0.66	0.62	0.01	<b>0.22</b>	<b>0.24</b>	
YPL061W	ALD6	D	20	1.33	0.86	1.36	1.59	0.01	0.05	0.09	
YPL063W		D	20	0.12	0.08	0.09	0.15	0	0	0	
YPL064C		D	20	0.11	0.08	0.05	0.05	0	0	0	
YPL065W	VPS28	D	20	0.11	0.08	0.05	0.1	0	0	0	
YPL066W		D	20	0.11	0.08	0.76	0.08	0	<b>0.8</b>	0	
YPL067C		D	21	0.21	0.49	1.76	0.52	0.01	<b>0.77</b>	0.02	
YPL068C		D	21	0.11	0.08	0.09	0.04	0	-0.12	0	

YPL069C	BTS1	D	21	0.11	0.08	0.04	0.05	0	0	0
YPL071C		D	20	0.11	0.08	0.06	0.06	0	0	0
YPL075W	GCR1	D	21	0.11	0.08	0.12	0.12	0	-0.08	0.05
YPL076W	GPI2	D	21	0.11	0.08	0.16	0.11	0	0	-0.05
YPL077C		D	20	0.11	0.09	0.04	0.04	0	0	0
YPL078C	ATP4	D	20	0.65	0.53	1.32	0.65	0	<b>0.31</b>	-0.05
YPL079W	RPL21B	D	20	17.13	10.75	16	9.9	-0.06	-0.05	-0.15
YPL080C		D	20	0.11	0.08	0.04	0.06	0	0	0
YPL081W	RPS9A	D	21	0.25	0.33	0.4	0.53	0.04	0.01	<b>0.25</b>
YPL084W	BRO1	D	21	0.11	0.08	0.08	0.06	0	0	0
YPL085W	SEC16	D	20	0.11	0.19	0.14	0.14	0	0	0
YPL086C	HPA1	D	21	0.11	0.11	0.07	0.06	0	<b>-0.26</b>	0
YPL087W		D	20	1.01	0.52	0.7	1.46	0	0.03	<b>0.2</b>
YPL088W		D	20	0.11	0.08	0.04	0.12	0	0	0
YPL089C	RLM1	D	20	0.11	0.12	0.17	0.27	-0.03	0.05	0.24
YPL090C	RPS6A	D	20	2.44	3.1	2.6	2.14	0.05	0.04	-0.14
YPL091W	GLR1	D	20	0.24	0.15	0.27	0.25	0	0.07	0
YPL092W	SSU1	D	21	0.11	0.08	0.24	0.13	0	<b>0.24</b>	0.03
YPL093W		D	20	0.11	0.08	0.05	0.1	0	0	0
YPL094C	SEC62	D	20	0.7	0.61	1.46	0.78	0.02	<b>0.24</b>	0.17
YPL095C		D	20	0.32	0.31	0.52	0.18	0.02	0.17	-0.13
YPL097W	MSY1	D	20	0.11	0.1	0.11	0.13	0	0	0
YPL098C		D	20	0.94	1.46	1.19	1.28	0.12	0.15	0.1
YPL100W		D	20	0.11	0.08	0.05	0.1	0	0	0
YPL101W		D	20	0.11	0.08	0.08	0.1	0	0	0
YPL104W	MSD1	D	20	0.11	0.08	0.04	0.07	0	0	0
YPL105C		D	20	0.11	0.08	0.16	0.07	0	-0.07	0
YPL106C	SSE1	D	20	0.83	0.49	0.97	1.72	-0.06	0.09	<b>0.32</b>
YPL107W		D	20	0.11	0.08	0.06	0.04	0	0	0
YPL111W	CAR1	D	20	0.11	0.09	0.1	0.12	0	0	0
YPL112C		D	21	0.11	0.1	0.08	0.08	0	0	0
YPL113C		D	20	0.11	0.08	0.05	0.04	0	0	0
YPL115C	BEM3	D	21	0.11	0.08	0.04	0.08	0	0	-0.11
YPL117C	IDI1	D	20	0.12	0.15	0.18	0.25	0	0	0.08
YPL118W		D	20	0.11	0.09	0.13	0.1	0	0	0
YPL122C	TFB2	D	20	0.11	0.08	0.07	0.09	0	0	0
YPL123C		D	20	0.11	0.08	0.04	0.08	0	0	0
YPL125W		D	21	0.11	0.08	0.07	0.04	0	<b>-0.24</b>	0
YPL127C	HHO1	D	20	0.34	0.24	0.22	0.12	-0.06	<b>-0.2</b>	<b>-0.34</b>
YPL128C	TBF1	D	21	0.16	0.2	0.11	0.23	0.06	<b>-0.22</b>	-0.04
YPL129W		D	20	0.16	0.16	0.15	0.18	0	-0.13	-0.06
YPL131W	RPL5	D	21	9.79	15.07	11.54	9.28	0.1	-0.05	-0.11
YPL132W	COX11	D	20	0.11	0.08	0.06	0.13	0	0	-0.12
YPL134C		D	20	0.24	0.2	0.77	0.22	0	<b>0.36</b>	-0.14
YPL135W		D	20	0.76	0.47	0.67	1.16	0.04	-0.02	<b>0.31</b>
YPL138C		D	20	0.11	0.08	0.04	0.1	0	0	0
YPL139C	UME1	D	20	0.11	0.17	0.14	0.08	0	-0.05	<b>-0.25</b>
YPL142C		D	21	0.13	0.1	0.06	0.13	0	0	0
YPL143W	RPL33A	D	18	12.45	7.79	8.49	7.04	-0.07	0	-0.11
YPL144W	SNR17B	D	20	0.32	0.24	0.23	0.22	-0.02	-0.07	-0.15
YPL145C	KES1	D	20	0.17	0.15	0.12	0.1	0	0	0
YPL148C	PPT2	D	20	0.13	0.11	0.08	0.13	0	0	0.02
YPL149W	APG5	D	21	0.42	0.42	0.5	0.49	0.02	0.11	0.09
YPL152W	RRD2	D	21	0.11	0.08	0.04	0.09	0	0	0
YPL154C	PEP4	D	20	1.94	1.3	1.85	3.12	-0.11	-0.04	0.18

YPL156C		D	20	0.11	0.08	0.05	0.06	0	0	0
YPL157W		D	20	0.11	0.08	0.05	0.04	0	0	0
YPL159C		D	20	0.11	0.08	0.11	0.1	0	0	0
YPL160W	CDC60	D	20	0.12	0.16	0.21	0.21	0.08	0.12	0.08
YPL162C		D	21	0.11	0.08	0.08	0.06	0	0	0
YPL163C	SVS1	D	20	0.48	0.82	0.87	0.61	0.18	0.09	0
YPL168W		D	20	0.11	0.08	0.04	0.06	0	0	0
YPL169C	MEX67	D	20	0.16	0.11	0.15	0.25	0	<b>-0.22</b>	0.07
YPL170W		D	21	0.42	0.26	0.51	0.75	0	0.16	<b>0.24</b>
YPL171C	OYE3	D	20	0.11	0.08	0.07	0.04	0	0	0
YPL172C	COX10	D	20	0.11	0.08	0.06	0.1	0	0	<b>-0.21</b>
YPL173W	MRPL40	D	20	0.11	0.09	0.12	0.12	0	0	-0.11
YPL175W		D	20	0.11	0.08	0.09	0.09	0	0	0
YPL176C		D	20	0.16	0.12	0.13	0.18	0	-0.13	-0.1
YPL177C	CUP9	D	21	0.2	0.25	0.27	0.32	-0.08	0.04	0.01
YPL178W	MUD13	D	21	0.16	0.2	0.17	0.19	0	-0.12	0
YPL179W	PPQ1	D	20	0.11	0.11	0.13	0.14	0	0	0
YPL180W		D	21	0.11	0.08	0.04	0.04	0	0	0
YPL182C		D	20	0.11	0.09	0.05	0.04	0	0	0
YPL183C		D	20	0.11	0.08	0.04	0.09	0	0	0
YPL184C		D	20	0.12	0.2	0.15	0.12	0.02	-0.05	0
YPL186C		D	21	0.11	0.08	0.07	0.09	0	0	-0.13
YPL187W	MFα1	D	20	0.11	2.88	0.07	0.04	<b>1.28</b>	0	0
YPL188W	POSS	D	20	0.11	0.08	0.13	0.09	0	0.03	0
YPL190C		D	20	0.11	0.08	0.06	0.06	0	0	0
YPL195W	APL5	D	21	0.11	0.08	0.08	0.06	0	0	<b>-0.33</b>
YPL196W		D	21	0.11	0.08	0.06	0.08	0	0	-0.12
YPL197C		D	21	0.11	0.08	0.04	0.07	0	0	0
YPL198W	RPL7B	D	39	0.81	0.76	1.02	1.97	0	-0.05	-0.04
YPL199C		D	20	0.23	0.21	0.29	0.21	0	-0.03	-0.06
YPL203W	PKA3	D	21	0.18	0.14	0.18	0.34	0	-0.01	0.1
YPL204W	HRR25	D	21	0.31	0.13	0.21	0.41	0	-0.15	0.02
YPL206C		D	20	0.44	0.14	0.36	0.45	<b>-0.25</b>	-0.05	0.1
YPL207W		D	20	0.11	0.18	0.18	0.22	-0.05	0.03	0.03
YPL208W		D	20	0.11	0.08	0.07	0.06	0	<b>-0.28</b>	0
YPL210C	SRP72	D	20	0.11	0.11	0.05	0.1	0	0	0
YPL211W	NIP7	D	21	0.11	0.15	0.17	0.11	0.08	0.03	-0.08
YPL212C	PUS1	D	21	0.11	0.08	0.08	0.06	0	<b>-0.23</b>	0
YPL214C	THI6	D	20	0.11	0.08	0.1	0.04	0	0	0
YPL215W	CBP3	D	21	0.11	0.1	0.16	0.11	0	0.15	-0.17
YPL218W	SAR1	D	20	2.18	1.36	3.16	2.2	-0.08	0.1	-0.06
YPL219W	PCL8	D	20	0.11	0.08	0.05	0.04	0	0	0
YPL220W	RPL1A	D	20	9.9	5.87	10.04	5.6	<b>-0.39</b>	-0.03	<b>-0.21</b>
YPL221W		D	21	0.26	0.14	0.48	0.52	<b>-0.22</b>	0.18	0.19
YPL222W		D	21	0.11	0.08	0.04	0.08	0	0	0
YPL223C	GRE1	D	21	0.11	0.08	0.06	1.04	0	0	<b>0.83</b>
YPL224C	MMT2	D	21	0.15	0.09	0.11	0.16	0	<b>-0.28</b>	0
YPL225W		D	21	0.24	0.18	0.64	0.57	0	<b>0.23</b>	<b>0.2</b>
YPL226W		D	21	0.11	0.13	0.07	0.09	0	-0.19	0
YPL227C	ALG5	D	20	0.11	0.08	0.07	0.1	0	0	0
YPL229W		D	21	0.3	0.22	0.32	0.48	0	-0.01	-0.01
YPL230W		D	20	0.11	0.08	0.09	0.11	0	0	0
YPL231W	FAS2	D	20	1.52	0.83	2.07	1.08	0	0.04	-0.12
YPL232W	SSO1	D	20	0.14	0.21	0.23	0.29	0	0	0.13
YPL234C	TFP3	D	21	2.78	1.14	2.44	1.56	-0.19	-0.04	-0.12

YPL235W		D	21	0.18	0.12	0.2	0.27	-0.06	-0.07	0.05
YPL236C		D	21	0.11	0.08	0.06	0.09	0	0	-0.07
YPL237W	SUI3	D	20	0.18	0.22	0.28	0.28	0.12	0.08	0.13
YPL238C		D	20	0.11	0.08	0.04	0.08	0	0	<b>-0.22</b>
YPL239W	YAR1	D	20	0.11	0.08	0.11	0.11	0	-0.09	0
YPL240C	HSP82	D	20	0.15	0.14	0.21	0.67	0	-0.12	<b>0.39</b>
YPL244C		D	21	0.21	0.17	0.27	0.22	0	0.06	0
YPL245W		D	20	0.11	0.14	0.08	0.13	-0.01	0	-0.08
YPL246C		D	20	0.96	0.72	0.81	0.68	0	-0.09	-0.13
YPL247C		D	20	0.43	0.09	0.55	0.38	<b>-0.3</b>	0.14	-0.09
YPL250C		D	21	1.05	0.53	0.73	0.48	-0.12	-0.17	0
YPL252C		D	20	0.88	0.78	0.97	1.09	0.02	0.01	0.1
YPL256C	CLN2	D	21	0.21	0.15	0.17	0.2	0	0	-0.02
YPL258C		D	21	0.11	0.08	0.05	0.05	0	0	0
YPL259C	APM1	D	20	0.11	0.11	0.09	0.06	0	0	0
YPL260W		D	21	0.11	0.08	0.04	0.1	0	0	<b>-0.25</b>
YPL262W	FUM1	D	21	0.97	0.64	3.11	1.42	<b>-0.28</b>	<b>0.4</b>	0.14
YPL263C	KEL3	D	20	0.11	0.08	0.05	0.04	0	0	0
YPL264C		D	20	0.11	0.09	0.08	0.08	0	0	0
YPL265W	DIP5	D	20	0.2	0.22	0.17	0.26	-0.08	-0.12	0.07
YPL266W	DIM1	D	20	0.11	0.08	0.09	0.06	0	0	0
YPL268W	PLC1	D	20	0.11	0.08	0.04	0.1	0	0	-0.19
YPL270W	MDL2	D	21	0.11	0.09	0.07	0.11	0	<b>-0.25</b>	0.02
YPL271W	ATP15	D	20	2.42	0.58	3.99	2.87	<b>-0.4</b>	0.16	-0.08
YPL273W		D	20	0.25	0.18	0.43	0.16	0	<b>0.24</b>	0
YPL274W		D	20	0.17	0.22	0.22	0.35	0.04	0.05	<b>0.22</b>
YPL275W		D	24	0.11	0.08	0.07	0.04	0	0	0
YPL276W		D	20	0.11	0.08	0.06	0.04	0	0	0
YPL278C		D	20	0.11	0.11	0.12	0.14	-0.06	0.03	-0
YPL279C		D	20	0.11	0.15	0.11	0.16	0	0	0.07
YPL280W		D	20	0.11	0.08	0.05	0.1	0	0	0
YPL282C		D	20	0.11	0.08	0.08	0.06	0	0	0
YPL283C		D	20	0.72	0.33	0.63	0.78	<b>-0.22</b>	-0.12	0
YPR004C		D	20	0.42	0.55	0.61	0.67	-0.03	0.01	0
YPR005C	HAL1	D	21	0.11	0.08	0.09	0.05	0	-0.16	0
YPR006C	ICL2	D	20	0.11	0.08	0.05	0.04	0	0	0
YPR008W		D	21	0.11	0.08	0.07	0.09	0	-0.19	-0.1
YPR009W		D	21	0.11	0.15	0.14	0.14	0	0	-0.01
YPR010C		D	20	0.27	0.41	0.36	0.37	0.1	0.02	0.05
YPR011C		D	20	0.11	0.08	0.08	0.09	0	0	0
YPR012W		D	21	0.12	0.08	0.14	0.12	0	-0.13	<b>-0.2</b>
YPR013C		D	20	0.11	0.08	0.08	0.05	0	0	0
YPR016C	CDC95	D	21	0.99	1.06	0.93	0.67	0.07	-0.02	-0.03
YPR017C	DSS4	D	20	0.11	0.08	0.08	0.05	0	-0.16	0
YPR019W	CDC54	D	21	0.11	0.08	0.06	0.04	0	0	0
YPR020W		D	20	0.32	0.15	0.61	0.16	0	<b>0.35</b>	<b>-0.21</b>
YPR021C		D	21	0.11	0.08	0.11	0.13	0	0	-0.11
YPR022C		D	21	0.11	0.08	0.08	0.09	0	0	0
YPR023C		D	20	0.24	0.32	0.23	0.36	0.04	0.08	0.13
YPR024W	YME1	D	21	0.11	0.08	0.05	0.09	0	0	0
YPR028W		D	41	4.33	1.52	3.02	3.43	-0.15	-0.1	0.01
YPR029C	APL4	D	20	0.11	0.08	0.05	0.08	0	0	<b>-0.2</b>
YPR030W		D	20	0.11	0.08	0.09	0.04	0	0	0
YPR033C	HTS1	D	20	0.33	0.31	0.6	0.47	0.07	0.18	0
YPR034W	ARP7	D	21	0.11	0.11	0.06	0.07	-0.01	<b>-0.28</b>	0

YPR035W	GLN1	D	20	1.04	0.63	1.73	2.74	-0.02	0.19	<b>0.43</b>
YPR036W	VMA13	D	21	1.16	1.1	1.57	1.97	-0.1	-0.02	<b>0.2</b>
YPR037C		D	20	0.46	0.39	0.46	0.41	-0.07	0.01	-0.1
YPR040W		D	20	0.11	0.08	0.06	0.08	0	0	0
YPR041W	TIF5	D	20	0.2	0.27	0.2	0.29	0	0	0.01
YPR042C		D	21	0.11	0.09	0.05	0.09	0	0	-0.16
YPR043W	RPL43A	D	20	15.59	9.63	9.66	7.48	-0.18	-0.13	<b>-0.22</b>
YPR044C		D	20	0.13	0.14	0.14	0.06	0	-0.1	0
YPR047W	MSF1	D	21	0.11	0.08	0.04	0.05	0	0	0
YPR048W		D	21	0.11	0.08	0.05	0.05	0	0	0
YPR051W	MAK3	D	21	0.11	0.08	0.11	0.07	0	0	0
YPR052C	NHP6A	D	21	1.5	0.49	1.39	1.2	-0.21	-0.08	-0.11
YPR053C		D	20	0.12	0.15	0.12	0.14	0	-0.15	0
YPR057W	BRR1	D	20	0.11	0.08	0.06	0.11	0	0	0
YPR058W	YMC1	D	21	0.36	0.22	0.61	0.3	0.05	<b>0.25</b>	-0.09
YPR060C	ARO7	D	20	0.11	0.12	0.06	0.11	0	0	0
YPR061C		D	21	0.11	0.08	0.07	0.04	0	<b>-0.31</b>	0
YPR062W	FCY1	D	20	0.62	0.55	0.79	0.7	-0.01	0.07	0
YPR063C		D	22	1.37	0.72	1.4	1.46	0	-0.02	0
YPR065W	ROX1	D	20	0.11	0.08	0.06	0.06	0	0	0
YPR066W	UBA3	D	21	0.11	0.08	0.05	0.05	0	0	0
YPR067W		D	20	0.2	0.16	0.2	0.3	0	0	0.07
YPR069C	SPE3	D	20	0.29	0.24	0.49	0.39	-0.03	0.09	0
YPR072W		D	20	0.12	0.11	0.14	0.09	0	0	0
YPR073C	LTP1	D	20	0.11	0.08	0.08	0.04	0	0	0
YPR074C	TKL1	D	20	1.97	1.53	2.79	2.72	-0.06	0.02	0.03
YPR075C	OPY2	D	20	0.11	0.16	0.2	0.21	0	0.04	0.13
YPR079W		D	21	0.11	0.08	0.14	0.16	0	0.05	0.12
YPR080W	TEF1	D	20	11.68	4.82	10.21	8.14	-0.13	-0.1	-0.14
YPR081C		D	21	0.11	0.08	0.04	0.1	0	0	0
YPR082C		D	21	0.13	0.17	0.48	0.2	0	<b>0.21</b>	0
YPR084W		D	20	0.11	0.08	0.06	0.08	0	0	-0.17
YPR085C		D	20	0.11	0.08	0.07	0.05	0	0	0
YPR086W	SUA7	D	20	0.12	0.17	0.25	0.14	-0.06	<b>0.22</b>	0.03
YPR088C		D	20	0.25	0.22	0.32	0.4	0	0.03	0.05
YPR091C		D	21	0.11	0.08	0.05	0.07	0	<b>-0.3</b>	0
YPR093C		D	21	0.11	0.08	0.07	0.05	0	0	0
YPR094W		D	20	0.11	0.08	0.06	0.09	0	0	-0.12
YPR098C		D	20	0.94	0.77	1.35	1.39	-0.1	0.06	0.05
YPR100W		D	20	0.13	0.2	0.27	0.2	0	0.07	-0.01
YPR101W	SNT309	D	20	0.11	0.08	0.04	0.05	0	0	0
YPR102C	RPL11A	D	28	4.58	1.3	3.45	3.44	<b>-0.28</b>	-0.01	-0.08
YPR103W	PRE2	D	20	1.33	0.57	1.21	1.25	0	-0.12	0.06
YPR106W	ISR1	D	20	0.28	0.29	0.19	0.31	0	0	-0.04
YPR107C	YTH1	D	20	0.11	0.08	0.08	0.09	0	0	0
YPR108W	RPN7	D	21	0.26	0.18	0.27	0.31	0	0.04	0.1
YPR109W		D	20	0.18	0.09	0.24	0.24	0	0	0.17
YPR110C	RPC40	D	20	0.16	0.19	0.22	0.19	-0.01	0.09	0.04
YPR113W	PIS1	D	20	2.51	1.89	1.65	1.64	-0.12	-0.09	-0.14
YPR114W		D	20	0.69	0.4	0.59	0.81	-0.2	0.03	0.05
YPR115W		D	21	0.11	0.08	0.21	0.1	0	-0.14	-0.13
YPR117W		D	20	0.11	0.08	0.04	0.07	0	0	0
YPR118W		D	20	0.17	0.17	0.16	0.21	0	0	-0.07
YPR119W	CLB2	D	20	0.11	0.08	0.08	0.06	0	0	0
YPR120C	CLB5	D	21	0.11	0.08	0.07	0.13	0	0	<b>-0.21</b>

YPR121W		D	20	0.11	0.08	0.06	0.08	0	0	0
YPR124W	CTR1	D	20	0.11	0.08	0.06	0.04	0	0	0
YPR125W		D	21	0.11	0.09	0.2	0.15	0	0.08	0.13
YPR126C		D	20	0.11	0.09	0.07	0.04	0	0	0
YPR127W		D	20	0.16	0.18	0.16	0.79	0	-0.03	<b>0.47</b>
YPR128C		D	21	0.17	0.13	0.13	0.22	0	<b>-0.22</b>	-0.08
YPR129W	SCD6	D	20	0.11	0.08	0.08	0.11	0	0	0
YPR131C		D	21	0.11	0.08	0.06	0.07	0	0	<b>-0.2</b>
YPR132W	RPS23B	D	40	3.53	4.34	5.31	2.72	0.01	0.05	-0.14
YPR133C		D	20	0.11	0.09	0.1	0.13	0	0	0
YPR134W	MSS18	D	21	0.11	0.08	0.05	0.09	0	0	-0.08
YPR135W	CTF4	D	20	0.11	0.08	0.06	0.07	0	0	0
YPR138C	MEP3	D	21	0.27	0.26	0.38	0.27	0	0	-0.05
YPR139C		D	20	0.13	0.08	0.14	0.1	0	-0.01	0
YPR140W		D	20	0.17	0.19	0.14	0.26	0	-0.15	0.16
YPR143W		D	21	0.11	0.08	0.05	0.07	0	0	<b>-0.26</b>
YPR144C		D	21	0.11	0.11	0.11	0.08	-0.07	-0.04	0
YPR145W	ASN1	D	20	0.46	0.39	0.96	0.47	0	<b>0.35</b>	0.06
YPR146C		D	20	0.17	0.16	0.33	0.39	0	0.11	0.17
YPR147C		D	20	0.24	0.25	0.45	0.38	0.03	<b>0.28</b>	0.18
YPR148C		D	20	0.14	0.08	0.23	0.23	0	0.02	0.12
YPR149W	NCE102	D	20	5.06	1.28	3.75	4.37	<b>-0.44</b>	-0.09	0.03
YPR151C		D	20	0.11	0.08	0.04	0.06	0	0	0
YPR153W		D	21	0.11	0.08	0.06	0.06	0	<b>-0.28</b>	0
YPR154W		D	20	0.27	0.28	0.42	0.52	0	0.07	<b>0.22</b>
YPR155C	NCA2	D	20	0.11	0.08	0.06	0.06	0	0	0
YPR156C		D	20	0.41	0.3	0.54	0.95	0	0	<b>0.24</b>
YPR157W		D	21	0.11	0.12	0.12	0.53	0	0	<b>0.47</b>
YPR158W		D	20	0.11	0.08	0.05	0.05	0	0	0
YPR159W	KRE6	D	20	0.37	0.46	0.84	0.69	0	0.26	0.12
YPR160W	GPH1	D	21	0.55	0.28	0.68	0.65	-0.13	<b>0.21</b>	0.09
YPR161C	SGV1	D	20	0.11	0.08	0.04	0.13	0	0	-0.03
YPR162C	ORC4	D	21	0.11	0.08	0.07	0.09	0	<b>-0.26</b>	0
YPR163C	TIF3	D	20	0.29	0.24	0.21	0.27	0	-0.19	-0.1
YPR165W	RHO1	D	20	1.57	0.41	1.85	1.32	<b>-0.4</b>	0.06	-0.08
YPR166C	MRP2	D	20	0.16	0.09	0.25	0.18	0	-0.03	0
YPR167C	MET16	D	20	0.11	0.08	0.06	0.05	0	0	0
YPR169W		D	20	0.11	0.08	0.05	0.09	0	0	-0.19
YPR172W		D	20	0.22	0.21	0.27	0.58	0	0.01	<b>0.26</b>
YPR173C	VPS4	D	20	0.11	0.08	0.09	0.16	0	0	0.09
YPR174C		D	21	0.11	0.08	0.07	0.04	0	<b>-0.33</b>	0
YPR176C	BET2	D	20	0.29	0.18	0.29	0.23	0	-0.06	-0.11
YPR178W	PRP4	D	21	0.11	0.08	0.07	0.07	0	0	0
YPR181C	SEC23	D	21	0.33	0.2	0.39	0.37	-0.1	0	0
YPR182W	SMX3	D	21	0.22	0.24	0.46	0.36	-0.04	0.13	0.1
YPR183W	DPM1	D	20	0.75	0.43	1.23	0.7	-0.16	0.18	-0.01
YPR184W		D	21	0.11	0.08	0.04	0.11	0	0	0
YPR185W	APG13	D	20	0.11	0.08	0.04	0.08	0	0	0
YPR187W	RPO26	D	20	0.23	0.15	0.26	0.19	0	0.04	-0.11
YPR188C		D	21	0.14	0.08	0.1	0.07	-0.11	-0.19	<b>-0.34</b>
YPR191W	QCR2	D	21	0.51	0.22	0.46	0.35	<b>-0.22</b>	<b>0.24</b>	-0.13
YPR194C		D	21	0.11	0.08	0.22	0.08	0	0	0
YPR198W	SGE1	D	20	0.14	0.11	0.16	0.28	0	-0.02	0.14
YPR199C	ARR1	D	20	0.14	0.1	0.14	0.15	0	-0.19	0
YPR204W		D	20	0.48	0.36	0.72	0.81	0	0.05	0.1

## References

1. **Wenzel, T.J., Teunissen, A.W. and de Steensma, H.Y.**, PDA1 mRNA: a standard for quantitation of mRNA in *Saccharomyces cerevisiae* superior to ACT1 mRNA, *Nucleic Acids Research*, 23(5), 883-884, 1995.
2. **Iyer, V. and Struhl, K.**, Absolute mRNA levels and transcription initiation rates in *Saccharomyces cerevisiae*., *Proceedings of the National Academy of Sciences of the United States of America*, 93, 5208-5212, 1996.

## Appendix D

### Transcripts Not Detected

in Four *Saccharomyces cerevisiae* Cultures

A number of ORFs were not detected, for one of two reasons. The first possibility is that probe pairs corresponding to the undetected ORF were simply not on the microarray. Since the list of ORFs in *S. cerevisiae*, as represented by the Saccharomyces Genome Database (SGD) has changed over time, since the design of the Affymetrix microarrays. The following ORFs were not detected for this reason.

### **ORFs Not Represented on the Affymetrix Yeast Microarrays Used**

ORF ID	Gene Name
YAL064C-A	
YAL064W-B	
YDL045W-A	MRP10
YDL134C-A	RPL47B
YDL184C	RPL41A
YFL002W-A	
YGL226C-A	OST5
YHR005C-A	MRS11
YHR021W-A	ECM12
YIL009C-A	EST3
YIL017C	
YIL071C	
YIL174W	
YKR035W-A	FTI1
YLR312W-A	MRPL15
YLR337C	VRP1
YLR391W-A	SSR1
YLR438C-A	SMX4
YMR307W	GAS1
YNL338W	
YOR008C-A	KIM1
YPR133W-A	TOM5

Detection thresholds were calculated as described in Chapter 3. The following table shows the detection thresholds applied for each microarray assay.

### **Detection Thresholds for each Microarray Assay**

	<b>a</b>	$\alpha$	gal	heat
microarray “A”	0.086	0.039	0.069	0.091
microarray “B”	0.069	0.072	0.066	0.046
microarray “C”	0.347	0.089	0.260	0.236
microarray “D”	0.105	0.082	0.044	0.045

These detection thresholds range from 0.2 to greater than 1 transcript per cell, based on the rough correspondence of absolute abundance units to number of transcripts per cell described in Appendix C.

Listed below are those ORFs with absolute abundance measures that were below detection thresholds in all four conditions, and which were undetectably changed between conditions. These ORFs have been split into four lists, one for each microarray type.

**ORFs not detected in any of four cultures on microarray ‘A’.**

YAL001C	TFC3	YBR184W	MEL1	YDL017W	CDC7	YDR159W	SAC3
YAL002W	VPS8	YBR186W	PCH2	YDL019C		YDR162C	NBP2
YAL004W		YBR190W		YDL020C	RPN4	YDR164C	SEC1
YAL010C	MDM10	YBR192W	RIM2	YDL021W	GPM2	YDR168W	CDC37
YAL011W		YBR193C	MED8	YDL023C		YDR169C	STB3
YAL013W	DEP1	YBR194W		YDL025C		YDR173C	ARG82
YAL015C	NTG1	YBR195C	MSI1	YDL026W		YDR175C	
YAL018C		YBR197C		YDL027C		YDR176W	NGG1
YAL020C	ATS1	YBR200W	BEM1	YDL028C	MPS1	YDR179C	
YAL024C	LTE1	YBR202W	CDC47	YDL030W	PRP9	YDR179W-A	
YAL025C	MAK16	YBR203W		YDL031W		YDR180W	SCC2
YAL026C	DRS2	YBR204C		YDL032W		YDR181C	SAS4
YAL028W		YBR208C	DUR1,2	YDL034W		YDR183W	
YAL029C	MYO4	YBR209W		YDL035C		YDR184C	ATC1
YAL031C	FUN21	YBR215W	HPC2	YDL036C		YDR186C	
YAL032C	FUN20	YBR216C		YDL037C		YDR189W	SLY1
YAL034C	FUN19	YBR217W		YDL041W		YDR191W	HST4
YAL034W-A		YBR219C		YDL043C	PRP11	YDR192C	NUP42
YAL035C-A		YBR223C		YDL044C	MTF2	YDR193W	
YAL037W		YBR224W		YDL045C	FAD1	YDR195W	REF2
YAL041W	CDC24	YBR225W		YDL050C		YDR197W	CBS2
YAL043C-A		YBR226C		YDL056W	MBP1	YDR198C	
YAL047C	SPI6	YBR228W		YDL058W	USO1	YDR199W	
YAL048C		YBR229C	ROT2	YDL060W		YDR200C	
YAL058C-A		YBR232C		YDL062W		YDR201W	
YAL058W	CNE1	YBR233W		YDL063C		YDR202C	
YAL059W	ECM1	YBR236C	ABD1	YDL065C	PEX19	YDR203W	
YAL064W	FLO9	YBR237W	PRP5	YDL068W		YDR206W	
YAL065C		YBR238C		YDL069C	CBS1	YDR207C	UME6
YAL065C-A		YBR240C	THI2	YDL070W	BDF2	YDR211W	GCD6
YAL066W		YBR245C	ISW1	YDL071C		YDR213W	
YAL067C	SEO1	YBR247C	ENP1	YDL073W		YDR215C	
YAL069W		YBR250W		YDL074C		YDR217C	RAD9
YAR002W		YBR251W	MRPS5	YDL077C	VAM6	YDR218C	SPR28
YAR008W	SEN34	YBR255W		YDL079C	MRK1	YDR219C	
YAR014C		YBR257W	POP4	YDL087C	EXM2	YDR221W	
YAR018C	KIN3	YBR259W		YDL088C	ASM4	YDR223W	
YAR019C	CDC15	YBR266C		YDL089W		YDR227W	SIR4
YAR029W		YBR267W		YDL090C	RAM1	YDR228C	PCF11
YAR030C		YBR270C		YDL091C		YDR229W	
YAR031W		YBR271W		YDL094C		YDR230W	
YAR037W		YBR272C		YDL096C		YDR237W	MRPL7
YAR040C		YBR273C		YDL098C		YDR240C	SNU56
YAR043C		YBR275C	RIF1	YDL099W		YDR241W	
YAR044W	OSH1	YBR277C		YDL101C	DUN1	YDR243C	PRP28
YAR047C		YBR278W	DPB3	YDL104C	QRI7	YDR244W	PEX5
YAR050W	FLO1	YBR281C		YDL105W	QRI2	YDR246W	

YAR052C		YBR284W		YDL106C	GRF10	YDR249C	
YAR053W		YBR285W		YDL107W	MSS2	YDR250C	
YAR060C		YBR289W	SNF5	YDL108W	KIN28	YDR251W	PAM1
YAR061W		YBR292C		YDL113C		YDR253C	MET32
YAR062W		YBR294W	SUL1	YDL114W		YDR254W	CHL4
YAR064W		YBR295W	PCA1	YDL115C		YDR255C	
YAR068W		YBR296C		YDL116W	NUP84	YDR256C	CTA1
YAR069C		YBR298C	MAL31	YDL117W		YDR257C	RMS1
YAR070C		YBR299W	MAL32	YDL118W		YDR259C	YAP6
YAR074C		YBR300C		YDL119C		YDR263C	DIN7
YBL004W		YCL003W	PEL1	YDL121C		YDR265W	PEX10
YBL005W-A		YCL004W	PEL1	YDL127W	PCL2	YDR268W	MSW1
YBL005W-B		YCL005W		YDL129W		YDR269C	
YBL008W	HIR1	YCL006C		YDL138W	RGT2	YDR270W	CCC2
YBL009W		YCL007C	CWH36	YDL139C		YDR273W	
YBL010C		YCL010C		YDL146W		YDR274C	
YBL012C		YCL012W		YDL148C		YDR277C	MTH1
YBL013W		YCL013W		YDL149W		YDR278C	
YBL014C	RRN6	YCL014W	BUD3	YDL150W	RPC53	YDR279W	
YBL018C		YCL020W		YDL151C		YDR281C	
YBL019W	ETH1	YCL021W		YDL152W		YDR282C	
YBL020W	RFT1	YCL022C		YDL154W	MSH5	YDR283C	GCN2
YBL023C	MCM2	YCL023C		YDL156W		YDR285W	ZIP1
YBL028C		YCL024W		YDL159W	STE7	YDR288W	
YBL029W		YCL026C		YDL161W		YDR289C	
YBL031W	SHE1	YCL031C	RRP7	YDL162C		YDR290W	
YBL035C	POL12	YCL032W	STE50	YDL163W		YDR295C	
YBL036C		YCL041C		YDL164C	CDC9	YDR299W	BFR2
YBL037W		YCL046W		YDL166C		YDR305C	HNT2
YBL044W		YCL048W		YDL167C	NRP1	YDR310C	SUM1
YBL046W		YCL051W	LRE1	YDL169C	UGX2	YDR311W	TFB1
YBL052C	SAS3	YCL052C	PBN1	YDL170W	UGA3	YDR312W	SSF2
YBL054W		YCL053C		YDL172C		YDR313C	
YBL059W		YCL054W		YDL175C		YDR314C	
YBL060W		YCL055W	KAR4	YDL176W		YDR316W	
YBL061C	SKT5	YCL058C		YDL177C		YDR317W	
YBL062W		YCL059C	KRR1	YDL183C		YDR324C	
YBL065W		YCL060C		YDL186W		YDR325W	
YBL066C	SEF1	YCL061C		YDL187C		YDR326C	
YBL067C	UBP13	YCL062W		YDL189W		YDR327W	
YBL070C		YCL063W		YDL194W	SNF3	YDR330W	
YBL073W		YCL065W		YDL196W		YDR331W	GPI8
YBL074C	AAR2	YCL068C		YDL197C	ASF2	YDR332W	
YBL075C	SSA3	YCL069W		YDL199C		YDR333C	
YBL079W	NUP170	YCL074W		YDL203C		YDR334W	
YBL080C	PET112	YCL075W		YDL206W		YDR336W	
YBL086C		YCL076W		YDL207W	GLE1	YDR340W	
YBL088C	TEL1	YCLX01W		YDL209C		YDR344C	
YBL090W	MRP21	YCLX02C		YDL210W	UGA4	YDR351W	SBE2
YBL093C	ROX3	YCLX03C		YDL211C		YDR355C	

YBL094C		YCLX04W		YDL214C		YDR356W	NUF1
YBL095W		YCLX05C		YDL216C		YDR359C	
YBL096C		YCLX07W		YDL218W		YDR360W	
YBL097W	BRN1	YCLX08C	FRM2	YDL219W		YDR361C	
YBL098W		YCLX09W		YDL221W		YDR363W	ESC2
YBL100C		YCLX10C		YDL225W		YDR366C	
YBL101W-B		YCLX11W		YDL227C	HO	YDR369C	XRS2
YBL104C		YCR001W		YDL231C		YDR370C	
YBL105C	PKC1	YCR003W	MRPL32	YDL233W		YDR371W	
YBL107C		YCR006C		YDL238C		YDR372C	
YBL108W		YCR007C		YDL239C		YDR374C	
YBL109W		YCR010C		YDL240W	LRG1	YDR379W	RGA2
YBL111C		YCR014C	POL4	YDL242W		YDR380W	
YBR002C		YCR015C		YDL243C		YDR383C	
YBR003W	COQ1	YCR016W		YDL244W		YDR386W	
YBR007C		YCR019W	MAK32	YDL245C	HXT15	YDR393W	
YBR012C		YCR022C		YDL247W		YDR396W	
YBR017C	KAP104	YCR024C		YDL248W	COS7	YDR401W	
YBR021W	FUR4	YCR025C		YDR004W	RAD57	YDR402C	
YBR027C		YCR026C		YDR008C		YDR403W	DIT1
YBR030W		YCR027C		YDR010C		YDR405W	MRP20
YBR032W		YCR028C	FEN2	YDR013W		YDR406W	PDR15
YBR033W		YCR032W	BPH1	YDR014W		YDR412W	
YBR040W	FIG1	YCR033W		YDR015C		YDR413C	
YBR044C		YCR038C	BUD5	YDR018C		YDR414C	ERD1
YBR045C	GIP1	YCR041W		YDR021W	FAL1	YDR416W	SYF1
YBR047W		YCR042C	TSM1	YDR022C	CIS1	YDR417C	
YBR051W		YCR045C		YDR026C		YDR419W	RAD30
YBR055C	PRP6	YCR049C		YDR028C	REG1	YDR420W	HKR1
YBR057C	MUM2	YCR050C		YDR029W		YDR421W	
YBR059C		YCR054C	CTR86	YDR030C	RAD28	YDR425W	
YBR060C	RRR1	YCR055C	PWP2	YDR034C	LYS14	YDR426C	
YBR064W		YCR056W		YDR040C	ENA1	YDR428C	
YBR065C	ECM2	YCR058C	PWP2	YDR042C		YDR430C	
YBR074W		YCR063W		YDR048C		YDR431W	
YBR075W		YCR064C		YDR049W		YDR437W	
YBR076W	ECM8	YCR066W	RAD18	YDR052C	DBF4	YDR438W	
YBR081C	SPT7	YCR068W		YDR053W		YDR439W	LRS4
YBR089W		YCR073C	SSK22	YDR054C	CDC34	YDR440W	PCH1
YBR094W		YCR074C		YDR057W		YDR442W	
YBR095C		YCR081W	SRB8	YDR058C	TGL2	YDR443C	SSN2
YBR097W	VPS15	YCR085W		YDR060W		YDR444W	
YBR098W		YCR086W		YDR061W		YDR445C	
YBR099C		YCR089W	FIG2	YDR065W		YDR446W	ECM11
YBR100W		YCR091W	KIN82	YDR066C		YDR448W	ADA2
YBR102C		YCR092C	MSH3	YDR068W	DOS2	YDR449C	
YBR103W		YCR093W	CDC39	YDR069C	DOA4	YDR455C	
YBR104W	YMC2	YCR094W	CDC50	YDR075W	PPH3	YDR458C	
YBR110W	ALG1	YCR095C		YDR076W	RAD55	YDR460W	TFB3
YBR112C	CYC8	YCR097WA	A1	YDR078C		YDR467C	

YBR113W		YCR097WB	A1	YDR080W	VPS41	YDR469W
YBR114W	RAD16	YCR098C	GIT1	YDR081C	PDC2	YDR473C
YBR119W	MUD1	YCR099C		YDR083W		YDR475C
YBR120C	CBP6	YCR100C		YDR085C	AFR1	YDR478W
YBR124W		YCR101C		YDR087C	RRP1	YDR480W
YBR128C		YCR102C		YDR088C	SLU7	YDR484W
YBR130C		YCR103C		YDR089W		YDR485C
YBR131W		YCR105W		YDR095C		YDR488C
YBR134W		YCR106W		YDR096W	GIS1	YDR491C
YBR136W	ESR1	YCR107W		YDR102C		YDR495C
YBR138C	HDR1	YCRX01W		YDR104C		YDR496C
YBR141C		YCRX02C		YDR106W	ARP10	YDR499W
YBR142W	MAK5	YCRX03C		YDR108W	GSG1	YDR501W
YBR144C		YCRX04W		YDR109C		YDR507C
YBR148W	YSW1	YCRX05W		YDR110W	FOB1	YDR509W
YBR150C		YCRX06W		YDR112W		YDR515W
YBR152W		YCRX09C		YDR113C	PDS1	SLF1
YBR153W	RIB7	YCRX10W		YDR114C		YDR521W
YBR155W	CNS1	YCRX11W		YDR118W	APC4	SPS2
YBR156C		YCRX12W		YDR122W	KIN1	YDR523C
YBR161W		YCRX14W		YDR124W		YDR524C
YBR167C	RPP2	YCRX15W		YDR125C	ECM18	YDR525W
YBR168W		YCRX16C		YDR131C		YDR526C
YBR170C	NPL4	YCRX18C		YDR132C		YDR527W
YBR172C	SMY2	YCRX20C		YDR135C	YCF1	SPS1
YBR174C		YDL002C	NHP10	YDR136C		YDR530C
YBR176W	ECM31	YDL003W	MCD1	YDR137W	RGP1	APA2
YBR178W		YDL006W	PTC1	YDR145W	TAF61	YDR532C
YBR179C	FZO1	YDL011C		YDR149C		YDR535C
YBR180W		YDL013W	HEX3	YDR150W	NUM1	STL1
YBR182C	SMP1	YDL016C		YDR157W		YDR540C
						YDR544C

**ORFs not detected in any of four cultures on microarray ‘B’.**

YEL003W	PFD2	YGL033W	HOP2	YGR140W	CBF2	YHR177W	
YEL004W	YEA4	YGL034C		YGR142W		YHR178W	STB5
YEL005C		YGL041C		YGR145W		YHR182W	
YEL008W		YGL042C		YGR150C		YHR184W	SSP1
YEL010W		YGL043W	DST1	YGR151C		YHR185C	
YEL014C		YGL046W		YGR152C	RSR1	YHR186C	
YEL016C		YGL049C	TIF4632	YGR153W		YHR189W	
YEL018W		YGL050W		YGR154C		YHR196W	
YEL019C	MMS21	YGL052W		YGR156W		YHR197W	
YEL022W		YGL059W		YGR158C	MTR3	YHR204W	
YEL023C		YGL060W		YGR160W		YHR207C	
YEL025C		YGL061C	DUO1	YGR164W		YHR209W	
YEL028W		YGL063W	PUS2	YGR166W	KRE11	YHR210C	
YEL029C		YGL064C		YGR168C		YHR211W	
YEL030W	ECM10	YGL065C	ALG2	YGR170W	PSD2	YHR212C	
YEL032W	MCM3	YGL066W		YGR171C	MSM1	YHR213W	
YEL033W		YGL069C		YGR176W		YHR214W	
YEL035C	UTR5	YGL071W	RCS1	YGR177C	ATF2	YHR214W-A	
YEL039C	CYC7	YGL072C		YGR179C		YHR216W	
YEL041W		YGL073W	HSF1	YGR186W	TFG1	YHR218W	
YEL044W		YGL074C		YGR187C	HGH1	YIL002C	INP51
YEL045C		YGL075C		YGR188C	BUB1	YIL003W	
YEL048C		YGL083W	SCY1	YGR190C		YIL004C	BET1
YEL053C	MAK10	YGL085W		YGR196C		YIL005W	
YEL055C	POL5	YGL086W	MAD1	YGR198W		YIL006W	
YEL061C	CIN8	YGL090W		YGR202C	PCT1	YIL012W	
YEL062W	NPR2	YGL092W	NUP145	YGR205W		YIL013C	PDR11
YEL064C		YGL093W		YGR208W	SER2	YIL016W	SNL1
YEL065W		YGL094C	PAN2	YGR212W		YIL017W	
YEL067C		YGL095C	VPS45	YGR213C	RTA1	YIL019W	
YEL068C		YGL098W		YGR219W		YIL024C	
YEL069C	HXT13	YGL108C		YGR221C		YIL025C	
YEL070W		YGL109W		YGR223C		YIL026C	IRR1
YEL072W		YGL110C		YGR225W		YIL028W	
YEL076C		YGL113W		YGR226C		YIL029C	
YEL076C-A		YGL116W	CDC20	YGR228W		YIL031W	SMT4
YEL076W-C		YGL118C		YGR230W		YIL032C	
YER002W		YGL120C	PRP43	YGR233C	PHO81	YIL035C	CKA1
YER006W		YGL129C		YGR236C		YIL037C	
YER007W	PAC2	YGL131C		YGR237C		YIL054W	
YER008C	SEC3	YGL132W		YGR238C	KEL2	YIL055C	
YER013W	PRP22	YGL133W		YGR239C		YIL057C	
YER015W	FAA2	YGL136C		YGR242W		YIL058W	
YER018C		YGL138C		YGR245C		YIL060W	
YER032W	FIR1	YGL139W		YGR247W		YIL061C	SNP1
YER033C		YGL140C		YGR249W	MGA1	YIL063C	YRB2

YER038C		YGL144C		YGR251W		YIL068C	SEC6
YER040W	GLN3	YGL145W	TIP20	YGR259C		YIL071W	
YER041W		YGL146C		YGR261C	APL6	YIL072W	HOP1
YER044C-A	MEI4	YGL149W		YGR265W		YIL073C	
YER047C	SAP1	YGL150C		YGR266W		YIL079C	
YER051W		YGL152C		YGR269W		YIL080W	
YER054C	GIP2	YGL158W	RCK1	YGR271W		YIL082W	
YER059W	PCL6	YGL163C	RAD54	YGR272C		YIL082W-A	
YER065C	ICL1	YGL164C		YGR273C		YIL084C	SDS3
YER066C-A		YGL165C		YGR274C	TAF145	YIL086C	
YER070W	RNR1	YGL168W		YGR276C	RNH70	YIL089W	
YER071C		YGL169W	SUA5	YGR278W		YIL091C	
YER075C	PTP3	YGL170C		YGR280C		YIL092W	
YER077C		YGL171W	ROK1	YGR283C		YIL095W	PRK1
YER085C		YGL174W		YGR287C		YIL096C	
YER093C		YGL175C	SAE2	YGR288W		YIL097W	
YER096W		YGL176C		YGR289C	AGT1	YIL100W	
YER097W		YGL177W		YGR290W		YIL102C	
YER098W	UBP9	YGL180W	APG1	YGR291C		YIL103W	
YER101C	AST2	YGL182C		YGR292W	MAL1	YIL105C	
YER104W		YGL183C		YGR293C		YIL107C	PFK26
YER105C	NUP157	YGL185C		YHL005C		YIL110W	
YER108C	FLO8	YGL190C	CDC55	YHL007C	STE20	YIL112W	
YER109C	FLO8	YGL192W	IME4	YHL009C	YAP3	YIL120W	
YER110C	KAP123	YGL194C	HOS2	YHL010C		YIL122W	
YER111C	SWI4	YGL201C	MCM6	YHL012W		YIL126W	STH1
YER116C		YGL204C		YHL013C		YIL127C	
YER119C-A		YGL205W	POX1	YHL014C	YLF2	YIL128W	MET18
YER123W	YCK3	YGL211W		YHL016C	DUR3	YIL130W	
YER128W		YGL212W	VAM7	YHL018W		YIL132C	
YER129W	PAK1	YGL214W		YHL022C	SPO11	YIL138C	TPM2
YER132C	PMD1	YGL217C		YHL023C		YIL139C	REV7
YER135C		YGL218W		YHL030W	ECM29	YIL141W	
YER137C		YGL222C		YHL036W	MUP3	YIL143C	SSL2
YER139C		YGL226W		YHL037C		YIL144W	TID3
YER140W		YGL227W	TIN1	YHL038C	CBP2	YIL146C	ECM37
YER142C	MAG1	YGL228W		YHL041W		YIL147C	SLN1
YER144C	UBP5	YGL229C	SAP4	YHL042W		YIL149C	
YER147C		YGL230C		YHL043W	ECM34	YIL150C	DNA43
YER149C	PEA2	YGL232W		YHL045W		YIL151C	
YER153C	PET122	YGL233W	SEC15	YHL047C		YIL153W	RRD1
YER161C	SPT2	YGL235W		YHR002W		YIL159W	BNR1
YER162C	RAD4	YGL237C	HAP2	YHR006W	STP2	YIL161W	
YER168C	CCA1	YGL239C		YHR011W		YIL163C	
YER169W	RPH1	YGL240W	DOC1	YHR014W	SPO13	YIL166C	
YER171W	RAD3	YGL241W		YHR015W	MIP6	YIL167W	
YER172C	BRR2	YGL243W		YHR023W	MYO1	YIL168W	SDL1
YER173W	RAD24	YGL246C		YHR029C		YIL171W	HXT12
YER179W	DMC1	YGL249W	ZIP2	YHR031C		YIL172C	
YER180C	ISC10	YGL250W		YHR035W		YIL173W	

YER181C		YGL251C	HFM1	YHR036W		YIL175W	
YER182W		YGL254W	FZF1	YHR038W	KIM4	YIR001C	
YER184C		YGL257C		YHR040W		YIR002C	
YER187W		YGL258W		YHR044C	DOG1	YIR004W	DJP1
YER188W		YGL259W	YPS5	YHR047C	AAP1'	YIR005W	
YER189W		YGL260W		YHR048W		YIR008C	PRI1
YFL001W	DEG1	YGL262W		YHR049C-A		YIR009W	MSL1
YFL003C	MSH4	YGL263W	COS12	YHR058C	MED6	YIR010W	
YFL004W		YGR002C		YHR059W		YIR014W	
YFL008W	SMC1	YGR003W		YHR060W	VMA22	YIR015W	
YFL011W	HXT10	YGR005C	TFG2	YHR061C	GIC1	YIR017C	MET28
YFL012W		YGR006W	PRP18	YHR066W	SSF1	YIR020C	
YFL013W-A		YGR012W		YHR073W		YIR023W	DAL81
YFL015C		YGR013W	SNU71	YHR075C		YIR025W	
YFL023W		YGR016W		YHR077C	NMD2	YIR027C	DAL1
YFL024C		YGR018C		YHR079BC	SAE3	YIR029W	DAL2
YFL025C	BST1	YGR022C		YHR079C	IRE1	YIR030C	DCG1
YFL029C	CAK1	YGR025W		YHR080C		YIR031C	DAL7
YFL032W		YGR030C		YHR081W		YIR032C	DAL3
YFL033C	RIM15	YGR035C		YHR085W		YIR033W	MGA2
YFL035C	MOB2	YGR039W		YHR088W		YIR039C	YPS6
YFL036W	RPO41	YGR040W	KSS1	YHR090C	NBN1	YIR040C	
YFL040W		YGR042W		YHR093W	AHT1	YIR042C	
YFL042C		YGR045C		YHR095W		YJL003W	
YFL046W		YGR046W		YHR099W	TRA1	YJL005W	CYR1
YFL047W		YGR047C	TFC4	YHR101C	BIG1	YJL006C	CTK2
YFL049W		YGR048W	UFD1	YHR102W	NRK1	YJL007C	
YFL050C	ALR2	YGR051C		YHR103W	SBE22	YJL009W	
YFL051C		YGR053C		YHR105W		YJL010C	
YFL052W		YGR056W	RSC1	YHR109W		YJL013C	MAD3
YFL053W	DAK2	YGR057C	LST7	YHR111W		YJL018W	
YFL055W	AGP3	YGR058W		YHR117W	TOM71	YJL019W	
YFL056C		YGR059W	SPR3	YHR118C	ORC6	YJL022W	
YFL060C	SNO3	YGR064W		YHR119W	SET1	YJL023C	PET130
YFL061W		YGR066C		YHR120W	MSH1	YJL024C	APS3
YFL063W		YGR067C		YHR121W		YJL025W	RRN7
YFL064C		YGR068C		YHR122W		YJL028W	
YFL065C		YGR070W	ROM1	YHR124W	NDT80	YJL029C	
YFL067W		YGR071C		YHR125W		YJL031C	BET4
YFL068W		YGR072W	UPF3	YHR126C		YJL033W	HCA4
YFR002W	NIC96	YGR081C		YHR127W	HSN1	YJL035C	
YFR005C		YGR087C	PDC6	YHR129C	ARP1	YJL036W	
YFR008W		YGR089W		YHR130C		YJL037W	
YFR012W		YGR091W	PRP31	YHR131C		YJL038C	
YFR013W		YGR092W	DBF2	YHR134W		YJL039C	
YFR014C	CMK1	YGR093W		YHR136C	SPL2	YJL043W	
YFR016C		YGR096W		YHR137W	ARO9	YJL046W	
YFR019W	FAB1	YGR098C	ESP1	YHR139C-A		YJL047C	
YFR023W	PES4	YGR099W	TEL2	YHR144C	DCD1	YJL049W	
YFR027W		YGR100W	MDR1	YHR148W		YJL050W	MTR4

YFR029W	PTR3	YGR103W		YHR149C		YJL051W	
YFR032C		YGR104C	SRB5	YHR150W		YJL054W	TIM54
YFR035C		YGR107W		YHR151C		YJL056C	ZAP1
YFR038W		YGR109C	CLB6	YHR152W	SPO12	YJL058C	
YFR039C		YGR112W	SHY1	YHR153C	SPO16	YJL059W	YHC3
YFR040W	SAP155	YGR113W	DIF1	YHR154W	ESC4	YJL064W	
YFR043C		YGR114C		YHR155W		YJL067W	
YFR046C		YGR115C		YHR156C		YJL069C	
YFR054C		YGR116W	SPT6	YHR157W	REC104	YJL070C	
YFR055W		YGR117C		YHR158C	KEL1	YJL071W	ARG2
YFR056C		YGR119C	NUP57	YHR159W		YJL072C	
YFR057W		YGR120C		YHR160C		YJL073W	JEM1
YGL005C		YGR122W		YHR164C	DNA2	YJL074C	SMC3
YGL007W		YGR123C	PPT1	YHR165C	PRP8	YJL075C	
YGL014W		YGR128C		YHR166C	CDC23	YJL076W	ESC5
YGL015C		YGR129W	SYF2	YHR167W		YJL077C	
YGL016W	PDR6	YGR130C		YHR168W		YJL084C	
YGL017W	ATE1	YGR131W		YHR169W	DBP8	YJL085W	EXO70
YGL018C	JAC1	YGR134W		YHR172W	SPC97	YJL086C	
YGL025C	PGD1	YGR139W		YHR173C		YJL087C	TRL1
YGL027C		CWH41					

**ORFs not detected in any of four cultures on microarray ‘C’.**

YJL089W	SIP4	YKL070W		YLR055C	SPT8	YLR444C	
YJL090C	DPB11	YKL071W		YLR057W		YLR445W	
YJL092W	HPR5	YKL072W	STB6	YLR062C		YLR446W	
YJL093C	TOK1	YKL073W	LHS1	YLR063W		YLR450W	HMG2
YJL094C		YKL074C	MUD2	YLR067C	PET309	YLR451W	LEU3
YJL095W	BCK1	YKL075C		YLR068W		YLR452C	SST2
YJL096W		YKL076C		YLR070C		YLR453C	RIF2
YJL098W		YKL078W		YLR071C	RGR1	YLR454W	
YJL099W	CHS6	YKL079W	SMY1	YLR072W		YLR455W	
YJL100W		YKL082C		YLR077W		YLR456W	
YJL101C	GSH1	YKL083W		YLR080W		YLR457C	NBP1
YJL102W	MEF2	YKL088W		YLR082C		YLR458W	
YJL103C		YKL089W	MIF2	YLR084C		YLR460C	
YJL104W		YKL090W		YLR085C	ARP6	YLR462W	
YJL105W		YKL092C	BUD2	YLR086W	SMC4	YLR463C	
YJL106W	IME2	YKL093W	MBR1	YLR087C		YLR464W	
YJL107C		YKL095W	YJU2	YLR090W	XDJ1	YLR465C	
YJL108C		YKL097C		YLR091W		YML002W	
YJL109C		YKL098W		YLR092W	SUL2	YML003W	
YJL110C	GZF3	YKL099C		YLR094C		YML005W	
YJL112W		YKL101W	HSL1	YLR096W	KIN2	YML006C	
YJL113W		YKL102C		YLR097C		YML007W	YAP1
YJL114W		YKL105C		YLR098C	CHA4	YML011C	
YJL115W	ASF1	YKL106W	AAT1	YLR101C		YML013C-A	
YJL118W		YKL107W		YLR102C	APC9	YML013W	
YJL119C		YKL108W		YLR103C	CDC45	YML015C	TAF40
YJL120W		YKL109W	HAP4	YLR105C	SEN2	YML016C	PPZ1
YJL122W		YKL110C	KTI12	YLR106C		YML017W	PSP2
YJL123C		YKL111C		YLR107W		YML020W	
YJL125C	GCD14	YKL112W	ABF1	YLR108C		YML021C	UNG1
YJL126W	NIT2	YKL113C	RAD27	YLR111W		YML023C	
YJL127C	SPT10	YKL114C	APN1	YLR114C		YML032C	RAD52
YJL128C	PBS2	YKL115C		YLR115W	CFT2	YML032C-A	
YJL129C	TRK1	YKL116C		YLR116W	MSL5	YML033W	
YJL131C		YKL118W		YLR117C		YML034W	
YJL132W		YKL119C	VPH2	YLR119W	SRN2	YML035C	AMD1
YJL135W		YKL121W		YLR122C		YML035C-A	
YJL137C	GLG2	YKL123W		YLR123C		YML036W	
YJL139C	YUR1	YKL124W	SSH4	YLR124W		YML037C	
YJL140W	RPB4	YKL125W	RRN3	YLR125W		YML038C	
YJL141C	YAK1	YKL129C	MYO3	YLR126C		YML041C	
YJL142C		YKL130C		YLR127C	APC2	YML042W	CAT2
YJL144W		YKL131W		YLR128W		YML043C	RRN11
YJL145W		YKL132C		YLR131C	ACE2	YML046W	PRP39
YJL146W	IDS2	YKL133C		YLR135W		YML047C	
YJL147C		YKL134C		YLR136C	TIS11	YML048W-A	
YJL148W	RPA34	YKL135C	APL2	YLR137W		YML049C	RSE1

YJL149W		YKL136W		YLR138W	NHA1	YML050W	
YJL150W		YKL137W		YLR139C	SLS1	YML053C	
YJL154C	VPS35	YKL138C	MRPL31	YLR140W		YML054C	CYB2
YJL155C	FBP26	YKL139W	CTK1	YLR141W	RRN5	YML058C-A	
YJL156C	SSY5	YKL143W	LTV1	YLR142W	PUT1	YML059C	
YJL160C		YKL147C		YLR143W		YML060W	OGG1
YJL161W		YKL149C	DBR1	YLR144C	ACF2	YML061C	PIF1
YJL162C		YKL153W		YLR145W		YML062C	MFT1
YJL163C		YKL154W		YLR147C	SMD3	YML065W	ORC1
YJL165C	HAL5	YKL155C		YLR148W	PEP3	YML066C	
YJL168C	SET2	YKL158W		YLR149C		YML068W	
YJL169W		YKL159C		YLR151C		YML069W	POB3
YJL170C	ASG7	YKL161C		YLR152C		YML071C	
YJL172W	CPS1	YKL162C		YLR156W		YML076C	
YJL175W		YKL166C	TPK3	YLR158C	ASP3	YML077W	
YJL176C	SWI3	YKL168C	KKQ8	YLR159W		YML080W	
YJL179W	PFD1	YKL169C		YLR161W		YML081W	
YJL180C	ATP12	YKL171W		YLR162W		YML082W	
YJL181W		YKL173W	SNU114	YLR163C	MAS1	YML083C	
YJL182C		YKL176C		YLR164W		YML084W	
YJL183W	MNN11	YKL177W		YLR165C		YML087C	
YJL184W		YKL179C		YLR166C	SEC10	YML088W	
YJL185C		YKL183W		YLR168C	MSF1'	YML089C	
YJL186W		YKL187C		YLR169W		YML090W	
YJL187C	SWE1	YKL188C	PXA2	YLR170C	APS1	YML091C	RPM2
YJL188C		YKL189W	HYM1	YLR171W		YML093W	
YJL193W		YKL193C	SDS22	YLR173W		YML094W	PFD5
YJL194W	CDC6	YKL194C	MST1	YLR174W	IDP2	YML095C	RAD10
YJL195C		YKL195W		YLR176C	RFX1	YML095C-A	
YJL197W	UBP12	YKL197C	PEX1	YLR181C		YML096W	
YJL198W		YKL198C	PTK1	YLR182W	SWI6	YML097C	VPS9
YJL200C		YKL200C		YLR183C		YML098W	TAF19
YJL201W	ECM25	YKL201C		YLR184W		YML099C	ARG81
YJL202C		YKL202W		YLR187W		YML100W-A	
YJL203W	PRP21	YKL203C	TOR2	YLR188W	MDL1	YML102C-A	
YJL204C		YKL204W		YLR189C		YML102W	CAC2
YJL206C		YKL205W	LOS1	YLR190W		YML103C	NUP188
YJL207C		YKL206C		YLR191W	PEX13	YML104C	MDM1
YJL208C	NUC1	YKL208W	CBT1	YLR193C		YML107C	
YJL209W	CBP1	YKL209C	STE6	YLR196W	PWP1	YML108W	
YJL211C		YKL215C		YLR198C		YML109W	ZDS2
YJL212C		YKL217W	JEN1	YLR200W	YKE2	YML111W	
YJL213W		YKL218C		YLR205C		YML115C	VAN1
YJL214W	HXT8	YKL219W	COS9	YLR207W	HRD3	YML117W	
YJL215C		YKL220C	FRE2	YLR210W	CLB4	YML118W	
YJL216C		YKL221W		YLR211C		YML119W	
YJL218W		YKL222C		YLR213C		YML120C	NDI1
YJL219W	HXT9	YKL223W		YLR214W	FRE1	YML122C	
YJL220W		YKL224C		YLR215C		YMR001C	CDC5
YJL221C	FSP2	YKL225W		YLR217W		YMR004W	MVP1

YJL222W		YKR001C	VPS1	YLR218C		YMR007W	
YJL223C		YKR002W	PAP1	YLR219W		YMR013C	SEC59
YJL225C		YKR003W		YLR221C		YMR014W	
YJR002W	MPP10	YKR005C		YLR223C	IFH1	YMR016C	SOK2
YJR003C		YKR007W		YLR225C		YMR017W	DBI9
YJR005W	APL1	YKR008W	RSC4	YLR226W		YMR018W	
YJR006W		YKR009C	FOX2	YLR227C		YMR019W	STB4
YJR010W	MET3	YKR010C	TOF2	YLR228C	ECM22	YMR020W	FMS1
YJR011C		YKR011C		YLR230W		YMR021C	MAC1
YJR012C		YKR012C		YLR232W		YMR023C	MSS1
YJR013W		YKR014C	YPT52	YLR233C	EST1	YMR025W	
YJR018W		YKR015C		YLR234W	TOP3	YMR026C	PEX12
YJR020W		YKR016W		YLR235C		YMR028W	TAP42
YJR021C	REC107	YKR017C		YLR236C		YMR029C	
YJR022W		YKR019C	IRS4	YLR238W		YMR030W	
YJR023C		YKR020W		YLR239C		YMR031C	
YJR030C		YKR021W		YLR240W	VPS34	YMR031W-A	
YJR031C	GEA1	YKR022C		YLR242C	ARV1	YMR032W	CYK2
YJR032W	CPR7	YKR023W		YLR243W		YMR033W	ARP9
YJR033C		YKR024C	DBP7	YLR245C		YMR034C	
YJR034W	PET191	YKR027W		YLR246W		YMR036C	MIH1
YJR035W	RAD26	YKR028W	SAP190	YLR247C		YMR037C	MSN2
YJR036C		YKR029C		YLR254C		YMR039C	SUB1
YJR037W		YKR031C	SPO14	YLR255C		YMR040W	
YJR038C		YKR032W		YLR260W	LCB5	YMR041C	
YJR039W		YKR033C		YLR261C		YMR044W	
YJR040W	GEF1	YKR034W	DAL80	YLR262C	YPT6	YMR045C	
YJR041C		YKR035C		YLR263W	RED1	YMR046C	
YJR042W	NUP85	YKR036C	CAF4	YLR265C		YMR048W	
YJR043C	POL32	YKR037C		YLR266C		YMR052C-A	
YJR046W		YKR040C		YLR267W		YMR052W	FAR3
YJR047C	ANB1	YKR041W		YLR269C		YMR053C	STB2
YJR049C	UTR1	YKR044W		YLR271W		YMR057C	
YJR050W	UTR3	YKR045C		YLR272C		YMR059W	SEN15
YJR051W	OSM1	YKR047W		YLR273C	PIG1	YMR060C	TOM37
YJR052W	RAD7	YKR050W	TRK2	YLR274W	CDC46	YMR061W	RNA14
YJR053W		YKR051W		YLR275W	SMD2	YMR063W	RIM9
YJR054W		YKR052C	MRS4	YLR276C	DBP9	YMR064W	AEP1
YJR055W	HIT1	YKR053C	YSR3	YLR277C	YSH1	YMR065W	KAR5
YJR056C		YKR054C	DYN1	YLR278C		YMR066W	
YJR057W	CDC8	YKR055W	RHO4	YLR279W		YMR068W	
YJR060W	CBF1	YKR058W	GLG1	YLR280C		YMR069W	
YJR061W		YKR060W		YLR281C		YMR070W	MOT3
YJR062C	NTA1	YKR061W	KTR2	YLR282C		YMR075C-A	
YJR066W	TOR1	YKR063C	LAS1	YLR283W		YMR075W	
YJR067C	YAE1	YKR064W		YLR284C	EHD1	YMR076C	PDS5
YJR068W	RFC2	YKR069W	MET1	YLR287C		YMR077C	
YJR071W		YKR072C	SIS2	YLR288C	MEC3	YMR078C	CTF18
YJR072C		YKR073C		YLR289W	GUF1	YMR080C	NAM7
YJR078W		YKR075C		YLR296W		YMR082C	

YJR079W		YKR077W		YLR298C	YHC1	YMR084W	
YJR082C		YKR078W		YLR299W	ECM38	YMR085W	
YJR083C		YKR079C		YLR302C		YMR086C-A	
YJR087W		YKR081C		YLR305C	STT4	YMR086W	
YJR088C		YKR082W	NUP133	YLR306W	UBC12	YMR093W	
YJR089W		YKR083C		YLR307W	CDA1	YMR094W	CTF13
YJR090C	GRR1	YKR084C	HBS1	YLR308W	CDA2	YMR095C	SNO1
YJR091C	JSN1	YKR085C	MRPL20	YLR309C	IMH1	YMR096W	SNZ1
YJR092W	BUD4	YKR086W	PRP16	YLR310C	CDC25	YMR097C	
YJR093C	FIP1	YKR087C		YLR311C		YMR098C	
YJR094C	IME1	YKR089C		YLR312C		YMR100W	MUB1
YJR095W	ACR1	YKR090W		YLR313C	SPH1	YMR101C	
YJR097W		YKR091W		YLR314C	CDC3	YMR102C	
YJR098C		YKR092C	SRP40	YLR315W		YMR103C	
YJR099W	YUH1	YKR095W	MLP1	YLR316C		YMR104C	YPK2
YJR100C		YKR096W		YLR318W	EST2	YMR106C	HDF2
YJR102C		YKR097W	PCK1	YLR319C	BUD6	YMR107W	
YJR106W	ECM27	YKR098C	UBP11	YLR320W		YMR109W	MYO5
YJR107W		YKR099W	BAS1	YLR321C	SFH1	YMR111C	
YJR108W		YKR101W	SIR1	YLR322W		YMR112C	
YJR109C	CPA2	YKR102W	FLO10	YLR323C		YMR114C	
YJR110W		YKR103W		YLR324W		YMR115W	
YJR111C		YKR104W		YLR326W		YMR117C	
YJR112W	NNF1	YKR105C		YLR329W	REC102	YMR118C	
YJR114W		YKR106W		YLR331C		YMR122C	
YJR119C		YLL001W	DNM1	YLR332W	MID2	YMR124W	
YJR120W		YLL002W	KIM2	YLR334C		YMR125W	STO1
YJR122W	CAF17	YLL003W	SFI1	YLR336C	SGD1	YMR126C	
YJR124C		YLL004W	ORC3	YLR337W		YMR127C	SAS2
YJR128W		YLL005C		YLR338W		YMR129W	POM152
YJR129C		YLL006W	MMM1	YLR339C		YMR130W	
YJR130C		YLL007C		YLR341W		YMR132C	
YJR131W	MNS1	YLL008W	DRS1	YLR343W		YMR133W	REC114
YJR132W	NMD5	YLL011W	SOF1	YLR345W		YMR134W	
YJR134C		YLL012W		YLR346C		YMR135W-A	
YJR135C	MCM22	YLL013C		YLR349W		YMR137C	SNM1
YJR136C		YLL015W		YLR352W		YMR138W	CIN4
YJR137C	ECM17	YLL016W	SDC25	YLR353W	BUD8	YMR139W	RIM11
YJR138W		YLL017W		YLR357W	RSC2	YMR140W	
YJR140C	HIR3	YLL019C	KNS1	YLR358C		YMR141C	
YJR141W		YLL021W	SPA2	YLR360W	VPS38	YMR144W	
YJR142W		YLL029W		YLR361C		YMR147W	
YJR144W	MGM101	YLL030C		YLR362W	STE11	YMR151W	
YJR146W		YLL032C		YLR363C	NMD4	YMR153C-A	
YJR147W	HMS2	YLL033W		YLR365W		YMR153W	
YJR149W		YLL034C		YLR366W		YMR154C	RIM13
YJR150C	DAN1	YLL035W		YLR368W		YMR155W	
YJR151C		YLL036C	PRP19	YLR369W		YMR156C	
YJR152W	DAL5	YLL037W		YLR371W		YMR158W	
YJR153W	PGU1	YLL038C		YLR373C		YMR158W-A	

YJR154W		YLL042C		YLR374C		YMR159C	SAP18
YJR155W		YLL046C	RNP1	YLR376C		YMR160W	
YJR156C	THI11	YLL047W		YLR377C	FBP1	YMR162C	
YJR157W		YLL052C		YLR379W		YMR163C	
YJR158W	HXT16	YLL054C		YLR381W		YMR164C	MSS11
YJR159W	SOR1	YLL055W		YLR382C	NAM2	YMR165C	SMP2
YJR160C		YLL057C		YLR383W	RHC18	YMR166C	
YJR162C		YLL059C		YLR385C		YMR167W	MLH1
YKL005C		YLL060C		YLR386W		YMR168C	CEP3
YKL006C-A	SFT1	YLL061W		YLR387C		YMR170C	ALD2
YKL011C	CCE1	YLL062C		YLR389C	STE23	YMR172C-A	
YKL012W	PRP40	YLL063C		YLR392C		YMR172W	
YKL014C		YLL065W	GIN11	YLR393W	ATP10	YMR176W	ECM5
YKL015W	PUT3	YLR002C		YLR394W		YMR178W	
YKL017C	HCS1	YLR003C		YLR396C	VPS33	YMR179W	SPT21
YKL020C	SPT23	YLR004C		YLR397C	AFG2	YMR180C	
YKL021C	MAK11	YLR006C	SSK1	YLR398C	SKI2	YMR182C	RGM1
YKL022C	CDC16	YLR007W		YLR399C	BDF1	YMR183C	SSO2
YKL023W		YLR009W		YLR400W		YMR185W	
YKL025C	PAN3	YLR010C		YLR401C		YMR187C	
YKL026C		YLR011W		YLR402W		YMR188C	
YKL027W		YLR012C		YLR403W	SFP1	YMR190C	SGS1
YKL030W		YLR013W		YLR407W		YMR192W	
YKL031W		YLR014C	PPR1	YLR408C		YMR193C-A	
YKL032C	IXR1	YLR015W		YLR409C		YMR193W	
YKL033W		YLR016C		YLR410W		YMR196W	
YKL036C		YLR020C		YLR411W	CTR3	YMR197C	VTI1
YKL037W		YLR021W		YLR415C		YMR198W	CIK1
YKL038W	RGT1	YLR022C		YLR416C		YMR199W	CLN1
YKL040C		YLR024C		YLR417W	VPS36	YMR201C	RAD14
YKL041W	VPS24	YLR026C	SED5	YLR418C	CDC73	YMR204C	
YKL042W	SPC42	YLR030W		YLR419W		YMR206W	
YKL044W		YLR031W		YLR422W		YMR207C	HFA1
YKL045W	PRI2	YLR032W	RAD5	YLR423C		YMR209C	
YKL047W		YLR033W		YLR424W		YMR210W	
YKL048C	ELM1	YLR035C		YLR425W		YMR212C	
YKL049C	CSE4	YLR036C		YLR427W		YMR213W	CEF1
YKL050C		YLR039C	RIC1	YLR428C		YMR214W	SCJ1
YKL052C		YLR041W		YLR430W	SEN1	YMR218C	
YKL055C		YLR045C	STU2	YLR431C		YMR219W	ESC1
YKL057C	NUP120	YLR046C		YLR433C	CNA1	YMR220W	ERG8
YKL059C		YLR047C		YLR434C		YMR223W	
YKL061W		YLR049C		YLR435W		YMR225C	MRPL44
YKL063C		YLR051C		YLR436C	ECM30	YMR227C	TAF67
YKL064W	MNR2	YLR052W		YLR440C		YMR228W	MTF1
YKL068W	NUP100	YLR053C		YLR442C	SIR3	YMR229C	FMI1
YKL069W		YLR054C		YLR443W	ECM7		

**ORFs not detected in any of four cultures on microarray ‘D’.**

YMR231W	PEP5	YNL318C	YOR118W	YPL151C		
YMR232W	FUS2	YNL319W	YOR127W	RGA1	YPL153C	RAD53
YMR233W		YNL324W	YOR139C		YPL155C	KIP2
YMR251W		YNL325C	FIG4	YOR144C	YPL158C	
YMR254C		YNL335W		YOR146W	YPL161C	BEM4
YMR265C		YNR003C	RPC34	YOR148C	SPP2	YPL164C
YMR268C	PRP24	YNR004W		YOR156C	NFI1	YPL165C
YMR270C	RRN9	YNR005C		YOR162C	YRR1	YPL166W
YMR273C	ZDS1	YNR008W		YOR169C		YPL167C
YMR277W	FCP1	YNR023W	SNF12	YOR170W		YPL174C
YMR279C		YNR024W		YOR171C	LCB4	YPL181W
YMR280C	CAT8	YNR042W		YOR177C		YPL185W
YMR282C	AEP2	YNR045W	PET494	YOR183W		YPL189W
YMR284W	HDF1	YNR056C	BIO5	YOR186W		YPL191C
YMR285C		YNR059W		YOR188W	MSB1	YPL192C
YMR287C	MSU1	YNR060W	FRE4	YOR190W	SPR1	YPL193W
YMR288W		YNR062C		YOR192C		YPL194W
YMR294W	JNM1	YNR063W		YOR193W		YPL200W
YMR306C-A		YNR064C		YOR195W	SLK19	YPL201C
YMR306W	FKS3	YNR066C		YOR199W		YPL202C
YMR313C		YNR069C		YOR211C	MGM1	YPL205C
YMR316C-B		YNR070W		YOR214C		YPL209C
YMR317W		YNR072W	HXT17	YOR216C	RUD3	YPL213W
YMR320W		YNR073C		YOR221C		YPL216W
YMR324C		YNR077C		YOR225W		YPL217C
YMR326C		YOL006C	TOP1	YOR235W	SNR17A	YPL228W
YNL012W	SPO1	YOL015W		YOR237W	HES1	YPL233W
YNL014W		YOL017W		YOR242C		YPL241C
YNL017C		YOL018C	TLG2	YOR252W		YPL242C
YNL018C		YOL023W	IFM1	YOR255W		YPL243W
YNL019C		YOL024W		YOR256C		SRP68
YNL020C	ARK1	YOL025W	LAG2	YOR263C		GAL4
YNL024C		YOL028C	YAP7	YOR268C		YPL248C
YNL027W	CRZ1	YOL029C		YOR274W	MOD5	YPL249C
YNL028W		YOL034W		YOR277C		YPL251W
YNL033W		YOL037C		YOR279C		YPL254W
YNL034W		YOL041C		YOR282W		HFI1
YNL041C		YOL044W	PEX15	YOR287C		BBP1
YNL047C		YOL045W		YOR295W		VIK1
YNL049C		YOL046C		YOR296W		IQG1
YNL057W		YOL047C		YOR298W		SRP68
YNL059C	ARP5	YOL050C		YOR300W		KAR9
YNL068C	FKH2	YOL054W		YOR308C		YPL277C
YNL077W		YOL067C	RTG1	YOR313C	SPS4	YPL281C
YNL082W	PMS1	YOL069W	NUF2	YOR314W		ERR2
YNL083W		YOL076W	DEC1	YOR324C		CIT3
YNL089C		YOL078W		YOR325W		YPL281C

YNL095C		YOL079W		YOR330C	MIP1	YPR014C
YNL102W	POL1	YOL085C		YOR333C		YPR015C
YNL105W		YOL089C		YOR334W	MRS2	YPR018W RLF2
YNL106C	INP52	YOL091W		YOR339C		YPR025C CCL1
YNL109W		YOL093W		YOR345C		YPR026W ATH1
YNL119W		YOL095C		YOR350C	MNE1	YPR027C
YNL120C		YOL099C		YOR351C	MEK1	YPR031W
YNL126W	SPC98	YOL100W		YOR353C		YPR032W SRO7
YNL127W		YOL104C	NDJ1	YOR364W		YPR038W
YNL128W	TEP1	YOL105C	WSC3	YOR365C		YPR039W
YNL139C	RLR1	YOL113W	SKM1	YOR366W		YPR045C
YNL140C		YOL114C		YOR368W	RAD17	YPR046W MCM16
YNL143C		YOL115W	TRF4	YOR371C		YPR049C
YNL146W		YOL116W	MSN1	YOR372C		YPR050C
YNL148C	ALF1	YOL117W		YOR376W		YPR054W SMK1
YNL152W		YOL118C		YOR378W		YPR055W SEC8
YNL161W		YOL131W		YOR379C		YPR056W TFB4
YNL164C		YOL132W		YOR381W	FRE3	YPR059C
YNL171C		YOL134C		YOR384W	FRE5	YPR064W
YNL172W	APC1	YOL138C		YOR386W	PHR1	YPR068C HOS1
YNL179C		YOL141W		YOR387C		YPR070W
YNL182C		YOL144W		YOR392W		YPR071W
YNL187W		YOL145C	CTR9	YPL005W		YPR076W
YNL188W	KAR1	YOL150C		YPL008W	CHL1	YPR077C
YNL196C	SLZ1	YOL152W	FRE7	YPL016W	SWI1	YPR078C
YNL197C	WHI3	YOL156W	HXT11	YPL021W	ECM23	YPR083W
YNL198C		YOL157C		YPL022W	RAD1	YPR087W
YNL203C		YOL160W		YPL025C		YPR089W
YNL204C	SPS18	YOL161C		YPL027W		YPR090W
YNL205C		YOL163W		YPL029W	SUV3	YPR092W
YNL207W		YOL166C		YPL033C		YPR095C
YNL210W	MER1	YOR003W	YSP3	YPL035C		YPR096C
YNL212W		YOR005C	DNL4	YPL038W		YPR097W
YNL214W	PEX17	YOR011W		YPL040C	ISM1	YPR099C
YNL215W		YOR012W		YPL041C		YPR104C FHL1
YNL218W		YOR017W	PET127	YPL043W	NOP4	YPR105C
YNL224C		YOR019W		YPL044C		YPR111W DBF20
YNL225C	CNM67	YOR024W		YPL045W	VPS16	YPR112C
YNL226W		YOR025W	HST3	YPL060W		YPR116W
YNL227C		YOR026W	BUB3	YPL062W		YPR122W AXL1
YNL228W		YOR028C	CIN5	YPL070W		YPR123C
YNL233W	BNI4	YOR029W		YPL072W		YPR130C
YNL235C		YOR030W	DFG16	YPL073C		YPR136C
YNL242W		YOR032C	HMS1	YPL074W		YPR137W
YNL250W	RAD50	YOR033C	DHS1	YPL082C	MOT1	YPR141C KAR3
YNL253W		YOR037W	CYC2	YPL083C	SEN54	YPR142C
YNL254C		YOR038C	HIR2	YPL096W		YPR150W
YNL257C	SIP3	YOR041C		YPL099C		YPR152C
YNL258C		YOR048C	RAT1	YPL102C		YPR164W KIM3
YNL260C		YOR049C		YPL103C		YPR168W NUT2

YNL266W		YOR050C		YPL108W		YPR170C	
YNL267W	PIK1	YOR055W		YPL109C		YPR171W	
YNL269W		YOR058C	ASE1	YPL110C		YPR175W	DPB2
YNL270C	ALP1	YOR060C		YPL114W		YPR177C	
YNL272C	SEC2	YOR068C		YPL116W	HOS3	YPR179C	
YNL273W	TOF1	YOR070C	GYP1	YPL119C	DBP1	YPR180W	AOS1
YNL275W		YOR073W		YPL120W	VPS30	YPR186C	PZF1
YNL276C		YOR075W	UFE1	YPL121C	MEI5	YPR189W	SKI3
YNL279W		YOR076C		YPL124W	NIP29	YPR190C	RPC82
YNL282W	POP3	YOR077W	RTS2	YPL126W		YPR192W	
YNL285W		YOR080W		YPL130W		YPR193C	HPA2
YNL286W	CUS2	YOR082C		YPL133C		YPR195C	
YNL295W		YOR083W		YPL136W		YPR196W	
YNL296W		YOR093C		YPL137C		YPR197C	
YNL297C		YOR100C		YPL140C	MKK2	YPR200C	ARR2
YNL298W	CLA4	YOR105W		YPL141C		YPR201W	ARR3
YNL299W	TRF5	YOR111W		YPL146C		YPR202W	
YNL309W	STB1	YOR113W	AZF1	YPL147W	PXA1	YPR203W	
YNL311C		YOR114W		YPL150W			

## Appendix E

Transcripts with the Highest Average Abundance  
among Four *Saccharomyces cerevisiae* Cultures

This appendix contains a table of the 500 ORFs with the most abundant transcripts. Ranking of abundance in this table is by the mean of absolute abundance across the four cultures measured, with absolute abundance calculated as described in Chapter 2.

It was interesting to find that eleven of the one hundred most abundant transcripts measured derive from ORFs which have not been assigned a gene name. A cursory examination of these ORFs showed that YDR154C (rank 1) overlaps YDR155C (gene CPH1, ranked 33), and the ORFs YDR134C (rank 16) and YDR133C (rank 44) overlap each other. This effectively reduces the number of abundant unnamed transcripts to 9 of the top 100.

### Unnamed transcripts in the 100 most abundant ORFs

Rank	ID	Notes	Homology (BLAST GenEMBL)
1	YDR154C	overlaps YDR155C (CPH1; rank 33)	CPH1, <i>C. albicans</i> CYP1, <i>S. Pombe</i> ISP4
3	YLR110C	convergent with YLR109W (rank 69)	YAR050W (FLO1), YKR102W (FLO10), YNR044W (AGA1)
16	YDR134C	overlaps YDR133C (unnamed; rank 44)	YLR110C, YAR050W (FLO1), YKR102W (FLO10), YNR044W (AGA1)
30	YMR173WA	overlaps YMR173W (DDR48; rank 1362)	DDR48
37	YKL056C		translationally controlled tumor protein (TCTP) conserved in animals and higher plants.
44	YDR133C	overlaps YDR134C (unnamed; rank 16)	YLR110C
52	YDR033W		YBR054W (YRO2), YCR021C (YRO1/HSP30)
55	YDR276C		<i>H. vulgare</i> blt101, <i>L. elongatum</i> salt-stress induced ESI3, YJL152W, YJL153C (APR1/INO1)
69	YLR109W	convergent with YLR110C (rank 3)	<i>L. kononenkoae</i> putative peroxisomal protein, <i>C. boidinii</i> peroxisomal membrane protein A and B, YDR077W (SED1)
76	YER150W		-
96	YNL208W		-

Homology searches were performed using TBLASTN against the non-redundant GenBank+EMBL+DDBJ+PDB databases (April 1997) using a web interface provided by the Saccharomyces Genome Database [Altschul, 1990 #340].

Guide to abundance table. The columns labeled ‘R’ refer to the rank of the transcript according to average abundance. ‘Avg’ is the average of four absolute abundances (which can be found for each ORF in Appendix C). ‘ID’ refers to the ORF identifier as assigned by the *Saccharomyces* Genome Database (SGD). An ORF identifier printed in italics indicates that the sequence of some of the mismatch probes for this ORF were not unique in the *cerevisiae* genome. In this case PM values were substituted for  $\Delta$  values in calculating absolute and relative abundance, so that the quantitation for these ORFs should be viewed more critically. The gene names were taken from the current (10 April 98) SGD table of gene names.

**ORFs with the highest average absolute abundance across four cultures assayed.**

R	Avg	ID	Gene	R	Avg	ID	Gene	R	Avg	ID	Gene
1	36.0	YDR154C		168	2.9	YPL037C	EGD1	335	1.3	YBR106W	PHO88
2	28.7	YKL097WA	CWP2	169	2.9	YPL028W	ERG10	336	1.3	YHR018C	ARG4
3	25.1	YLR110C		170	2.8	YDR447C	RPS17B	337	1.3	YLR354C	TAL1
4	22.0	YGR192C	TDH3	171	2.8	YBR067C	TIP1	338	1.2	YGL202W	ARO8
5	21.1	YDR382W	RPP2B	172	2.8	YDR178W	SDH4	339	1.2	YLR395C	COX8
6	21.0	YBR191W	RPL21A	173	2.7	YML073C	RPL6A	340	1.2	YLL041C	SDH2
7	18.9	YHR174W	ENO2	174	2.7	YOR167C	RPS28A	341	1.2	YPR063C	
8	17.8	YDL130W	RPP1B	175	2.7	YLR441C	RPS1A	342	1.2	YDR404C	RPB7
9	17.0	YKL060C	FBA1	176	2.7	YNR050C	LYS9	343	1.2	YBR109C	CMD1
10	16.6	YDR050C	TPI1	177	2.7	YLL024C	SSA2	344	1.2	YDR025W	RPS11A
11	16.3	YBL072C	RPS8A	178	2.6	YER091C	MET6	345	1.2	YLR150W	MPT4
12	14.2	YBR031W	RPL4A	179	2.6	YNL302C	RPS19B	346	1.2	YPL098C	
13	13.4	YPL079W	RPL21B	180	2.6	YDR055W		347	1.2	YNL096C	RPS7B
14	13.4	YGL189C	RPS26A	181	2.6	YPL090C	RPS6A	348	1.2	YLR303W	MET17
15	13.2	YOL040C	RPS15	182	2.6	YBL092W	RPL32	349	1.2	YMR195W	
16	12.1	YDR134C		183	2.6	YNL134C		350	1.2	YDR471W	RPL27B
17	11.8	YLR044C	PDC1	184	2.5	YDR353W	TRR1	351	1.2	YGL187C	COX4
18	11.7	YCR012W	PGK1	185	2.5	YNL209W	SSB2	352	1.2	YKL085W	MDH1
19	11.5	YHR021C	RPS27B	186	2.5	YJR145C	RPS4A	353	1.2	YKR094C	RPL40B
20	11.4	YIL018W	RPL2B	187	2.5	YMR083W	ADH3	354	1.2	YPL048W	CAM1
21	11.4	YPL131W	RPL5	188	2.5	YJL151C		355	1.2	YBR009C	HHF1
22	11.4	YHR053C	CUP1	189	2.5	YEL026W		356	1.2	YOR187W	
23	10.7	YOL039W	RPP2A	190	2.5	YJL138C	TIF2	357	1.2	YLR286C	CTS1
24	10.7	YMR251WA	HOR7	191	2.5	YPL271W	ATP15	358	1.2	YOL139C	CDC33
25	10.6	YPR043W	RPL43A	192	2.4	YDL137W	ARF2	359	1.2	YJR139C	HOM6
26	10.4	YBR118W	TEF2	193	2.4	YER011W	TIR1	360	1.2	YDL128W	VCX1
27	10.3	YKL180W	RPL17A	194	2.4	YMR297W	PRC1	361	1.2	YER009W	NTF2
28	10.3	YJR073C	OPI3	195	2.4	YBR189W	RPS9B	362	1.2	YIL094C	
29	10.2	YOL086C	ADH1	196	2.4	YDR450W	RPS18A	363	1.2	YDL232W	OST4
30	9.9	YMR173WA		197	2.4	YHR183W	GND1	364	1.2	YGR285C	ZUO1
31	9.3	YJL190C	RPS22A	198	2.4	YIL043C	CBR1	365	1.2	YLR229C	CDC42
32	9.1	YGR254W	ENO1	199	2.4	YKL156W	RPS27A	366	1.2	YBL099W	ATP1
33	9.1	YDR155C	CPH1	200	2.4	YLL050C	COF1	367	1.2	YLR375W	STP3
34	8.9	YPL143W	RPL33A	201	2.3	YKR059W	TIF1	368	1.1	YDR304C	CYP5
35	8.9	YOL053CA	DDR2	202	2.3	YDR233C		369	1.1	YPR052C	NHP6A
36	8.7	YPR080W	TEF1	203	2.3	YGL037C		370	1.1	YPL198W	RPL7B
37	8.7	YKL056C		204	2.3	YGR060W	ERG25	371	1.1	YOR374W	ALD7
38	8.6	YHR055C	CUP1	205	2.3	YOL127W	RPL25	372	1.1	YLR178C	TFS1
39	8.5	YGL135W	RPL1B	206	2.3	YJL159W		373	1.1	YFL045C	SEC53
40	8.3	YOR182C	RPS30B	207	2.3	YOR234C		374	1.1	YPR098C	
41	8.2	YJR009C	TDH2	208	2.3	YJL191W	RPS14B	375	1.1	YFL010C	
42	7.9	YPL220W	RPL1A	209	2.3	YPR074C	TKL1	376	1.1	YKL080W	VMA5
43	7.6	YKL152C	GPM1	210	2.2	YLR048W	RPS0B	377	1.1	YLR179C	
44	7.5	YDR133C		211	2.2	YPL218W	SAR1	378	1.1	YMR256C	COX7
45	7.5	YOL120C	RPL18A	212	2.2	YDR345C	HXT3	379	1.1	YIL062C	ARC15
46	7.4	YNL031C	HHT2	213	2.2	YER117W	RPL23B	380	1.1	YCL035C	

47	7.2	YMR116C	BEL1	214	2.2	YNL030W	HHF2	381	1.1	YLR056W	ERG3
48	7.2	YNL055C	POR1	215	2.2	YNR018W		382	1.1	YKL067W	YNK1
49	7.1	YNL135C	FPR1	216	2.2	YKL035W		383	1.1	YPR103W	PRE2
50	7.0	YGL008C	PMA1	217	2.2	YDR502C	SAM2	384	1.1	YGL026C	TRP5
51	7.0	YNL178W	RPS3	218	2.2	YDR298C	ATP5	385	1.1	YIR022W	SEC11
52	6.8	YDR033W		219	2.1	YBL030C	PET9	386	1.1	YLR027C	AAT2
53	6.7	YCR031C	RPS14A	220	2.1	YDL191W	RPL35A	387	1.1	YDL131W	LYS21
54	6.6	YLR061W	RPL22A	221	2.1	YGR209C	TRX2	388	1.1	YOR303W	CPA1
55	6.6	YDR276C		222	2.1	YDR158W	HOM2	389	1.1	YBL003C	HTA2
56	6.6	YDR500C	RPL37B	223	2.1	YNL327W	EGT2	390	1.1	YNL268W	LYP1
57	6.5	YEL027W	CUP5	224	2.1	YHR193C	EGD2	391	1.1	YCL018W	LEU2
58	6.5	YDR077W	SED1	225	2.1	YOL109W	ZEO1	392	1.1	YHR001WA	QCR10
59	6.5	YLR340W	RPP0	226	2.1	YPL154C	PEP4	393	1.1	YOR007C	SGT2
60	6.4	YDR012W	RPL4B	227	2.0	YOR045W	TOM6	394	1.0	YCR024CA	PMP1
61	6.4	YHR203C	RPS4B	228	2.0	YLR264W	RPS28B	395	1.0	YOL030W	
62	6.3	YHR026W	PPA1	229	2.0	YNL300W		396	1.0	YFR044C	
63	6.3	YGL123W	RPS2	230	2.0	YMR202W	ERG2	397	1.0	YOR120W	GCY1
64	6.2	YML028W	TSA1	231	2.0	YGR282C	BGL2	398	1.0	YKL182W	FAS1
65	6.2	YLR388W	RPS29A	232	2.0	YBL002W	HTB2	399	1.0	YMR241W	
66	6.1	YNL145W	MFA2	233	2.0	YLR406C	RPL31B	400	1.0	YML092C	PRE8
67	6.1	YLR075W	RPL10	234	2.0	YNL044W		401	1.0	YGR180C	RNR4
68	6.0	YJL158C	CIS3	235	2.0	YPL234C	TFP3	402	1.0	YER072W	
69	5.9	YLR109W		236	2.0	YMR295C		403	1.0	YDR328C	SKP1
70	5.9	YJL052W	TDH1	237	2.0	YOR270C	VPH1	404	1.0	YBR115C	LYS2
71	5.9	YFL014W	HSP12	238	1.9	YOR136W	IDH2	405	1.0	YHR051W	COX6
72	5.7	YDR064W	RPS13	239	1.9	YLR355C	ILV5	406	1.0	YMR305C	
73	5.6	YIL133C	RPL16A	240	1.9	YCL043C	PDI1	407	1.0	YGL220W	
74	5.6	YLR300W	EXG1	241	1.9	YNL190W		408	1.0	YJR105W	
75	5.6	YJL136C	RPS21B	242	1.9	YPR113W	PIS1	409	1.0	YMR315W	
76	5.5	YER150W		243	1.9	YMR142C	RPL13B	410	1.0	YMR008C	PLB1
77	5.4	YGR085C	RPL11B	244	1.9	YGL256W	ADH4	411	1.0	YDL048C	STP4
78	5.3	YAL038W	CDC19	245	1.9	YLL045C	RPL8B	412	1.0	YNL305C	
79	5.3	YDL081C	RPP1A	246	1.9	YDR388W	RVS167	413	1.0	YHR064C	PDR13
80	5.3	YKR042W	UTH1	247	1.9	YEL054C	RPL12A	414	1.0	YLR208W	SEC13
81	5.3	YOR063W	RPL3	248	1.9	YDR032C		415	1.0	YPL106C	SSE1
82	5.2	YGL030W	RPL30	249	1.9	YHR025W	THR1	416	1.0	YER057C	HIG1
83	5.2	YER102W	RPS8B	250	1.9	YNL067W	RPL9B	417	1.0	YIL123W	SIM1
84	5.2	YKL164C	PIR1	251	1.9	YLR350W		418	1.0	YCL009C	ILV6
85	5.2	YER177W	RPL23B	252	1.8	YGL055W	OLE1	419	1.0	YHR179W	OYE2
86	5.1	YDL125C	HNT1	253	1.8	YBR020W	GAL1	420	1.0	YJR121W	ATP2
87	5.1	YKL096W	CWP1	254	1.8	YML012W	ERV25	421	1.0	YNL244C	SUI1
88	5.1	YKR057W	RPS21A	255	1.8	YER056CA	RPL34A	422	1.0	YHR039BC	VMA10
89	5.0	YNL069C	RPL16B	256	1.8	YBR082C	UBC4	423	1.0	YBR029C	CDS1
90	5.0	YJR104C	SOD1	257	1.8	YHR141C	RPL42B	424	1.0	YIL041W	
91	4.9	YDL192W	ARF1	258	1.8	YBR249C	ARO4	425	1.0	YML100W	TSL1
92	4.9	YLR167W	RPS31	259	1.8	YGL200C	EMP24	426	1.0	YER023W	PRO3
93	4.7	YMR194W	RPL36A	260	1.8	YJR085C		427	1.0	YDR519W	FKB2
94	4.6	YNL160W	YGP1	261	1.8	YNL015W	PBI2	428	1.0	YGL089C	MFα2
95	4.6	YLR185W	RPL37A	262	1.8	YNL301C	RPL18B	429	1.0	YIL078W	THS1
96	4.5	YNL208W		263	1.7	YBR196C	PGI1	430	1.0	YNR036C	

97	4.5	YGL103W	RPL28	264	1.7	YOR248W		431	1.0	YHR094C	HXT1
98	4.4	YDR342C	HXT7	265	1.7	YKR013W	PRY2	432	1.0	YBR018C	GAL7
99	4.4	YDL182W	LYS20	266	1.7	YDL055C	PSA1	433	1.0	YGL077C	HNM1
100	4.4	YEL017CA	PMP2	267	1.7	YLR325C	RPL38	434	0.9	YDR513W	TTR1
101	4.4	YOR247W		268	1.7	YFL031W	HAC1	435	0.9	YLL023C	
102	4.4	YFR053C	HXK1	269	1.7	YOL129W		436	0.9	YOR185C	GSP2
103	4.4	YDL083C	RPS16B	270	1.7	YDR224C	HTB1	437	0.9	YDR368W	YPR1
104	4.4	YJR123W	RPS5	271	1.7	YHR162W		438	0.9	YMR318C	
105	4.4	YDL229W	SSB1	272	1.7	YBL087C	RPL23A	439	0.9	25SRRNAA	
106	4.3	YLR448W	RPL6B	273	1.7	YMR002W		440	0.9	YPL252C	
107	4.3	YDR497C	ITR1	274	1.7	YML058W		441	0.9	YBR086C	
108	4.2	YDR343C	HXT6	275	1.7	YLR333C	RPS25B	442	0.9	YBR126C	TPS1
109	4.2	YCL040W	GLK1	276	1.6	YGR214W	RPS0A	443	0.9	YER094C	PUP3
110	4.1	YJR094WA	RPL43B	277	1.6	YMR143W	RPS16A	444	0.9	YLL039C	UBI4
111	4.1	YJL189W	RPL39	278	1.6	YER178W	PDA1	445	0.9	YER062C	HOR2
112	4.1	YOR285W		279	1.6	YOR099W	KTR1	446	0.9	YPL087W	
113	4.1	YLR391W		280	1.6	YLR259C	HSP60	447	0.9	YFL038C	YPT1
114	4.1	YEL034W	HYP2	281	1.6	YGR183C	QCR9	448	0.9	YBR181C	RPS6B
115	4.1	YDR418W	RPL12B	282	1.6	YGL253W	HXK2	449	0.9	YNL130C	CPT1
116	4.0	YOR369C	RPS12	283	1.6	YMR226C		450	0.9	YBR011C	IPP1
117	4.0	YHL015W	RPS20	284	1.6	YGR118W	RPS23A	451	0.9	YER056C	FCY2
118	4.0	YPR132W	RPS23B	285	1.6	YOR020C	HSP10	452	0.9	YLR294C	
119	4.0	YEL009C	GCN4	286	1.6	YLR293C	GSP1	453	0.9	YPR016C	CDC95
120	4.0	YCR021C	HSP30	287	1.6	YHL033C	RPL8A	454	0.9	YIR038C	
121	3.9	YBR010W	HHT1	288	1.5	YAL005C	SSA1	455	0.9	YKR065C	
122	3.9	YGL255W	ZRT1	289	1.5	YPR035W	GLN1	456	0.9	YCR053W	THR4
123	3.8	YLR043C	TRX1	290	1.5	YPL262W	FUM1	457	0.9	YLR180W	SAM1
124	3.8	YKL006W	RPL14A	291	1.5	YNL322C	KRE1	458	0.9	YOL154W	
125	3.8	YFR031CA	RPL2A	292	1.5	YDL067C	COX9	459	0.9	YNL064C	YDJ1
126	3.8	YOR122C	PFY1	293	1.5	YNL162W	RPL42A	460	0.9	YLR378C	SEC61
127	3.8	YGL076C	RPL7A	294	1.5	YPL004C		461	0.9	CONTROL2	
128	3.7	YJL177W	RPL17B	295	1.5	YER120W	SCS2	462	0.9	YPL094C	SEC62
129	3.7	YDR533C		296	1.5	YKR066C	CCP1	463	0.9	YMR145C	
130	3.7	YOR230W	WTM1	297	1.5	YDL181W	INH1	464	0.9	YLR081W	GAL2
131	3.7	YFL039C	ACT1	298	1.5	YML078W	CPR3	465	0.9	YPL010W	RET3
132	3.7	YKL192C		299	1.5	YJL079C	PRY1	466	0.9	YBR019C	GAL10
133	3.6	YOL121C	RPS19A	300	1.5	YLR029C	RPL15A	467	0.9	CONTROL10	
134	3.6	YPR149W	NCE102	301	1.5	YDL004W	ATP16	468	0.9	YGR181W	
135	3.6	YIL148W	RPL40A	302	1.5	YNL104C	LEU4	469	0.9	YGR027C	RPS25A
136	3.6	YDR461W	MFA1	303	1.5	YAL012W	CYS3	470	0.8	YBR159W	
137	3.6	YLR287CA	RPS30A	304	1.5	YDL124W		471	0.8	YML052W	SUR7
138	3.5	YIR034C	LYS1	305	1.5	YDL075W	RPL31A	472	0.8	YOR332W	VMA4
139	3.5	YHR010W	RPL27A	306	1.5	YPR036W	VMA13	473	0.8	YNL071W	LAT1
140	3.5	YDL022W	GPD1	307	1.4	YLR372W	SUR4	474	0.8	YMR215W	
141	3.5	YDR226W	ADK1	308	1.4	YNL007C	SIS1	475	0.8	YGL148W	ARO2
142	3.5	YIL053W	RHR2	309	1.4	YNL052W	COX5A	476	0.8	YMR205C	PKF2
143	3.4	YGR037C	ACB1	310	1.4	YBR054W	YRO2	477	0.8	YHR008C	SOD2
144	3.4	YIL051C	MMD1	311	1.4	YGL147C	RPL9A	478	0.8	YDL188C	PPH22
145	3.3	YML024W	RPS17A	312	1.4	YBR072W	HSP26	479	0.8	YBR025C	
146	3.3	YIL052C	RPL34B	313	1.4	YOR224C	RPB8	480	0.8	YDR070C	

147	3.3	YER043C	SAH1	314	1.4	YOR383C		481	0.8	YJR065C	ARP3
148	3.3	YGR279C		315	1.4	YHR007C	ERG11	482	0.8	YGR240C	PKF1
149	3.3	YIR037W	HYR1	316	1.4	YPL231W	FAS2	483	0.8	YMR242C	RPL20A
150	3.2	YLR058C	SHM2	317	1.4	YNR001C	CIT1	484	0.8	YGR155W	CYS4
151	3.2	<i>YHL001W</i>	RPL14B	318	1.4	YML026C	RPS18B	485	0.8	YGR106C	
152	3.2	YKL163W	PIR3	319	1.4	YDR433W		486	0.8	YJL153C	INO1
153	3.2	YPR102C	RPL11A	320	1.4	YGL225W	GOG5	487	0.8	YOL058W	ARG1
154	3.2	YOR133W	EFT1	321	1.3	YJL034W	KAR2	488	0.8	YDR234W	LYS4
155	3.2	YBR286W	APE3	322	1.3	YLR249W	YEF3	489	0.8	YDR483W	KRE2
156	3.1	YOR096W	RPS7A	323	1.3	YAL003W	EFB1	490	0.8	YLL014W	
157	3.1	YDL061C	RPS29B	324	1.3	YDR297W	SUR2	491	0.8	YER055C	HIS1
158	3.1	YDR225W	HTA1	325	1.3	YOR375C	GDH1	492	0.8	YGR295C	COS6
159	3.1	YDR385W	EFT2	326	1.3	YML126C	HMGS	493	0.8	YAL044C	GCV3
160	3.1	YPR028W		327	1.3	YOR010C	TIR2	494	0.8	YFR047C	
161	3.0	YJR077C	MIR1	328	1.3	YGR148C	RPL24B	495	0.8	YPL246C	
162	3.0	YML106W	URA5	329	1.3	YPR165W	RHO1	496	0.8	YML132W	COS3
163	2.9	YOR293W	RPS10A	330	1.3	YDL136W	RPL35B	497	0.8	YBR127C	VMA2
164	2.9	YGR034W	RPL26B	331	1.3	YPL061W	ALD6	498	0.8	YGL012W	ERG4
165	2.9	YGL031C	RPL24A	332	1.3	YDL072C		499	0.8	<i>YLR367W</i>	RPS22B
166	2.9	YDR454C	GUK1	333	1.3	YGR008C	STF2	500	0.8	YMR272C	SCS7
167	2.9	YDL082W	RPL13A	334	1.3	<i>YOR312C</i>	RPL20B				

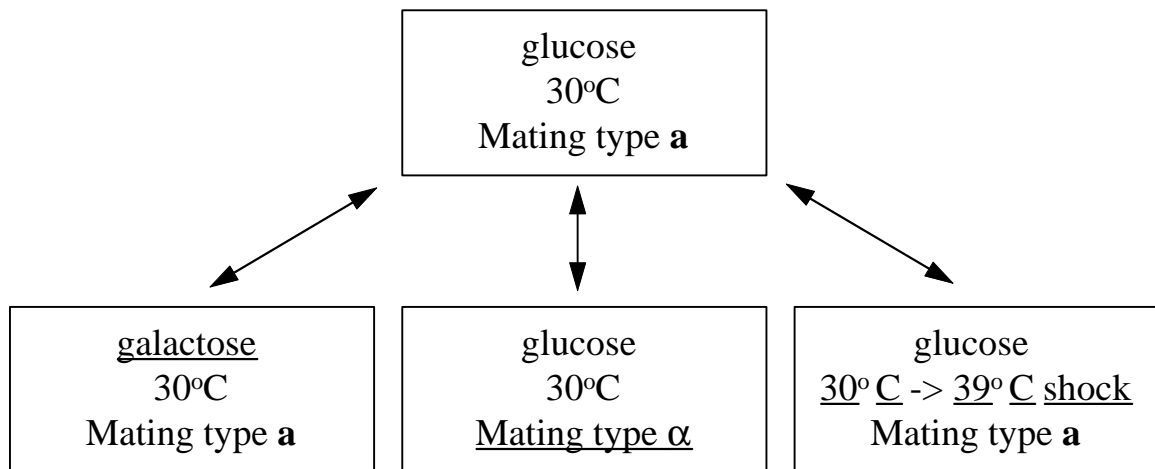
## References

## Appendix F

Transcripts Most Changed in Abundance

among Four Cultures Assayed

The four cultures examined in Chapter 3 consisted of a ‘baseline’ condition, and three ‘experimental’ conditions, where only one variable (either genotypic or environmental) was changed relative to baseline. This allows for three whole-genome scale comparisons of transcript abundance. The following table contains those genes most changed in these comparisons. Since there are three comparisons, there are six sets of extrema—a set of ORFs most increased and most decreased for each comparison.



Guide to relative abundance table. The first column (“ID”) contains the ORF identifier as issued by the Saccharomyces Genome Database. An ORF identifier printed in italics indicates that the sequence of some of the mismatch probes for this ORF were not unique in the *cerevisiae* genome. In this case PM values were substituted for  $\Delta$  values in calculating absolute and relative abundance, so that the quantitation for these ORFs should be viewed more critically.

The second column (“Gene”) contains the common gene names corresponding to each ORF identifier. The gene names were taken from the current (10 April 98) SGD table of gene names.

The fourth and fifth columns contain absolute abundances of the ORF's transcript in the two conditions being compared. Transcripts which fell below the detection threshold of the corresponding hybridization experiment are indicated by abundance values in italics. In this case,  $\Delta$  values used to calculate the abundance value were adjusted to the detection threshold if they fell below it. The sixth column contains the logarithm (base 10) of the median  $\Delta$ -ratio value for this comparison. Transcripts considered below detection threshold in one or both conditions being compared are indicated by median log  $\Delta$ -ratio values in italics. If a transcript is below detection threshold in both conditions being compared, the median log  $\Delta$ -ratio is set to zero. For each of the relative abundance values, a measure of significance is calculated by dividing the median log  $\Delta$ -ratio by the median deviation of log  $\Delta$ -ratios. If this measure of significance is one or greater, and the median log  $\Delta$ -ratio is 0.2 or greater, the median log  $\Delta$ -ratio value is in bold type. Absolute and relative abundance calculations are described in Chapters 2 and 3.

### ORFs most abundant in mating type a relative to mating type a culture.

R	ID	Gene	a	alpha	log α/a	Brief SGD Gene Description
1	YPL187W	MF(α)1	0.11	2.88	<b>1.28</b>	mating factor α
2	YGL089C	MF(α)2	0.07	3.67	<b>1.22</b>	α mating factor
3	YCL066W	α1	0.09	0.51	<b>0.67</b>	transcription factor involved in the regulation of the alpha-specific genes
4	YCR040W	α1	0.09	0.37	<b>0.63</b>	transcription factor involved in the regulation of the alpha-specific genes
5	YJR004C	SAG1	0.35	1.74	<b>0.48</b>	α-agglutinin
6	YLR040C		0.35	1	<b>0.42</b>	
7	YHR053C	CUP1	5.96	17	<b>0.4</b>	copper-binding metallothionein
8	YHR128W	FUR1	0.44	1.09	<b>0.38</b>	UPRTase
9	YHR141C	RPL42B	1.03	1.98	<b>0.35</b>	Ribosomal protein L42B (YL27) (L41) (YP44)
10	YGL106W	MLC1	0.16	0.51	<b>0.35</b>	myosin light chain
11	YGR038W	ORM1	0.17	0.3	<b>0.35</b>	
12	YLR355C	ILV5	1.09	2.59	<b>0.33</b>	acetohydroxyacid reductoisomerase
13	YLR029C	RPL15A	0.97	2.84	<b>0.32</b>	Ribosomal protein L15A (YL10) (rp15R) (L13)
14	YGL030W	RPL30	4.86	9.72	<b>0.32</b>	Large ribosomal subunit protein L30 (L32) (rp72) (YL38)
15	YGR159C	NSR1	0.21	0.48	<b>0.31</b>	nuclear localization sequence binding protein
16	YOR309C		0.41	0.93	<b>0.29</b>	
17	YIL052C	RPL34B	2.34	4.11	<b>0.28</b>	Ribosomal protein L34B
18	YLR056W	ERG3	0.65	1.53	<b>0.28</b>	C-5 sterol desaturase
19	YNL112W	DBP2	0.16	0.33	<b>0.27</b>	ATP-dependent RNA helicase of DEAD box family
20	YGR232W		0.19	0.54	0.26	
21	YIL133C	RPL16A	4.77	8.84	<b>0.26</b>	Ribosomal protein L16A (L21) (rp22) (YL15)
22	YLR229C	CDC42	0.72	1.6	<b>0.26</b>	member of the Rho subfamily of Ras-like proteins
23	YJR145C	RPS4A	2.08	3.91	<b>0.26</b>	Ribosomal protein S4A (YS6) (rp5) (S7)
24	YLR150W	MPT4	0.77	1.74	0.25	
25	YEL026W		1.59	2.96	<b>0.24</b>	
26	YOL040C	RPS15	10.86	20.6	<b>0.24</b>	40S ribosomal protein S15 (S21) (rp52) (RIG protein)
27	YLR293C	GSP1	1.16	2.37	<b>0.24</b>	GTP-binding protein
28	YMR292W		0.48	0.86	<b>0.23</b>	
29	YGL055W	OLE1	0.65	1.19	<b>0.22</b>	delta-9-fatty acid desaturase
30	YJL153C	INO1	0.35	1.25	0.22	L-myo-inositol-1-phosphate synthase
31	YNL255C		0.25	0.51	<b>0.22</b>	
32	<i>YFR031C-A</i>	RPL2A	2.22	5.11	<b>0.22</b>	Ribosomal protein L2A (L5) (rp8) (YL6)
33	YDR471W	RPL27B	0.82	1.28	<b>0.21</b>	60S ribosomal protein L27, identical to Yhr010p
34	YOR310C	NOP5	0.42	0.76	<b>0.21</b>	nucleolar protein
35	YER086W	ILV1	0.13	0.36	<b>0.21</b>	threonine deaminase
36	YOL021C	DIS3	0.11	0.21	<b>0.21</b>	
37	YOR247W		3.99	5.53	<b>0.21</b>	
38	<i>YER117W</i>	RPL23B	1.82	3.53	<b>0.21</b>	Ribosomal protein L23B (L17a) (YL32)
39	YMR276W	DSK2	0.54	0.64	0.21	ubiquitin-like protein
40	YLR333C	RPS25B	1.58	2.59	<b>0.21</b>	Ribosomal protein S25B (S31) (rp45) (YS23)

41	YDR450W	RPS18A	1.45	3.12	<b>0.2</b>	Ribosomal protein S18A
42	YOR021C		0.11	0.23	<b>0.2</b>	
43	YMR321C		0.46	0.63	<b>0.2</b>	
44	<i>YIL069C</i>	RPS24B	0.45	0.93	<b>0.2</b>	40S ribosomal protein S24B
45	<i>YIL018W</i>	RPL2B	8.69	15.9	<b>0.2</b>	Ribosomal protein L2B (L5) (rp8) (YL6)
46	YGR124W	ASN2	0.25	0.25	0.2	asparagine synthetase
47	YGL198W		0.21	0.82	0.2	
48	YEL040W	UTR2	0.36	0.75	<b>0.2</b>	
49	YHR193C	EGD2	1.12	2.16	0.19	GAL4 enhancer protein, homolog of human alpha NAC subunit of the nascent-polypeptide-associated complex
50	YLR286C	CTS1	1.1	1.61	<i>0.19</i>	Endochitinase

### ORFs most abundant in mating type a relative to mating type a culture.

R	ID	GENE	a	alpha	log a/α	Brief SGD Gene Description
1	YDR461W	MFA1	4.42	0.04	<b>1.98</b>	a-factor mating pheromone precursor
2	YNL145W	MFA2	7.14	0.09	<b>1.64</b>	mating a-factor pheromone precursor
3	YGL032C	AGA2	0.6	0.07	<b>0.9</b>	adhesion subunit of a-agglutinin
4	YFL026W	STE2	0.57	0.07	<b>0.8</b>	alpha-factor pheromone receptor; seven-transmembrane domain protein
5	YIL015W	BAR1	0.45	0.07	<b>0.68</b>	encodes a-cell barrier activity on alpha factor
6	YCR024C-A	PMP1	1.83	0.54	<b>0.6</b>	Proteolipid associated with plasma membrane H(+)-ATPase (Pma1p)
7	YJL164C	SRA3	0.47	0.15	<b>0.56</b>	putative catalytic subunit of cAMP-dependent protein kinase
8	YLL040C	VPS13	0.35	0.11	<b>0.55</b>	
9	YKR071C		0.35	0.11	<b>0.53</b>	
10	YBR147W		0.39	0.11	<b>0.52</b>	
11	YJR086W	STE18	0.35	0.11	<b>0.51</b>	gamma subunit of G protein coupled to mating factor receptors
12	YML027W	YOX1	0.35	0.15	<b>0.5</b>	Homeobox-domain containing protein
13	YMR042W	ARG80	0.35	0.14	<b>0.5</b>	Regulator of arginine-responsive genes with ARG81 and ARG82
14	YMR047C	NUP116	0.35	0.15	<b>0.5</b>	Nuclear pore complex protein that is member of GLFG repeat-containing family of nucleoporins and is highly homologous to Nup100p
15	YKR018C		0.35	0.19	<b>0.49</b>	
16	YLL031C		0.35	0.17	<b>0.49</b>	
17	YKL214C		0.35	0.14	<b>0.48</b>	
18	YKL170W	MRPL38	0.35	0.12	<b>0.47</b>	mitochondrial ribosomal protein L14
19	YMR119W		0.35	0.14	<b>0.47</b>	
20	YBR011C	IPP1	1.17	0.63	<b>0.46</b>	Inorganic pyrophosphatase
21	YBR106W	PHO88	2.11	0.76	<b>0.46</b>	May be a membrane protein involved in inorganic phosphate transport and regulation of Pho81p function
22	YAL061W		0.46	0.16	<b>0.45</b>	
23	YBL015W	ACH1	0.46	0.11	<b>0.44</b>	acetyl CoA hydrolase
24	YKL128C	PMU1	0.35	0.15	<b>0.44</b>	Phospo-mutase homolog
25	YMR003W		0.35	0.13	<b>0.44</b>	
26	YPR149W	NCE102	5.06	1.28	<b>0.44</b>	involved in secretion of proteins that lack classical secretory signal sequences
27	YCR012W	PGK1	23.1	5.85	<b>0.44</b>	3-phosphoglycerate kinase
28	YKL066W		0.35	0.13	<b>0.43</b>	
29	YBR268W	MRPL37	0.26	0.05	<b>0.42</b>	Probable mitochondrial protein L37
30	YDR343C	HXT6	6	2.42	<b>0.42</b>	Hexose transporter
31	YPR165W	RHO1	1.57	0.41	<b>0.4</b>	GTP-binding protein of the rho subfamily of ras-like proteins
32	YBR072W	HSP26	0.68	0.24	<b>0.4</b>	heat shock protein 26
33	YMR090W		0.35	0.21	<b>0.39</b>	
34	YPL220W	RPL1A	9.9	5.87	<b>0.39</b>	Ribosomal protein L1A, forms part of the 60S ribosomal subunit
35	YML075C	HMG1	0.35	0.17	<b>0.38</b>	3-hydroxy-3-methylglutaryl-coenzyme A (HMG-CoA) reductase isozyme

36	YJL210W	PEX2	0.6	0.26	<b>0.38</b>	CH3HC4 zinc-binding integral peroxisomal membrane protein
37	YBL045C	COR1	0.4	0.17	<b>0.37</b>	44 kDa core protein of yeast coenzyme QH2 cytochrome c reductase
38	YJR103W	URA8	0.35	0.17	<b>0.36</b>	CTP synthase
39	YOL058W	ARG1	0.65	0.22	<b>0.35</b>	arginosuccinate synthetase
40	YPL271W	ATP15	2.42	0.58	<b>0.35</b>	nuclear gene for ATP synthase epsilon subunit
41	YKL196C	YKT6	0.35	0.16	<b>0.34</b>	v-SNARE
42	YLR028C	ADE16	0.35	0.23	<b>0.34</b>	5-aminoimidazole-4-carboxamide ribonucleotide (AICAR) transformylase/IMP cyclohydrolase
43	YMR038C	LYS7	0.35	0.22	<b>0.34</b>	
44	YMR184W		0.35	0.2	<b>0.34</b>	
45	YDL047W	SIT4	0.09	0.05	<b>0.33</b>	SIT4 suppress mutations in DBF2
46	YDR490C		0.12	0.05	<b>0.33</b>	
47	YDR506C		0.09	0.07	<b>0.33</b>	
48	YDR342C	HXT7	6.13	3.01	<b>0.33</b>	Hexose transporter
49	YBR107C		0.09	0.06	<b>0.32</b>	
50	YEL031W	SPF1	0.21	0.07	<b>0.32</b>	P-type ATPase

### ORFs most abundant in galactose vs. glucose-fed culture.

R	ID	Gene	glu	gal	log gal/glu	Brief SGD Gene Description
1	YBR020W	GAL1	0.09	7.12	<b>1.81</b>	galactokinase
2	YBR018C	GAL7	0.09	3.59	<b>1.62</b>	galactose-1-phosphate uridyl transferase
3	YBR019C	GAL10	0.09	3.24	<b>1.57</b>	UDP-glucose 4-epimerase
4	YOR120W	GCY1	0.11	3.21	<b>1.09</b>	Similar to mammalian aldo/keto reductases
5	YLR081W	GAL2	0.35	2.84	<b>0.91</b>	galactose permease
6	YPL066W		0.11	0.76	<b>0.8</b>	
7	YPL067C		0.21	1.76	<b>0.77</b>	
8	YMR318C		0.37	1.89	<b>0.6</b>	
9	YNL015W	PBI2	0.95	3.03	<b>0.59</b>	Proteinase inhibitor I2B (PBI2), that inhibits protease Prb1p (yscB)
10	YOL058W	ARG1	0.65	1.99	<b>0.53</b>	arginosuccinate synthetase
11	YGL055W	OLE1	0.65	2.44	<b>0.51</b>	delta-9-fatty acid desaturase
12	YHR033W		0.21	0.65	<b>0.5</b>	
13	YDR009W	GAL3	0.09	0.29	<b>0.49</b>	galactokinase
14	YGR244C		0.17	0.53	<b>0.48</b>	
15	YNL052W	COX5A	1.09	2.69	<b>0.47</b>	Cytochrome-c oxidase chain Va
16	YMR256C	COX7	0.54	2.43	<b>0.45</b>	subunit VII of cytochrome c oxidase
17	YOL031C		0.11	0.43	<b>0.45</b>	
18	YGL121C		0.15	0.43	<b>0.44</b>	
19	YGR232W		0.19	0.56	<b>0.42</b>	
20	YGR234W	YHB1	0.37	1.38	<b>0.41</b>	Flavohemoglobin
21	YNL239W	LAP3	0.26	0.88	<b>0.41</b>	Aminopeptidase of cysteine protease family
22	YPL262W	FUM1	0.97	3.11	<b>0.4</b>	mitochondrial and cytoplasmic fumarase (fumarate hydralase)
23	YGL126W	SCS3	0.31	0.81	<b>0.39</b>	
24	YHR193C	EGD2	1.12	2.79	<b>0.38</b>	GAL4 enhancer protein, homolog of human alpha NAC subunit of the nascent-polypeptide-associated complex
25	YER069W	ARG5,6	0.27	0.5	<b>0.37</b>	N-acetyl-gamma-glutamyl-phosphate reductase and acetylglutamate kinase
26	YGL187C	COX4	0.88	1.94	<b>0.37</b>	subunit IV of cytochrome c oxidase
27	YER067W		0.35	1.03	<b>0.36</b>	
28	YOR288C	MPD1	0.18	0.53	<b>0.36</b>	Disulfide isomerase related protein
29	YPL134C		0.24	0.77	<b>0.36</b>	
30	YHR001W-A	QCR10	0.81	2.1	<b>0.35</b>	8.5 kDa subunit of the ubiquinol-cytochrome c oxidoreductase complex
31	YHR018C	ARG4	1.11	2.01	<b>0.35</b>	argininosuccinate lyase
32	YHR057C	CYP2	0.11	0.51	<b>0.35</b>	Peptidylprolyl isomerase (cyclophilin) ER or secreted
33	YHR179W	OYE2	0.78	1.1	<b>0.35</b>	NAPDH dehydrogenase (old yellow enzyme), isoform 2
34	YNL104C	LEU4	1.2	1.98	<b>0.35</b>	alpha-isopropylmalate synthase (2-Isopropylmalate Synthase)
35	YNL112W	DBP2	0.16	0.44	<b>0.35</b>	ATP-dependent RNA helicase of DEAD box family
36	YPR020W		0.32	0.61	<b>0.35</b>	
37	YPR145W	ASN1	0.46	0.96	<b>0.35</b>	asparagine synthetase
38	YGL117W		0.08	0.28	<b>0.34</b>	
39	YGR183C	QCR9	1.45	3.17	<b>0.34</b>	7.3 kDa subunit 9 of the ubiquinol cytochrome c oxidoreductase complex
40	YHR008C	SOD2	0.62	1.24	<b>0.34</b>	Manganese-containing superoxide dismutase

41	YIL050W	PCL7	0.1	0.29	<b>0.34</b>	
42	YOL143C	RIB4	0.32	0.66	<b>0.34</b>	6,7-dimethyl-8-ribityllumazine synthase (DMRL synthase)
43	YGR008C	STF2	1.26	1.79	<b>0.33</b>	
44	YGR037C	ACB1	2.26	6.31	<b>0.33</b>	Acyl-CoA-binding protein (ACBP)/Diazepam binding inhibitor (DBI)/endozepine (EP)
45	YHR051W	COX6	0.56	2.02	<b>0.33</b>	subunit VI of cytochrome c oxidase
46	YHR141C	RPL42B	1.03	2.78	<b>0.33</b>	Ribosomal protein L42B (YL27) (L41) (YP44)
47	YOR202W	HIS3	0.23	0.69	<b>0.33</b>	imidazoleglycerol-phosphate dehydratase
48	YFL030W		0.14	0.69	0.32	
49	YHR071W	PCL5	0.07	0.18	<b>0.32</b>	PHO85 cyclin
50	YNL259C	ATX1	0.22	0.35	<b>0.32</b>	Antioxidant protein and metal homeostasis factor, protects against oxygen toxicity

### ORFs most abundant in glucose- vs. galactose-fed culture.

R	ID	Gene	glu	gal	log glu/gal	Brief SGD Gene Description
1	YDR345C	HXT3	3.77	0.09	<b>1.4</b>	High-affinity glucose transporter
2	YGL189C	RPS26A	14.83	1.19	<b>0.89</b>	
3	YHR094C	HXT1	0.84	<i>0.07</i>	<b>0.8</b>	High-affinity hexose (glucose) transporter
4	YOL154W		1.89	0.17	<b>0.78</b>	
5	YGL030W	RPL30	4.86	0.89	<b>0.73</b>	Large ribosomal subunit protein L30 (L32) (rp72) (YL38)
6	YFL045C	SEC53	1.25	0.29	<b>0.71</b>	phosphomannomutase
7	YBR106W	PHO88	2.11	0.34	<b>0.7</b>	May be a membrane protein involved in inorganic phosphate transport and regulation of Pho81p function
8	YER190W		0.73	0.1	<b>0.69</b>	
9	YBR011C	IPP1	1.17	0.41	<b>0.58</b>	Inorganic pyrophosphatase
10	YER178W	PDA1	1.88	0.32	<b>0.54</b>	alpha subunit of pyruvate dehydrogenase (E1 alpha)
11	YCR005C	CIT2	1.05	0.19	<b>0.52</b>	non-mitochondrial citrate synthase
12	25srRnaa		1.54	0.32	<b>0.51</b>	
13	YHR092C	HXT4	0.76	0.12	<b>0.51</b>	High-affinity glucose transporter
14	YFR024C		0.27	<i>0.07</i>	<b>0.51</b>	
15	YJR073C	OPI3	14.51	4.73	<b>0.47</b>	Methylene-fatty-acyl-phospholipid synthase (unsaturated phospholipid N-methyltransferase)
16	YKL096W	CWP1	4.38	1.36	<b>0.47</b>	cell wall mannoprotein
17	YLL024C	SSA2	2.07	0.76	<b>0.46</b>	member of 70 kDa heat shock protein family
18	YJL190C	RPS22A	19.08	3.19	<b>0.44</b>	Ribosomal protein S22A (S24) (rp50) (YS22)
19	YFR051C	RET2	0.55	0.16	<b>0.43</b>	
20	YKL035W		2.32	0.81	<b>0.42</b>	
21	YBR072W	HSP26	0.68	0.18	<b>0.39</b>	heat shock protein 26
22	YJL191W	RPS14B	2.33	0.94	<b>0.39</b>	Ribosomal protein S14B (rp59)
23	YGL256W	ADH4	2.66	0.52	<b>0.39</b>	alcohol dehydrogenase isoenzyme IV
24	YCR024C-A	PMP1	1.83	0.8	<b>0.38</b>	Proteolipid associated with plasma membrane H(+)-ATPase (Pma1p)
25	YBL087C	RPL23A	2.07	1.01	<b>0.38</b>	Ribosomal protein L23A (L17a) (YL32)
26	YNL054W	VAC7	<i>0.11</i>	0.05	<b>0.37</b>	
27	YJL158C	CIS3	9.57	3.2	<b>0.36</b>	Protein with homology to Hsp150p and Pir1p, Pir2p, and Pir3p
28	YOR352W		<i>0.11</i>	0.08	<b>0.36</b>	
29	YCR012W	PGK1	23.1	9.14	<b>0.35</b>	3-phosphoglycerate kinase
30	YJR009C	TDH2	7.93	3.96	<b>0.35</b>	glyceraldehyde 3-phosphate dehydrogenase
31	YOR377W	ATF1	<i>0.11</i>	0.05	<b>0.35</b>	Alcohol acetyltransferase
32	YML073C	RPL6A	3.12	1.66	<b>0.35</b>	Ribosomal protein L6A (L17) (rp18) (YL16)
33	YLL045C	RPL8B	1.68	0.74	<b>0.34</b>	Ribosomal protein L8B (L4) (rp6) (YL5)
34	YGL209W	MIG2	0.21	0.08	<b>0.33</b>	Protein containing zinc fingers very similar to zinc fingers in Mig1p
35	YOL158C		<i>0.11</i>	0.05	<b>0.33</b>	
36	YPR174C		<i>0.11</i>	0.07	<b>0.33</b>	
37	YJR094W-A	RPL43B	3.91	1.9	<b>0.33</b>	Ribosomal protein L43B
38	YBR101C		0.29	0.11	<b>0.32</b>	
39	YGL157W		0.26	<i>0.07</i>	<b>0.32</b>	
40	YDR171W	HSP42	0.5	0.27	<b>0.31</b>	Similar to HSP26; expression is regulated by stress conditions

41	YNL084C	END3	<i>0.11</i>	0.07	<b>0.31</b>	Protein necessary for internalization of alpha-factor receptor when bound to ligand
42	YPR061C		<i>0.11</i>	0.07	<b>0.31</b>	
43	YLR109W		3.58	1.96	<b>0.31</b>	
44	YPR091C		<i>0.11</i>	0.05	<b>0.3</b>	
45	YJR123W	RPS5	5.23	1.26	<b>0.3</b>	ribosomal protein RPS5 (mammalian S5) (previously called rp14, S2 or YS8)
46	YLR043C	TRX1	2.64	2.07	<b>0.3</b>	thioredoxin
47	YKL097W-A	CWP2	40.86	15.05	<b>0.29</b>	cell wall mannoprotein
48	YFL021W	GAT1	0.17	<i>0.07</i>	<b>0.29</b>	transcriptional activator with GATA-1-type Zn finger DNA-binding motif
49	YMR116C	BEL1	9.06	3.58	<b>0.29</b>	
50	YLR264W	RPS28B	2.16	0.52	<b>0.29</b>	Ribosomal protein S28B (S33) (YS27)

### ORFs most abundant in heat-shocked vs. 30 °C culture.

R	ID	Gene	30°C	heat	log heat/30°C	Brief SGD Gene Description
1	YFL014W	HSP12	2.53	16.82	<b>0.89</b>	12 kDa heat shock protein
2	YDR453C		0.2	1.66	<b>0.88</b>	
3	YPL223C	GRE1	0.11	1.04	<b>0.83</b>	Induced by osmotic stress
4	YGL121C		0.15	1.53	<b>0.82</b>	
5	YLR303W	MET17	0.39	3.15	<b>0.77</b>	O-Acetylhomoserine-O-Acetylserine Sulphydralase
6	YBR072W	HSP26	0.68	4.62	<b>0.75</b>	heat shock protein 26
7	YGR256W	GND2	0.08	0.53	<b>0.75</b>	6-phosphogluconate dehydrogenase
8	YLR178C	TFS1	0.39	3.31	<b>0.65</b>	suppressor of cdc25
9	YDR533C		1.53	9.8	<b>0.65</b>	
10	YDR019C	GCV1	0.16	1	<b>0.64</b>	glycine cleavage T protein (T subunit of glycine decarboxylase complex
11	YGL055W	OLE1	0.65	3.08	<b>0.62</b>	delta-9-fatty acid desaturase
12	YLR058C	SHM2	1.52	6.78	<b>0.59</b>	serine hydroxymethyltransferase
13	YGR250C		0.07	0.52	<b>0.59</b>	
14	YLL039C	UBI4	0.35	2.2	<b>0.57</b>	ubiquitin
15	YDR055W		1.54	5.63	<b>0.57</b>	
16	YHR104W	GRE3	0.43	1.63	<b>0.57</b>	Induced by osmotic stress\; similar to xylose reductase from other fungi
17	YDR214W		0.27	1.09	<b>0.53</b>	
18	YLR216C	CPR6	0.35	1.4	<b>0.53</b>	a cyclophilin related to the mammalian CyP-40\; physically interacts with RPD3 gene product
19	YDR070C		0.51	2.18	<b>0.52</b>	
20	YMR174C	PAI3	0.35	1.45	<b>0.51</b>	Cytoplasmic inhibitor of proteinase Pep4p
21	YNL281W		0.16	0.69	<b>0.51</b>	
22	YER103W	SSA4	0.26	0.84	<b>0.5</b>	member of 70 kDa heat shock protein family
23	YER062C	HOR2	0.59	2.05	<b>0.5</b>	DL-glycerol-3-phosphatase
24	YMR175W	SIP18	0.35	1.33	0.5	
25	YKL163W	PIR3	1.28	9.38	<b>0.49</b>	Protein containing tandem internal repeats
26	YGL196W		0.31	0.96	<b>0.48</b>	
27	YOR120W	GCY1	0.11	0.72	<b>0.48</b>	Similar to mammalian aldo\keto reductases
28	YPR127W		0.16	0.79	<b>0.47</b>	
29	YHR007C	ERG11	1.02	2.6	<b>0.47</b>	cytochrome P450 lanosterol 14a-demethylase
30	YML128C		0.35	1.06	<b>0.47</b>	
31	YPR157W		0.11	0.53	<b>0.47</b>	
32	YMR246W	FAA4	0.2	0.65	<b>0.47</b>	long-chain fatty acid--CoA ligase and synthetase 4
33	YDL222C		0.23	0.97	<b>0.45</b>	
34	YBR117C	TKL2	0.09	0.3	<b>0.44</b>	transketolase, homologous to tk11
35	YGR088W	CTT1	0.11	0.67	<b>0.44</b>	cytoplasmic catalase T
36	YOL053C-A	DDR2	5.4	16.53	<b>0.44</b>	
37	YHR055C	CUP1	6.8	15.95	<b>0.43</b>	copper-binding metallothionein
38	YMR276W	DSK2	0.54	1.2	<b>0.43</b>	ubiquitin-like protein
39	YPR035W	GLN1	1.04	2.74	<b>0.43</b>	glutamine synthetase
40	YOR020C	HSP10	1.22	2.71	<b>0.42</b>	10 kDa mitochondrial heat shock protein
41	YER042W		0.07	0.29	<b>0.41</b>	
42	YGR043C		0.07	0.37	<b>0.41</b>	
43	YIR038C		0.66	1.67	<b>0.41</b>	

44	YOR007C	SGT2	0.71	1.86	<b>0.41</b>	small glutamine-rich tetratricopeptide repeat containing protein
45	YML092C	PRE8	0.56	2.15	<b>0.39</b>	proteasome component Y7
46	YBR054W	YRO2	1.05	2.94	<b>0.39</b>	Homolog to HSP30 heat shock protein Yro1p
47	YPL240C	HSP82	0.15	0.67	<b>0.39</b>	heat shock protein
48	YDL223C		0.11	0.42	<b>0.39</b>	
49	YER160C		0.12	0.39	<b>0.39</b>	
50	YLR375W	STP3	0.76	2.35	<b>0.39</b>	Involved in pre-tRNA splicing and in uptake of branched-chain amino acids

### ORFs most abundant in 30 °C vs. heat-shocked culture.

R	ID	Gene	30°C	heat	log heat/30° C	Brief SGD Gene Description
1	YJL052W	TDH1	9.02	0.05	<b>-1.69</b>	Glyceraldehyde-3-phosphate dehydrogenase 1
2	YOL154W		1.89	0.08	<b>-0.99</b>	
3	YGR234W	YHB1	0.37	0.11	<b>-0.62</b>	Flavohemoglobin
4	YBR010W	HHT1	5.04	1.29	<b>-0.53</b>	Histone H3 (HHT1 and HHT2 code for identical proteins)
5	YBL072C	RPS8A	23.04	7.03	<b>-0.49</b>	Ribosomal protein rp19 (YS9) (Mammalian S8)
6	YBL002W	HTB2	2.74	0.73	<b>-0.48</b>	Histone H2B (HTB1 and HTB2 code for nearly identical proteins)
7	YBL003C	HTA2	1.31	0.47	<b>-0.48</b>	Histone H2A (HTA1 and HTA2 code for nearly identical proteins)
8	YFR015C	GSY1	0.16	0.05	<b>-0.46</b>	Glycogen synthase (UDP-glucocse--starch glucosyltransferase)
9	YBR009C	HHF1	1.7	0.55	<b>-0.41</b>	Histone H4 (HHF1 and HHF2 code for identical proteins)
10	YIR034C	LYS1	4.01	2.33	<b>-0.4</b>	saccharopine dehydrogenase
11	YNL030W	HHF2	2.55	1.03	<b>-0.39</b>	Histone H4 (HHF1 and HHF2 code for identical proteins)
12	YGL256W	ADH4	2.66	0.99	<b>-0.38</b>	alcohol dehydrogenase isoenzyme IV
13	YCR034W	FEN1	0.75	0.22	<b>-0.37</b>	Probable subunit of 1,3-beta-glucan synthase\; homolog of ELO1
14	YNL117W	MLS1	0.11	0.05	<b>-0.36</b>	carbon-catabolite sensitive malate synthase
15	YNL199C	GCR2	0.11	0.08	<b>-0.35</b>	Activates transcription of glycolytic genes\; homologous to GCR1\; may function in complex with Gcr2p
16	YPL127C	HHO1	0.34	0.12	<b>-0.34</b>	histone H1
17	YPR188C		0.14	0.07	<b>-0.34</b>	
18	YMR283C	RIT1	0.11	0.06	<b>-0.34</b>	Initiator methionine tRNA 2'-O-ribosyl phosphate transferase
19	YGL255W	ZRT1	4.53	1.99	<b>-0.34</b>	
20	YJL158C	CIS3	9.57	4.62	<b>-0.33</b>	Protein with homology to Hsp150p and Pir1p, Pir2p, and Pir3p
21	YDR382W	RPP2B	30.31	13.72	<b>-0.33</b>	Ribosomal protein P2B (YP2b) (L45)
22	YPL195W	APL5	0.11	0.06	<b>-0.33</b>	delta-like subunit of the yeast AP-3 adaptin component of the membrane-associated clathrin assembly complex
23	YBL015W	ACH1	0.46	0.14	<b>-0.33</b>	acetyl CoA hydrolase
24	YCR024C-A	PMP1	1.83	1.02	<b>-0.32</b>	Proteolipid associated with plasma membrane H(+)-ATPase (Pma1p)
25	YBL092W	RPL32	3.47	1.7	<b>-0.32</b>	Ribosomal protein L32
26	YDL081C	RPP1A	7.2	2.72	<b>-0.31</b>	Acidic ribosomal protein P1A (YP1a) (A1)
27	YDR516C		0.54	0.26	<b>-0.31</b>	
28	YOR081C		0.11	0.11	<b>-0.31</b>	
29	YOR154W		0.11	0.07	<b>-0.31</b>	
30	YOL053W		0.11	0.06	<b>-0.3</b>	
31	YJL190C	RPS22A	19.08	6.52	<b>-0.29</b>	Ribosomal protein S22A (S24) (rp50) (YS22)
32	YJL088W	ARG3	0.28	0.1	<b>-0.29</b>	Ornithine carbamoyltransferase
33	YMR240C	CUS1	0.11	0.06	<b>-0.29</b>	U2 snRNP protein

34	YBR115C	LYS2	1.82	0.66	<b>-0.28</b>	alpha amino adipate reductase
35	<i>YBL027W</i>	RPL19B	0.64	0.23	<b>-0.28</b>	Ribosomal protein L19B (YL14) (L23) (rpl5L)
36	YOR290C	SNF2	0.11	0.06	<b>-0.27</b>	transcriptional regulator
37	YDL182W	LYS20	6.35	3.4	<b>-0.27</b>	homocitrate synthase, highly homologous to YDL131W
38	YPL046C	ELC1	0.11	0.07	<b>-0.27</b>	Elongin C transcription elongation factor
39	YJR073C	OPI3	14.51	9.55	<b>-0.26</b>	Methylene-fatty-acyl-phospholipid synthase (unsaturated phospholipid N-methyltransferase)
40	YDR064W	RPS13	7.08	4.32	<b>-0.26</b>	Ribosomal protein S13 (S27a) (YS15)
41	YPR143W		0.11	0.07	<b>-0.26</b>	
42	YML073C	RPL6A	3.12	1.81	<b>-0.25</b>	Ribosomal protein L6A (L17) (rp18) (YL16)
43	YDL130W	RPP1B	20.92	13.86	<b>-0.25</b>	Ribosomal protein P1B (L44') (YP1b) (Ax)
44	YPL139C	UME1	0.11	0.08	<b>-0.25</b>	Transcriptional modulator
45	YPL260W		0.11	0.1	<b>-0.25</b>	
46	YHL015W	RPS20	3.39	3.35	<b>-0.25</b>	Ribosomal protein S20
47	YIL052C	RPL34B	2.34	1.76	-0.25	Ribosomal protein L34B
48	YCR005C	CIT2	1.05	0.48	<b>-0.24</b>	non-mitochondrial citrate synthase
49	YDR133C		10.29	5.16	<b>-0.24</b>	
50	YBR268W	MRPL37	0.26	0.11	<b>-0.24</b>	Probable mitochondrial protein L37

## Appendix G

Sizes of Intergenic Regions in *S. cerevisiae*,

*E. coli* and *H. influenzae*

This appendix contains the size distribution of intergenic regions for three organisms—*Saccharomyces cerevisiae*, *Escherichia coli*, and *Haemophilus influenzae*. The size of intergenic regions in *S. cerevisiae* is relevant to Chapter 3, in which a choice was made about how much upstream non-coding sequence to examine, i.e., at what distance from translation start are we unlikely to find regulatory sequences? The size of intergenic regions for prokaryotes *E. coli* and *H. influenzae* is not relevant to any other work in this thesis, but I include it here as a reference.

For each organism, each intergenic region was classified as being one of three types: divergent, convergent or tandem. A divergent region is a region between two flanking genes which have opposite directions of translation. A divergent intergenic region must then contain transcription regulation signals for two genes. A convergent region is defined as having two flanking genes, both having directions of translation oriented towards the intergenic region. Therefore, a convergent intergenic region presumably contains no transcription regulation signals. A tandem intergenic region is flanked by two genes, one oriented away from and one towards the intergenic region, so that a tandem intergenic region contains the transcription signals for one gene (or possibly none if the intergenic region is within an operon). In addition to these three types, we might also consider the intron to be a type of intergenic region.

Convergent intergenic regions have the shortest length distribution in all three of the organisms examined, which was to be expected since these regions will in general not contain any transcriptional control sequences. Tandem intergenic regions were the next highest length distribution in all three organisms, consistent with the expectation that these regions will, in general, contain the transcriptional control elements of one gene.

The largest intergenic regions are divergent regions, which is to be expected since these will often contain transcriptional control elements for two genes.

In Chapter 3, AlignACE was used to find conserved upstream DNA elements. It was important to have an estimate of how great a distance upstream of translation start one might expect to find transcriptional regulatory elements. It is instructive to look at the size distribution of tandem intergenic regions, since these should in general contain a set of transcriptional elements for one (and only one) gene. Setting an upper length bound of 600 base pairs seemed reasonable, since more than 75% of tandem intergenic regions that are greater than zero in length are less than 600 base pairs long. An upper limit of 975 base pairs would be required to include the full width of 90% of the intergenic regions with non-negative length.

It is also worth noting that the distribution of tandem regions in the two eubacterial genomes appeared bimodal. Presumably this is due to the fact that operon structure is found in these organisms, with shorter intergenic regions corresponding to genes within operons.

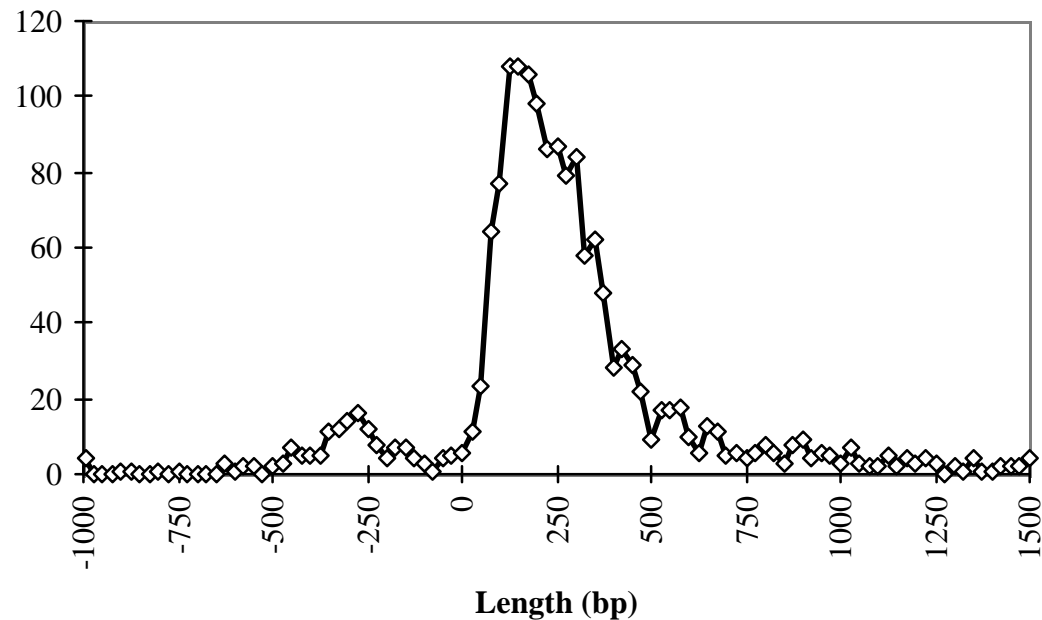
It is intriguing to find that intron lengths in *S. cerevisiae* also form a bimodal distribution. This may be an artifact due to the software used to predict intron positions, or it reflects distinct types of introns (perhaps the difference is in length is due to introns containing genes). This observation bears further investigation.

For the purpose of this appendix, the collection of regions between open reading frames (ORFs) was taken as a surrogate for intergenic regions, i.e., non-protein-coding regions such as tRNAs and rRNAs were not included as genes. This decision was made for the sake of convenience and excluded roughly 400 genes from *S. cerevisiae*, and

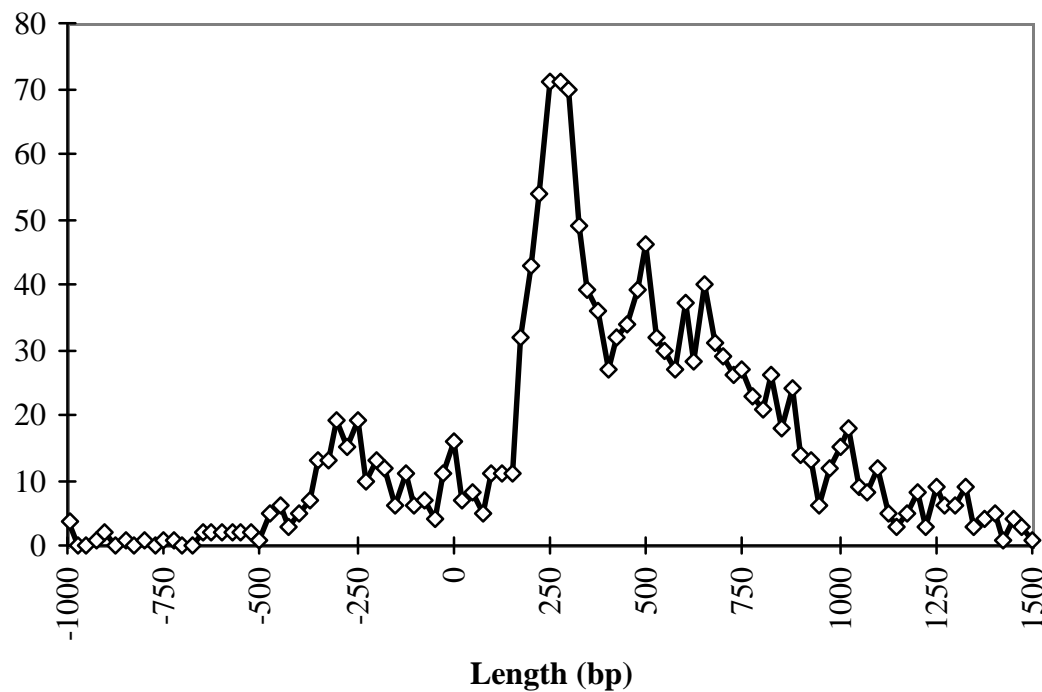
roughly 100 *E. coli* & *H. influenzae* genes. Thus, the distributions presented here are slightly biased towards larger intergenic regions.

The positions of start and stop codons for each ORF in *S. cerevisiae* were obtained from SGD, and are current as of August 1997. The positions of start and stop codons in *E. coli* were derived from the M52 version of the *E. coli* K-12 sequence (September 1997) and were obtained from NCBI at <ftp://ncbi.nlm.nih.gov/genbank/genomes/bacteria/Ecoli/>. The positions of start and stop codons for *H. influenzae* are current as of February 1998 and were obtained from the Institute for Genomic Research (TIGR) Microbial Database at <http://www.tigr.org/tdb/mdb/hidb/hidb.html>.

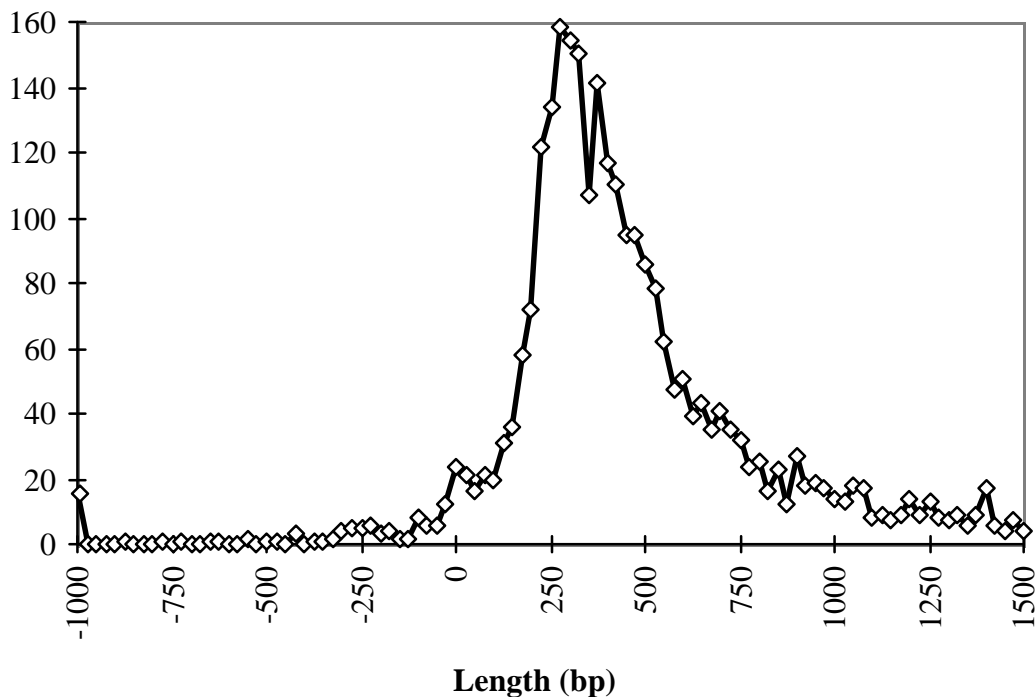
**Size Distribution of Convergent Intergenic Regions in *S. cerevisiae*.**



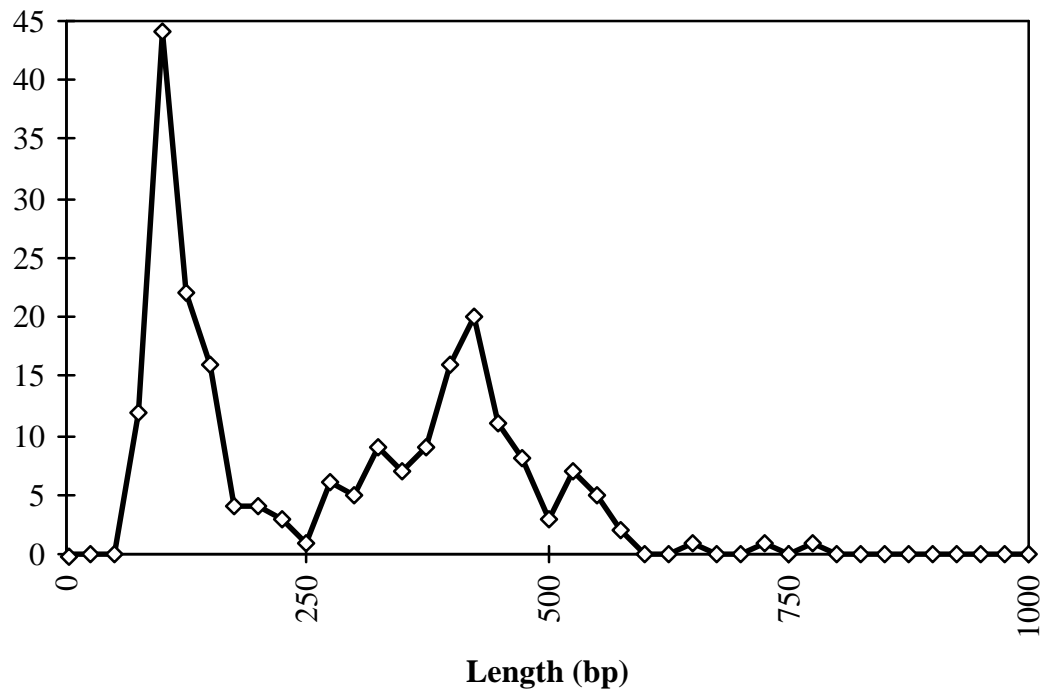
**Size Distribution of Divergent Intergenic Regions in *S. cerevisiae*.**



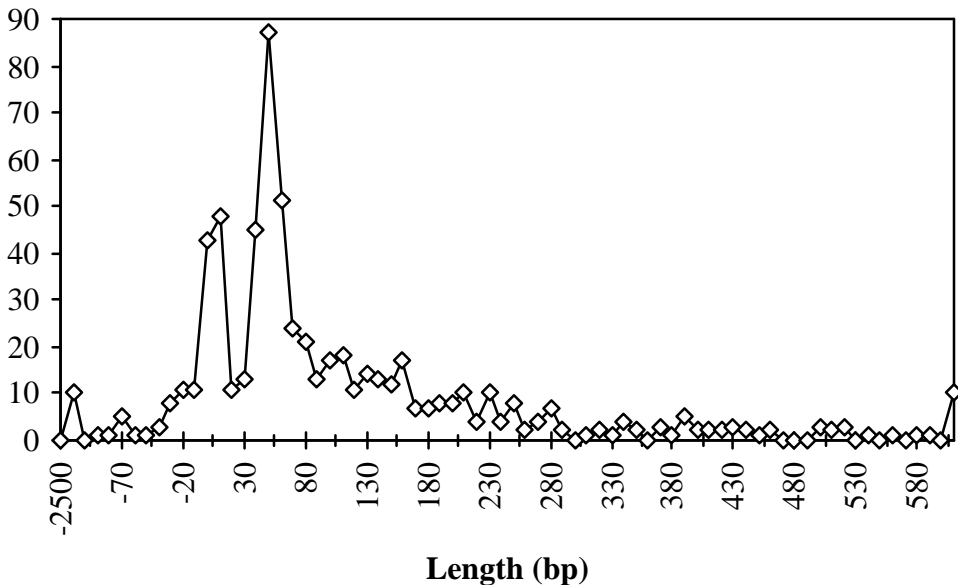
### Size Distribution of Tandem Intergenic Regions in *S. cerevisiae*.



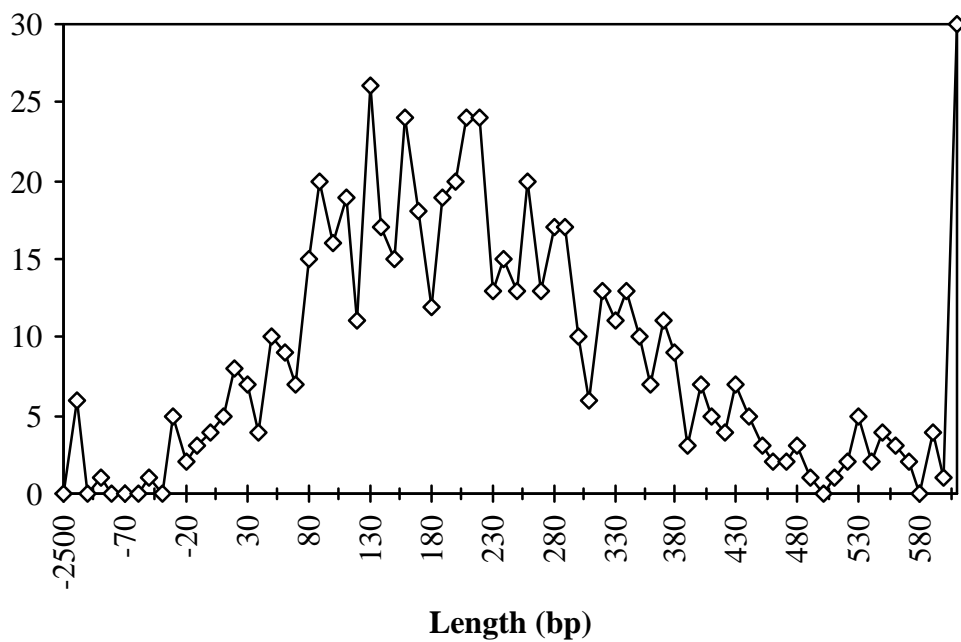
### Size Distribution of Introns in *S. cerevisiae*.



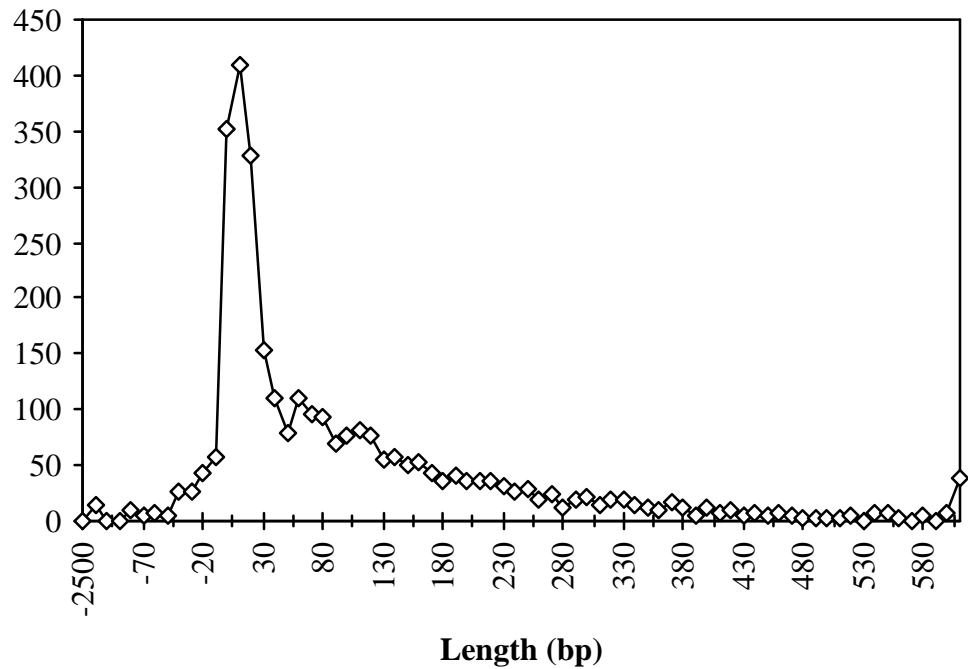
### Size Distribution of Convergent Intergenic Regions in *E. coli*.



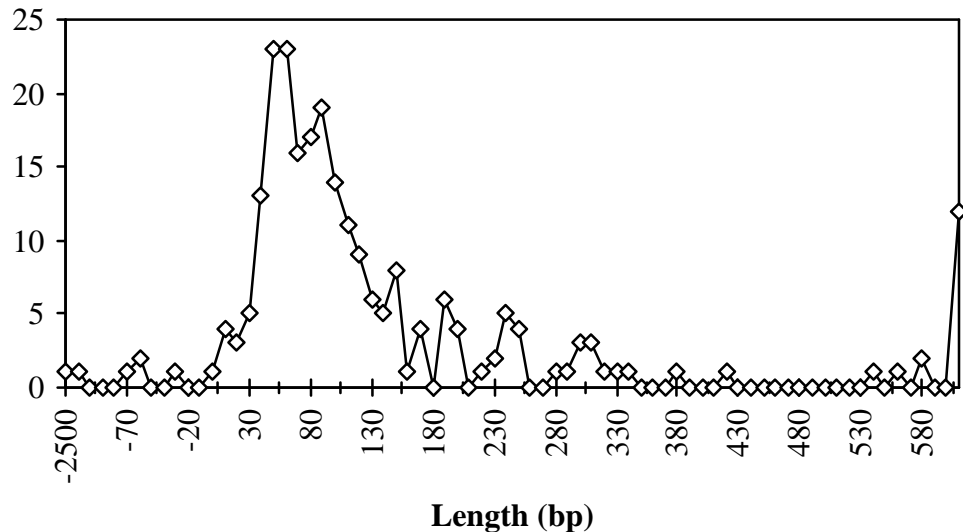
### Size Distribution of Divergent Intergenic Regions in *E. coli*.



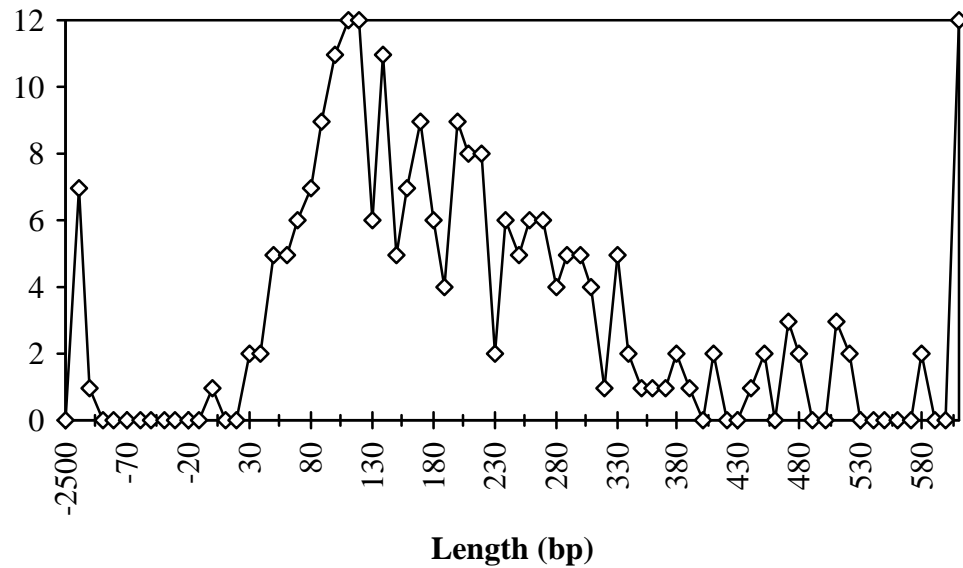
### Size Distribution of Tandem Intergenic Regions in *E. coli*.



**Size Distribution of Convergent Intergenic Regions in *H. influenzae*.**



**Size Distribution of Divergent Intergenic Regions in *H. influenzae*.**



**Size Distribution of Tandem Intergenic Regions in *H. influenzae*.**

